DANMARKS OG GRØNLANDS GEOLOGISKE UNDERSØGELSE **RAPPORT 2022/26**

CCS2022-2024 WP1: The Stenlille structure

Seismic data and interpretation to mature potential geological storage of CO_2

Ulrik Gregersen, Lars Hjelm, Henrik Vosgerau, Florian W.H. Smit, Carsten M. Nielsen, Rasmus Rasmussen, Kenneth Bredesen, Mads Lorentzen, Finn Mørk, Bodil W. Lauridsen, Gunver K. Pedersen, Lars Henrik Nielsen, Anders Mathiesen, Shahjahan Laghari, Lars Kristensen, Emma Sheldon, Trine Dahl-Jensen, Karen Dybkjær, Christian A. Hidalgo & Lasse M. Rasmussen

GEOLOGICAL SURVEY OF DENMARK AND GREENLAND
DANISH MINISTRY OF CLIMATE, ENERGY AND UTILITIES

G E U S

DANMARKS OG GRØNLANDS GEOLOGISKE UNDERSØGELSE **RAPPORT 2022/26**

CCS2022-2024 WP1: The Stenlille structure

Seismic data and interpretation to mature potential geological storage of CO_2

Ulrik Gregersen, Lars Hjelm, Henrik Vosgerau, Florian W.H. Smit, Carsten M. Nielsen, Rasmus Rasmussen, Kenneth Bredesen, Mads Lorentzen, Finn Mørk, Bodil W. Lauridsen, Gunver K. Pedersen, Lars Henrik Nielsen, Anders Mathiesen, Shahjahan Laghari, Lars Kristensen, Emma Sheldon, Trine Dahl-Jensen, Karen Dybkjær, Christian A. Hidalgo & Lasse M. Rasmussen

GEOLOGICAL SURVEY OF DENMARK AND GREENLAND
DANISH MINISTRY OF CLIMATE, ENERGY AND UTILITIES

G E U S

Preface

A new Danish Climate Act was decided by the Danish Government and a large majority of the Danish Parliament on June 26th, 2020. It includes the aim of reducing the Danish greenhouse gas emissions with 70 % by 2030 compared to the level of emissions in 1990. The first part of a new Danish CCS-Strategy of June 30th, 2021 includes a decision to continue the initial investigations of sites for potential geological storage of CO_2 in Denmark. GEUS has therefore from 2022 commenced seismic acquisition and investigations of potential sites for geological storage of CO_2 in Denmark.

The structures decided for maturation by the authorities, are some of the largest structures onshore Zealand, Jutland and Lolland and in the eastern North Sea (Fig. 1.1). The onshore structures include the Havnsø, Gassum, Thorning, and Rødby structures, and in addition the small Stenlille structure as a demonstration (pilot) site. The offshore structures include the Inez, Lisa and Jammerbugt structures. A GEUS Report is produced for each of the structures to mature the structure as part of the CCS2022–2024 project towards potential geological storage of CO_2.

The intension with the project reporting for each structure is to provide a knowledge-based maturation with improved database and solid basic descriptions to improve the understanding of the formation, composition, and geometry of the structure. It includes a description overview and mapping of the reservoir and seal formations, the largest faults, the lowermost closure (spill-point) and structural top point of the reservoir, estimations of the overall closure area and gross-rock volume. In addition, the database will be updated, where needed with rescanning of some of the old seismic data, and acquisition of new seismic data in a grid over the structures, except for the Inez and Lisa structures, which have sufficient seismic data for this initial maturation.

The reports will provide an updated overview of the database, geology, and seismic interpretation for all with interests in the structures and will become public available. Each reporting is a first step toward geological maturation and site characterization of the structures. A full technical evaluation of the structures to cover all site characterization aspects related to CO_2 storage including risk assessment is recommended for the further process.

Content

Dansk sammendrag

Regeringen og et bredt flertal i Folketinget vedtog i juni 2021 en køreplan for lagring af CO_2, der inkluderer undersøgelser af potentielle lagringslokaliteter i den danske undergrund. Der er derfor udvalgt fire store strukturer på land med dataindsamling og kortlægning til videre modning: Havnsø, Gassum, Rødby og Thorning, samt den mindre Stenlille struktur til demonstrationslagring (Fig. 1.1–1.4). Derudover indsamles nye data til kortlægning og modning for den kystnære Jammerbugt struktur, mens de to Inez og Lisa strukturer, længere mod vest i Nordsøen, kortlægges og modnes med eksisterende data.

Stenlille strukturen er den mindste af de strukturer, der undersøges i projektet, men er til gengæld den struktur med den mest omfattende database og med erfaringer fra mere end 30 års sikker geologisk lagring af naturgas. Stenlille strukturen i Sorø Kommune kan blive det første lagringssted på land i Danmark i form af et demonstrationsanlæg for geologisk lagring af CO_2.

Dette sammendrag opsummerer kort forundersøgelsen og den initiale vurdering af lagringsmuligheden i Stenlille strukturen. Vurderingen bygger på tolkning af eksisterende samt nye geologiske og geofysiske data og viden (Kapitel 3−4), og belyser geologien i og omkring Stenlille strukturen (Kapitel 5–7). I et område af strukturens nordøst flanke med mindre datadækning, lige nordøst for det 3D seismiske survey område, er der i 2022 indsamlet 5 nye 2D seismiske profiler, der også indgår i vurderingen. Vurderingen har fokus på strukturens form, størrelse, overordnede opdeling inklusive reservoir- og seglforhold, geologiske risikofaktorer, især større forkastninger og segl, og der foretages en volumenvurdering for det primære reservoir (Kapitel 5, 8). Desuden opsummeres anbefalinger (Kapitel 9, 10) til yderligere modning af strukturen hen imod en mulig CO_2 lagring.

Datagrundlag

Stenlille strukturen er dækket af et net af refleksionsseismiske data (Fig. 4.1.1) med 2D profiler af varierende tæthed og kvalitet indsamlet i 1960'erne, 1970'erne, 1980'erne, 1990'erne og i 2022, samt et 3D seismisk datasæt fra 1997 af den bedste kvalitet, men de nyere 2D datasæt fra 1980'erne og frem har dog også en god kvalitet. Derudover er der logs og geologiske data og rapporter fra 20 boringer (den første fra 1980), hvoraf de fleste har gennemboret den primære reservoir-holdige formation (Fm): Gassum Fm, og kun én boring er væsentlig dybere (Stenlille-19 med TD i Bunter Sandsten Fm) (Kapitel 4).

Der blev i februar 2022 indsamlet fem nye 2D refleksionsseismiske profiler (i alt c. 13 km) ved hjælp af 2 vibrator trucks (kilde), tilkoblet en land-streamer med geofoner, samt trådløse geofoner i vejsiden. Disse data har forbedret datadækningen og tolkningsmulighederne over den nordøstlige flanke af strukturen. Dette blev også gennemført som en test af det seismiske udstyr og indsamlingslayout til senere indsamling over andre strukturer i projektet (Fig. 4.2.1–4.2.7). Uppsala Universitet gennemførte indsamlingen og processeringen på vegne af GEUS, med seismiske kilder (2 vibrator-lastbiler) fra polske Geopartner Sp. zo.o og med feltassistance fra universitetsstuderende fra Københavns- og Uppsala universiteter. COWI varetog ansøgninger om tilladelser, og sammen med Gas Storage Denmark A/S logistik, kommunikation og borgerkontakt. Der blev forud for indsamlingen informeret på et borgermøde hos Gas Storage Denmark A/S (GSD), via webside information hhv. af GEUS og GSD, via informationsbreve og flyers, samt på to besøgsdage under indsamlingen.

Tolkning

Stenlille strukturen er en geologisk 4-vejs lukning med forkastninger, som er dannet fra Jura til Tidlig Kridt tid over en dyb salt pude med Zechstein salt (Fig. 1.4, 3.4, 6.2.2). De primære reservoir-segl-par i *Stenlille strukturens geologiske lagringskompleks* er vist i Figur 1.4: Det primære reservoir-segl-par er Gassum−Fjerritslev formationerne; De to dybere, sekundære reservoir-segl-par er hhv. Intra Oddesund sandstone beds med overliggende mudderstens-segl (Oddesund Formation), og Bunter Sandstone Formation med overliggende mudder-stenssegl (Ørslev Fm) – se også den generelle lithostratigrafi for det Danske Bassin i Figur 3.3.

Strukturen lukker på flere stratigrafiske niveauer fra Trias til Jura. Særligt vigtigt er lukningen på toppen af Gassum Formation (Sen Trias alder) med det primære reservoir, som har fokus i denne vurdering (Kapitel 6). Formationen er opdelt i 6 zoner (Zone 1–6), som indeholder reservoir sandsten af forskellig tykkelse med de tykkeste sandsten i de to nederste zoner (5 og 6). Reservoir zonerne indeholder primært sandsten men lersten og siltsten indgår i zonerne med varierende tykkelse.

Gassum Fm er c. 140–160 meter tyk baseret både på boringer og seismisk kortlægning og den består primært af sandsten med lerstenslag. Formationen har varierende reservoir-egenskaber, som er beregnet både fra logs og fra kerne målinger med gennemsnit beregnet fra begge datasæt nedenfor (se også Afsnit 7.1). De to nederste og tykkeste reservoir zoner (5 og 6) har de bedste reservoir egenskaber med henholdsvis op til c. 25 % og c. 27 % porøsitet i gennemsnit, samt en gennemsnitlig permeabilitet på henholdsvis c. 300 mD og 4000 mD. De øverste reservoirzoner (1, 2b, 3, 4) har gode, men dog lidt mere moderate reservoir egenskaber end de nederste zoner, med et summeret gennemsnit på c. 23% porøsitet og en gennemsnitlig permeabilitet på op til c. 170 mD. Selvom reservoir Zone 3 er relativt tynd sammenlignet med Zone 5 and 6, så har den reservoir parametre, der er sammenlignelige med disse to zoner, med en gennemsnits porøsitet på c. 25% og permeabilitet på c. 350 mD. Net til Gross for Gassum Fm-sandsten er i gennemsnit for f.eks. ST-19 boringen c. 0,76 totalt for alle seks reservoir sand zoner, samt c. 0,67 for de øverste fire zoner, samt c. 0,78 og c. 1 for hhv. Zone 5 og 6. Reservoir zonerne 1–3 og 5 bruges til lagring af naturgas (Fig. 1.3).

De nye data med ny kortlægning bekræfter, at Stenlille strukturen lukker på top reservoir niveau ved Top Gassum Fm og ved toppen af de sekundære reservoirholdige formationer i Oddesund Fm (Intra Oddesund sst. beds) og Bunter Sandstone Fm (Fig. 6.2.3). Lukningens størrelse på Top Gassum dybde-struktur kortet (Fig. 6.2.3C, 8.1.1) er c. 5,4 km^2 ved den lukkende kontur på c. 1475 m dybde under havniveau (below mean sea level - b.msl). Toppen af strukturen ved Top Gassum Fm er c. 1449 m (b.msl) og højden (relief) af strukturen fra spill-point er derfor kun c. 26 m. Arealet af den lukkende kontur er større på tids-struktur kortet (Fig. 6.2.2D) end på dybde-struktur kortet i meter (Fig. 6.2.3C). Forskellen skyldes primært effekten af dybdekonvertering af kort fra to-vejs tid til dybde i meter, og især på grund af tykkelsesvariationen af den overliggende Chalk Group (se Kapitel 5 og Appendix A).

Beregningerne i denne undersøgelse viser en begrænset potentiel lagringskapacitet (storage capacity) af CO_2 i Gassum Formationen i Stenlille strukturen. Lagringskapaciteten er her estimeret for fire forskellige scenarier ud af mange mulige og inkluderer 4-vejs lukning (spill-punkt) samt et konceptuelt flankescenarie, og begge er beregnet for henholdsvis reservoir Zone 1–4 og Zone 5. Den gennemsnitlige (mean) lagringskapacitet i Gassum Formationen for Stenlille strukturen er for 4-vejs lukningen af strukturen estimeret til: 2,4 megaton (MT)

CO_2 i Zone 1–4 og 2,7 MT CO_2 i Zone 5. De konceptuelle flankescenarie er i størrelsesordenen: 6,2 MT CO_2 i Zone 1–4 og 8,0 MT CO_2 i Zone 5.

Da scenarierne er forskellige, bør tallene ikke summeres. Det er dog muligt at et par af scenarierne kunne kombineres afhængig af nærmere undersøgelser. Lagringskapaciteten i Gassum Formationen (Zone 1–5) for Stenlille strukturen kan være i størrelsesordenen c. 6–10 MT CO_2. Lagringskapaciteten og de mulige lagringsscenarier bør dog undersøges nærmere, f.eks. med mere konkrete data (herunder placering af injektionsboringer) og reservoir simuleringsmodeller. Der kan desuden være lagringspotentiale af CO_2 i nedre sandsten i Gassum Formationen (Zone 6), samt i dybereliggende sandsten i Oddesund og Bunter Sandstone formationerne, men dette er ikke undersøgt her. Se Kapitel 5 og 8 for flere detaljer om lagringskapacitet. Sandsten i Oddesund og Bunter Sandstone formationerne er i Stenlille området kun dokumenteret i én dyb boring (ST-19), og der må derfor forventes variationer igennem området og måske også flere sandstenslag dybere i Bunter Sandstone Fm end påvist med boringen.

Det primære segl for Gassum Fm er Fjerritslev Fm, som er en flere hundrede meter tyk succession af lersten af seneste Trias til Tidlig Jura alder. Den nederste del af formationen (F-Ia Mb) indeholder nogle tynde lag af silt- og sandsten, som kan gøre denne del lidt ringere som segl, mens den øverste og tykkeste del (F-Ib til F-IV Mb) vurderes at have de bedste seglegenskaber. Over Fjerritslev Fm ligger sekundære segl med lersten fra Vedsted Fm, mergel og kalk fra Rødby Fm (begge Nedre Kridt) og derover en kilometer-tyk enhed (Chalk Group) med skrivekridt og kalk fra Øvre Kridt til tidlig Paleocæn (Danien) tid samt tyndere Paleocæne mergel- og lerlag. Øverst er der lag af Kvartær alder. Sikker naturgas lagring i Gassum Formationen gennem mere end 30 år i Stenlille strukturen har vist, at seglene er effektive.

Der er identificeret en række især SV–NØ strygende forkastninger (samt færre S–N), med mindre forsætninger af Gassum Fm og Fjerritslev Fm i toppen af strukturen, og med større forsætninger i den østlige til sydlige del af strukturen. Langt de fleste forkastninger ser ud til at stoppe nær toppen af Fjerritslev Fm eller i Nedre Kridt. Der er også observeret mindre forkastninger med primært tre retninger (SV–NØ; VNV–ØNØ; SØ–NV) et stykke oppe i Chalk Group.

Den vestlige til nordvestlige del af strukturen synes mindre påvirket af forkastninger i Gassum og Fjerritslev Formationerne end de mere centrale til østlige dele af strukturen. Det er ældre, inaktive forkastninger og der er ikke i området registreret jordskælv.

Eventuel CO_2 injektion bør ske væk fra større forkastninger og derfor ikke i den østlige til sydlige del af strukturen. Ligeledes er der et område nær et saddelpunkt og den nederste lukkende kontur på Top Gassum kortet (Fig. 6.2.3C) i den sydlige del af strukturen ved Stenlille-4 boringen og et saddelpunkt i den nordøstligste del, der skal undgås (Afsnit 8.2).

Nye 2D seismiske data er blevet indsamlet over den nordøstlige flanke af Stenlille strukturen og har forbedret datagrundlaget med større linjedækning og tolkningsmulighederne af bl.a. strukturens størrelse, lukning på top reservoir niveau, volumen, detaljer i reservoir- og segl enheder, samt forkastninger til denne initiale modning af Stenlille strukturen.

Der anbefales indsamling af nye 3D seismiske data over områder, der vurderes egnede til injektion og CO_2 lagring. Dette ville kunne øge den foreliggende viden om reservoir, segl og forkastninger, og forbedre mulighederne for modellering af CO_2 migration, risiko analyser og detail planlægning før injektion (Kapitel 10).

Under en eventuel injektion kan gentagne indsamlinger af seismiske data de samme steder, sammen med anden monitering og målinger (f.eks. via forskellige målinger i observations-boringer og i overfladeære lag, seismometre, satellit, osv.), desuden bidrage væsentligt til monitering af CO_2 udbredelse.

Viden fra forundersøgelsen af Stenlille strukturen vil indgå i myndighedernes videre arbejde med at afdække muligheder og behov, samt eventuelle krav til flere data og undersøgelser for yderligere modning af et potentielt lager. Det besluttes på politisk niveau, hvorledes og hvor der skal udbydes og etableres et CO_2-lager.

1. Summary

The subsurface in Denmark has a large number of deep structures offshore and onshore, and some of these are suited for CO_2 storage and some are located near emission sources (Fig. 1.1). The named structures are selected for initial investigation and maturation through seismic acquisition, geological analyses, and mapping from 2022 to 2024 by GEUS, and with cooperating partners on acquisition and processing (see database chapter below).

This report provides basic descriptions of the Stenlille structure (Fig. 1.1–1.4) based on a comprehensive database to improve the understanding of the formation, composition, and geometry of the structure. It includes a description overview and mapping of the reservoir and seal formations, the largest faults, the lowermost closure (spill-point) and top point at the top of the reservoir, estimations of the overall closure area, gross-rock volume and potential storage capacity. In addition, the database is updated with acquisition of new seismic data over the NE part of the structure to improve mapping of this part.

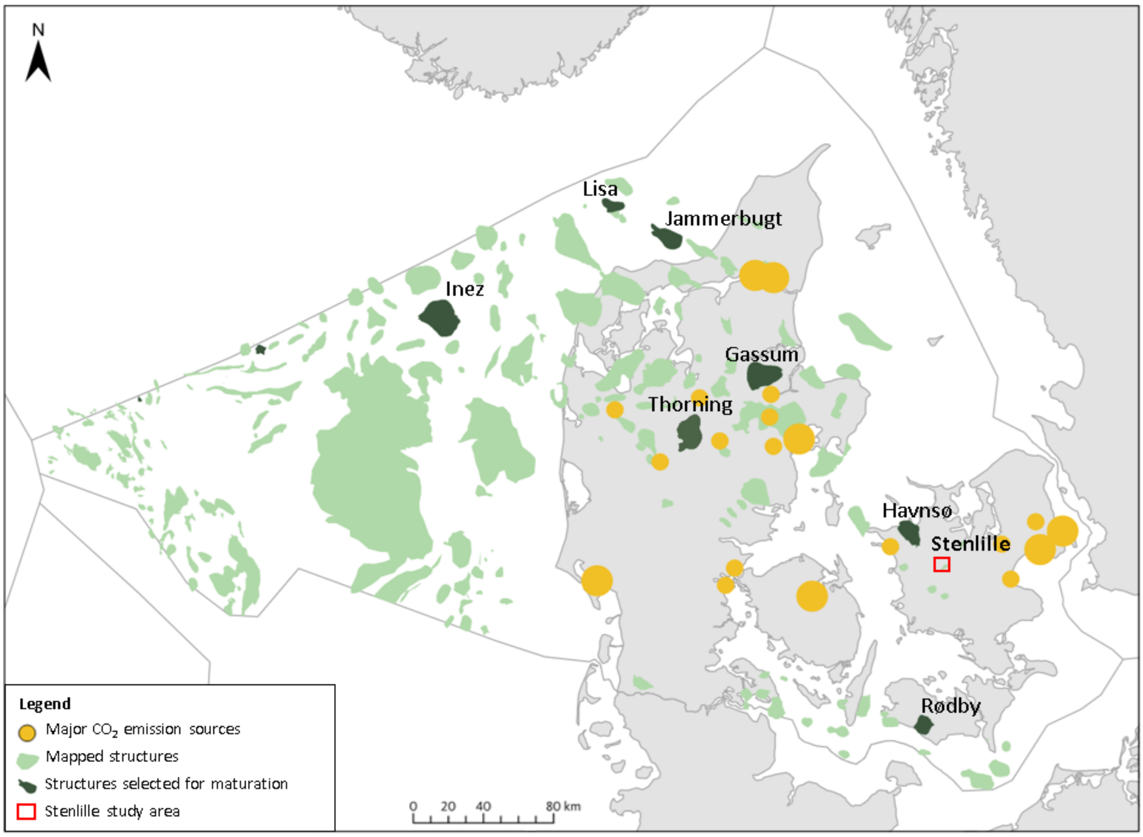

Figure 1.1. *Map of Danish structures with potential for geological storage of CO_2. The named structures (Stenlille, Havnsø, Rødby, Gassum, Thorning, Jammerbugt, Lisa and Inez) are currently investigated with new data and updated mapping in GEUS' CCS project during 2022–2024. The study area of the Stenlille structure in Zealand is marked with a small red square. From Hjelm et al. (2022).*

The Stenlille structure is a geological 4-way dip structure with faults probably formed during mainly late Early to Late Jurassic time over a deep salt pillow with Zechstein salt (Fig. 1.4, 3.4). The main reservoir-seal couples of the *Stenlille geological storage complex* are shown in Figure 1.4. The primary reservoir-seal couple is the Gassum−Fjerritslev Formations. The secondary reservoir-seal couples are the Intra Oddesund sandstone beds with overlying seal mudstones (Oddesund Formation), and the Bunter Sandstone Formation with overlying seal mudstones (Ørslev Fm) – see also the general lithostratigraphy of the Danish Basin in Figure 3.3.

The structure has closing contours at several stratigraphic levels in the Triassic to Jurassic successions. Of particular importance is the structural closure at the top of the Gassum Formation (Fm) level (Late Triassic age) (Fig. 1.2), which contains the primary reservoir sandstones and is the main focus for this study. It is overlain by the primary seal of the several hundred-meter-thick Fjerritslev Formation of latest Triassic to Early Jurassic age.

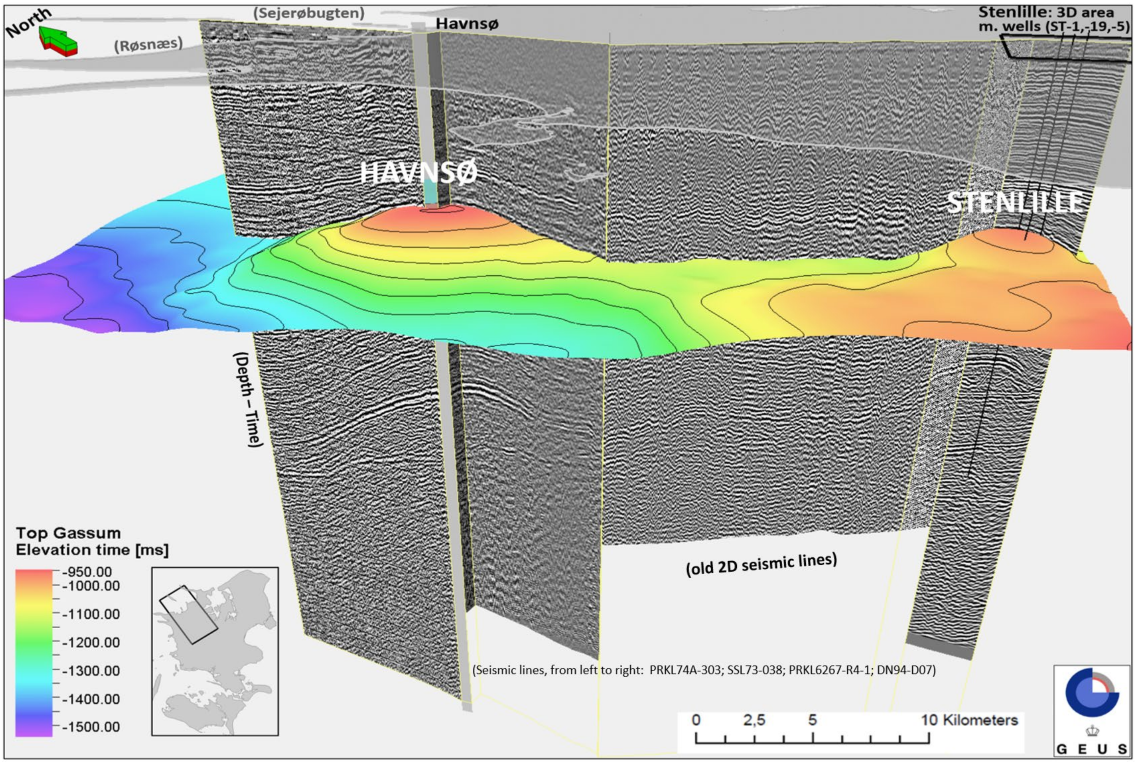

Figure 1.2. *Simplified map of the Top Gassum surface in time (ms TWT) with seismic sections (PRKL74A-303; SSL73-038; PRKL6267-R4-1_part1&2; DN94-D07), showing the Stenlille and the Havnsø structures and the mapped connection with their common saddle-point (near spill-point). The Havnsø structure is much larger and has a slightly shallower top than the Stenlille structure.*

The Gassum Formation is c. 140−160 m thick with large lateral continuity based on the Stenlille wells and the seismic mapping (Section 6.2) and it consists primary of sandstones with interbedded claystones. The Gassum Formation is divided into 6 reservoir zones (Zone 1–6; Fig. 1.3) with various thicknesses, variable reservoir properties and variable content of mudstones and siltstones. The quality of the reservoir zones is calculated from both logs and measured in cores (see Section 7.1).

The two lowermost and thickest reservoir zones (5 and 6) have the best reservoir properties, with up to c. 25 % and c. 27 % porosity in average, respectively, and a permeability up to c. 300 mD and 4000 mD in average, respectively. The uppermost reservoir sandstone zones (1, 2b, 3 and 4) have good, but slightly more moderate reservoir properties with a summarized average of c. 23 % porosity and an average permeability up to c. 170 mD. Although Reservoir Zone 3 is relatively thin compared to Zones 5 and 6, it has specific reservoir properties comparable to the lowermost zones, with average porosities of 25% and a permeability of 350 mD. The Net to Gross ratio of the Gassum Fm sandstones in e.g., the ST-19 well is for these six zones in average 0.76 in total, and 0.67 for Zones 1–4 sand (0.93 for Zone 3), 0.78 for Zone 5, and 1 for Zone 6 sand. The reservoir zones 1–3 and 5 are utilized for storage of natural gas (Fig. 1.3).

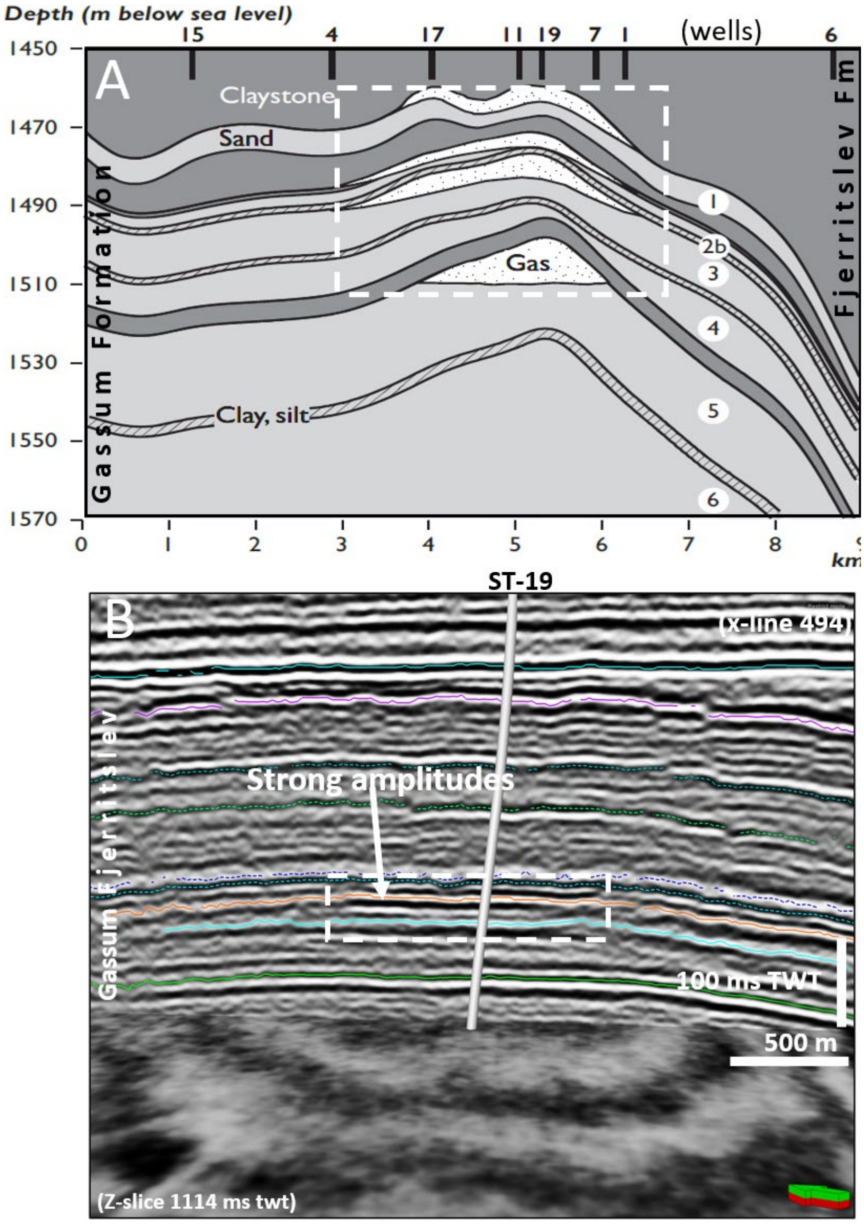

Figure 1.3. *The Gassum Fm–Fjerritslev Fm reservoir–seal couple of the Stenlille structure. A: Geological model the structure with reservoir zones (Zone 1–6) in the Gassum Fm, where natural gas is stored and used for consumers. Safe storage has been carried out for more than 30 years (since 1989). Dashed white rectangle approximately in a similar position as in the figure below, although they are different e.g., in scale and depth versus time. Modified from Laier & Øbro (2009). B: 3D seismic data (1997) near the Stenlille-19 well with strong, bright amplitudes in the upper part of the Gassum Fm probably reflecting the gas filled sandstones, as illustrated in the model above within the dashed white rectangle. Notice vertical exaggeration.*

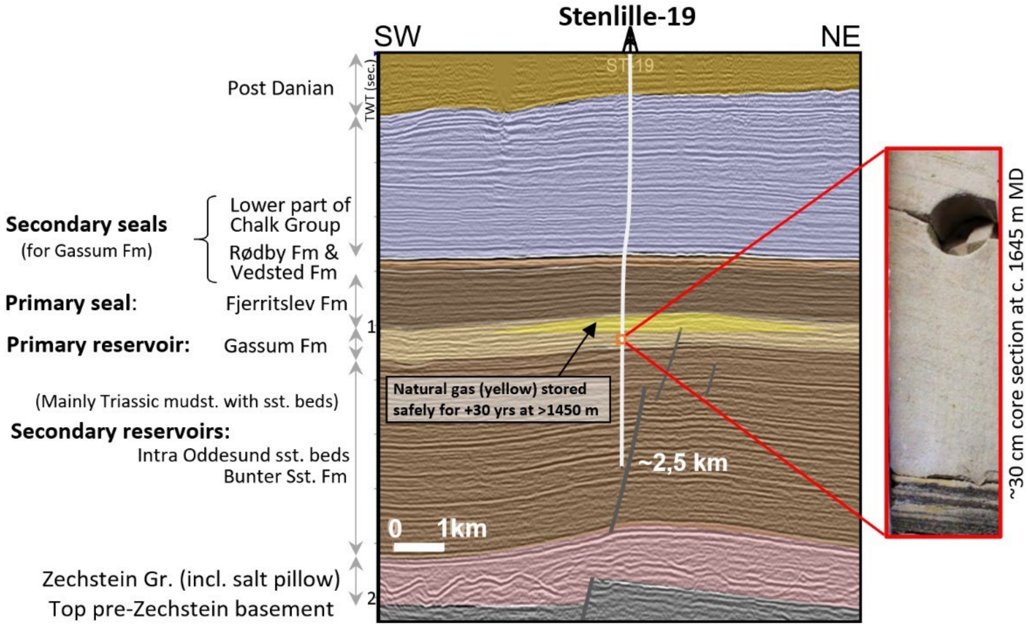

Figure 1.4. *The Stenlille geological storage complex. Interpretation of a SW–NE seismic profile (DN94_D01) through the Stenlille structure with the Stenlille-19 well to illustrate the overall geological formations with reservoir and seals. See Fig. 6.1.1 for more detailed lithostratigraphy, seismic stratigraphy and well-tie. A small core section at c. 1645 m MD with cross-bedded sandstones overlaying coaly debris in a fluvio-estuarine complex of the Gassum Fm is also shown from Hovikoski & Pedersen (2020). The Stenlille structure geological storage complex consists of: The primary reservoir–seal couple of the Gassum Fm–Fjerritslev Fm and its overlying secondary seal successions of the Vedsted Fm, Rødby Fm and Chalk Group. The deeper Triassic secondary reservoir–seal couples with potential reservoirs include the Bunter Sst. Fm and the Intra Oddesund sandstone (sst.) beds, and their respectively interbedded and overlying mudstone dominated seals. The larger structural and stratigraphic context are outlined in Fig. 3.1–3.4.*

The new data and mapping confirm that the Stenlille structure has closures at the Top Gassum Fm and also at the top of the deeper secondary reservoirs of the Intra Oddesund sandstone beds (Oddesund Fm) and the Bunter Sandstone Fm (Fig. 6.2.3). The area of lowermost closure on the Top Gassum depth-structure map is 5.4 km^2 at the closing contour of c. 1475 m depth b.msl (Fig. 6.2.3C, 8.1.1). The top of the structure at the Top Gassum map is at c. 1449 m (b.msl), and the relief of the structure at Top Gassum is thus c. 26 m. The closure is larger on the time-depth map (Fig. 6.2.2D), and the difference is mainly due to the effect of thickness variations of the overlying Chalk Group on the time-to-depth conversion (Fig. 6.2.4A, Appendix A).

The calculations in this study show a limited storage capacity of the Gassum Formation. The storage capacity of the Gassum Formation is estimated for four out of several possible scenarios, here including the 4way closure and a conceptual Flank scenario for reservoir Zone 1–4 and Zone 5, respectively. The mean storage capacities of CO_2 in the Gassum Formation of the Stenlille structure are estimated respectively for each of the scenarios and are within the 4way closure: 2.4 MT CO_2 of Zone 1–4 and 2.7 MT CO_2 of Zone 5. The possible Flank scenarios may be in the order of 6.2 MT CO_2 of Zone 1–4 and 8.0 MT CO_2 of Zone 5. As the scenarios are different, the values may not be summarized. However, possibly two of the scenarios may be combined. Possible mean storage capacity estimates for the Gassum Formation in the Stenlille structure, may be in the order of c. 6–10 MT CO_2. However, the capacity and possible scenario combinations must be investigated further by more site-specific assessments and reservoirs simulation modelling. There may also be potential for CO_2

storage in the lower reservoir sandstones of the Gassum Formation (Zone 6), and deeper in sandstones of the Oddesund and Bunter Sandstone Formations, but their storage capacities have not been investigated here. Sandstone-dominated units in the Oddesund Formation and Bunter Sandstone Formations are only documented in one well (ST-19) and variations of thicknesses and reservoir properties are expected across the structure. See Chapters 5, 7 and 8 for more details on the reservoirs.

The primary seal for the Gassum Fm is the Fjerritslev Fm, which is several hundred-meter-thick mudstone successions of a latest Triassic to Early Jurassic age, and it includes generally good to very good sealing mudstones. The lowermost part of the formation (F-Ia Mb) includes a number of thin siltstone and sandstone beds, which probably to some extent reduce the seal quality, whereas the upper and thickest part of the formation (F-Ib to F-IV Mb) is a good quality seal. Above this formation are the secondary seals, which in particular includes the Vedsted Fm mudstones and Rødby Fm marl and chalk of Early Cretaceous ages. Above these follows the km-thick Chalk Group, which is overlain by thinner Cenozoic to Quaternary deposits. Safe storage of natural gas through many years in the Gassum Fm has proven that the seals are efficient in the Stenlille structure. See also Section 7.2 for more details on the seals.

There are located a number of mainly SW–NE trending faults with less trending c. S–N at the Top Gassum (Fig. 6.2.3C). The faults have mainly minor throws of the Gassum Fm and the Fjerritslev Fm at the top of the structure. Towards east and south in the structure, there are more larger faults with more throws. By far the most faults seem to terminate near the Top Fjerritslev Fm or slightly above. There are also observed smaller faults with three main directions (SW– NE; WNW–ENE; SE– NW) further up within the Chalk Group. The west to north-western part of the structure seems less affected by faults in the Gassum and Fjerritslev Formations than the more central to south-eastern parts. Thus, possible CO_2 injection should be away from the larger faults and not in the south-eastern to southern part of the structure. The faults are old with mostly minor throws, and no earthquakes have been detected in the Stenlille area. An area close to the mapped saddle-point low and lowest contour at the Top Gassum map (Fig. 6.2.3C) in the southernmost part of the structure (near the ST-4 well), as well as the area with the saddle-point and lowest contour in the north-eastern part of the structure, should also be avoided.

New 2D seismic data has been acquired in the north-eastern part of the structure and has improved the database with more dense good quality seismic sections. This gives the opportunity for an improved interpretation of the size, spill-point, volume, details of reservoir- and seal successions, and faults of the Stenlille structure for this initial maturation.

New 3D seismic acquisition over the potential injection- and storage areas is recommended, for more detailed interpretation prior to CO_2 injection. This can improve site-specific knowledge with more details on reservoir, seal, and faults, and can improve modelling of CO_2 migration and risk analyses. Repeated 3D surveys in same place can contribute to monitor the extent of the CO_2 migration, together with other monitoring (e.g., via wells, seismometers, sampling, satellite, etc).

New necessary data acquisition and sampling, analyses and evaluations should be carried out for further maturation, including risk analyses, to cover geological and other technical uncertainties and risks. The knowledge from the investigated structures will be included in the further work of the authorities to reveal opportunities and requirements towards further maturation, site selection and licensing of geological CO_2 storage.

2. Introduction

Carbon capture and storage (CCS) is an important instrument for considerably lowering atmospheric CO_2 emissions (IPCC 2022). Geological storage of CO_2 is known from many countries, including Norway (Sleipner), Canada (Weyburn) and Germany (Ketzin), since the first started more than 25 years ago (e.g., Chadwick et al. 2004).

The Danish subsurface is highly suited for CO_2 storage, and screening studies document an enormous geological storage potential that is widely distributed below the country and adjacent sea areas (Larsen et al. 2003; Anthonsen et al. 2014; Hjelm et al. 2022; Mathiesen et al. 2022). The significant Danish storage potential is based on the favorable geology that includes excellent and regionally distributed reservoirs, tight seals, large structures, and a relatively quiescent tectonic environment. The largest storage potential is contained within saline aquifers and the Danish onshore and nearshore areas contain a number of these structures with a potentially significant CO_2 storage potential (Fig. 1.1; Hjelm et al. 2022). The Stenlille structure is one of these structures and is a relatively small structure geographically located in the central part of Zealand (Fig. 1.1), and geologically in the south-eastern part of the Danish Basin (Fig. 3.1). The structure is covered by a large database with 2D and 3D seismic data and 20 wells, mainly acquired to develop it for storage of natural gas to consumers, first by DONG and now by Gas Storage Denmark A/S (Energinet). The natural gas is stored in reservoir zones with sandstones interbedded by mudstones of the Gassum Formation below the thick sealing mudstones of the Fjerritslev Formation (Fig. 1.3). It is mainly this part of the structure, which is the focus of this study, but also deeper reservoir-seals of the structure are described.

Earlier screening projects by GEUS for structures relevant for CCS have also evaluated the Stenlille structure for potential CO_2 storage. The GESTCO project reported in 2003 (Larsen et al. 2003) that the Stenlille structure can be a relevant CO_2 storage site in the closed structure of the Gassum Formation (Fm) sealed by Fjerritslev Fm mudstones. The recent CCS related major project CCUS2020 was carried out by GEUS during 2020 and included comprehensive studies of particularly the Stenlille structure applying many analyses and methods, including: Sequence stratigraphic interpretation of seismic data and well-logs (Vosgerau et al. 2020; Gregersen et al. 2020); Quantitative seismic interpretation (Bredesen 2020); Sedimentology (Hovikoski & Pedersen 2020); Palynology (Lindström 2020); Reservoir data - Stenlille area (Kristensen 2020). In addition, the 2020 work also included other studies such as: Seal capacity and geochemical modelling (Springer et al. 2020); Reservoir characterisation and geochemical reactions between CO2 and reservoir rock (Holmslykke et al. 2020); Geophysical Methods to monitor injection and storage of CO_2 (Keiding 2021); Seismology (Larsen et al. 2020); Static reservoir models (Frykmann 2020), Provenance of the Gassum Fm (Olivarius et al. 2020); Potential chemical reaction of CO_2 leakage in water systems (Jakobsen 2020), and a comprehensive summary with an evaluation of the CO_2 storage potential in Denmark (Hjelm et al. 2022). GEUS reports of the CCUS2020 project are available from www.geus.dk web-site (link to the pdf files: CCUS-projekt 2020 (geus.dk)). Thus, there is a comprehensive knowledge available, which is improved with the present study with many new details and the updated database with new seismic profiles.

In this study, the Stenlille structure is investigated further based on evaluation of the well data and the existing and new seismic data to characterize its tectonic and depositional evolution, composition with reservoir-seal couples, faults and geometry towards maturation for potentially geological storage of CO_2.

3. Geological setting

The central to western Zealand area, including the Stenlille structure, is located in the eastern part of the Norwegian–Danish Basin (Vejbæk 1997), which is also termed the Danish Basin (Nielsen 2003). This Danish Basin trends WNW−ESE between the Ringkøbing–Fyn High and the North German Basin to the south and the Sorgenfrei–Tornquist Zone at the southern boundary of the Skagerrak–Kattegat Platform to the north (Fig. 3.1, 3.2).

The Danish Basin is an eastern part of the larger Norwegian–Danish Basin with connections to the North Sea region and an intracratonic structure formed since the Palaeozoic (Vejbæk 1997) as a major basin at the base of the Zechstein or top pre-Zechstein surface, as shown in Figure 3.2. The deep structures of the crystalline basement and the Cambrian to Lower Permian sedimentary successions constitute the base below the Danish Basin.

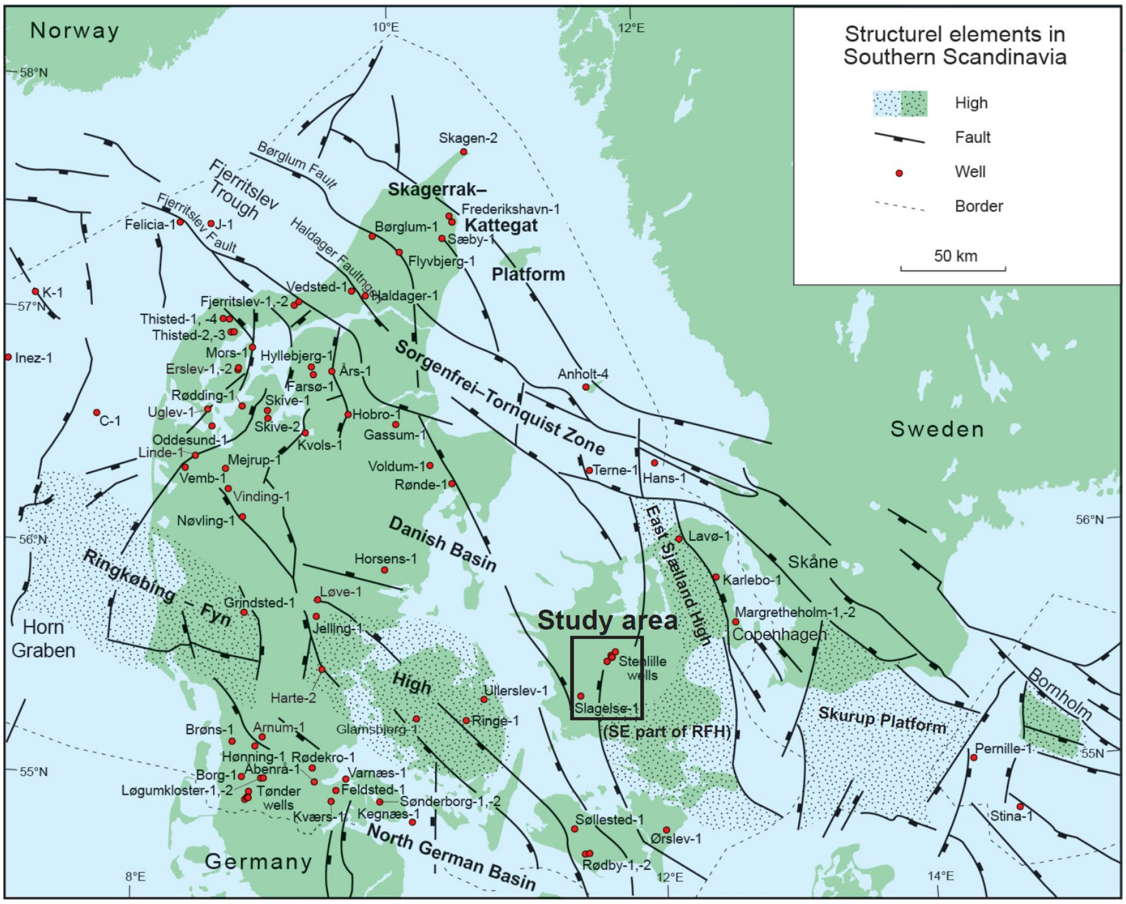

Figure 3.1. *Map of the main structural elements including highs, basins, and main faults onshore and offshore Denmark. The study area is within the black square. The elements include the Danish Basin, the Sorgenfrei–Tornquist Zone, the Skagerrak–Kattegat Platform, the Ringkøbing–Fyn High and the northern part of the North German Basin. Positions of deep wells are also marked. Modified from Nielsen (2003).*

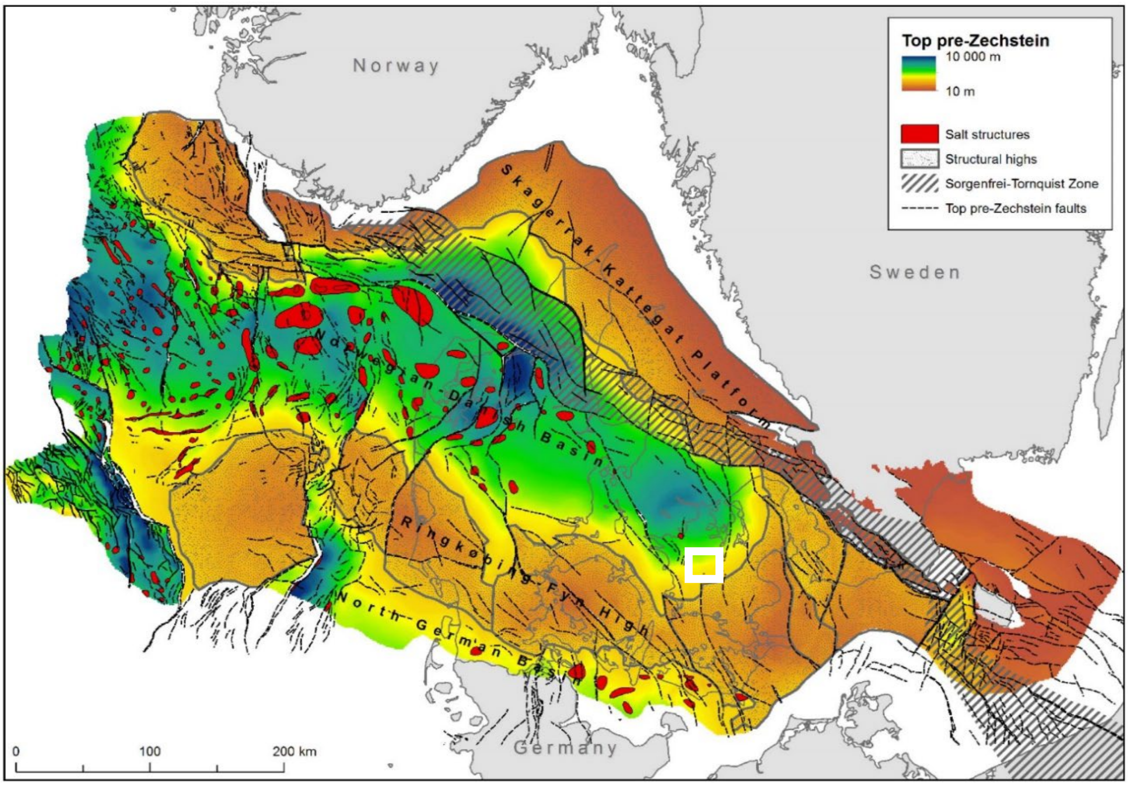

Figure 3.2. *Map of the main structural elements onshore and offshore Denmark, including highs, basins, and main faults. The location of the study area around Stenlille area is marked with a white square. The elements include the Norwegian–Danish Basin (of which the eastern part in Denmark is the Danish Basin), the Sorgenfrei–Tornquist Zone, the Skagerrak–Kattegat Platform, the Ringkøbing–Fyn High and the northern part of the North German Basin. Modified from Vejbæk & Britze (1984).*

Stretching of the lithosphere below the Danish–Norwegian Basin caused Carboniferous−Permian rifting with extension, normal faulting followed by basin subsidence, and the Ringkøbing–Fyn High probably formed at same time due to less stretch than basin areas (Vejbæk 1997). The tectonism led to large, rotated fault blocks, intrusive volcanism, extensive erosion, and mostly coarse siliciclastic deposition (Rotliegende) affecting large parts of the basin (Vejbæk 1997; Michelsen & Nielsen 1991, 1993; Nielsen 2003). After mainly evaporites (Zechstein Group) developed in shallow basin areas during late Permian time, the region subsided and thick Triassic clay and mud-dominated successions formed with a few sandstones (Bunter Shale, Bunter Sandstone, Ørslev, Falster, Tønder, Oddesund, Vinding Formations; Fig. 3.3, 3.4, 3.5A,B), and sandstones are in particular known from the Bunter Sandstone Formation (Bertelsen 1978, 1980). During the Late Triassic−Early Jurassic time, sand-rich continental–fluvial, coastal near and shallow marine sand-rich systems interbedded by more clay-rich intervals formed and now constitute the widely distributed Gassum Formation (Fig. 1.4, 3.4, 3.5C). During the latest Triassic (Rhaetian) and into the earliest Jurassic (Hettangian – early Sinemurian) times the coastal to continental areas were repeatedly overstepped by the sea (Fig. 3.6). The relative sea-level rise resulted in the deposition of thick clay-dominated successions with some silty and sandy layers (Fjerritslev Formation), which have been correlated basin wide in several depositional sequences and members (Nielsen 2003; Michelsen et al. 2003).

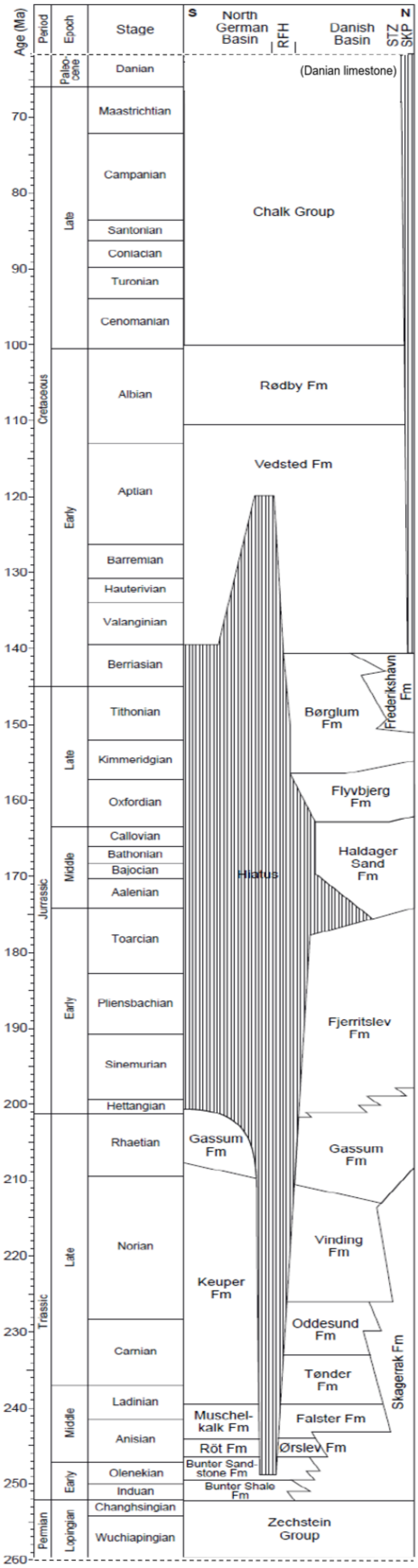

Figure 3.3. *Generalized stratigraphy in the Danish Basin from north to south, mostly representative of the Jutland part of the basin. The Stenlille area is located in the eastern part of the Danish Basin, just north of Ringkøbing-Fyn High (RFH), equivalent to the central figure part, without M-L Jurassic formations. Dashed horizontal lines at the top and base of the scheme indicate omitted Selandian + Quaternary and pre-Zechstein successions, respectively, due to space limitation. Based on Bertelsen (1980) and Nielsen (2003).*

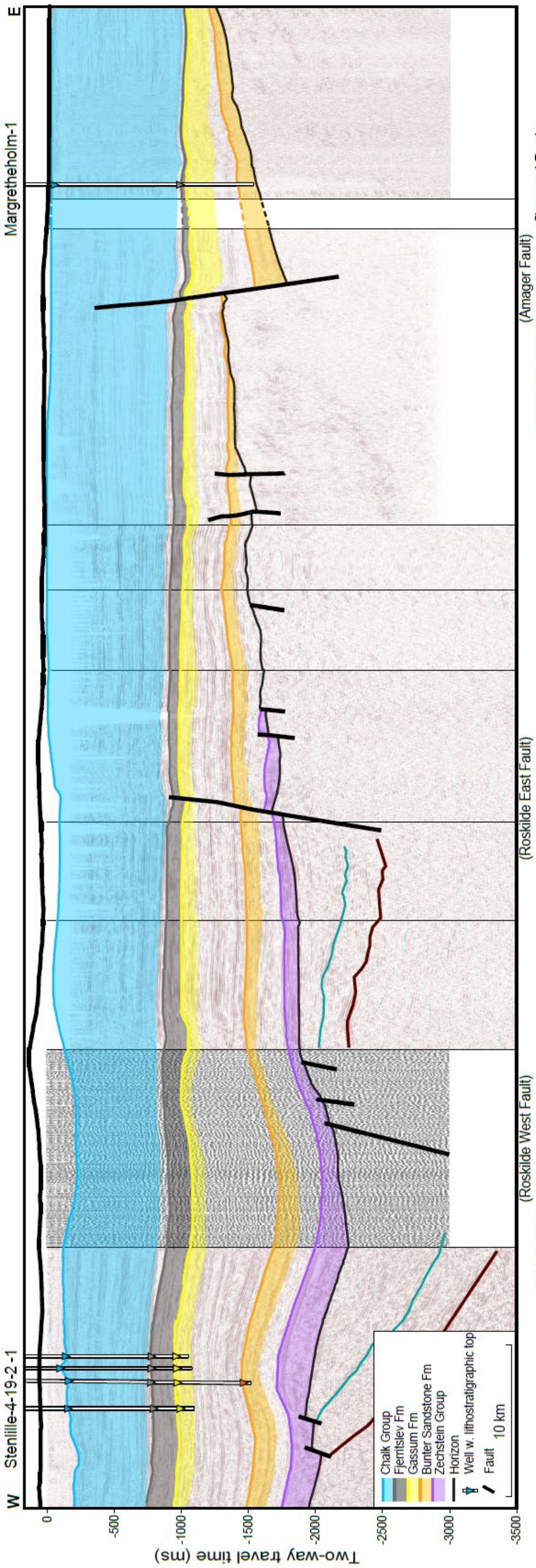

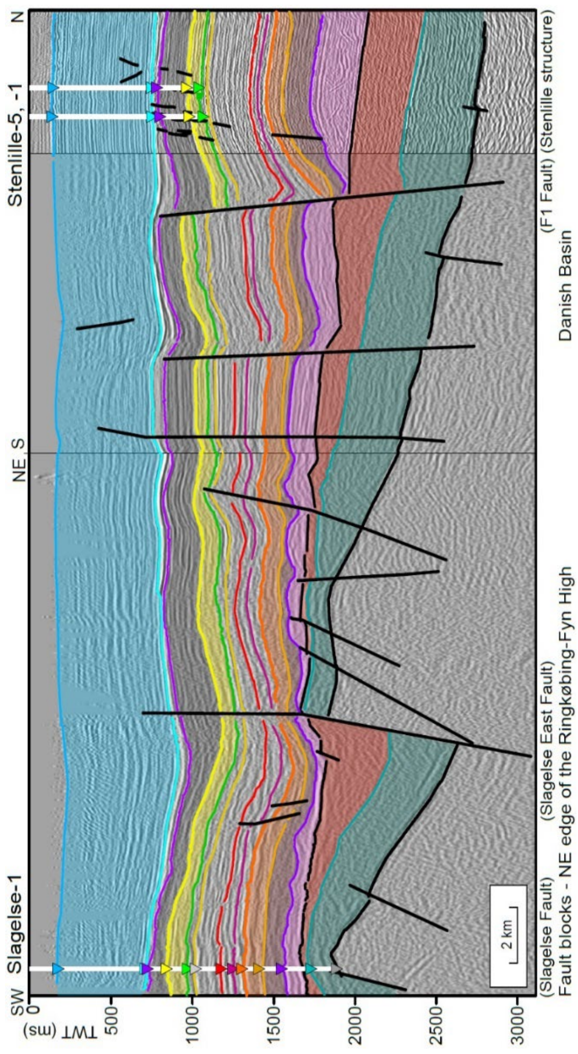

Figure 3.4. *Two regional profiles through the eastern Danish Basin and the Stenlille structure with interpreted stratigraphy: The upper blue unit indicates the Chalk Group and Danian. The Gassum (yellow unit) and Fjerritslev (dark-grey unit) Formations form the upper part of the Stenlille structure, which is formed by the deep Zechstein salt pillow (purple). Bunter Sandstone Formation is orange. Triangle positions mark lithostratigraphic well-top ties. All wells are projected onto the profiles. The upper W−E composite seismic profile from the Stenlille-1,-2,-4,-19 wells to the Margretheholm-1 well is modified from https://dybgeotermi.geus.dk/. The lower SW−NE−N composite seismic profile (lines: SSL72_001, SSL73_036 and DN94_D07) from the Slagelse-1 to the Stenlille-1,-5 wells is from Gregersen et al. (2022).*

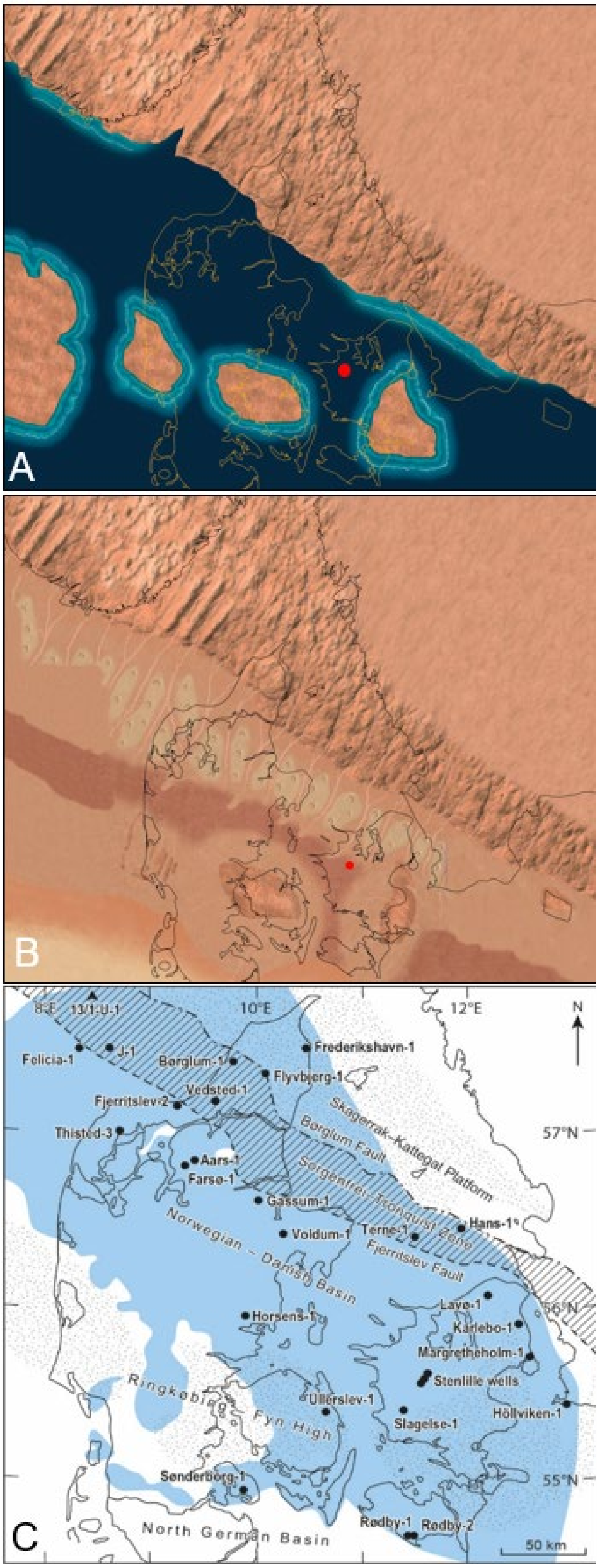

Figure 3.5. *Paleogeographic maps of Denmark and southern Scandinavia illustrating the possible distribution of general depositional environments.*

A. Late Permian (Zechstein) sea (dark blue), coastal near areas (light blue) and onshore areas (orange red). From Rasmussen & Nielsen (2020).

B. Early–Middle Triassic (incl. the Bunter Sandstone Fm) dominated by desert with local sand dunes, lakes and sabkhas. From Rasmussen & Nielsen (2020).

C. Late Triassic (Rhaetian) to earliest Jurassic (Hettangian – early Sinemurian) Gassum Fm distribution in Denmark. (Olivarius et al. 2022).

The study area is located at the Stenlille wells. This report (Section 7.1) and other work show, that the Gassum Fm is composed of several depositional sequences with regressions–transgression cycles and deposition in onshore, nearshore, and shallow marine environments.

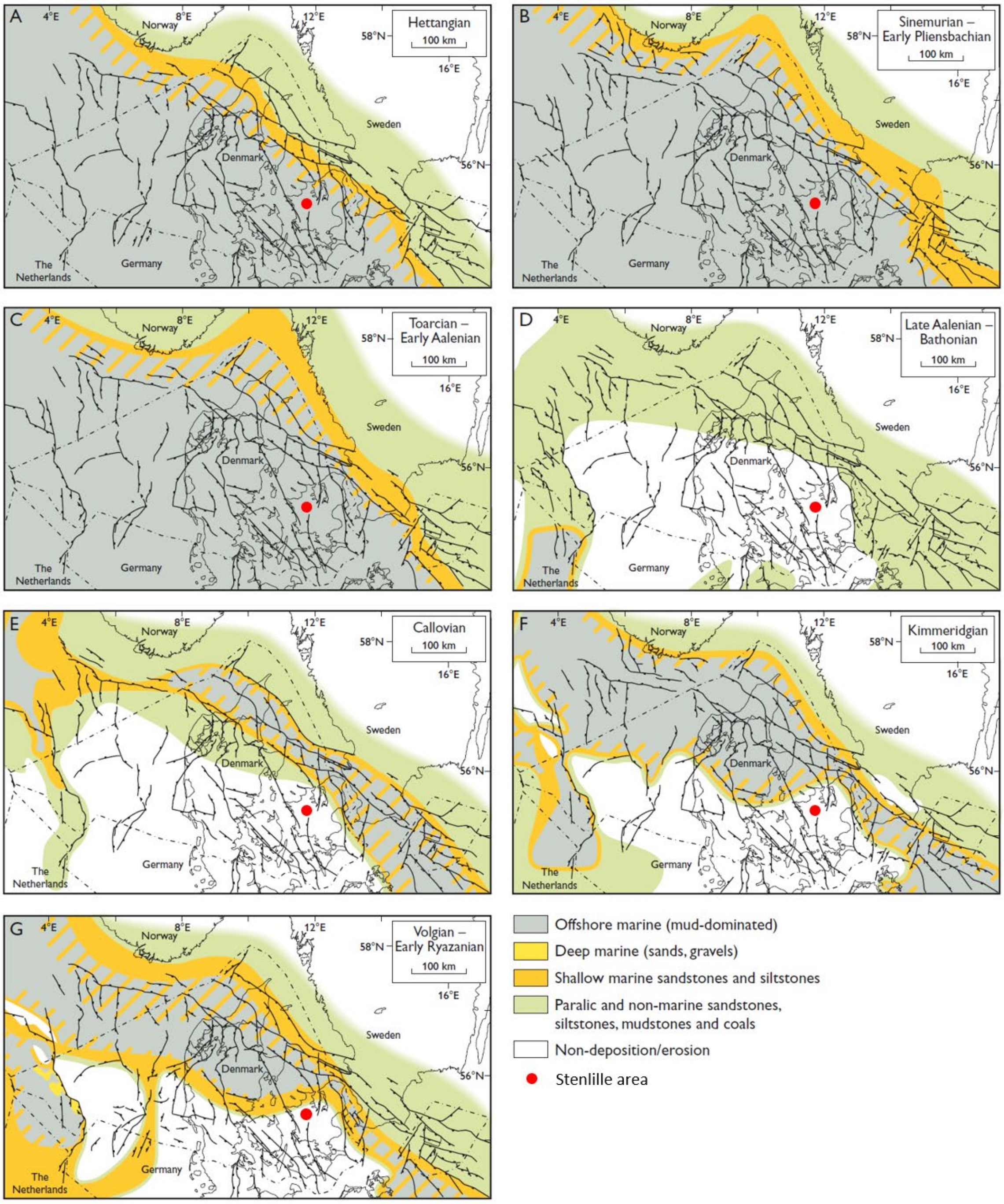

Figure 3.6. *Paleogeographic maps of Denmark showing the inferred distribution of general depositional environments during the Jurassic time, when the primary seal of the Fjerritslev Formation was deposited. The central to western Zealand, incl. the Stenlille area (red circle), is dominated by deposition of marine clays with some layers and beds of siltstone and sandstone, from Hettangian to Toarcian or Aalenian (A–C), whereas sedimentary successions are not shown (removed or not deposited?) during the Middle- and Late Jurassic times. From Petersen et al. (2008) modified from Michelsen et al. (2003).*

Mainly Middle−Late Jurassic regional uplift and salt mobilization led to formation of structures, associated faults, and major erosion in large parts of the eastern Danish Basin, with a hiatus expanding towards the Ringkøbing–Fyn High (Fig. 3.3) (Nielsen 2003). Renewed subsidence in the Early Cretaceous resulted in mudstones dominated successions with local sandstones, which became gradually more calcareous during the Albian (Rødby Formation). Chalk (Chalk Group) was formed throughout the Danish Basin in the Late Cretaceous, and structures were elevated due to regional inversion. Finally, Cenozoic incl. Quaternary successions were deposited in the Danish Basin, with episodic uplift (Japsen & Bidstrup 1999; Japsen 2007).

4. Database

4.1 Seismic data

The geophysical and geological database on the Stenlille structure is comprehensive and includes a 3D seismic survey (STENLILLE-97), 2D seismic lines at different angles across and outside the structure, and 20 wells with logs, cores and cuttings samples. This chapter will focus on the data used here for description and interpretation of the structure (Fig. 4.1.1).

The seismic database is diverse, with very good 3D seismic data, and 2D seismic data which ranges from good new and relatively recent data to old very poor data. The used seismic data are described below, and positions are shown in Figures 4.1.1,–2 and Table 4.1.1.

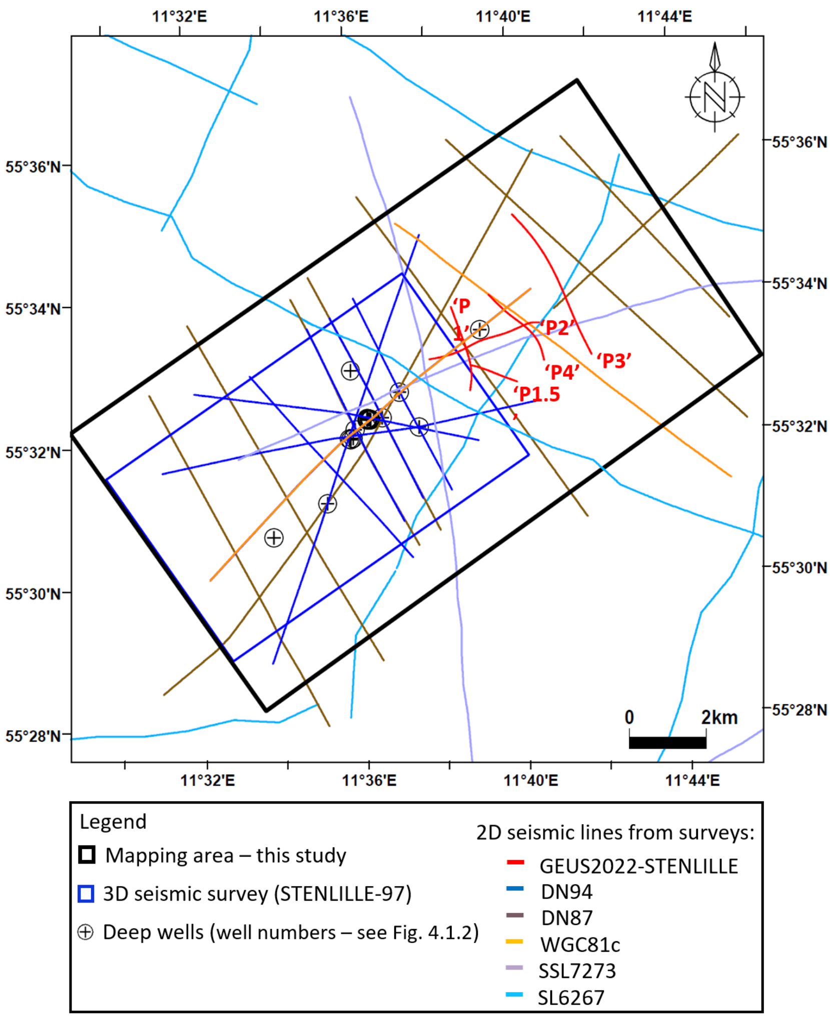

Figure 4.1.1. *Database at the Stenlille structure with positions of wells, the 3D seismic survey (STENLILLE-97) and 2D seismic lines, including the new GEUS2022-STENLILLE survey (red lines with abbreviated numbers), acquired in February 2022, See also positions of the new lines in Fig. 4.2.1.*

The 2D seismic survey GEUS2022-STENLILLE is a new survey acquired February 2022, organized by GEUS as part of the CCS maturation of this reporting and is acquired and processed by Uppsala University. The survey is located at the NE flank of the structure, near the NE boundary of the 3D seismic survey (Fig. 4.1.1). The purpose of the survey was to add quality data and coverage to this data poor part of the structure flank, where only few and old seismic lines exist, for a better definition of the structure geometry and closure, reservoir–seal successions, and faults. In addition, it was a test of equipment, settings and lay-out for possible further site investigations. Five seismic lines with a total of approximately 13 km were acquired (see more details in Section 4.2).

The 3D seismic survey STENLILLE-97 was carried out in 1997 by THOR Geophysikalische Prospektion GmbH on behalf of Dansk Olie og Naturgas A/S (DONG) and it covers totally 56.4 km^2 and was acquired as vibroseis with 1−3 vibrators conducting minimum 4 sweeps in 20 seconds with a frequency range of 10–120 Hz (THOR, 1997). The survey was processed by CGG, and the survey datum plane elevation is at the mean seal level, the data is in zero phase with reverse SEG polarity, the nominal bin size is 20 m x 20 m, and the nominal stacking fold is 16 (CGG 1998).

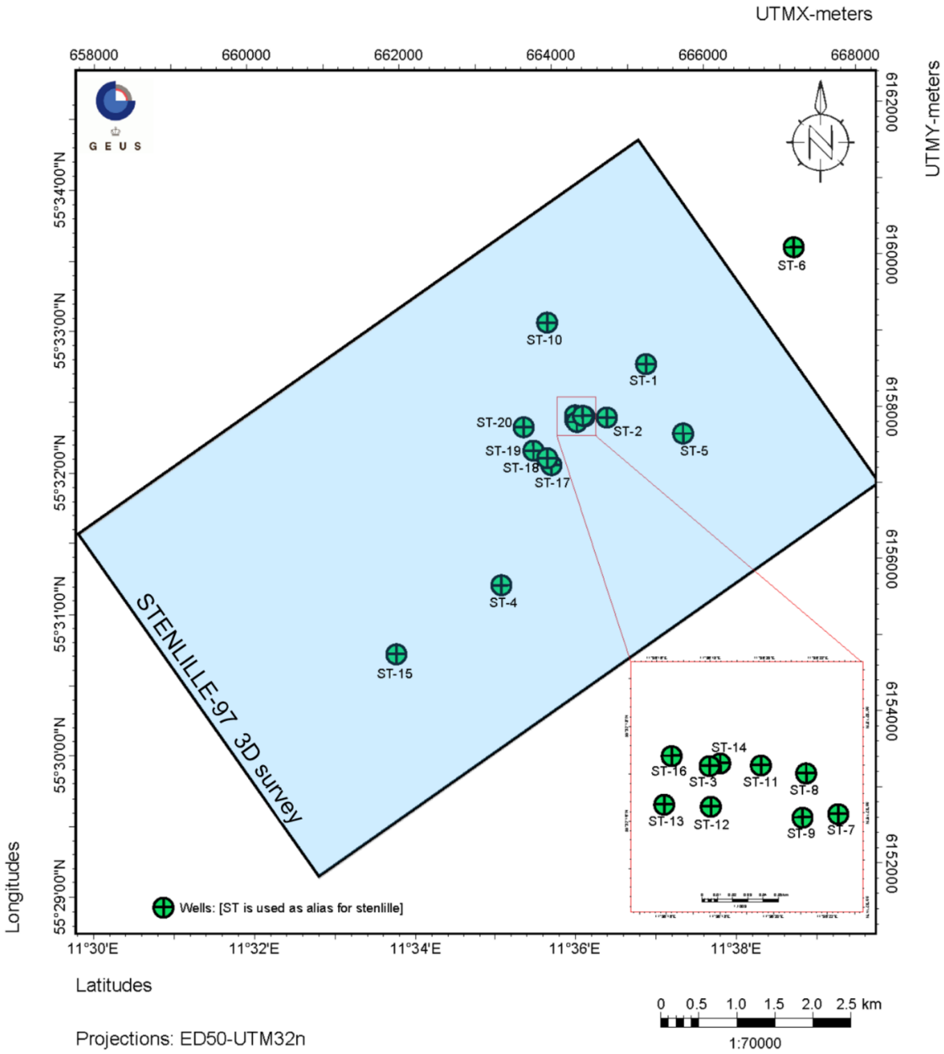

Figure 4.1.2. *Database at the Stenlille structure with positions of wells and the 3D seismic survey (STENLILLE-97). See Fig. 4.1.1 for position of seismic 2D lines and surveys.*

The 2D seismic survey DN94O was acquired in 1994 by Compagnie Générale de Géophysique (CGG) for Dansk Olie og Naturgas A/S (DONG). The eight survey lines are located across the Stenlille structure in the area of the later 3D survey and more details are available in the acquisition report.

The 2D seismic survey DN87 (DN87O and DN87I) was acquired in 1987 by Prakla-Seismos AG for Dansk Operatørselskab i.s. (Danop) and nine lines of the survey were used in the study area. The seismic lines are located across the Stenlille structure in the area of the later 3D survey with a few lines further to the SW and NE, and more details are available in the acquisition report.

The more recent vintage data (1987 to 1997) were acquired mainly to develop gas storage in the Stenlille structure. Older data were mainly acquired more regionally to map for structures relevant for petroleum exploration.

The 2D seismic survey WGC81 was carried out in 1981 by Western Geophysical Co. for DONG, and here only two of the lines were used, as some of the lines were approximately acquired again by better quality data of the DN94O survey.

The 2D seismic survey SSL7273 was carried out in 1972 and 1973 by Gulf Oil Co. Denmark for Dansk Undergrunds Consortium (DUC) and six lines were used, although mostly of poor quality.

The oldest seismic dataset is the 2D seismic survey SSL6267, which was acquired in 1962–67 by Gulf Oil Co. Denmark and Shell for DUC, and four lines were used in area where other lines are missing, although they mostly are of very poor quality (Table 4.1.1).

Seismic surveys, and acquisition and processing reports are available through GEUS (www.geus.dk), or by requests to the GEUS Subsurface Archive: info-data@geus.dk.

The quality of the seismic data is highly variable from very good to very poor (Table 4.1.1, Fig. 4.1.3, 4.1.4). Most of the oldest 2D seismic surveys from the 1960s and 1970s in the Stenlille area are generally very poor to poor in quality, whereas the more recent 2D and 3D seismic data are generally of good quality and are all digital data.

Table 4.1.1. *The seismic surveys and lines used in the mapped area at Stenlille and the data quality. STELILLE-97 is a 3D seismic survey, and all other datasets are from 2D seismic surveys.*

Seismic survey	Seismic lines	Data quality
GEUS22_STL (new)	P1, P1.5, P2, P3, P4	Good
STENLILLE-97 3D survey	all	Very Good
DN94	01, 02, 03, 04, 05, 06, 07, 08	Good
DN87	001, 003, 004, 005, 006, 007, 008, 009, 010	Good
SSL6267 (R-lines)	R4-37117, R9-37126, R9-1-37126, R13-37131	Very Poor
WGC81	8110, 8113	Moderate and Good
SSL7273	72-001, 73-025, -036, -037, -038, -039	Poor and moderate

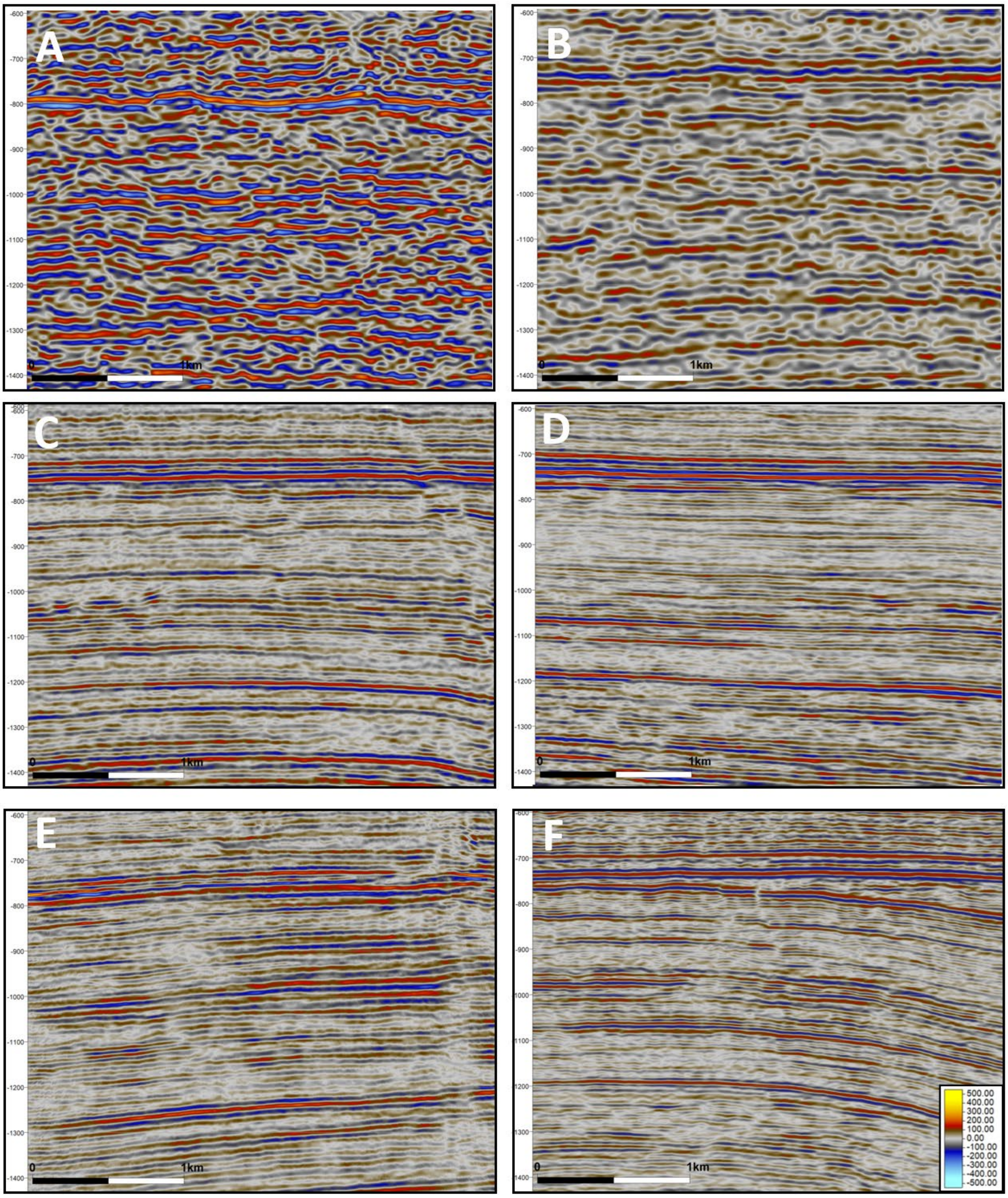

Figure 4.1.3. *Examples of seismic data quality (two-way time sections). A. Very poor data quality of 1960s data (SSL6267_R4). B. Poor to moderate quality of 1973s data (73-036). C. Good quality of the 1987 data (DN87-007), (D) 1994 data (DN94-D01), and (E) 2022 data ('P3'). F. Very good quality of the 1997 3D data (Xline495). All the surveys are represented in the study area (Fig. 3.1). All lines except the 3D Xline are time shifted.*

Seismic data mis-ties

The 2D seismic profiles in the study area (Fig. 4.1.1) have different datum elevations, mostly related to different static corrections, topography, etc. In this context and in relation to the data acquired, also the level of the water saturated zone (groundwater) plays a role and will be slightly different depending on the season of the year and wet or dry periods. The topography near Stenlille is variable, with ca. 30–45 m a. msl. NE of the 3D survey and ca. 40–60, and even 70 m a. msl. within the new 2D survey area.

In order to compensate for many differences in the datum elevation between seismic profiles, it was decided for mapping purpose in this project to conduct static (constant and non-data stretched) vertical time shifts of each 2D seismic profile in order to match it with the 3D seismic survey STENLILLE-97. The 3D survey is also used for tying the seismic data with wells using synthetic seismic data. The reported datum plane elevation of the 3D seismic survey STENLILLE-97 is the mean sea level, and the final data are with reverse SEG polarity convention (white trough representing an increase of acoustic impedance), in zero phase (CGG, 1998: Final report of seismic data processing. Survey: STENLILLE-97 3D survey).

Mis-ties were investigated visually and manually, and also digitally with the Petrel Survey Manager to constrain the time-shifts. The visual mis-tie screening and the Petrel mis-tie analysis show that there are data mis-ties between different seismic surveys, but also between lines of the same surveys in the order of mostly approx. 10−40 ms TWT, but up to as much as 80 ms TWT. Some of the mis-ties requires a dynamic shift (gradual time shifts stretching the data) on the same line to make a full fit at crossing seismic sections, and thus this is not straight forward, and dynamic shift is omitted here. In the Stenlille area this may be related to other factors including different parameters and different amounts of gas storage at the difference acquisition times, which affects the seismic signals differently. However, this has not been studied further in this project.

It was decided to conduct a manual time-shift for each seismic line and the used time-shifts are shown in Table 4.1.2 below, which also show the large differences in the datum elevation.

Table 4.1.2. *Seismic surveys and lines used in the mapped Stenlille area, with time-shift and data quality.*

Survey	Line and survey: Vertical time-shift (millisecond TWT) - to fit the Stenlille 3D survey
GEUS2022-STENLILLE	GEUS22_STL_P1, P1.5: 30ms; P2, P4: 56ms; P3: 68ms
STENLILLE-97 (3D)	0ms (datum plane elevation: mean seal level)
DN94O	01, 05: 10ms; 02, 03, 07: 14ms; 04, 06: 18ms; 08: 12ms
DN87O	001, 004, 007: 12ms; 003: 22ms; 005: 32ms; 006: 39ms; 008, 009: 35ms; 010: 40ms
SSL6267 (R-lines)	80ms
WGC81	8110: 55ms; 8113: 46ms
SSL7273	002: 70ms; 003A, 0033: 35ms; 007: 40ms; 034: 45ms; 037: 40ms; 72-001: 55ms; 73-025,-037,-038, 039: 40ms; 73-036: 45ms

First, the 2D seismic profile DN94_D01 is shifted 10 ms (up) to fit the 3D seismic survey close NE of ST-1 (at Trace 725 on DN94_D01), and next other 2D lines are shifted to fit the 3D survey and the DN94_D01 profile. Figure 4.1.4 shows an example, where the new line 'P2' is shifted 56 ms to fit the 3D survey. Mis-tie corrections for the surveys were not applied to the original files of the project database, as it was not possible within the frame of this study to sort out all mis-ties and adjust surveys properly but is described here for future consideration. It is important to be aware of the mis-ties and adjust data to compensate for these, to avoid bad ties and errors in interpretation and mapping.

Another new onshore seismic survey was acquired by Uppsala University for GEUS in 2022 across the Havnsø structure. The southernmost profile starts with a tie within the 3D seismic survey at the Stenlille-19 well to connect with the Stenlille data and interpretation in order to tie to the Havnsø structure. This is also important in order to contribute to sort out the mis-fit of the older data and optimize correlation of formations and sequence surfaces. It can be suggested for further studies to perform more detailed analyses to set the elevation plane of each seismic line and survey compensating e.g., statics, topography, groundwater level, etc. more accurate and to fit all the seismic profiles. However, this may be rather resource demanding.

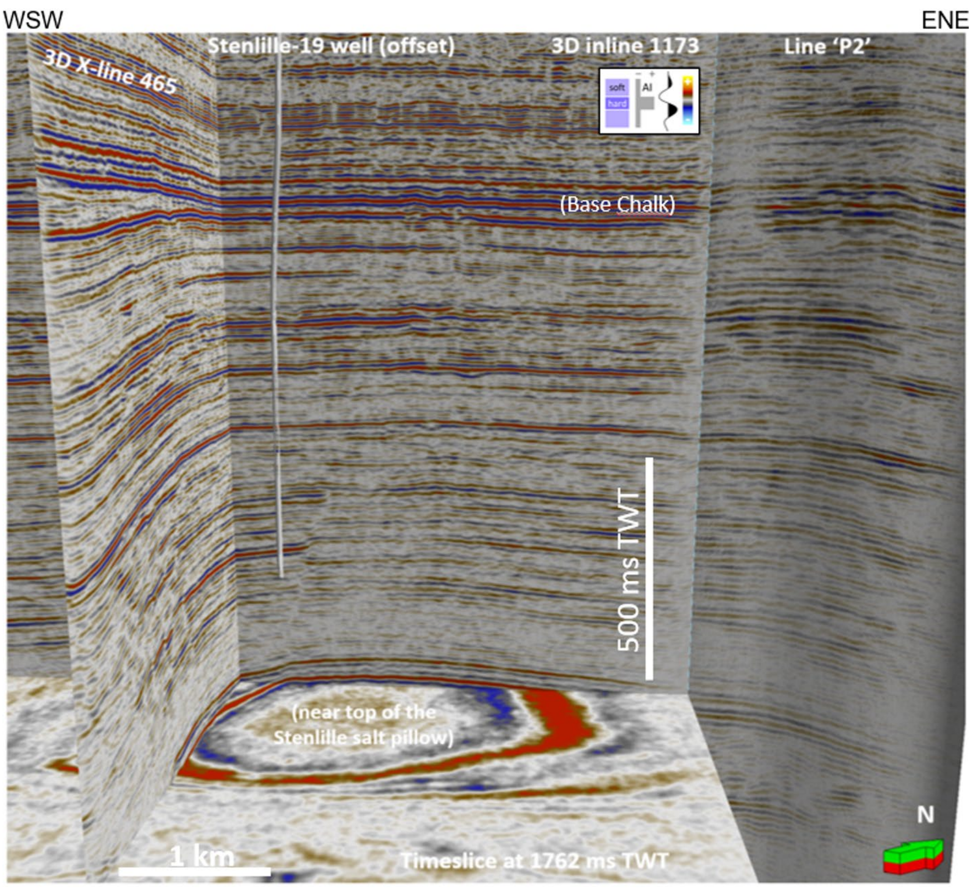

Figure 4.1.4. 3D seismic inline (1173) and crossline (465) with the Stenlille-19 well (offset), and the line GEUS_STL_P2 ('P2')*, which is time-shifted 56 ms to fit the 3D survey. View is towards NW, green and red arrow points towards north. Base Chalk reflection is a strong near horizontal red amplitude and the time slice (1762 ms TWT) cuts the top of the Stenlille salt pillow, shown in Fig. 1.4.*

4.2 New seismic data acquired in this project

The new seismic survey: GEUS2022-STENLILLE

The new survey acquired in Stenlille in 2022 is organized by GEUS for the initial maturation described in this report, and with Uppsala University in charge of acquisition and processing is named: GEUS2022-STENLILLE. Each of the survey profiles are named: GEUS22_STL_P1; GEUS22_STL_P1.5; GEUS22_STL_P2; GEUS22_STL_P3; GEUS22_STL_P4, with line km lengths respectively of 2.3 km, 1.3 km, 3 km, 4.2 km and 2.3 km, in total ~13 km. The positions of the profiles are shown in Fig. 4.2.1, where they are abbreviated P1 – P4. Line extensions include a reference to the type of the geophone recording: streamer, wireless and merged (streamer & wireless together), and if the version is stacked (stk), or stacked and migrated (mig) - e.g., GEUS22_STL_P1_merged_stk. Info on access to the survey at GEUS can be provided via email: info-data@geus.dk.

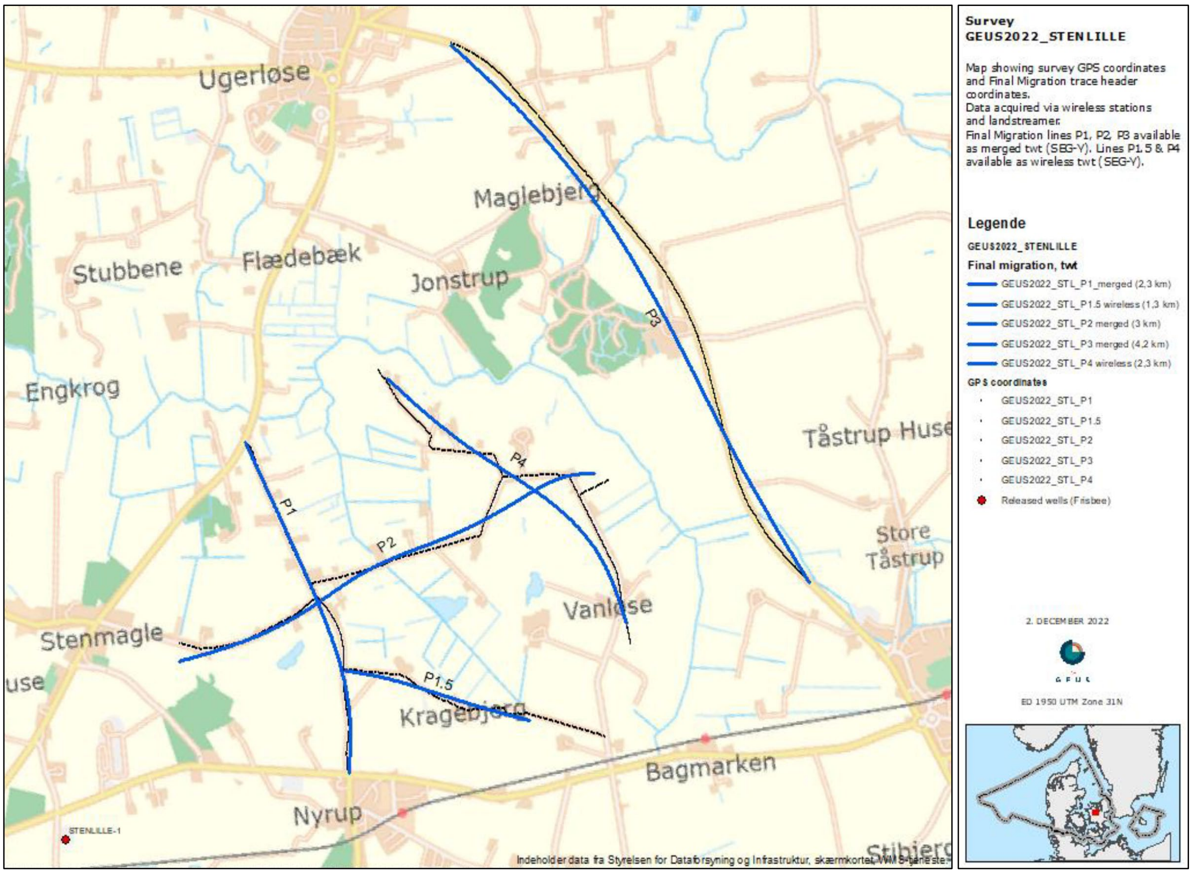

Figure 4.2.1. *Map with locations of the seismic profiles abbreviated to P1, P1.5, P2, P3, P4 - see legend for specified profile names. Blue lines are locations of the final migrated seismic profiles (here the profiles of wireless and merged files). Black dots are locations at the roads, where the seismic data were recorded. From the information flyer of GEUS (contact on data: email to info-data@geus.dk).*

Acquisition of the survey by Uppsala University

Background and purpose

In November 2021, GEUS contracted Uppsala University to acquire and process a new small seismic survey with five reflection seismic profiles of the survey GEUS2022_STENLILLE, to the NE of the STENLILLE-97 3D survey in a research and development cooperation. The survey was conducted in February 2022 (Fig. 4.2.1, 4.2.2) and is delivered and reported in the acquisition and processing report of June 2022 by Malehmir & Papadopoulou (2022) (Fig. 4.2.3).

The purposes of this cooperation acquisition project are mainly:

(1) to improve the database at the data-poor area NE of the STENLILLE-97 3D survey to mature the Stenlille structure towards potential demonstration storage of CO_2;

2) to test the equipment and the survey design to be used here and potentially other structures for similar targets;

(2) to acquire new seismic lines to improve the data coverage with modern data;

(3) to acquire modern high fold data for imaging and interpretation of the shallow and deeper subsurface, in particular the key reservoirs (mainly Gassum Fm), seals (mainly Fjerritslev Fm), faults and the geometry of the NE flank of the Stenlille structure.

(4) to expand knowledge of CCS operations through research and education, here in cooperation with universities.

Collaboration partners

Uppsala University contracted the Polish company Geopartner Sp. zo.o with two small trucks with vibration hydraulic pistons as source for the vibro-seismic data. Students in Geophysics and Geoscience from both University of Copenhagen and Uppsala University were hired as field assistants to conduct field support, including handling and moving the wireless geophones with Differential GPS surveying, adjusting the landstreamer, handling the road traffic signs, distributing information folders and flyers to citizens. Gas Storage Denmark A/S supported the acquisition with much help, including logistics of housing project meetings, storage of equipment, information and contacts to local population. COWI was contracted for acquiring permits, logistical planning, assessments in relation to landowners and supported on external contacts to authorities and citizens.

Communication & meetings

Communication with the local community was provided through a public information meeting on February 12th, 2022, at Gas Storage Denmark A/S, public visit days on February 9th and 13th, information flyers and folders to landowners in the vicinity of the acquisition, and with information mainly on the website of Gas Storage Denmark A/S. In addition, local media (e.g., Sjællandske Medier/www.sn.dk – ex. Feb. 7th and 8th) made interviews and articles on the acquisition. On Feb. 2, the day before the tests and first acquisition, the field personnel followed a road-safety course, and were equipped with safety wests during fieldwork.

Figure 4.2.2. *Survey design and equipment. Uppermost two rows are photos of field acquisition at roads near Stenlille in February 2022 with two mini-trucks with vibration pistons, and behind a landstreamer on the road and separate wireless geophones with a 10 m distance along the road. The lowermost row are close-up photos of (left to right) a wireless geophone and the landstreamer below it, next is a sensitive tool (MicroMate) to control-measure the vibration level to avoid too strong vibrations near properties, and finally safety road signs. The drawing in the uppermost row is the acquisition lay-out, showing the gradual proceeding of the acquisition train, with the two mini-trucks vibrating at every 10 meters, dragging the landstreamer with MEMs at 2 meters intervals, and the wireless geophones at every 10 meters along the road. The uppermost row of figures is from Papadopoulou et al. (2022).*
Acquisition with initial tests

On Feb. 3, after briefing of field personnel, equipment was checked, and acquisition tests were performed for optimal acquisition. Tests included use of 1 or 2 trucks for source, different frequency ranges (5–160 Hz) and different number of sweeps and sweeping periods (16 and 18 seconds) (Fig. 4.2.4).

The acquisition took place for 13 days (February 3rd to 15th 2022) and the seismic data are recorded along the five lines shown in Figure 4.1.1, with a total length of c. 12.5 km. The most crocked lines were later geometrically adjusted to become more straight lines, during the processing work to the final lines (Fig. 4.2.1).
As seismic source, two small trucks (INOVA UNIVIB, PLS-334; peak-force: 151 kN) were used with synchronized vibrating hydraulic pistons lowered in firm contact with the road (Fig. 4.2.2). Each truck has a weight of 9 ton but were loaded to be 12 ton in total for a better earth contact.
The trucks generated simultaneous a sweep lasting 16 seconds, increasing in frequency from 10 Hz to 140 Hz (Fig. 4.2.4). At every shot-point location this sweep was repeated three times. The three sweeps were later stacked to one shot-point during the processing to improve signal-to-noise ratio. After each shot-point with three sweeps, the trucks move 10 meters (shot-point distance) to the next shot-point. The last truck drags the attached landstreamer, adjusted along the road by field assistants (Fig. 4.2.2). When passing close to properties, control measurements with a sensitive 'Micromate' devise were carried out at the properties to secure, that vibrations stay below a threshold, as defined by the German norm DIN 4150-3. If the vibrations approached the threshold, the vibrations were stopped or continued with smaller vibration level, and in some cases with sensitive properties the shot-point was skipped.

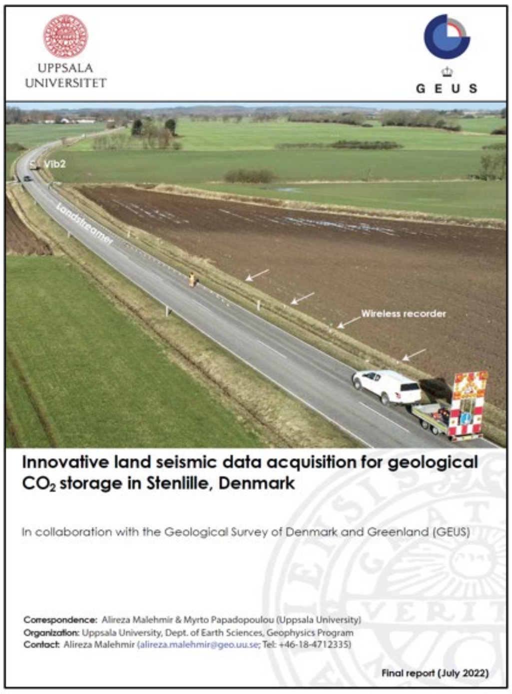

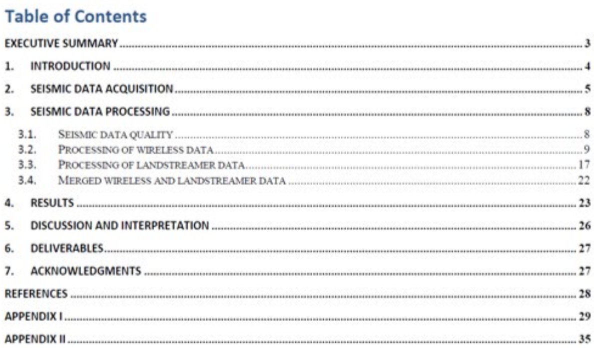
Table of Contents

Figure 4.2.3. *The front page and contents of the Final Acquisition and Processing Report of the GEUS2022-STENLILLE survey (Malehmir & Papadopoulou, 2022), which can be purchased through GEUS (email: info-data@geus.dk).*

As recording equipment connected to the truck data system was used both landstreamer mounted geophones attached to the last truck and road-side wireless geophones (Fig. 4.2.2) and the recording time of the geophones was 22 seconds. The wireless geophones were placed in the roadside with a 10-meter distance and used a frequency of 10 Hz and a 2 ms sampling interval (Table 4.2.1). The landstreamer has mounted a Micro-Electro-Mechanical (MEM) based geophone at every 2 meters with a sampling interval of 1 ms (Table 4.2.1). The landstreamer is developed by Uppsala University and is constructed of attached sections providing a flexible length up to c. 238 meter in this survey. It was shortened after logistical conditions, such as crookedness and other road conditions. From the shortest line (P1.5 or 'P1-leg') to the longest line (P3) the receiver positions varied from 382 to 4,291, and the total number of traces (vertical component) from 3,040 to 58,053 (Table 4.2.1).

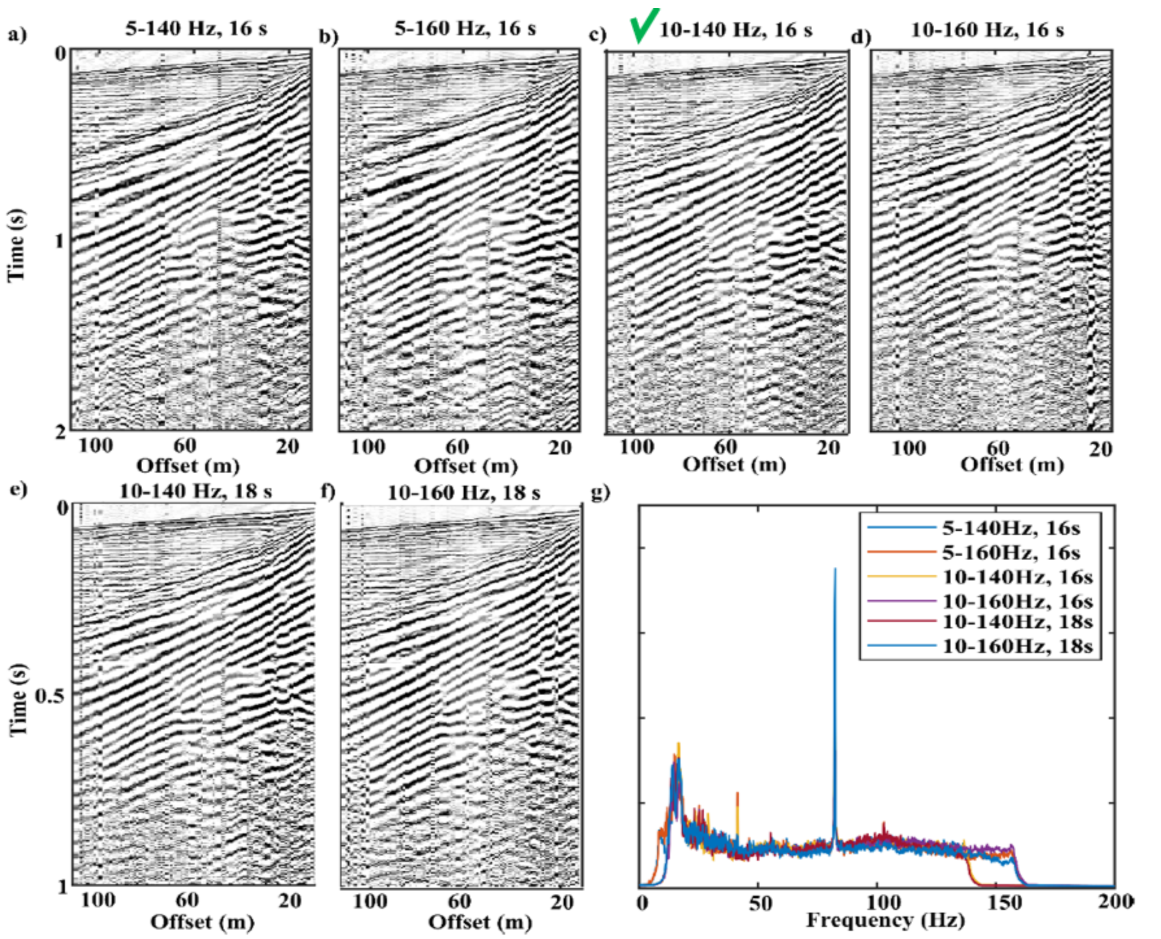

Sweep parameter tests conducted prior to the start of the acquisition. (a)-(f) The same shot gather corresponding to different sweep parameters. (g) Corresponding frequency spectra. Note that although the chosen sweep parameters in (d) presented the best compromise between of frequency band and noise contamination. An 80 Hz harmonic signal is very evident in the data.

Figure 4.2.4. *Sweep parameter tests prior to the start of acquisition, with the chosen parameters by the green 'v'-sign. From the Acquisition & Processing Report for the seismic survey GEUS2022-STENLILLE (Malehmir & Papadopoulou 2022).*

Table 4.2.1. *Table (table 1) showing the main seismic data acquisition parameters of the Stenlille seismic survey. From the Acquisition & Processing Report for the seismic survey GEUS2022-STENLILLE (Malehmir & Papadopoulou 2022).*

Survey parameters	**Profile P1**	**Profile P1-leg**	**Profile P2**	**Profile P3**	**Profile P4**
Recording system	Sercel Lite	Sercel Lite	Sercel Lite	Sercel Lite	Sercel Lite
Survey geometry	Fixed / Landstreamer	Fixed / Landstreamer	Fixed / Landstreamer	Fixed / Landstreamer	Fixed / Landstreamer
No. of shots	208 (3 records / point)	78 (3 records / point)	309 (3 records / point)	414 (3 records / point)	231 (3 records / point)
Shot spacing	10 m	10 m	10 m	10 m	10 m
Geodetic surveying	DGPS	DGPS	DGPS	DGPS	DGPS
Wireless					
No. of receivers	231 (1000-1230)	184 (1501-1684)	350 (2001-2350)	420 (3001-3420)	285 (4001-4285)
Receiver spacing	10 m	10 m	10 m	10 m	10 m
Maximum offset	~ 2,226 m	~ 1,772 m	~ 3,026 m	~ 4,143 m	~ 2,264 m
Geophone	10 Hz, Spike	10 Hz, Spike	10 Hz, Spike	10 Hz, Spike	10 Hz, Spike
Sampling interval	2 ms	2 ms	2 ms	2 ms	2 ms
Record length	22 s (5 s for processing)	22 s (5 s for processing)	22 s (5 s for processing)	22 s (5 s for processing)	22 s (5 s for processing)
Wireless data harvesting	GPS time	GPS time	GPS time	GPS time	GPS time
Total no. of traces	47840	14352	108150	173880	65835
Landstreamer					
No. of receiver positions	1,143 (10000-12300)	382 (15010-15780)	1,677 (19912-23280)	4,291 (3001-3420)	1236 (400170-42648)
Receiver spacing	2 m	2 m	2 m	2 m	2 m
Maximum offset	~ 238 m	~ 88 m	~ 130 m	~ 108 m	~ 88 m
Sampling interval	1 ms	1 ms	1 ms	1 ms	1 ms
Record length	22 s (5 s for processing)	22 s (5 s for processing)	22 s (5 s for processing)	22 s (5 s for processing)	22 s (5 s for processing)
Total no. of traces	20,437 (vertical component)	3,040 (vertical component)	17,380 (vertical component)	58,053 (vertical component)	8,300 (vertical component)

Processing of the seismic survey by Uppsala University

Immediately after seismic data acquisition seismic processing from raw SEG-D field data to final post stack migration were performed at Uppsala University. Slightly different processing sequences have been applied to the wireless data recordings and to the short offset landstreamer recordings. In the first processing step shot and receiver geometry are included in the seismic trace header and output data are in SEG-Y data format. Secondly cross correlation of the raw recorded vibrator signal with the theoretical source sweep has been applied to get the seismic response. Subsequently the 3 sweeps for each source location are then summed together to increase the signal to noise level.

The relatively small vibrator source (2x12 ton in total) is a big advantage in survey planning of line lay out and is also relatively easy to operate in the field in comparison to heavier equipment. In comparison to earlier reflection seismic surveys, the very short shot-point distance (10 m) and the long offset wireless receiver layout (10 m receiver distance) strongly supports noise attenuation tools both in source, receiver, and common offset domain.

The first run Uppsala University processing of the GEUS2022-STENLILLE seismic survey is a relatively fast-track seismic processing of the dataset and the results have immediately been included in an updated seismic mapping of the Stenlille structure. For getting this fast-track processing conventional post stack migration has been applied to the dataset. However, GEUS are also doing further tests of the processing sequence including pre-stack time migration and preliminary results are presented in section 4.3.

Landstreamer and wireless data were combined into a merged version (Fig. 4.2.5), for the sections: GEUS22_STL_P1; GEUS22_STL_P2; GEUS22_STL_P3. However, logistical restrictions in the field with a shortened streamer (only 1 segment) and poor data quality, caused that streamer data and consequently merged data are not available for two sections: GEUS22_STL_P1.5 and GEUS22_STL_P4. Wireless data are available for these sections. Examples of the final delivered sections are shown in Figures 4.2.6 (with interpretation notes) and 4.2.7.

Processing workflow for the wireless data from the Final Acquisition and Processing Report of the GEUS2022-STENLILLE survey (Malehmir & Papadopoulou 2022):

1 Read SEGD data
2 Vertical shot stacking (3 shot records)
3 Geometry setup (CDP spacing 5 m)
4 First break picking
5 Trace editing (noisy and dead)
6 AGC (200 ms)
7 Bandpass filter (10-25-130-150 Hz)
8 Bandstop filter (79-80-82-83)
9 Spectral balancing: 10-30-110-140 Hz
10 Gap deconvolution (filter length: 100 ms, gap length: 28 ms)
11 Gap deconvolution (filter length: 100 ms, gap length: 10 ms)
12 Median filter (window length: 9 traces, velocity: 1800 m/s)
13 Airwave attenuation (Velocity 330 m/s)
14 First-break mute
15 Elevation statics (40 m, 2500 m/s)
16 Surface-consistent refraction corrections (one-layer model)
17 Surface-consistent residual static corrections lopped with NMO (2 rounds)
18 AGC (100 ms)
19 Velocity analysis
20 NMO corrections (30% stretch mute)
21 Stack (normal)
22 FX-deconvolution
23 Balance amplitude
24 Migration (Finite difference with a maximum dip of 60 degrees)

Processing workflow for the landstreamer data from the Final Acquisition and Processing Report of the GEUS2022-STENLILLE survey (Malehmir & Papadopoulou 2022):

1 Read SEGD
2 Vertical shot stacking (3 shot records)
3 Geometry setup (CDP spacing 5m)
4 First break picking
5 Trace editing
6 Bandpass filter (30-35-130-170 Hz)
7 Bandstop filter (79-80-82-83)
8 Gap deconvolution (Filter length: 100 ms, Gap length: 28 ms)
9 Gap deconvolution (Filter length: 100 ms, Gap length: 10 ms)
10 First-break mute (P1 and P4)
11 Elevation statics (40 m, 2500 m/s)
12 Refraction statics (P1 and P4)
13 Residual statics (P1 and P3)
14 AGC (100 ms)
15 Velocity analysis
16 NMO corrections (30% stretch mute)
17 Stack
18 Bandpass filter (10-30-100-120 Hz)
19 FX-deconvolution
20 Balance amplitude
21 Migration (finite-difference)

Note that a notch filter (Bandstop filter ,79-80-82-83 Hz) has been applied for removing a strong frequency peak at 80 Hz, probably related to the source engine (point 8 in the wireless data and point 7 in the landstreamer data).
The wireless and the landstreamer data resulting from the corresponding pre-stack processing works were merged together providing a unique dataset by combining the traces corresponding to each of the recorded shots. The stacked section generated from the merged dataset combines the detailed imaging from the landstreamer data in the uppermost part of the seismic section (down to 500–1000 ms) with the better penetration depth from the longer offset wireless data in the deeper part of the seismic section (Fig. 4.2.5).

Deliverables from Uppsala University

The list of deliverables is shown below from the Final Acquisition and Processing Report of the GEUS2022-STENLILLE survey (Malehmir & Papadopoulou 2022):

6. Deliverables

These items have been delivered (or available) as separate files:

1. Peg and shot positions (xyz and pegs) (.txt)
2. Raw data (uncorrelated and correlated) (.sgys)
3. Progress reports (.ppt)
4. Brute stacks (wireless and streamer) (.sgys)
5. Version 1 unmigrated stacks (wireless only) (.sgys)
6. Version 2 unmigrated stacks (wireless and landstreamer and merged) (.sgys)
7. Version 3 unmigrated and migrated, merged (landstreamer & wireless) data (.sgy).
8. Velocity model (.txt)
9. CDP sorted processed gathers (.sgy)
10. 3D views and visualizations (figures)
11. EAGE-NSG 2022 conference extended abstract (Papadopoulou et al., 2022).

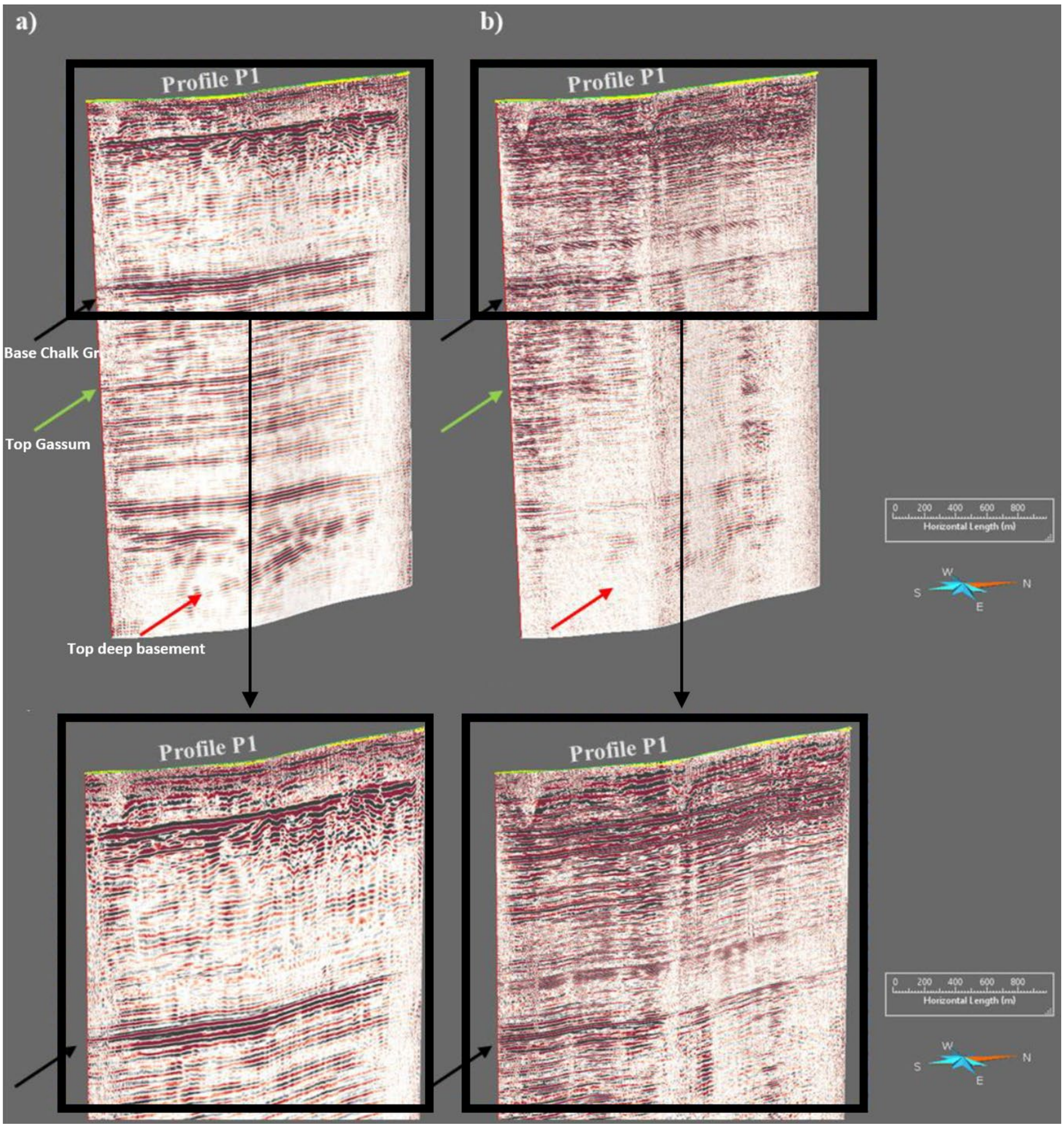

Figure 4.2.5. *Data examples from line P1 (stacked, unmigrated data) of the GEUS2022-STEN-LILLE survey. a) Data from wireless receiver with a zoom below. b) Landstreamer receiver with a zoom below. Note the differences with more details in depth for the wireless data, e.g., better reflection of the Top Gassum (a) but more details in the shallow parts for the landstreamer data (b) with more details in the Chalk Group successions. See Fig. 4.1.1 for position of the seismic profile. Modified from Malehmir & Papadopoulou (2022).*

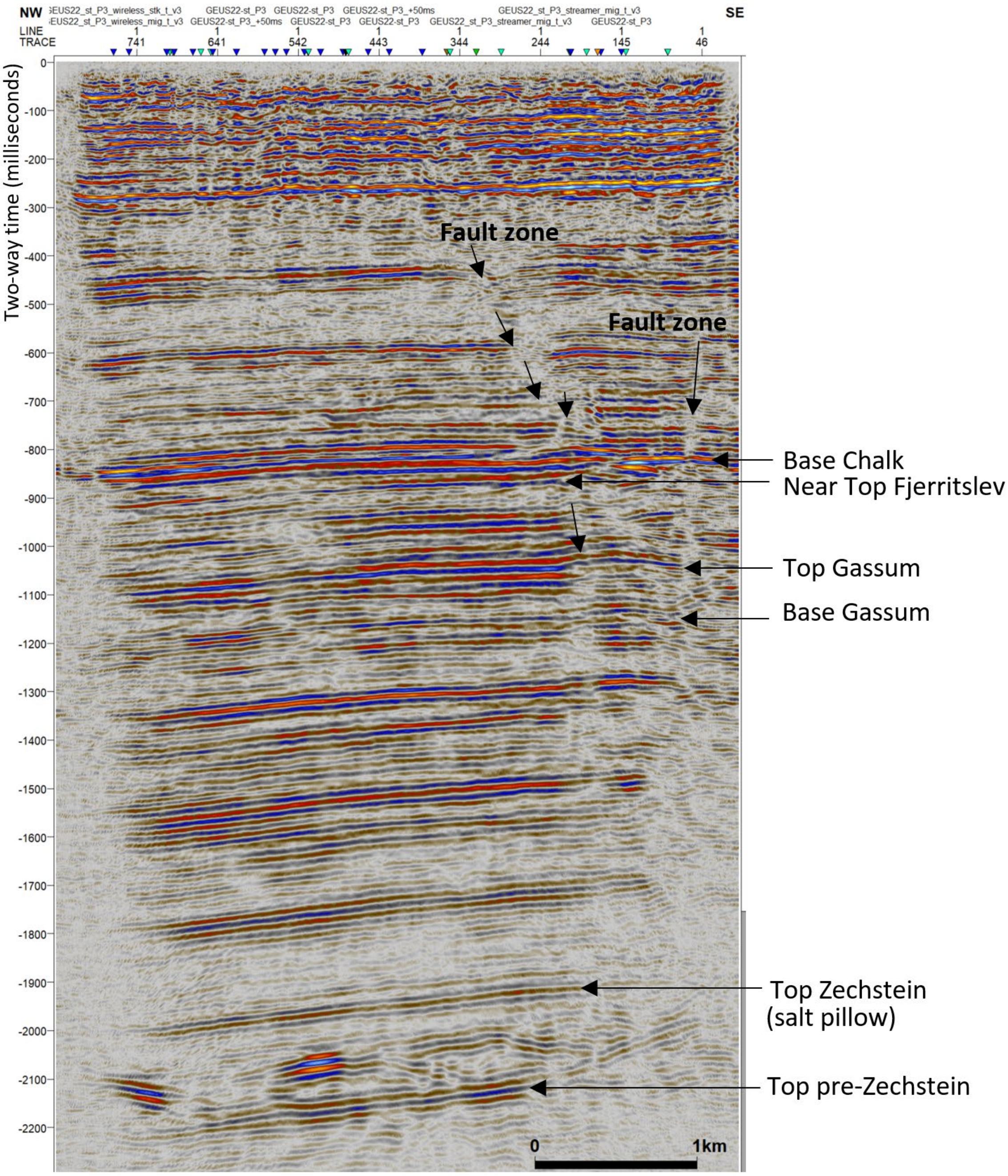

Figure 4.2.6. *Data example of line P3 with stacked and migrated data, merged from both the wireless and the landstreamer receivers, as the final deliverable, received from Uppsala University after processing. Interpretation annotation of this study. Note the reflections of the Gassum Formation (Base to Top Gassum) and the faults and fault zones towards SE. See Fig. 4.1.1 for position of the seismic profile.*

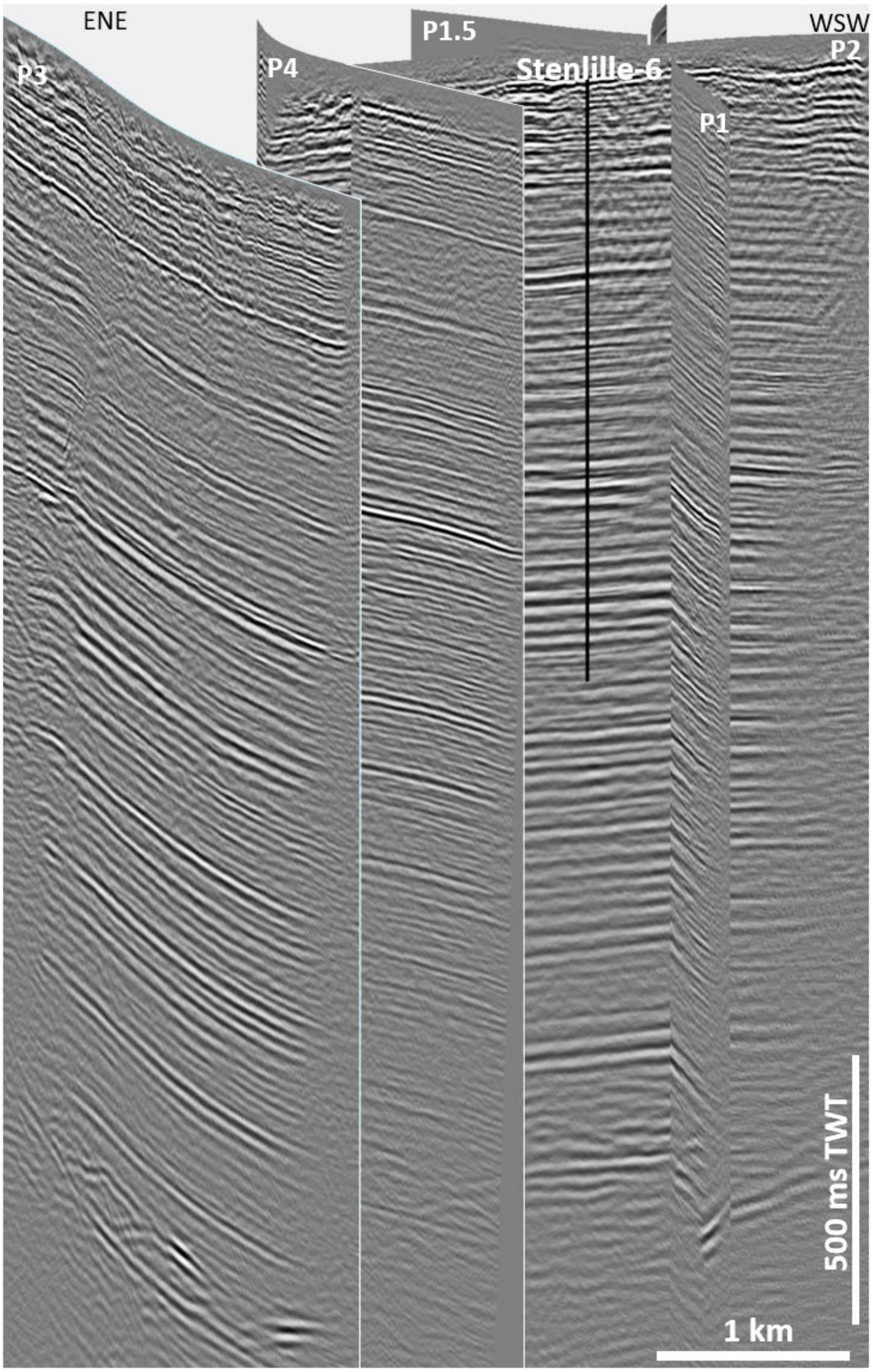

Figure 4.2.7. *The seismic survey GEUS2022_STENLILLE with the five final version seismic profiles (P1–P4) and the projected older Stenlille-6 well. Seismic data available from GEUS (info-data@geus.dk). See Fig. 4.1.1 for positions of the seismic profiles.*

4.3 Reprocessed seismic data in this project

Various seismic processing sequences of the Stenlille 2D acquired February 2022 by Uppsala University have been investigated. The objective is to identify and select a robust processing sequence that improves the overall signal-to-noise ratio (S/N) and resolution of the seismic data. A set of processing tools have been applied in a systematic order and sequentially evaluated by how well noise is suppressed and the reflection events are preserved. The data is processed in such a manner that it should be optimized both for structural and sedimentological interpretations, as well as being input to pre-stack quantitative interpretation workflows, e.g., AVO inversion.

An example of a seismic processing flow that has been used for the testing is the following:

Table 4.3.1. *Seismic processing sequence tested for the 2D Stenlille data.*

1.	Data input with diversity stack
2.	Near trace mute (<50m) and TPower
3.	Refraction statics
4.	Spiking deconvolution
5.	Denoising #1 (shot domain)
6.	Surface-Consistent Amplitude Correction
7.	Velocity picking
8.	Residual static correction
9.	Common Offset Binning
10.	Denoising #2 (OFFBIN domain)
11.	Kirchoff Pre-Stack Time Migration
12.	Post-Stack processing

In the following, some examples with key learnings from the seismic processing are presented in the common-shot domain and brute stacks along the P3 profile. We emphasize that the examples presented herein are subject to further testing and possible improvements, as seismic processing is an iterative process, and the quality of the result is ultimately a subjective opinion.

- Using a 'Diversity' stack of the repeating shot records of sweeps prior to a cross-correlation on the raw field records (SEG-D format) instead of a conventional vertical stack seems to significantly suppress traffic noise in the data. Figure 4.3.1 shows a shot record after vertical stacking (left) and diversity stacking (right), where the latter yields a significantly better S/N of the hyperbolic reflection events.
- Whether deconvolution should be applied prior to the first round of denoising or vice versa is a matter of testing and an open question. In the presented processing flow, a spiking and whitening deconvolution was applied to the shot gathers assuming zero-phase before the denoising. There may be a significant uplift potential in applying a spiking gap deconvolution instead, where the data must firstly be converted to minimum phase.

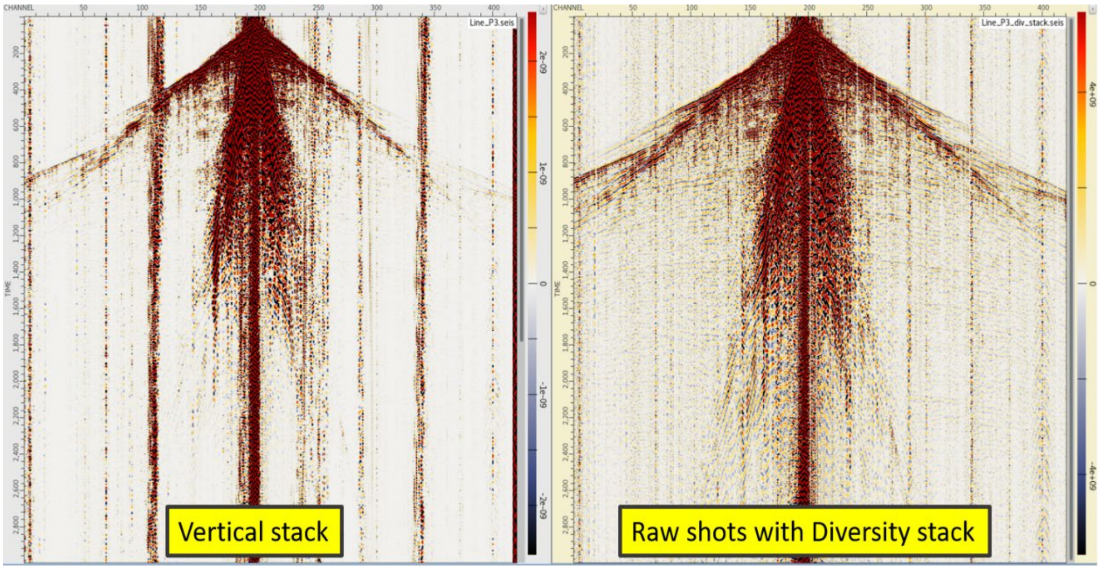

Figure 4.3.1. *Raw field records (SEG-D) after (left) cross-correlation and vertical stacking and (right) diversity stacking and cross-correlation.*

- Amplitudes of the near-offset traces exhibits some very high values that needs to be balanced or removed properly for subsequent processing. In our testing, we applied a set of high-cut bandpass (upper frequency around 70–90 Hz focusing on the Gassum Formation interval), FXSwell, TF denoise, near-offset mute, linear dip attenuation and air blast attenuation. Figure 4.3.2 shows before (left) and after (middle) applying a linear dip filter that attenuates linear events at 400 m/s velocities. The difference plot (right) shows linear dipping events through the shot-gather. The filter was applied to the whole shot gather except for the nearest offset traces (white cone in the right plot).

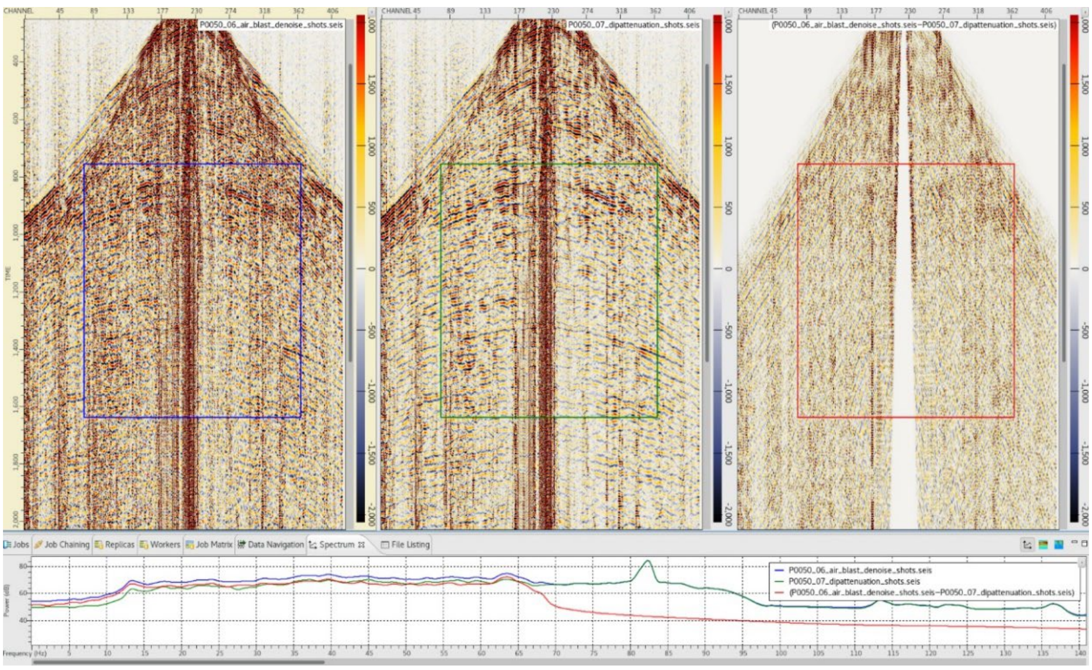

Figure 4.3.2. *Example of linear dip attenuation filter applied. Left: input, middle: output, and right: difference between input and output.*

- Improving the refraction and residual static corrections can be some of the most critical steps for improving the seismic image. However, the 2D Stenlille survey was acquired during the wet season where the shallow part is more water saturated and, therefore, contains a lower proportion of low-velocity, dry, unconsolidated sediments that tends to absorb much of the propagated seismic energy. Hence, static corrections will be even more important for seismic surveys acquired during dry seasons to compensate for the shallow part, i.e., the weathering layer. Moreover, we are fortunate that the Stenlille-6 well is located close to the 2D seismic lines at Stenlille, which we used to specify the depth of the first refraction event as recorded by the first break events, namely the top of the chalk package. The velocities of the weathering layer were estimated to be around 1800–2100 m/s. Figure 4.3.3 shows brute stacks after picking NMO velocities (left) and after calculating and applying residual static corrections (right). Notice that more continuous and consistent reflection events are obtained particularly in the middle of the section.

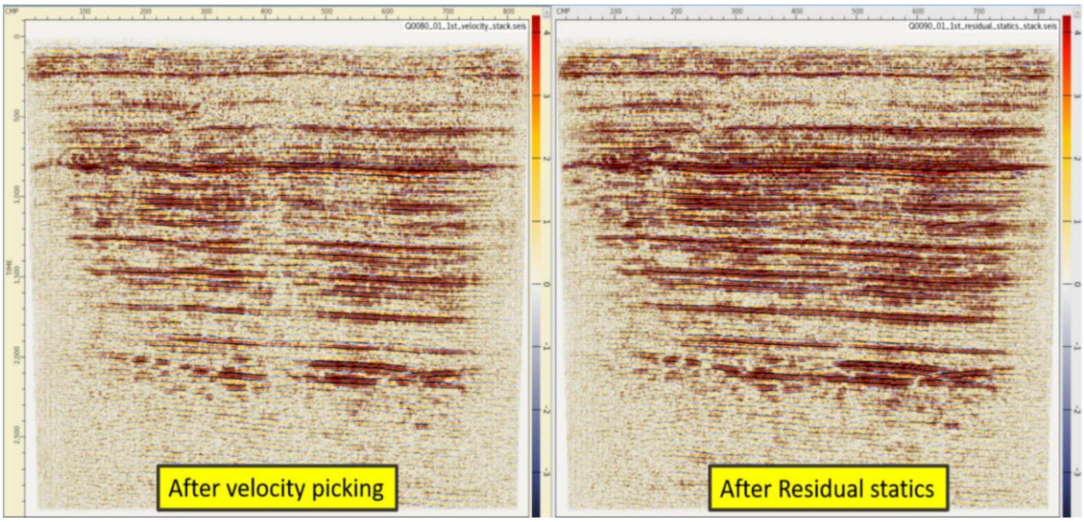

Figure 4.3.3. *Brute stacks after velocity picking (left) and subsequent residual static corrections (right).*

- Gentle use of Automatic Gain Control (AGC) is recommended to avoid making artificial AVO signatures for any subsequent pre-stack quantitative seismic analysis or reservoir characterization. However, by appropriately denoising, scaling and muting the extreme noise at the near-offset traces, there will be less dependency of strong AGC operators to boost the reflection events.
- Various Kirchoff pre-stack time migrations (PSTM) have been tested, where the current preliminary results are subject to additional calibration and optimization. Figure 4.3.4 shows brute stacks after 2nd denoising (left) in the common offset domain and after PSTM (steps 10 and 11 in Table 4.3.1, respectively). Some edge artefacts appear on both sections and are subjects to more testing and improvements. A fault lineation that can be used for testing various PSTM parameters on the P3 profile is observed at around CMPs 200–250 and 500–600 ms time, where the PSTM seems to reinforce the consistency of the fault lineation. On the PSTM section to the right (Fig. 4.3.4), it can be tracked from the strong base chalk reflection event and up towards the surface.

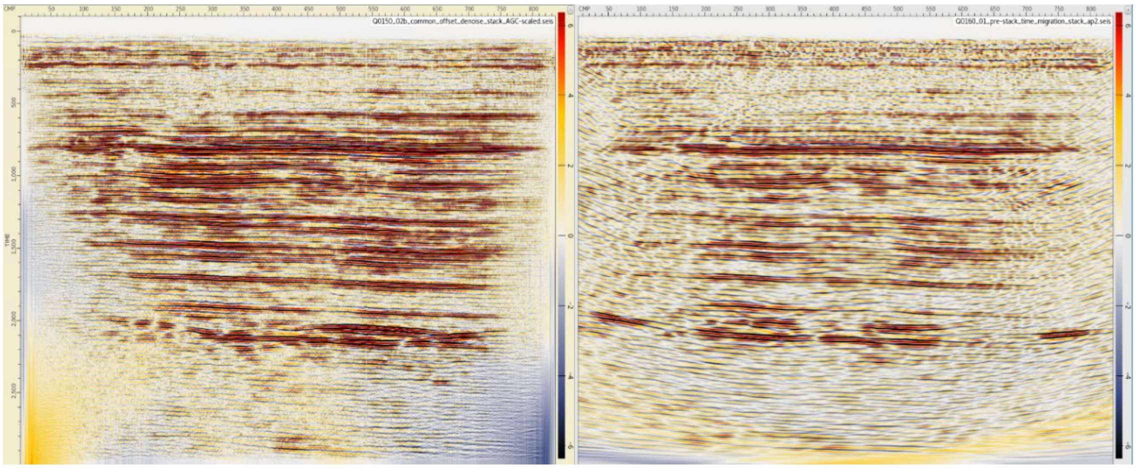

Figure 4.3.4. *Brute stacks after 2nd denoising (Step 10 in Table 4.3.1) (left) and after PSTM (right).*

Acknowledgement – The new seismic data

The good cooperation with Professor Alireza Malehmir and his researcher team from Uppsala University, and Geopartner Sp. zo.o (mini-vibs), on the planning, and during acquisition and completion of the GEUS2022-STENLILLE seismic survey, and the great field assistance from all the students from the University of Copenhagen and Uppsala University, are highly acknowledged and appreciated.

Also, the good cooperation with Gas Storage Denmark A/S and COWI during the planning and acquisition on application and logistics is highly acknowledged and appreciated.

4.4 Well data

The Stenlille structure is drilled by the 20 wells: Stenlille-1 to Stenlille-20 (ST-1 to ST-20), with 19 of the wells located within the 3D seismic survey area, and one (ST-6) just NE of the survey (Fig. 4.1.2, Table 4.4.1). The first well ST-1 was drilled in 1980 and the latest well ST-20 is from 2009.

Well logs have been used here for interpretation in particular of lithology, and selected logs were used for well log-based sequence stratigraphy, seismic to well ties and for seismic reservoir characterization and interpretation. See Chapters 5–7 for the specific used well logs.

Original logs: Caliper (CAL), Gamma-Ray (GR), compressional Sonic (SON, DT, DTLF, DT4P), shear Sonic (DTS, DT4S), Resistivity (R_deep mostly used), Neutron Porosity (NPHI) and Density (RHOB) logs.

Derived (interpreted) logs: Shale volume (V_{shale}), Effective porosity (PHIE), and Permeability estimates. The latter were derived from porosity-permeability relationships, established based on an analysis of core analysis data.

Table 4.4.1. *List of the Stenlille wells, with information on the year of drilling completed, Kelly Bushing (KB, meter above mean seal level), Total Depth (TD, meter below Kelly Bushing, measured depth) and deviation. Most wells have TD in lowermost Gassum Fm or in Vinding Fm, except Stenlille-3, which has TD in lowermost Fjerritslev Fm, and Stenlille-19 with TD in Bunter Sandstone Fm. All wells were drilled by DONG as Operator.*

Well	Year	KB a. msl (m)	TD b. KB (m)	Deviated
Stenlille-1	1980	41.6	1664	no
Stenlille-2	1987	47.7	1662	no
Stenlille-3	1987	47.7	1504	no
Stenlille-4	1988	38.4	1686	no
Stenlille-5	1988	55.9	1718	no
Stenlille-6	1988	32.4	1722	no
Stenlille-7	1990	40.0	1800	no
Stenlille-8	1992	40.0	1745	no
Stenlille-9	1992	40.0	1675	no
Stenlille-10	1992	41.5	1695	yes
Stenlille-11	1992	40.0	1900	no
Stenlille-12	1994	45.7	1780	no
Stenlille-13	1994	45.7	1840	no
Stenlille-14	1995	45.7	1815	no
Stenlille-15	1995	52.8	1703	yes
Stenlille-16	1996	40.0	1695	no
Stenlille-17	1996	47.6	1774	no
Stenlille-18	1996	47.6	1740	yes
Stenlille-19	2000	49.3	2570	yes
Stenlille-20	2009	40.0	1825	no

Well samples: Cores, SWC and ditch cutting samples

A number of cores, sidewall cores (SWC) and ditch cutting samples exist from the Stenlille wells and the cores and sidewall cores are listed in Table 4.4.2 below. Stenlille-4 is excluded from the list. The used samples and results are further discussed in Chapter 7.

Table 4.4.2. *Overview of the different cores, SWC and cuttings related to formation and well site. Chalk Group lower part is including the "Basal Chalk" and "Lower Chalk" and is of Cenomanian, Turonian and Coniacian age. Rødby Fm is Albian to lowermost Cenomanian age. Vedsted Fm is late Hauterivian to late Aptian age. Fjerritslev Fm is of latest Triassic to Early Jurassic age.*

Cores at Stenlille	St-1	St-2	St-3	St-5	St-6	St-7	St-8	St-9	St-10	St-11	St-12	St-13	St-14	St-15	St-16	St-17	St-18	St-19	St-20
Chalk Group (lower part)	-	-	-	Core 1	-	-	-	-	-	-	-	-	-	-	-	-	-	-	-
Rødby Fm	Core 1	-	-	-	-	-	SWC	-	-	-	-	-	-	-	-	-	-	-	-
Vedsted Formation	Core 1 + SWC	-	-	-	-	-	SWC	SWC	SWC	-	-	-	-	-	-	-	-	-	-
Fjerritslev Fm	Cores 2; 3; 4; 5; 6	Cores 1; 2; 3	-	Cores 2; 3; 4	Cores 1; 2; 3; 4	-	SWC	SWC	SWC + Cores 1;2	-	-	-	-	-	-	-	-	-	-
Gassum Fm	Core 6	Cores 4, 5	-	Cores 4, 5; 6		-	SWC	-	Cores 3	SWC	Cores 1 and 2	Cores 1,2,3, 4	Cores 1,2,3, 4	Cores 1,2,3, 4,5,6	-	Cores 1,2,3,4 ,5,6	Cores 1; 2; 3	Core 1	-
Bunter Sandstone	-	-	-	-	-	-	-	-	-	-	-	-	-	-	-	-	-	Cores 2; 3	-
Cuttings	Yes	Yes	Yes	Yes	?	?	Yes	Yes	Yes	Yes	Yes	Yes	Yes	Yes	Yes	Yes	Yes	Yes	Yes

5. Methods

Seismic interpretation and well-ties (Chapter 6)

The Stenlille structure storage complex, its formation and stratigraphy with reservoir-seal pairs, are investigated and evaluated from structural and stratigraphic analysis, based on the available 2D- and 3D seismic data and well-ties. Seismic horizons, seismic successions and seismic facies are identified and interpreted, using seismic attributes and reflector terminations such as onlap, downlap and truncation. The seismic stratigraphic horizons are essential sequence stratigraphic and chronostratigraphic surfaces but in this limited area they can be regarded as near base or near top formation boundaries. Horizon names are for simplicity similar to the formation names tied from the wells, which are in particular the Stenlille-1, 6, and 19 wells. The seismic stratigraphic boundaries and sequence stratigraphic surfaces and units should on a regional scale have more neutral naming (as e.g., in Nielsen 2003; Boldreel et al. in review). At the same time, faults, salt structures, and folds were identified and mapped together with internal configuration and thickness patterns. A structural and tectonic analysis was concluded by integrating the structural observations with the chronostratigraphic framework permitted by the well ties for tectonostratigraphic evolution.

Petrel (2021) software was used for establishing the database (Chapter 4), seismic interpretation with manual and auto-tracking of the horizons and well-ties with synthetic seismograms.

PaleoScan™ (2022) software was additionally used in the 3D survey area, with selection of generated horizons, which correspond to well-tied (ST-19) key formation tops from the Top Bunter Sandstone to the Top Oddesund. A few deeper horizons were also generated below TD (Top Bunter Shale and Top Zechstein). The generated horizons were correlated out to 2D seismic sections.

In total 18 horizons were mapped systematically over the area to determine the stratigraphy, geological evolution of the area, and most important to define reservoir-seal pairs and structural closures (see Chapter 6). The deepest horizons (below Top pre-Zechstein) were interpreted manually on selected lines and correlated from Stenlille area to the Slagelse-1 well, in order to describe the oldest part of the tectonostratigraphic evolution of the region. However, the most comprehensive and detailed mapping of horizons and faults has been performed of the successions from the Top Vinding (Base Gassum) to the Base Chalk, comprising the primary reservoir (Gassum Fm), primary seal (Fjerritslev Fm) and part of the secondary seal to the Gassum Fm.

In addition, the Gassum Fm are detailed interpreted in special studies of quantitative seismic modelling, log-based sequence stratigraphy, and seismic morphology, as a reservoir characterization. The methods used are described in each of these studies (see Chapters 6 and 7).

Lithostratigraphic and sequence stratigraphic well-log boundaries (well-tops) are adjusted by time-depth relations to the seismic data and synthetic seismograms of the wells are used to constrain the seismic interpretation (see below; Fig. 5.1).

Well-to-seismic tie and synthetic seismograms (Chapter 6)

In order to utilize well log data and well tops (depth domain) with seismic data (time domain), seismic-well tie procedure have been performed on wells that contain sonic and density logs (Fig. 5.1). In total, 13 wells contained density and sonic logs (see database section 4.4), though some wells only contained information in the vicinity of the reservoir section. A statistical wavelet was extracted within the interval of the Fjerritslev – Gassum Formations, resembling a zero-phased wavelet with reverse polarity, and having several sidelobes due to the noisy seismic data (Fig. 5.1).

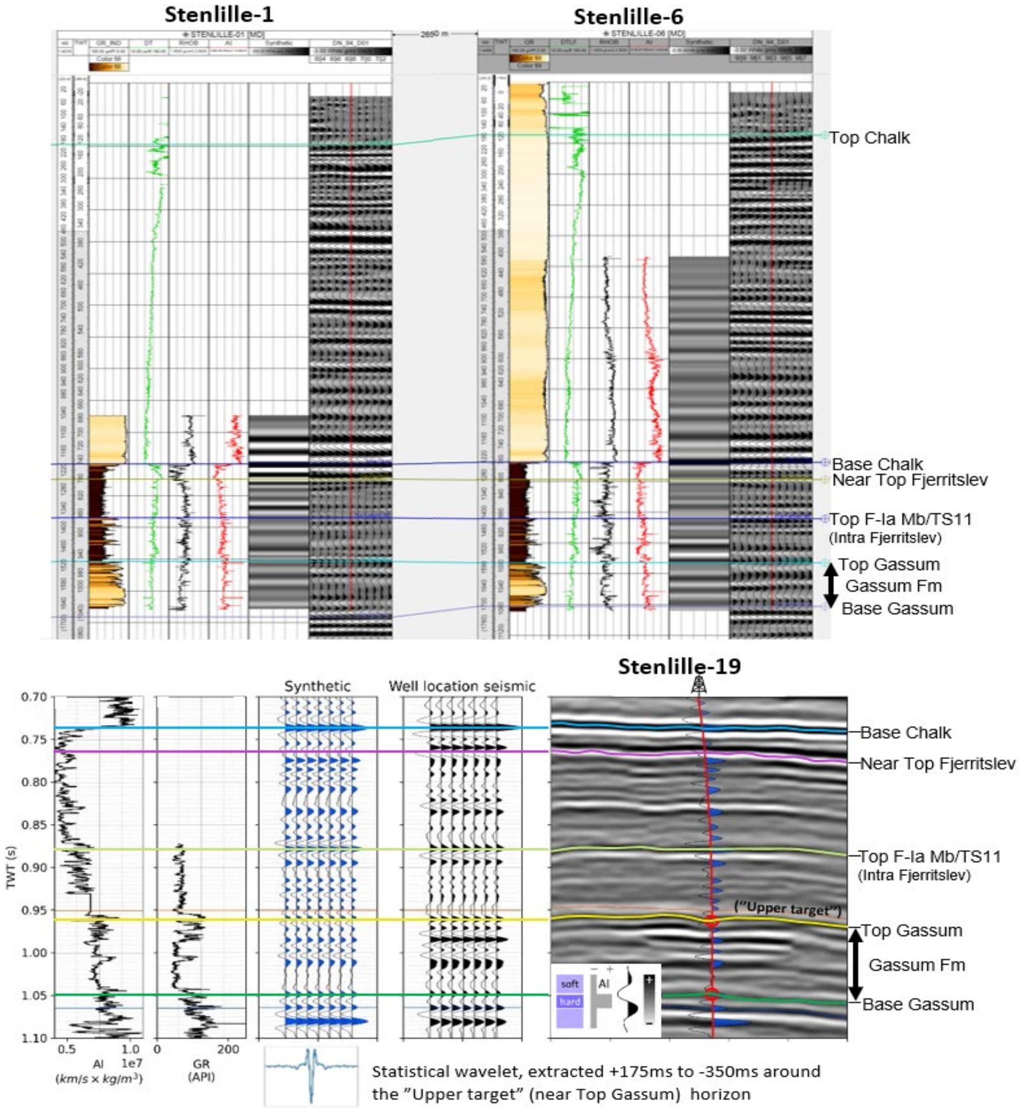

Figure 5.1. *Well to seismic ties with well-logs, synthetic seismic and seismic line displays of Stenlille-1, -6, -19 wells. Correlated seismic stratigraphic horizons from Base Gassum to Top Chalk are shown. The well-tied synthetic seismic displays are based on a statistical wavelet approach. The lower Stenlille-19 figure is modified from Bredesen (2022).*

Check shots were only available within Stenlille-1 and -19, which were used as an initial time-depth relationship, and using the density and sonic logs, a synthetic seismogram could be produced and compared to seismic data. A combination of bulk shifts (initial shift to match Base Chalk Group reflection and top Gassum reflection), and slight stretching or squeezing, QC'ed by observing reasonable interval velocities for the given lithologies, resulted in a good correlation of synthetic seismogram and seismic, thereby ensuring correct depths of well log information and well tops. For the other 11 wells without check shot information, check shots from Stenlille-1 and -19 were used as well as initial time-depth relationship. We evaluated this to be justified considering the relatively small distances (several kilometers at maximum), similar well trajectories and expected similar interval velocities due to the relative homogenous geological buildup. Some minor mismatch of the seismic-to-well tie in the gas saturated areas occur due to different years (data vintage) of drilling, seismic acquisition, and gas injection and volume. The Stenlille-1 to Stenlille-6 wells were drilled prior to the gas-injection initiated in 1989, and the Stenlille-18 was the latest well drilled prior to the 3D seismic survey in 1997. In addition, other factors may also affect the ties such as the seismic datum, static correction, the level of the ground-water table, and other factors also affect the seismic velocities (e.g., lithology variations) and thus time-depth relations.

Seismic time to depth conversion (Chapter 6)

A comprehensive velocity model was constructed to convert the interpreted horizons from the time domain to the depth domain. The model area was defined so that the velocity model includes the NE flank with closing contours of the Stenlille structure, so that depth-converted horizons can be used for simulation purposes (red polygon Fig. 5.2C). The model area is significantly extended beyond the 3D seismic survey outline, since this only covers the central part of the Stenlille structure (black polygon Fig. 5.2C). Extra figures on the depth conversion process are available in Appendix A.

The data available include: 1) TWT seismic horizons of the main stratigraphic units, utilizing the 3D seismic survey and 2D lines (including new GEUS2022-STENLILLE lines); 2) Time-Depth-Relationships (TDRs) for 13 wells; 3) Well top markers; 4) Seismic migration velocities (true interval velocities) from the 3D seismic volume (STENLILLE-97).

In order to account for vertical and lateral variations in interval velocities found within the stratigraphic units as seen in the TDRs and 3D seismic migration velocities, the velocity model was constructed in two steps, followed by depth-conversion of the TWT seismic horizons:

1. First, the interval velocities obtained from TDRs (1D) and seismic migration velocities (3D) were modelled within a 3D grid using kriging with parameters derived from comprehensive data analyses.
2. Second, a multi-layer velocity model was created using the modelled 3D interval velocities as velocity input, and 3D horizons and well tops to correct the velocity model.
3. Finally, TWT seismic horizons were depth-converted using the created velocity model.

The workflow was performed within Petrel by the following steps:

- QC of the input data:
    - seismic-well-ties; removing outliers in interval velocities observed in the TDRs originating from overstretching and squeezing in the seismic-to-well tie procedure.
    - adjusting the TWT seismic horizons to well markers since seismic peaks or troughs not necessarily coincide with the well tops, in order to get a good TWT to MD fit of main stratigraphic units (Fig. 5.1); checking TWT thicknesses for

bullseyes originating from horizon mis-picks or extrapolation, smoothening anomalies.

- Defining a 3D modelling grid (100x100m) based on the QC-ed TWT horizons using the Petrel structural modelling tool:
    - Model zonation according to the following horizons: surface (0 ms), Top Tertiary, Top Chalk Group, Intra-Chalk 1, Intra-Chalk 2, Base Chalk, Near Top Fjerritslev, Top Gassum, Base Gassum, Top Oddesund, Intra Oddesund sst. beds, Top Falster, Top Ørslev, Top Bunter Sst., Top Zechstein, Top pre-Zechstein. Top Tertiary and Top Chalk Group could only be picked on the 2D datasets (DN94O and DN87I).
    - Vertical layering was defined such that layer thickness is between 10 – 20 m, with higher resolutions within the Gassum Formation.
    - Upscaling the interval velocity data from the wells to the 3D grid.
    - Sampling seismic migration velocities at 3D grid resolution and extrapolated to the model extend, as input to data analysis and as 3D trend in the kriging step.
- Comprehensive data analysis for each zone separately using variograms and directional trends to obtain geostatistical parameters of vertical and lateral changes in interval velocities observed in detrended and normalized well and seismic migration velocity data (major/minor/vertical axes lengths, azimuth of data trends).
- Population of the 3D grid with interval velocities per zone, using the kriging parameters from the data analysis (min/max distribution, variogram ranges, 3D trends using extrapolated seismic migration velocities):
    - Perform blind testing by removing a well from the modelling, running the simulation, and compare the interval velocity data and prediction from the 3D model until satisfactory.
    - Convert the 3D interval velocity model volume to an 3D average velocity volume.
- Create an "advanced velocity model" with the same zonation as the 3D modelling grid and using modelled 3D interval velocities as velocity input and 3D surfaces/well tops as hard ties.
- Depth-convert the TWT horizons using the constructed velocity model.

Incisions into the Chalk Group from the middle part of the model area towards the SW causes a general thinning (Fig. 5.2A and B). As the infill of the incision has a lower velocity compared to the Chalk Group, the thinning creates a lower average velocity trend from NE to SW in the velocity model, resulting in changing architecture of the TWT horizon after depth-conversion (Fig. 5.2C and D). This will have an impact on volumetric calculations. Further iterations of the velocity model will aim to take into account uncertainties in depth and thicknesses of the units and their velocity values, resulting in some modification of the depth contours.

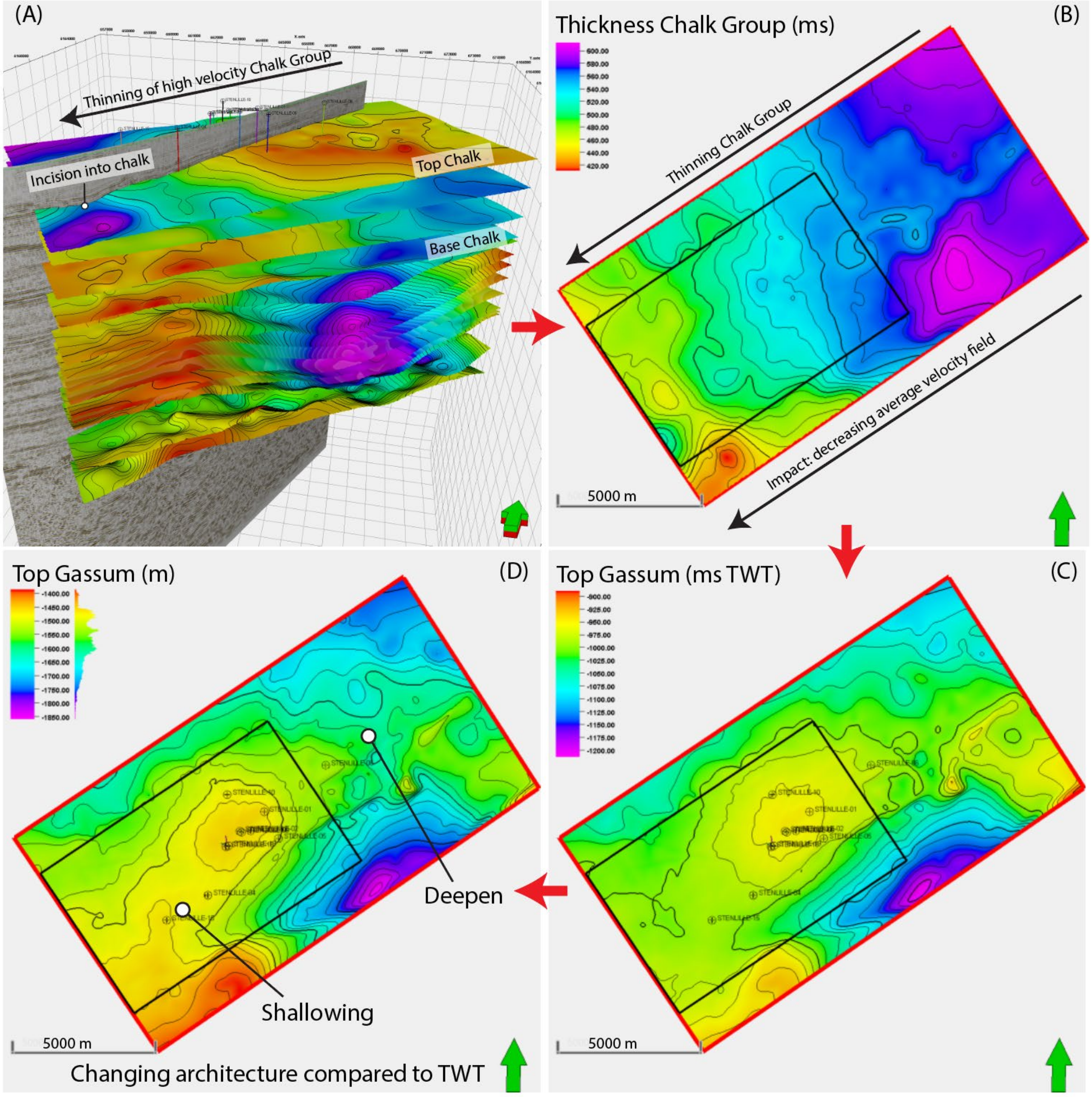

Figure 5.2. *(A) 3D perspective of horizons considered in the velocity model. 2D seismic line DN87I_001 shown as well, since it resolves top Chalk Group whereas this surface cannot be seen in the 3D seismic survey. Note the incision into the Chalk Group towards the SW. (B) TWT thickness map of the Chalk Group. Note the thinning to the SW. As the Chalk Group has a relative high velocity compared to the infill into the incision, average velocities will be lower where the Chalk is thinner, causing a change in geometry of TWT horizons compared to depth horizons. (C) Top Gassum depth-structure map in TWT. (D) Top Gassum depth-structure map in meters. Note the changed architecture between TWT and meters, with the SW flank becoming shallower and NE flank deeper as a result of the difference in Chalk Group thickness.*

Investigation of reservoir and seal (Chapter 7)

The geology of the reservoir and seal successions are described using well completion reports, publications, and in-house studies of well-logs and geological well samples mainly from cores. In addition, a limited number of studies focusing on lithology and biostratigraphy are available. The aim of these studies is to provide a more detailed understanding of reservoir and seal characteristics (see Chapter 7).

The reservoir characteristics presented below and discussed in Chapter 7 are derived mainly from the acquired wireline logs that are calibrated against conventional core analysis, descriptions of cuttings and sidewall cores. Potential reservoir units were identified from wireline logs by low formation resistivity, characteristic neutron-density log responses, and low natural radioactivity as recorded by the GR log and documented by cuttings containing sand-sized quartz grains. Reservoir parameters were evaluated based on well data with emphasis on data from e.g., the ST-1, 2, 5, 6, 18 and 19 wells. In petrophysical terms, a sandstone reservoir is herein defined as a rock having < 50% volume of shale, and an effective porosity (PHIE) of > 10%.

The volume of shale is estimated based on a combination of the gamma ray, deep resistivity, density, and neutron porosity logs, whereas the effective porosity is calculated based on the volume of shale combined with an analysis of the density-neutron porosity logs. The permeability is estimated using in-house established relationships between porosity and permeability, which is based on conventional core measurements. These relations are derived from core analysis data, i.e., porosities and permeabilities measured on core samples originating both from the Gassum Formation (e.g., the ST-1, 2, 5, 6, 18, 19 wells) and Bunter Sandstone Formation (the ST-19 well).

Seal thickness and grain-sizes were similarly evaluated based on petrophysical logs. Mudstone sections that will act as seal were identified from wireline logs by having high formation resistivity, high formation density and high natural radioactivity reflected in high GR log readings.

Storage capacity modeling (Chapter 8)

The storage capacity of reservoir units with buoyant trapping is estimated via this equation:

$$SC = GRV * N{:}G * \varphi * \rho_{CO2R} * S(Eff.)$$

Where:

SC Storage Capacity

GRV Gross Rock Volume is confined within the upper and lower boundary of the gross reservoir interval and above of the deepest closing contour from where spillage from the trap will occur

N/G Average net to gross reservoir ratio of aquifer across the entire trap (GRV)

φ Average effective reservoir porosity of aquifer within trap (GRV)

ρ_{CO2R} The average CO_2 density at reservoir conditions across all of trap.

$S(Eff.)$ Storage efficiency factor relates to the fraction of the available pore volume that will store CO_2 within the trap (GRV). This fraction depends on the size of storage domain, heterogeneity of formation, compartmentalization, permeability, porosity, and compressibility, but is also strongly influenced by different well designs and injection schemes (Wang et al. 2013).

To address the uncertainties associated with seismic data quality and density, interpretation and seismic well tie, depth conversion challenges, mapping, reservoir parameters assessment and fluid parameter assumptions in the reservoir, a simple Monte Carlo methodology has been applied. Ranges of each of the four input parameters (GRV, N/G, φ and ρ_{CO2R}) have been chosen to reflect parameter uncertainty and distribution modelled utilizing a simple Monte Carlo simulation tool built in MS Excel®. To achieve stable and adequate statistical representation of both input distribution and result output, 10,000 trials are calculated for each simulation. The methodology is simplistic and does not incorporate e.g., correlations of input parameters. However, for the purpose of estimating reliable screening volumes, the methodology is considered relevant and adequate. The method is used for the calculations in Chapter 8.

6. Results of seismic and well-tie interpretation

6.1 Stratigraphy of the structure

In total eighteen seismic stratigraphic horizons were interpreted in the study area of the Stenlille structure and they are from the deepest to the shallowest: (1) Top pre-Cambrian basement (2), Top Cambrian, (3) Top Lower Palaeozoic, (4) Top pre-Zechstein (Base Zechstein or Top Rotliegende), (5) Top Zechstein, (6) Top Bunter Shale (Sh), (7) Top Bunter Sandstone (Sst.), (8) Top Ørslev, (9) Top Falster, (10) Intra Oddesund sst. beds, (11) Top Oddesund, (12) Top Vinding (Base Gassum) (13) Top Gassum (TS7), (14) Top F-Ia Mb (TS11), (15) Top F-Ib Mb (SB13) (intra Fjerritslev Fm horizons), (16) Near Top Fjerritslev, (17) Base Chalk, and (18) Top Chalk (Fig. 6.1.1−6.1.7).

The three oldest pre-Zechstein horizons (1−3) are used to correlate selected sections for investigating the structural evolution, with interpretation only on a few selected 2D seismic lines, with the purpose of tying the Stenlille area to the Slagelse area (Slagelse-1 well). The uppermost Top Chalk horizon (Fig. 6.1.5) is mainly used for the Chalk Group isochore map for the time to depth conversion. The other fourteen horizons constitute the key stratigraphic framework in the present description of the Stenlille structure throughout the study area from 2D and 3D seismic data with well-ties. Horizons from Top Bunter Sst. and shallower can be correlated to the Stenlille-19 (ST-19) well (Fig. 3.4, 6.1.1). Horizons from Base Gassum and shallower can be correlated to well-tops in nearly all Stenlille wells. The Stenlille-3 well is the only well not reaching the Gassum Fm and having its TD in the lower part of the Fjerritslev Fm. The interpreted seismic stratigraphic horizon with well-ties documents the local stratigraphy of the Stenlille structure and the key tie between seismic stratigraphy and the regional generalized lithostratigraphy is shown in Figure 6.1.1. Parts of the Triassic lithostratigraphy should be revised in the future for this part of the Danish Basin. The horizons are essentially interpreted as sequence stratigraphic (approximately chronostratigraphic) boundaries, which are traced in a certain reflection (here a trough or a peak). However, they are in most cases also, on a local scale, near-formation boundaries as correlated to the well-tops. Thus, the seismic horizons are here named after the approximate formation boundaries. More regionally, it may be considered to use lithostratigraphic independent naming such as letters or ages, as on a regional scale, some of the lithostratigraphic units are diachronous. For example: The top of the Gassum Formation is Rhaetian in age (at the sequence stratigraphic flooding surface TS7) in the Stenlille area, whereas it is of a younger Hettangian – early Sinemurian age in central to northern Jutland, where the formation top occurs at different sequence stratigraphic flooding surfaces e.g., TS9–TS11 (Nielsen 2003). However, here in this local area, the naming serves to more directly relate formations and thus key reservoir-seal pairs.

Synthetic seismograms have been produced to study and connect wells to seismic reflections for interpretation of the horizons (Fig. 5.1). Most seismic data, including 3D and most 2D lines are European SEG reverse polarity, where a peak is a soft kick with downward decreasing acoustic impedance (AI), such as the Base Chalk. Figure 7.1.1 shows a significant drop in velocity from chalk of the Chalk Group into lower velocity marl and chalk of the Rødby Fm. We use here mostly coloured profiles displayed in red-white-blue (red peaks and blue troughs) or black-grey-white (black peaks and white troughs) (Fig. 6.1.1–6.1.3). Several factors affect the seismic reflection responses (velocity and/or density), not only lithology variation, but also variations in e.g., compaction, cementation, fluids and gas. Various amounts of natural gas have been stored in the Gassum Formation, which in the seismic data impact locally decrease of the velocities and densities in the reservoir zones. We define here each interpreted horizon in either a peak or a trough seismic reflection (note the reverse polarity), which are stated in Figure 6.1.5, where e.g., the Base Chalk follows a peak, the Near Top Fjerritslev follows a trough, and the Top Gassum follows a peak reflection.

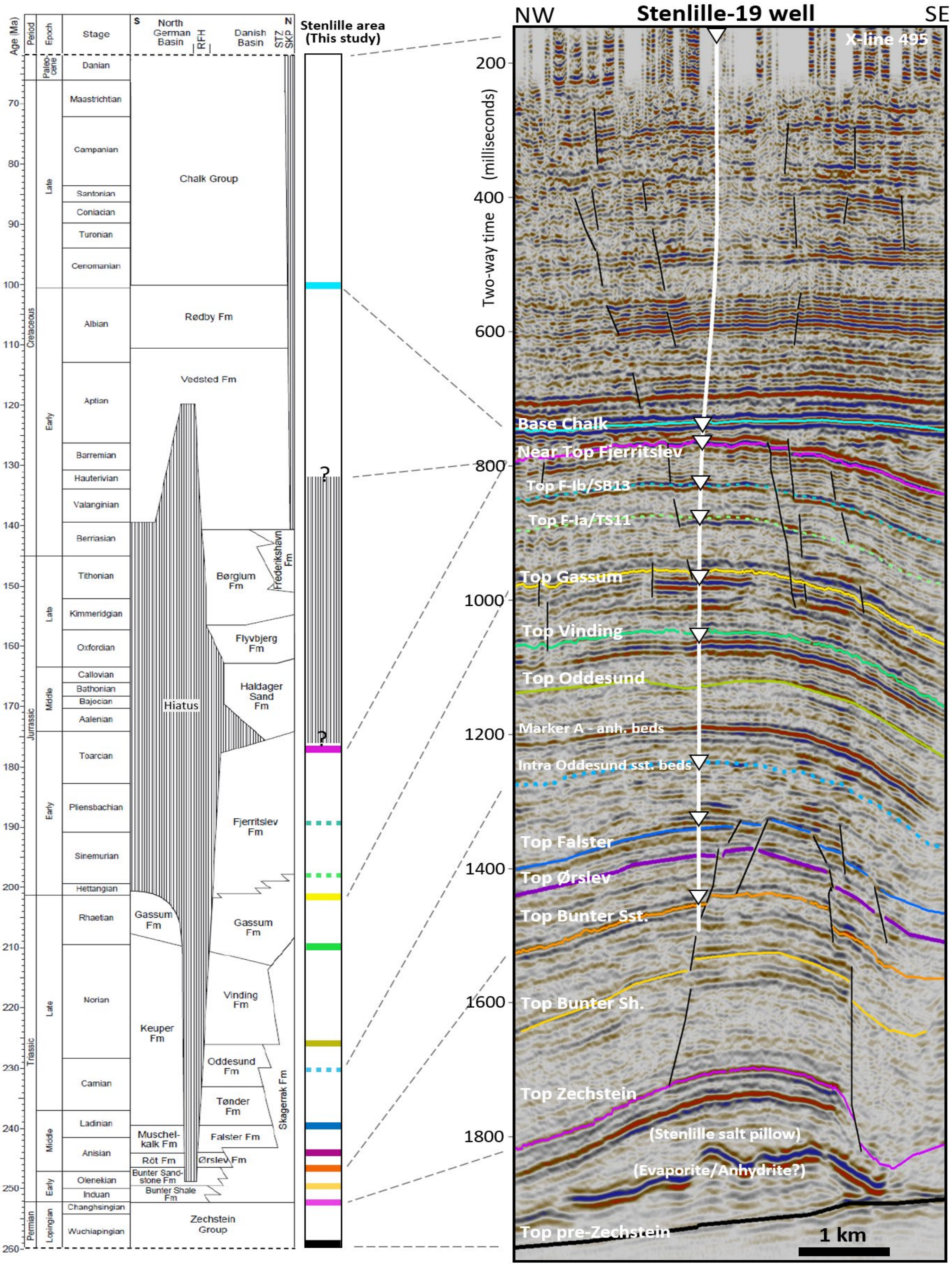

Figure 6.1.1. *(figure text next page)*

Figure 6.1.1. *Lithostratigraphy and seismic horizons with well-tie at the Stenlille-19 well in the eastern part of the Danish Basin, north of the Ringkøbing–Fyn High (RFH). The lithostratigraphic scheme, based on Bertelsen (1980) and Nielsen (2003), summarizes a more western part of the basin (Jutland), but most of the formations of the area just north of the RFH are partly comparable to the Stenlille region (excluding M.+U. Jurassic formations). Colored seismic stratigraphic horizons are shown in age in the separate stratigraphic column (this study), and in a seismic profile (X-line 495) in two-way time, with correlation to the Stenlille-19 well with well-tops (triangles, centers). In addition, some of the large faults (vertical black lines) are shown. Dashed horizontal lines at the top and base of the scheme indicate omitted younger Cenozoic and Quaternary successions, and pre-Zechstein successions, respectively due to space limitation. Location of the seismic section is shown in Fig. 6.1.3. Modified from Gregersen et al. (2022).*

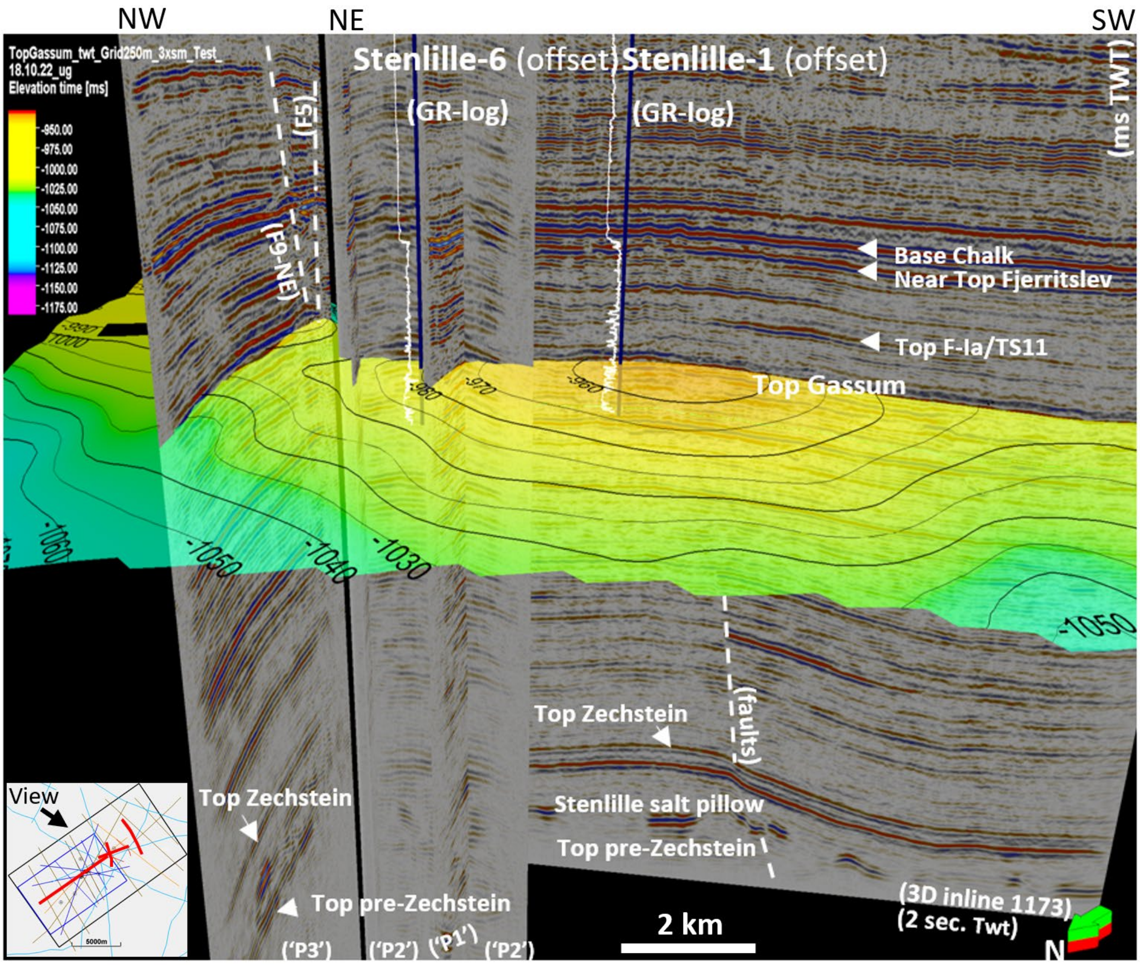

Figure 6.1.2. *3D perspective view with Stenlille-1,6 wells and 3D inline-1173, aligned with the new 'P1', 'P2' and 'P3' (GEUS22-STL-P1,-P2,-P3) seismic sections, and a Top Gassum time-structure map (ms twt), with indicated positions of Top pre-Zechstein, Stenlille salt pillow, Top Zechstein, Top F-Ia/TS11, Near Top Fjerritslev, Base Chalk, and faults. The Top Gassum structural closure towards NE was confirmed with the new data, and faults were detected and mapped in the Gassum–Fjerritslev Formations, but some also up into the Chalk Group. The new 2D sections are time-shifted to fit the 3D survey. Line positions (red) are shown in the small database map and viewed towards SE.*

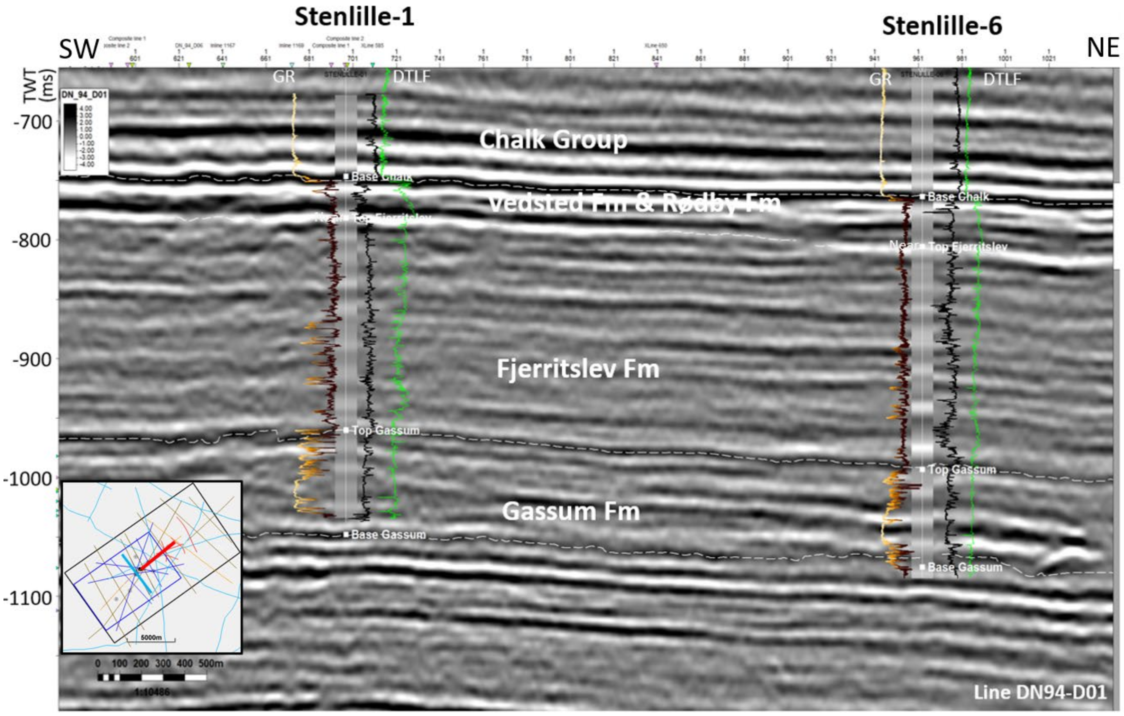

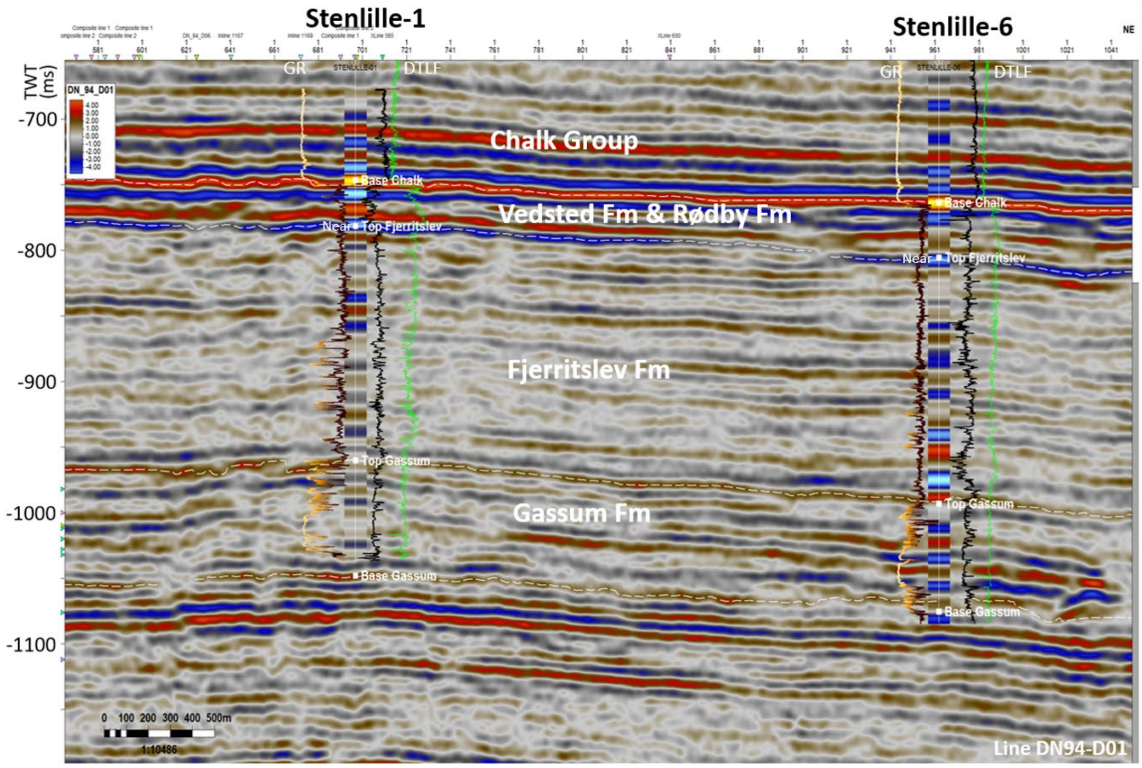

Figure 6.1.3. *Seismic section DN94-D01 (SW–NE) with well to seismic ties and well-logs (gamma ray- and sonic log) of the Stenlille-1 and Stenlille-6 wells. Synthetic seismic columns are shown down along the wells in black-grey-white and red-white-blue displays. Well-tops and formations are also marked. Location of the line (red) with projected wells is shown in the small map, where the blue line is Fig. 6.1.1.*

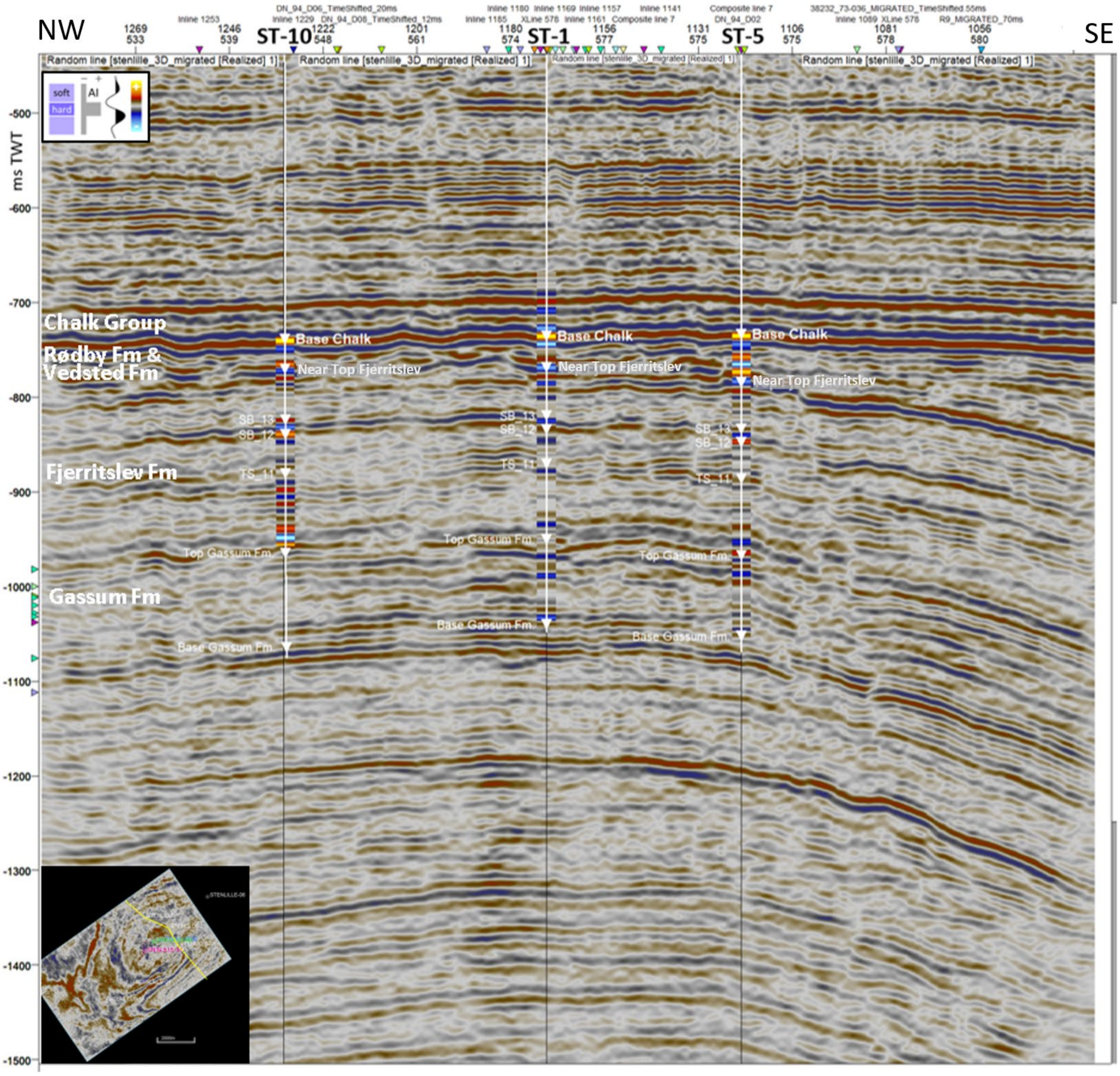

Figure 6.1.4. *Well to seismic ties to the Stenlille-10, -1, -5 wells and synthetic seismic columns on a random seismic section NW–SE through the 3D seismic survey in a red-white-blue display. Well-tops are also marked. The location of the line with projected wells is shown in the map with a time slice through the structure.*

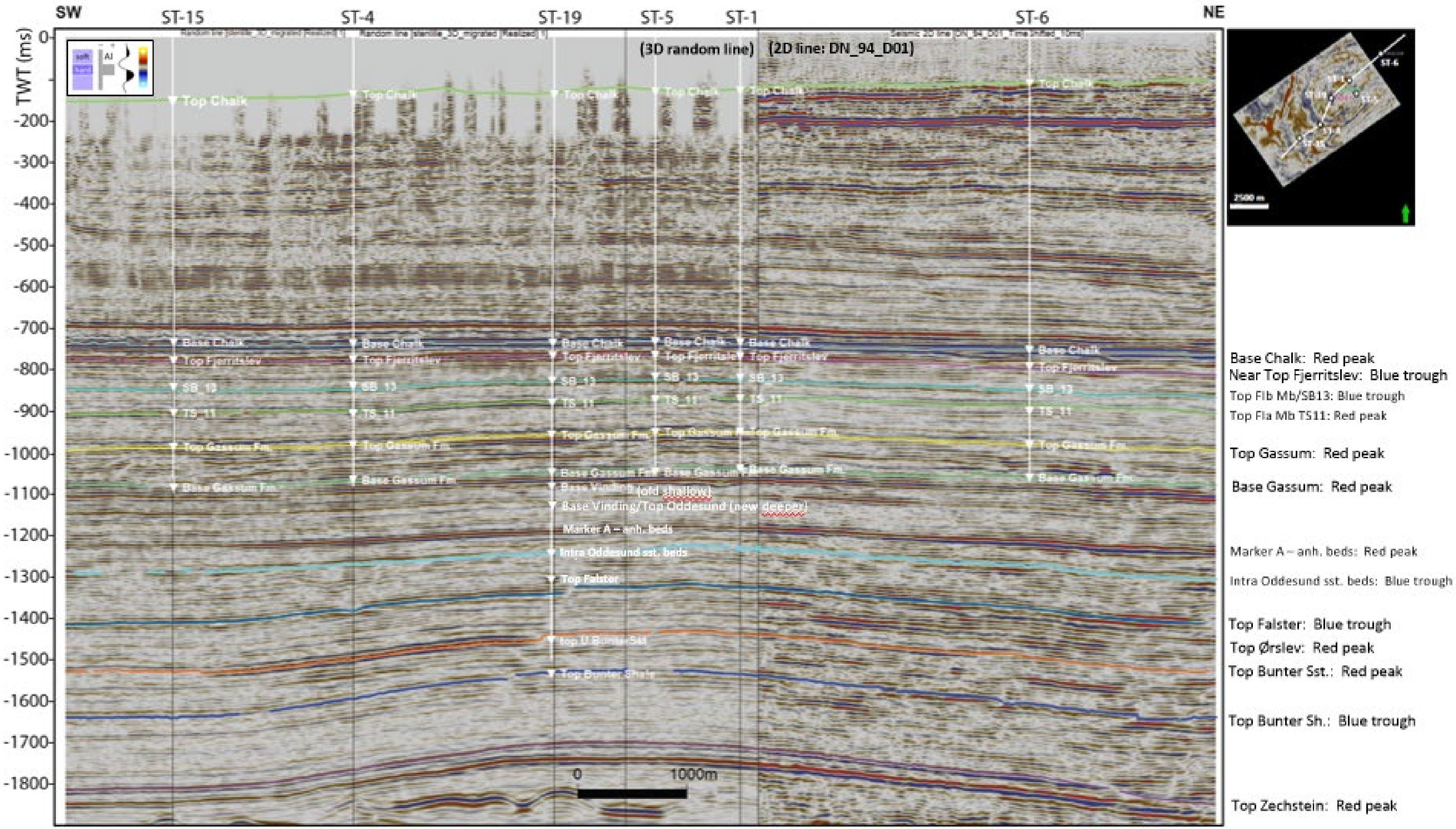

Figure 6.1.5. *Composite (3D random) seismic line and the 2D line DN94-D01 (right of ST-1), which is adjusted (10 ms) to fit the random line, including the Stenlille-15,-4,-19,-5,-1,-6 wells, well-tops, and interpreted horizons, which are defined in amplitude peak or trough.*

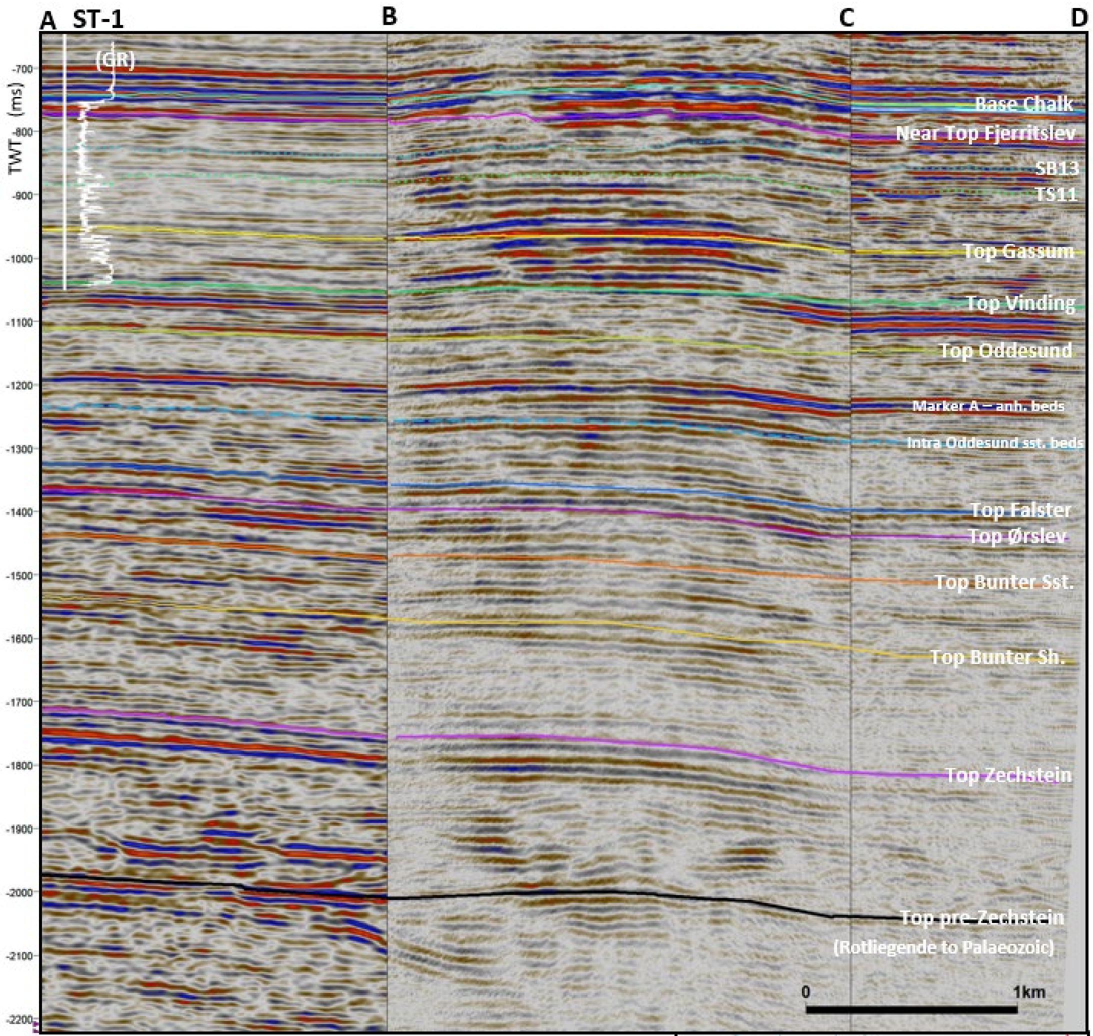

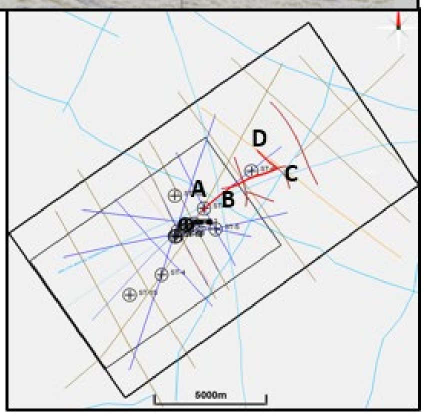

Figure 6.1.6. *Interpreted, time-shifted 2D seismic sections, including DN94-D01 (left) with the projected Stenlille-1 well (gamma ray log), and the new seismic lines GEUS22-STL-P2 (middle) and GEUS22-STL-P4 (right). Location of lines with the projected well is shown in the map.*

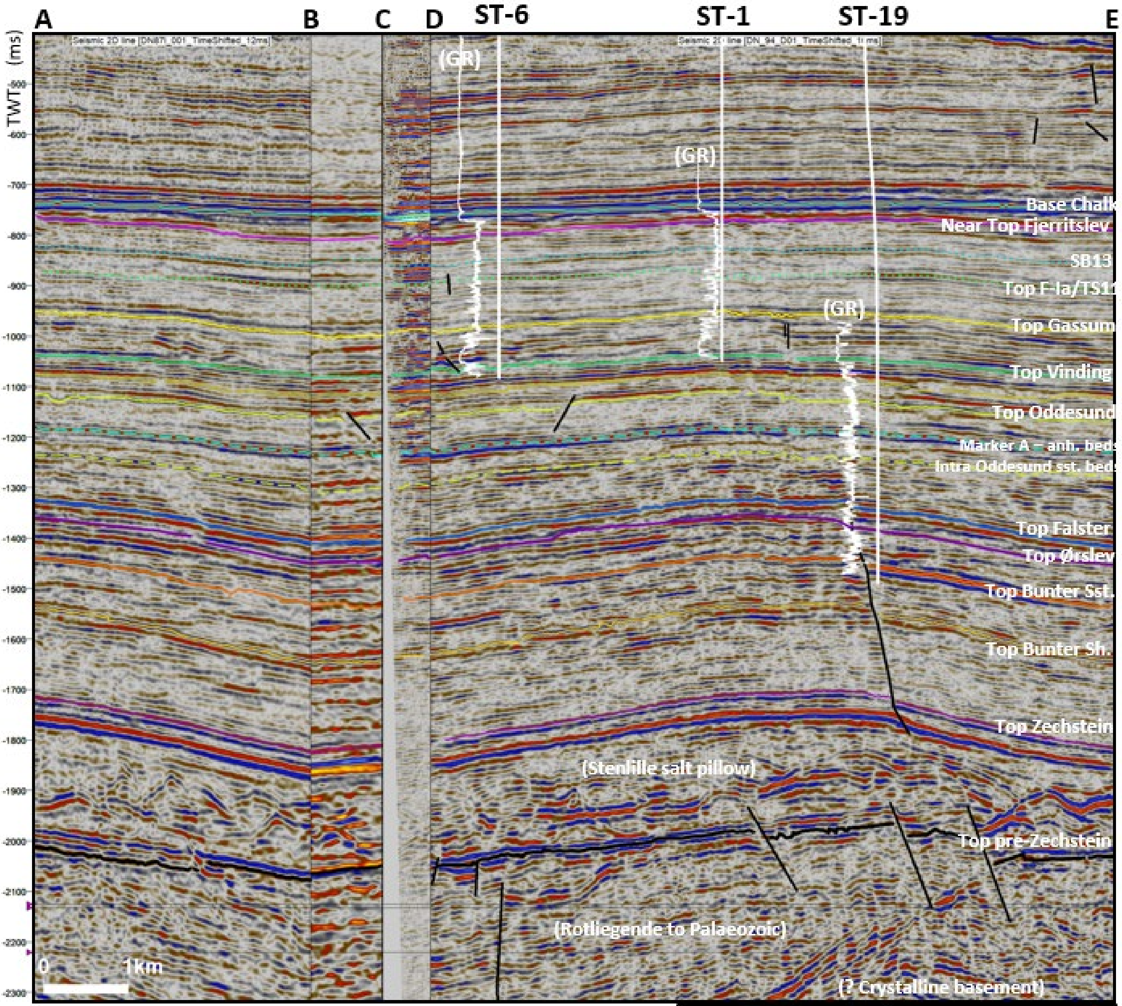

Figure 6.1.7. *Interpreted, time-shifted 2D seismic sections with older (1987, 1994) and new sections (2022), from left to right: DN87I-001, WGC81c, GEUS22-STL-P4, and DN94-D01 with interpreted horizons and few of the faults. The Stenlille-6,-1,-19 wells (offset) are shown with gamma ray log (GR). The location of composite section with projected wells is shown in the map.*

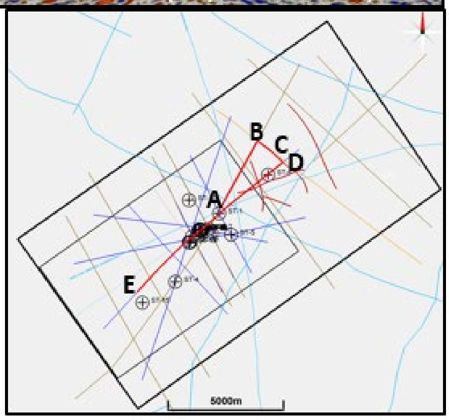

6.2 Structure description and tectonostratigraphic evolution

The seismic stratigraphic interpretation is tied to well-tops in the 3D seismic survey in most wells and extended further into the 2D seismic lines (fitted to the 3D survey) outside the 3D area, where one well (Stenlille-6) is located (Section 6.1). Maps in two-way time have been generated from horizons by gridding and smoothing (parameters - see each map figure). Figure 6.2.1 shows e.g., the three key-top reservoir surfaces in two-way time: Top Gassum, Intra Oddesund sst. beds and Top Bunter Sst. with their lowermost closing contour.

In Figure 6.2.2 the most important for the gross stratigraphy and top reservoir division are shown (shallow to deep): (A) Base Chalk, (B) Near Top Fjerritslev, (C) Top F-Ia Mb, (D) Top- & (E) Base Gassum, (F) Intra Oddesund sst. beds, (G) Top Bunter Sst., and (H) Top Zechstein is included to show a morphology affecting overlying horizons.

Figure 6.2.3 shows the depth converted maps of the five key horizons for the gross division of the Stenlille structure into top reservoir and seal containing formations (shallow to deep): (A) Base Chalk, (B) Near Top Fjerritslev, (C) Top Gassum, (D) Intra Oddesund sst. beds, (E) Top Bunter Sst. For depth conversion procedure see Chapter 5.

Fig. 6.2.4 shows key isochore maps including the (A) Chalk Group, important for depth conversion, and the primary seal and reservoir formations: (B) Fjerritslev Fm, and (C) Gassum Fm.

The maps are mainly used in the descriptions below in the sections: Description of Faults, Tectonostratigraphic evolution at the Stenlille structure, and in Section 8.1. Volumetrics and Storage Capacity.

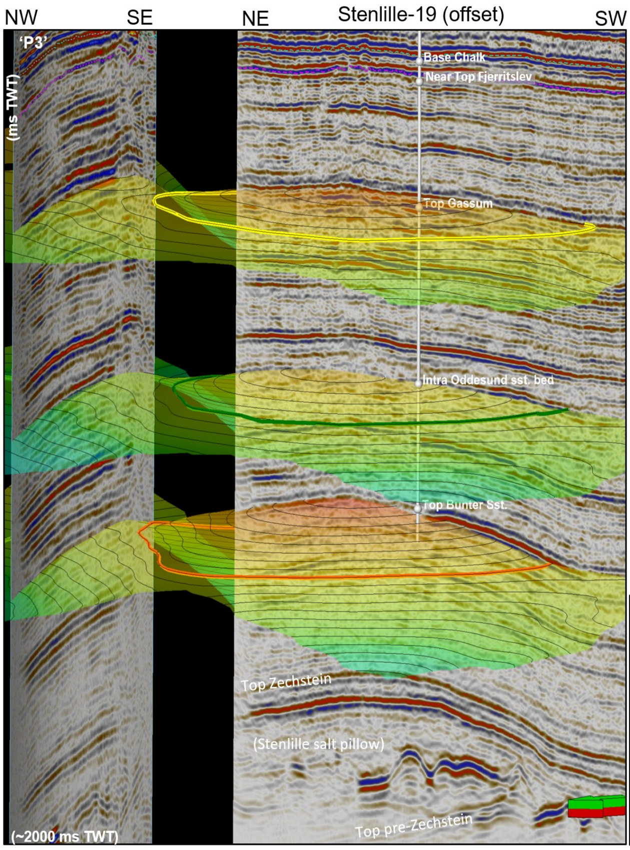

Figure 6.2.1. *Seismic sections with interpreted key horizons (no faults shown here) in a 3D display in two-way time down to c. 2 sec. and viewed towards SE. Right: A random 3D seismic section (c. 7 km long) SW–NE through a number of wells, with the Stenlille-19 well (projected) and well-tops shown. Left: The new 'P3' seismic section (GEUS22_STL_P3). Two-way time maps (3x smooth iteration, no faults shown), individually coloured by depth in time, are shown with the lowermost closing contour coloured for each of the surfaces: Top Bunter (orange), Intra Oddesund sst. beds (green) and Top Gassum (yellow). The small green and red arrow in the lower right corner points north and the small map shows the location of the sections and the view (blue arrow) towards SE.*

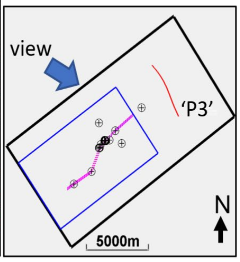

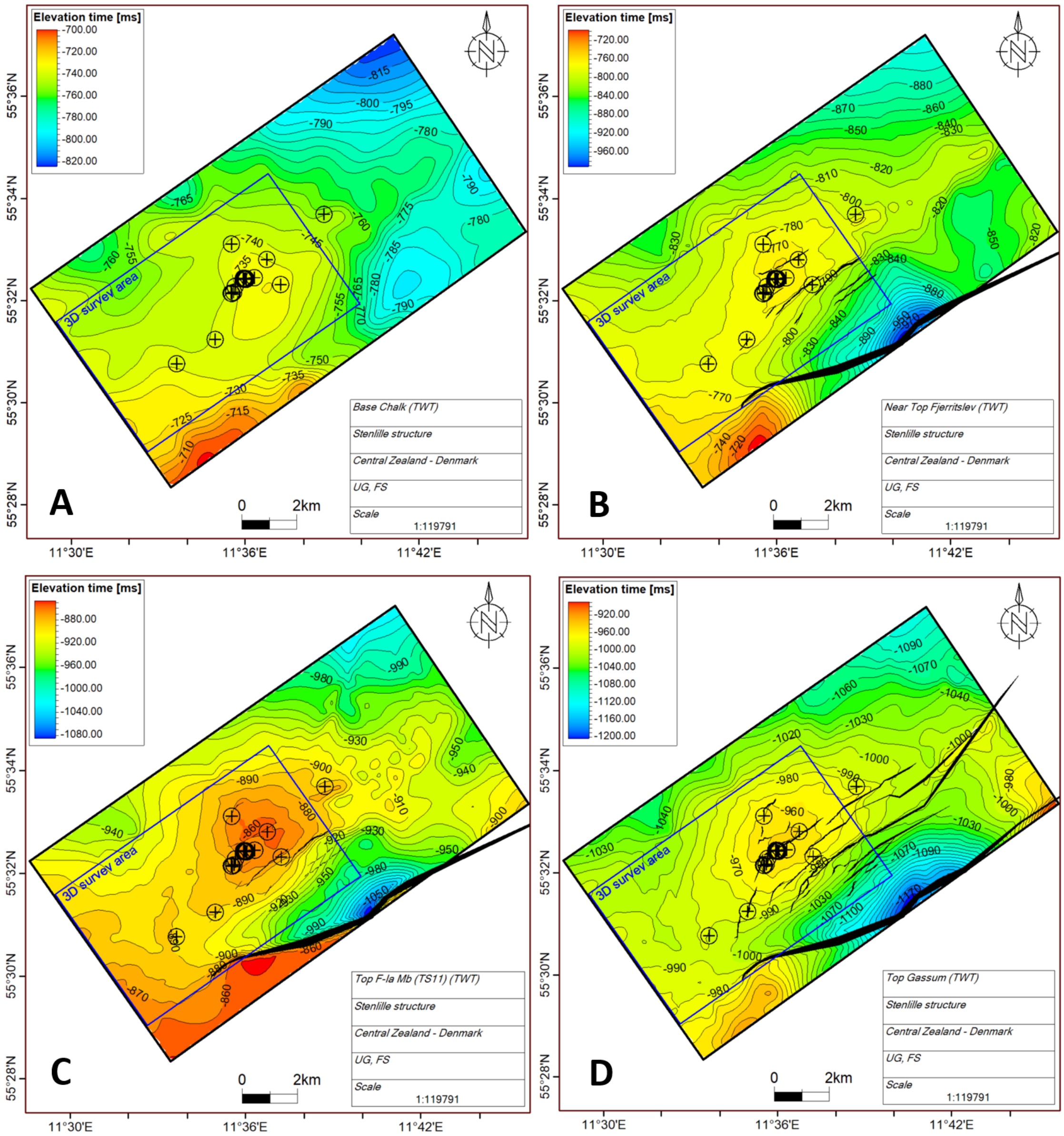

Fig. 6.2.2. *Depth-structure maps in milliseconds two-way time (ms TWT) with largest faults shown in B–D (black polygons). The maps are produced with a 100x100 m grid and smoothed (iterations: x10 for A; x1 for B–D) and a contour interval of 5 ms TWT (A) and 10 ms TWT (B–D).*

A: Base Chalk map; B: Near Top Fjerritslev map; C: Top F-Ia (TS11) map; D: Top Gassum map.

The maps show increasing relief with depth of the central Stenlille structure, trending SW–NE, mostly as a 4-way dip closed structure, but partly cut by SW–NE trending faults, mostly near Top Gassum. The deepest closing contour at Top Gassum is 990 ms TWT, which has an area of ~25 km2 and the surface has its top point within the closure at c. 950 ms TWT (depths are below mean seal level).

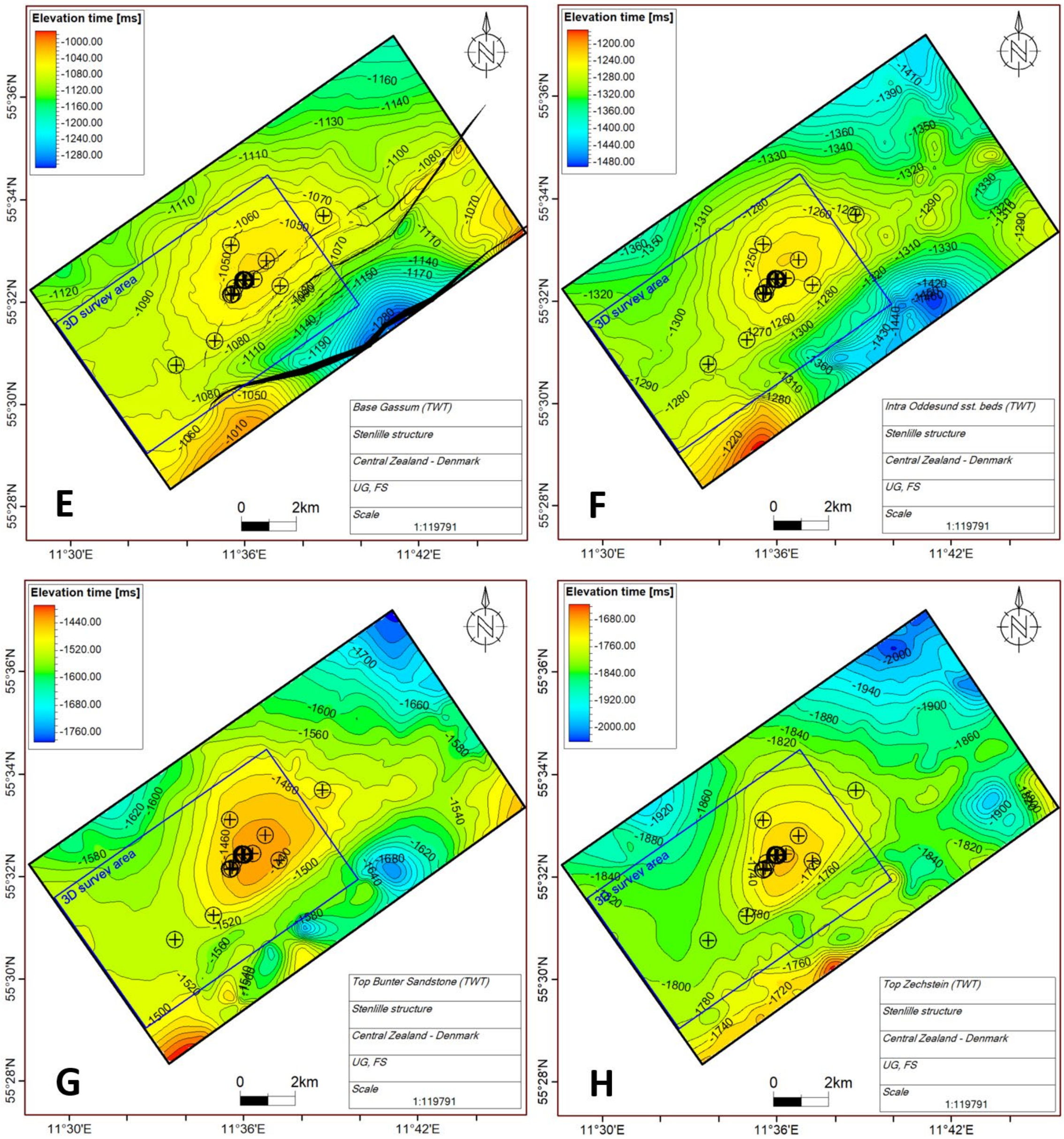

(**Fig. 6.2.2. – continued**). *Depth-structure maps in milliseconds two-way time (ms TWT).*

E: Base Gassum map; F: Intra Oddesund Sst. map; G: Top Bunter Sst. map; H: Top Zechstein map. The largest faults shown only in E (black polygons). Faults of F and G are shown from Machine Learning in Fig. 6.2.7b and 6.2.7a, respectively. The maps are produced with a 100x100 m grid and smoothed (iterations x1) and a contour interval of 10 ms TWT for E & F and 20 ms for G & H (depths are below mean seal level).

The maps show approximately similar outlines of the central Stenlille structure, trending SW–NE, mostly as a 4-way dip closed structure, but slightly more triangular at depth. The similar outline and similar position of the mapped structure overlying the domed Top Zechstein, which is cored by salt, support that the Stenlille structure is mainly formed by the salt pillow evolution. See also cross sections (Figs 6.2.1, 6.2.2). Mapping of F, G, and H include PaleoScan™ in the 3D area.

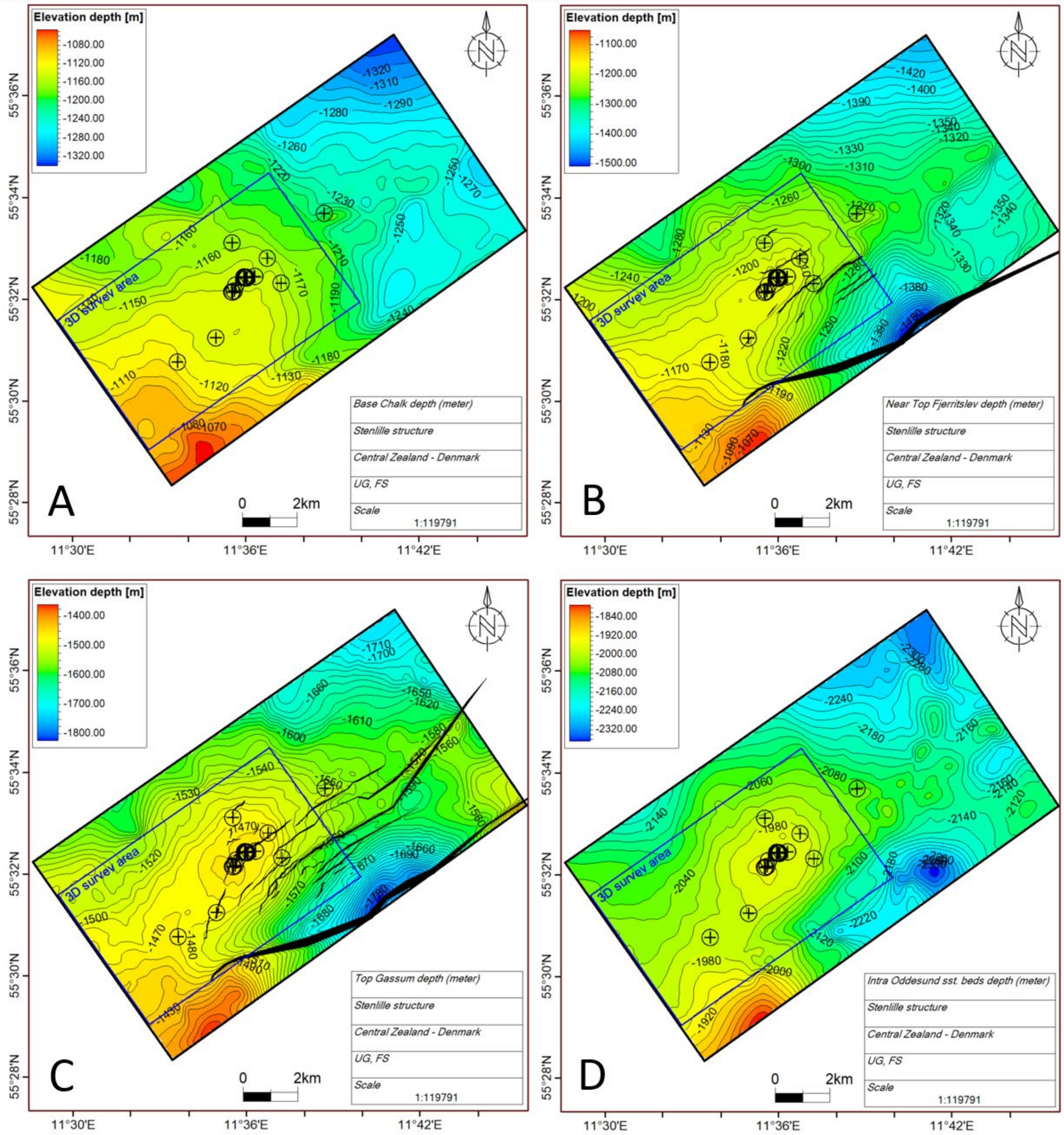

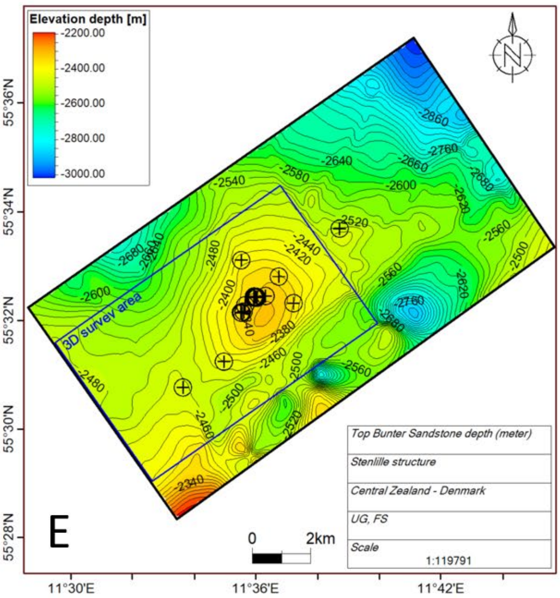

Fig. 6.2.3. *Depth-structure maps in meter (m): A: Base Chalk; B: Near Top Fjerritslev; C: Top Gassum; D: Intra Oddesund Sst.; E: Top Bunter Sst. The largest faults are shown in B & C (black polygons). The maps are produced with a 100x100 m grid and smoothed (iterations: x10 for A; x1 for B–E). The contour interval is 10 m for A, B & C, and 20 m for D & E.*

Note that the area within the lowest closed contour at Top Gassum (C) is smaller than in the time depth map of the horizon (Fig. 6.2.2.D). The unsmoothed Top Gassum depth map, with the closure shown at 1475 m in Fig. 8.1.1 is used for volumetrics (Chapter 8). The deepest closing contour of the Intra Oddesund sst. beds (D) and the Top Bunter Sandstone (E) shown here are 1980 m and 2460 m, respectively (depths are below mean seal level).

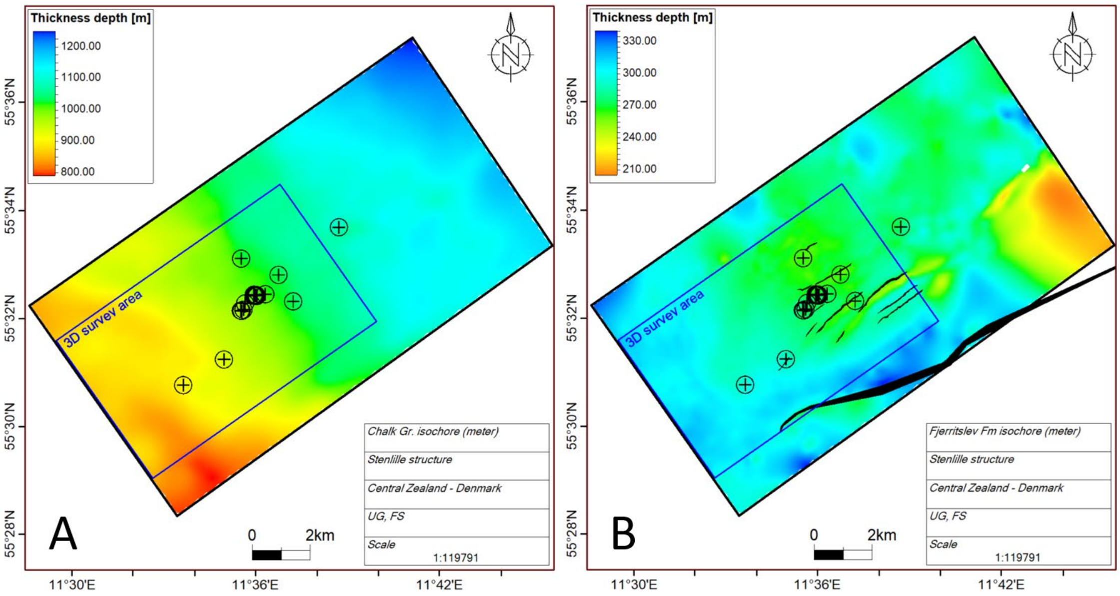

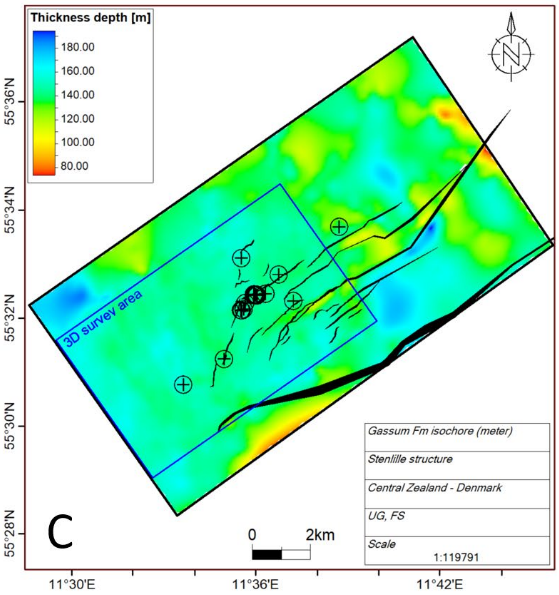

Fig. 6.2.4. *Isochore maps in meter (m) with largest faults shown in B & C (black polygons). A: Chalk Group; B: Fjerritslev Fm; C: Gassum Fm. The maps are produced with a 100x100 m grid and smoothed (10x iterations). In B & C the largest peak values are removed a few places along the southern mapping boundary and the major F1 fault.*

In the central part of the Stenlille structure the thicknesses mostly are A: Chalk Group: c. 900–1100 m; B: Fjerritslev Formation: c. 260–300 m; C: Gassum Formation: c. 140–160 m.

Description of faults

Faults may act as potential leakage pathways across and along faults but may also act as potential barriers for pore-fluids. Therefore, fault interpretation and mapping are important for evaluating reservoir fluid mobility and cap-rock integrity. Furthermore, mapping of faults may provide insight into the geological evolution and setting of the investigated area.

A manual interpretation of the 2D and 3D reflection seismic sections is performed, and supported by various seismic attributes, including ant-tracking, semblance and coherency. The focus was on larger faults in the primary reservoir succession in the Gassum Fm and the primary seal successions of the Fjerritslev Fm and in overlying secondary seal successions of the Vedsted−Rødby Formations and in the Chalk Group. The faults were interpreted vertically and laterally (Fig. 6.2.2–6.2.6).

In particular, fault systems that appear to be connected vertically from top reservoir up through the seal successions are important to reveal for describing the seal integrity. Some of the deeper faults near the top and above the Bunter Sandstone Fm and intra Oddesund Fm sandstone beds were also identified in connection to a possible secondary reservoir-seal potential. Faults interpreted manually in this study, are compared to the Machine Learning (ML) derived fault probability, both vertically and laterally (Fig. 6.2.5–6.2.8). In addition, deep faults to basement were interpreted at sections from the Stenlille area to the Slagelse-1 (Fig. 6.2.14, -15) to describe the regional structural evolution. See also description of these studies in Gregersen et al. (2022) and Lorentzen et al. (2022).

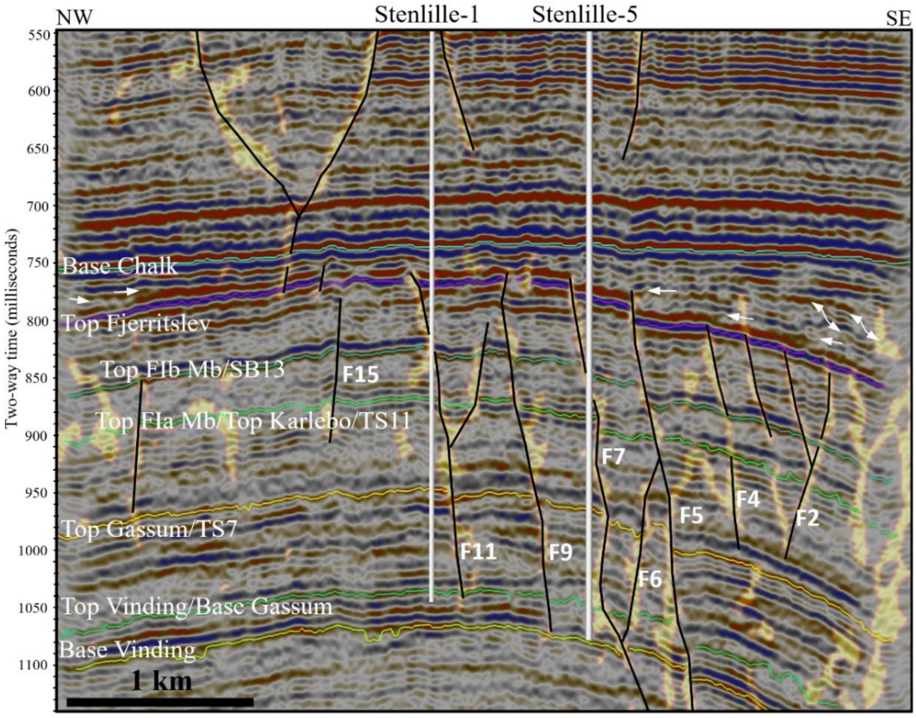

Figure 6.2.5. *X-line 578 (3D) with ST-1,-5 wells (projected) and details of the Stenlille structure. Interpreted horizons are coloured and manually interpreted faults (numbers – see Fig. 6.2.6) are vertical black lines. Vertical yellow zones mark fault probability (0.8−1.0) from a Machine Learning study by Lorentzen et al. (2022), which helped to predict fault patterns both vertically and laterally (Fig. 6.2.6). White arrows indicate onlap and toplap probably of the Vedsted Formation interval, that overlies the inconformity at the (Near) Top Fjerritslev horizon, where most deeper faults terminate. Cretaceous faults seem to have minor connections into the Fjerritslev Formation below Top Fjerritslev. From Gregersen et al. (2022).*

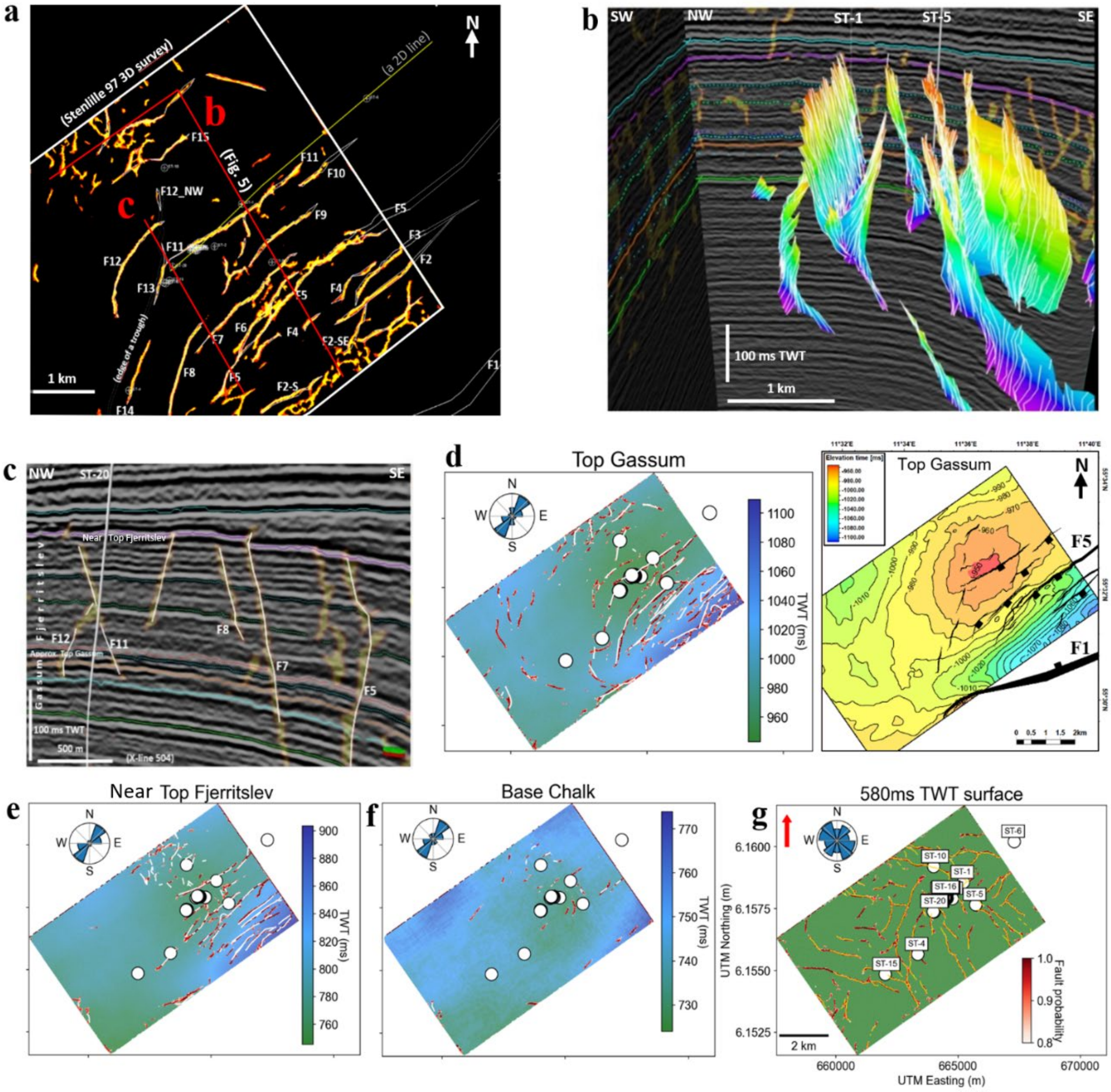

Figure 6.2.6. *More than fifteen manually interpreted fault polygons (thin white numbered lines) and numerous yellow Machine Learning (ML) faults of Gassum Formation-Fjerritslev Formation (5 ms below to 15 ms TWT above Top Gassum); b. Manually interpreted fault sticks (3D) coloured by TWT depth in Gassum-Fjerritslev Formations and yellow ML faults. Location & scale are similar to Fig. 5; c. Manually interpreted fault sticks (2D) and yellow ML traces on Xline 504 (location in 6a); d. Left: Map of Top Gassum with both fault stick traces (white) and ML fault traces (red). Right: Same horizon with manual interpreted fault polygons (black). Northing/Easting, km-scale and wells (white circles) are shown in g; e. Map of (Near) Top Fjerritslev with both fault stick-traces (white) and ML fault traces (red); f. Map of Base Chalk with both fault stick-traces (white) and ML fault traces (red); g. Map of 580 ms TWT (time slice) cutting through the lower part of the Chalk Group (see e.g., this time level and faults in Fig. 6.2.7) with ML fault traces (red) and Petrel generated fault traces (yellow). ML faults are generated and described by Lorentzen et al. (2022). Note the dominant NE-SW fault directions of Top Gassum-Fjerritslev, and the changed fault directions in the lower-mid (at 580 ms) Chalk Group, mostly trending NW−SE and WNW−ESE, and some NE−SW. From Gregersen et al. (2022).*

Machine Learning to support fault identification and interpretation

In addition to manual interpretation and mapping of faults through seismic sections using various attributes, a Machine Learning (ML) model was applied to the seismic data to highlight likely fault locations. Many seismic attributes exist that provide some indication of where faults may exist in the subsurface such as semblance, coherency and ant-tracking and are often used for extracting faults and manual interpretation of faults. These attributes rely on the seismic reflection continuities and discontinuities to locate the faults. However, outlining faults in seismic data based on such attributes can be ambiguous and time-consuming, and the methods are inclined to map other stratigraphic or lithological facies variations. Using a supervised machine learning approach, the fault mapping task can be regarded as a basic image segmentation task. By applying a Convolutional Neural Network (CNN) model, faults can be segmented based on learning from synthetic or interpreted field data with faulting (Lorentzen et al. 2022).

A state-of-the-art open-source CNN model has been used with a U-Net structure on 3D post-stack seismic data covering the Stenlille structure by Lorentzen et al. (2022) and included for this project. The CNN model has previously been trained on synthetic post-stack seismic cubes with planar faulting and has proved to map faults accurately in field data compared to other fault mapping methods in other studies. The input to the trained CNN model is the 3D post-stack seismic data from Stenlille, and the output is a 'fault posterior probability' cube. The fault mapping results from Stenlille are compared with traditional seismic attributes such as the variance and ant-tracking as well as a manual interpretation. The results show that the CNN model predicts fault patterns that are more consistent with the manual interpretation. In some cases, the CNN model even predicted subtle faults that were overlooked in a manual interpretation. The CNN model has provided new fault details in the Stenlille reservoir unit that may serve as an important input to build a robust static model. The neural network predictions are, however, in some cases patchy and lack coherence, which may lead to erroneous fault predictions. Therefore, the CNN model should be treated as an additional fault interpretation tool for the interpreter to quality check in a critical manner. The fault-probability, here shown in yellow, are scaled to 80−100% probability (binary colour coded: '1'= 80-100% fault probability, whereas '0' (no colour) < 80%) of reflection discontinuity, which represents mostly faults (Fig. 6.2.5, 6.2.6a-c). This comparison between the manual interpreted and ML faults improves the understanding significantly of the fault patches and provide more accurate and detailed fault networks. Manually interpreted faults are mainly located at clear breaks and displacements in reflections and successions, whereas the ML fault predictions are also sensitive to less visible breaks and subtle features (Fig. 6.2.5, 6.2.6c). Such features may also include boundaries of channels, mounds, seismic facies change due to changed lithology, fluids, etc., but also seismic noise. The significant details of ML fault-probability traces can provide important data for evaluations of fault risks, seal-integrity, etc., not least of prospects for storage CO_2 or other resources.

Fault interpretation

We focus here on the Gassum and Fjerritslev Formations as the primary reservoir and seal successions, respectively. The Stenlille structure has a number of faults in its top and eastern flank, in particular in the Gassum and Fjerritslev Formations, and less apparently in the overlying successions of the Vedsted to Rødby Formations and the lowermost part of the Chalk Group (Fig. 6.2.5−6.2.8).

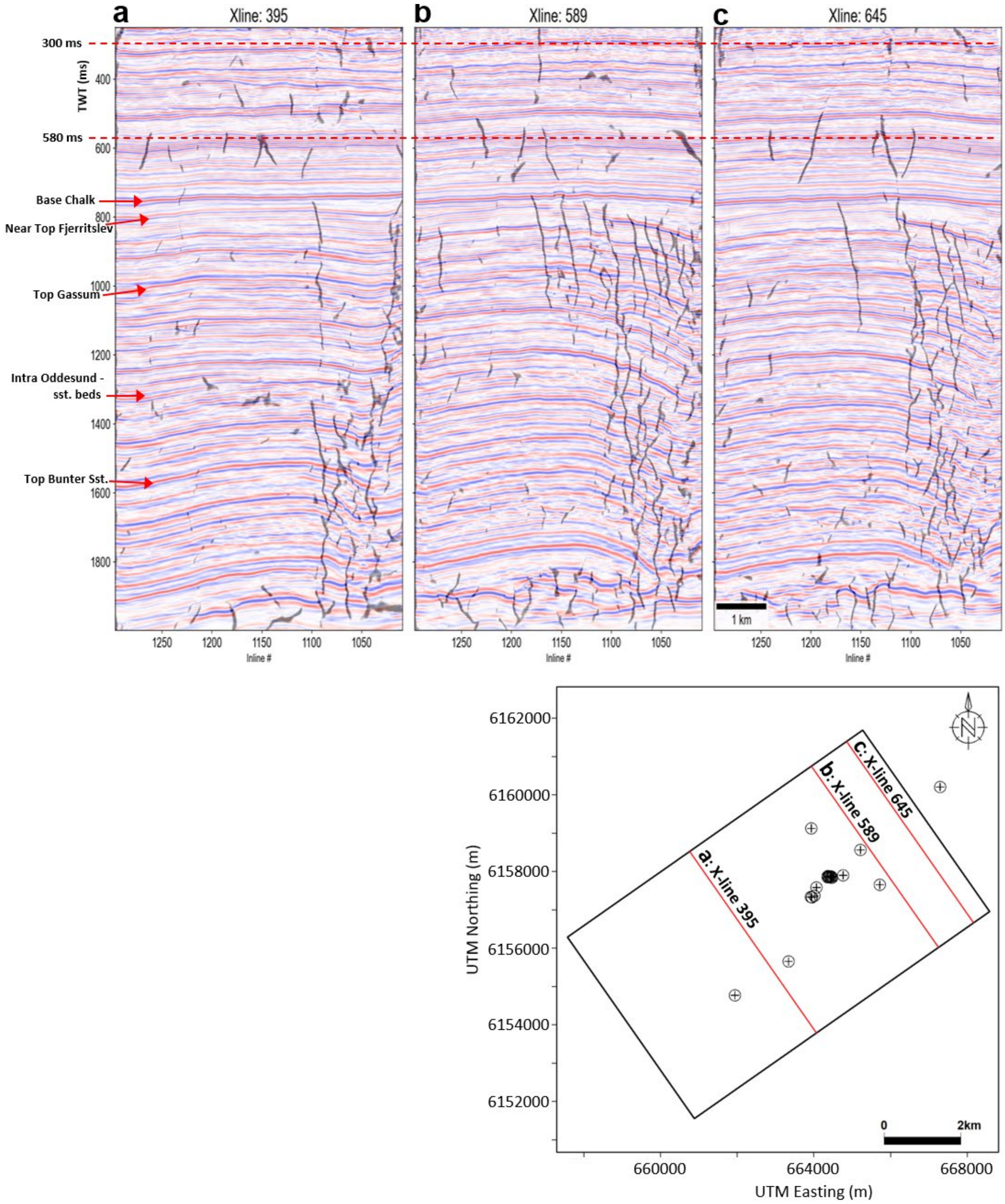

Figure 6.2.7. *Seismic sections (a: x-line 395; b: x-line 589; c: x-line 645) with ML faults (80–100% probability) and surfaces in Fig. 6.2.6 and 6.2.8, where fault probabilities have been extracted. Note the many faults towards SE, most terminates at Near Top Fjerritslev horizon level and some appear further up within the Chalk Group (above Base Chalk), apparently with few connections in these displays. Others displays show few connections from Near Top Fjerritslev and up into the Chalk Group, where faults are rather segmented and most extensive in lower parts around the 580 ms TWT level. Locations of the X-lines are shown in the insert map with outline of the 3D seismic survey Stenlille-97.*

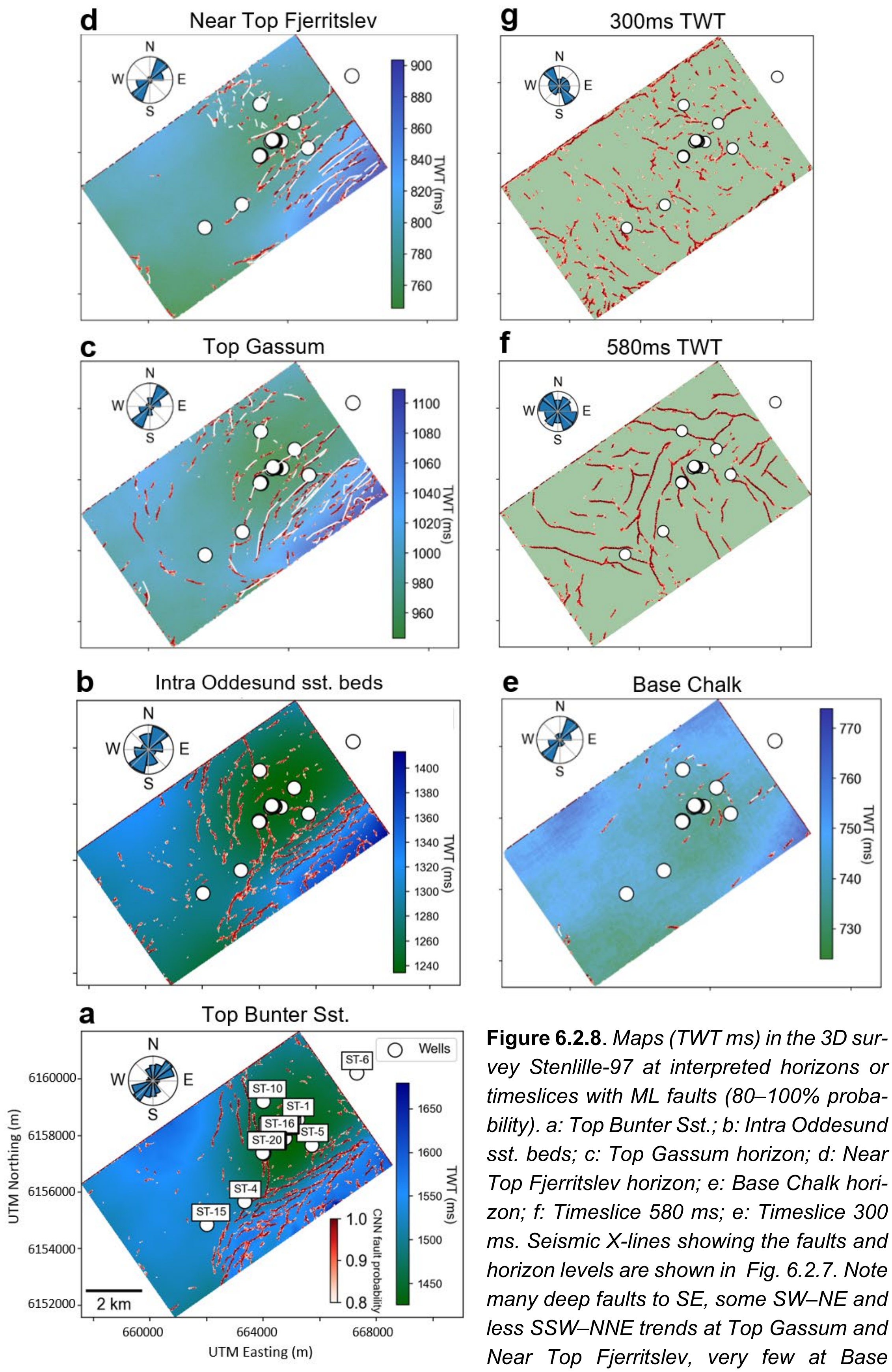

Figure 6.2.8. *Maps (TWT ms) in the 3D survey Stenlille-97 at interpreted horizons or timeslices with ML faults (80–100% probability). a: Top Bunter Sst.; b: Intra Oddesund sst. beds; c: Top Gassum horizon; d: Near Top Fjerritslev horizon; e: Base Chalk horizon; f: Timeslice 580 ms; e: Timeslice 300 ms. Seismic X-lines showing the faults and horizon levels are shown in Fig. 6.2.7. Note many deep faults to SE, some SW–NE and less SSW–NNE trends at Top Gassum and Near Top Fjerritslev, very few at Base Chalk, some with new directions at 580ms and some, less continuous at 300ms. Work extended from Lorentzen et al. (2022).*

In large parts of the structure, most faults to the Top Fjerritslev horizon seem to displace more or less equal thicknesses in both the Gassum and Fjerritslev successions (Fig. 6.2.4B,C, 6.2.5) and as the Gassum Fm has little thickness variations, this imply that most of the significant faults are formed after the deposition of the Gassum Fm and most of the Fjerritslev Fm.

As some of the significant faults continues up through the Fjerritslev Fm and more or less stops at the unconformable Near Top Fjerritslev horizon, they were probably formed during late part or after deposition of the Fjerritslev Fm, related to the doming of the structure, mainly caused by the salt pillow growth.

The Stenlille F1 fault SE in the study area, south of the Stenlille structure (Fig. 3.4, 6.2.6), is a large, deep normal fault, seated SE of the salt dome, which evolved from mid-Jurassic time. The F1 fault shows throw at the Top Gassum of c. 150−180 ms, with similar order of throws of the deeper horizons and units (c. 170−200 ms) down to Top Zechstein. The Stenlille structure was formed as response to the formation of the salt pillow, and faults at the flanks are probably related to the growth of the structure, and at the fault zone to the SE (F1 fault) also related to salt withdrawal and roll-over.

The Fjerritslev Formation between Top Gassum and Near Top Fjerritslev horizons thickens in the hanging wall syncline towards fault F1 (Fig. 6.2.4B), indicating growth fault evolution of a primary syncline of salt doming, and the throw at the Near Top Fjerritslev is less than c. 70–80 ms and mostly 10–30 ms, possibly in part due to erosion (Fig. 3.4, 6.1.1, 6.2.5). Apparently, it is primary the uppermost part of the Fjerritslev Formation succession (probably the F-III and F-IV members), that thickens towards the fault. The structure top is offset by faults, south and east of the Stenlille-1 well, at the southern flank of the doming structure (Fig. 6.2.2B, 6.2.5).

Most faults in Gassum and Fjerritslev Formations in the Stenlille structure have mainly minor, normal and in some cases reverse throws, mostly less than c. 30 ms or c. 30−50 m (Fig. 6.2.5). Most faults are located along the anticlinal NE−SW trending axis of the structure, in its top and its SE flank, and a few faults trend N-S (Fig. 6.2.6). The deepest-seated faults occur along the SE structure flank, and some of these sole out deep into the salt pillow (Fig. 6.1.1, 6.2.7), indicating that they are related to the structural deformation due to the doming of the structure. The most prominent fault in the structure top SE of well ST-5, is the F5 fault (Fig. 6.2.5, 6.2.6). Also, the shallower Gassum−Fjerritslev faults ending at the Near Top Fjerritslev horizon are mainly related to the doming of the salt pillow in parts of Middle- to Late Jurassic times.

The manually interpreted fault polygons and ML fault trends both show consistent, mostly NE−SW fault directions at both the Top Gassum and Near Top Fjerritslev surface maps (Fig. 6.2.2, 6.2.3, 6.2.8c,d). Recent studies show that some of the near Top Gassum faults identified by mapping (F11, F13 and F14) and Machine Learning may compart the Gassum Formation reservoir zones and seem to restrict predicted natural gas in some cases (see section below: Seismic reservoir characterization; Bredesen et al. 2022).

At the Base Chalk surface (Fig. 6.2.8e) there are less faults, but still with NE−SW trends. This indicates relatively few clear fault connections between the Lower Cretaceous successions and the Upper Cretaceous Chalk Group. However, breach of seals may occur even with few and subtle faults, and such risks have to be investigated and assessed thoroughly before injecting CO_2. There as some faults in the Chalk Group, but faults in the shallow section is difficult to reveal, e.g., due to noise, and storage should in general keep safely away from faults. However, the long-term, safe storage of natural gas at Stenlille indicates competent sealing successions.

The Near Top Fjerritslev is a significant seismic reflection trough with increasing acoustic impedance and the overlying successions (mostly of the Vedsted Formation) onlap this horizon (Fig. 6.1.1, 6.2.5). The Near Top Fjerritslev horizon is close to (or near below) a major unconformity (hiatus), separating Lower Jurassic (Toarcian age) deposits of the Fjerritslev Formation from the Lower Cretaceous Vedsted Formation (Fig. 6.1.1; see also discussion of ages in Section 8.2).

The youngest part of the Fjerritslev Formation in the Stenlille area is correlated to the F-III and F-IV members of the Fjerritslev Formation. In some of the Stenlille wells the uppermost preserved part of the Fjerritslev Formation (at or slightly above the Near Top Fjerritslev horizon) seems to be of a latest Early Jurassic (Toarcian) age, whereas overlying deposits may belong to the Vedsted Formation of an Early Cretaceous age (Nielsen 2003; Pedersen et al. 2022) - see the discussion in Section 7.2. Thus, Middle and Late Jurassic deposits may be missing at the crest of the structure. The erosion and hiatus may be slightly different depending on the position on the structure, and flanks of the structure would probably have less erosion and more preserved successions, possibly also including uppermost parts of the Fjerritslev F-IV member. The major unconformity (hiatus) marks the formation of the Stenlille structure mainly due to formation of the underlying salt pillow, but possibly also due to regional uplift and erosion. The unconformity may be equivalent to the 'Base Middle Jurassic unconformity' or 'Mid-Cimmerian Unconformity' (Nielsen 2003), and is associated with uplift and erosion or nondeposition (a major Middle- to Late Jurassic hiatus) over structures and margins of the Danish Basin, including the Ringkøbing-Fyn High in central and southern Denmark (Fig. 3.6).

The Lower Cretaceous Vedsted and Rødby Formations are part of the seismic stratigraphic wedge, which onlapped the Near Top Fjerritslev horizon after the formation of the elevated Stenlille structural dome and seems to have only few faults (Fig. 6.2.5, 6.2.7). The Rødby Formation is overlain by the regional Upper Cretaceous Chalk Group, and around this transition and in basalt parts of the Chalk Group (at Base Chalk), also only few faults are observed from the ML method (Fig. 6.2.7, 6.2.8). Slightly shallower, in the lower to middle parts of the Chalk Group (e.g., at 580 ms TWT), more extensional faults occur (Fig. 6.2.7, 6.2.8) as sets of small half-grabens in and below the high-reflective succession (c. 550−600 ms) trending in three directions, mostly NW−SE and WNW−ESE, and less NE−SW, due to renewed tectonism (Fig. 6.2.8f). Slight inversion may be recognized as gentle elevation over the top of the Stenlille structure (Fig. 6.2.5).

In the shallower successions above c. 500 ms TWT, faults are more difficult to track in the 3D seismic data mainly due to noise dat. Thus, data improvements and new data focused on the shallow section is recommended for further evaluations. The new seismic data of the GEUS2022_ST (e.g., in P3) demonstrate, that some subtle faults can be detected in the shallow successions (Fig. 4.2.6, 6.1.2).

In the deeper Triassic successions, near Top Bunter Sst. Fm and Intra Oddesund sst. beds, some faults are also observed, mostly trending NW–SE in the SE part of the structure and more northward or NNE further north in the structure (Fig. 6.2.7, 6.2.8a,b). Also, at these formation tops, the overlying seals are thick mudstones, as described in the well completion report and shown in well-logs (Fig. 7.1.1).

Seismic reservoir characterization: Prediction of Gassum Formation gas-sandstones and reservoir zonation

The quantitative seismic interpretation study (Bredesen et al. 2022) of the Gassum Formation in the Stenlille structure used the geophysical data of the 3D seismic post-stack volume STENLILLE-97 and the 20 wells to interrogate the following questions: (1) Is the seismic response of the natural gas stored in the Stenlille aquifer similar to a modelled CO_2 fluid at equivalent burial depths?; (2) Can the injected natural gas distributions stored within the various reservoir zones and compartments in the Stenlille aquifer be mapped?; and (3) Can the spatial reservoir heterogeneities and zone boundaries in the Gassum Formation be better resolved? The approach involved employing a set of quantitative interpretation tools based on the available 3D seismic post-stack volume and well logs to interrogate the three questions above as presented in the following sections. The approach involves employing a set of quantitative interpretation tools based on the available 3D seismic post-stack volume and well logs, including rock physics and pore-fluid substitution modelling, a relative seismic inversion, and an absolute Bayesian seismic inversion for classifying various litho-facies with separable acoustic impedances in a probabilistic framework.

Pore-fluid substitution modelling – Seismic response of natural gas vs. CO_2

To investigate the seismic response for different fluid scenarios in the Stenlille aquifer, a Gassmann fluid substitution was used. We consider three different scenarios: (1) in situ conditions, (2) replacing the natural gas with a 80%CO_2/20%CH_4 mixture, and (3) 100% water saturation. For scenario (2), the bulk modulus and density of the CO_2 and CH_4 were estimated individually as functions of the temperature and pressure conditions measured in the Gassum Formation in the Stenlille-19 well.

After calculating the acoustic properties for a 80%CO_2/20%CH_4 mixture, the seismic response for various fluid scenarios is evaluated from fluid replacement modelling. Figure 6.2.9 shows, from left to right, porosity, water saturation, density, P-velocity, and S-velocity, and synthetic seismic traces for various fluid scenarios in the Stenlille-19 well. To the right, a statistical seismic wavelet and the frequency spectrum of the 3D Stenlille seismic data is shown.

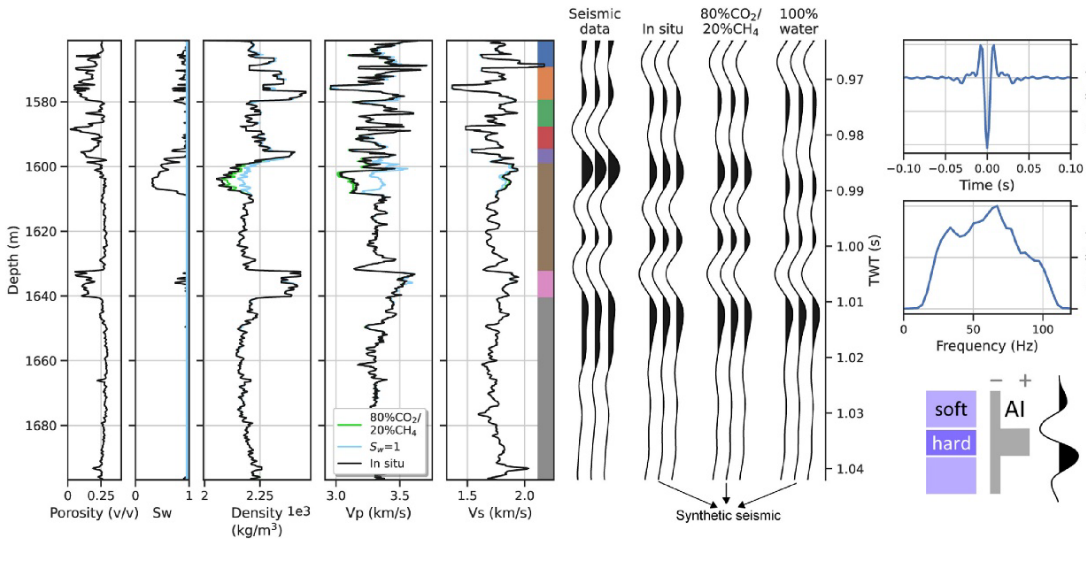

Figure 6.2.9. *Fluid replacement and synthetic seismic modelling for different fluid scenarios tied to Stenlille-19. TWT: Two-Way-Time.*

For the logs, a Gassmann fluid substitution was applied to predict two possible fluid scenarios: (1) replacing the in situ natural gas saturation with a (1) 80%CO_2/20%CH_4 mixture, and (2) 100% brine. Note how substituting 100% water decreases the peak response at the top of Zone 5 due to reduced acoustic impedance contrast. This plot indicates that the natural gas storage at Stenlille represents a good case analogue for studying how variable CO_2 saturation affects the seismic response in the Gassum Formation with a similar lithology and burial depth.

Absolute Bayesian seismic inversion – Mapping gas distributions in the Stenlille aquifer

A Bayesian inversion method has been applied based on the Stenlille post-stack 3D cube as input. In general, this type of seismic inversion can be useful for boosting reservoir resolution, incorporating geological information and classifying the seismic data into litho-fluid classes (LFC) in a probabilistic manner. The inversion requires a certain setup of preconditioned data extracted from the seismic and well log data before execution, such as interpreted horizons, a wavelet and the elastic properties of specific LFCs. Figure 6.2.10 shows a posterior probability section of the gas sandstone LFC covering the Gassum interval along an arbitrary line, intersecting Stenlille-4, 17, 18 and 1. In Stenlille-1 and 4, shale volume logs are projected on top of the probability section because the wells were drilled respectively in 1980 and 1988 prior to the start-up of gas injection.

A laterally consistent high-probability gas anomaly is prominent that aligns with the zone 3 gas saturations in Stenlille-17 and 18. The inversion also captures some more shallow gas anomalies representing zone 1 and 2, and some deeper discontinuous anomalies representing zone 5.

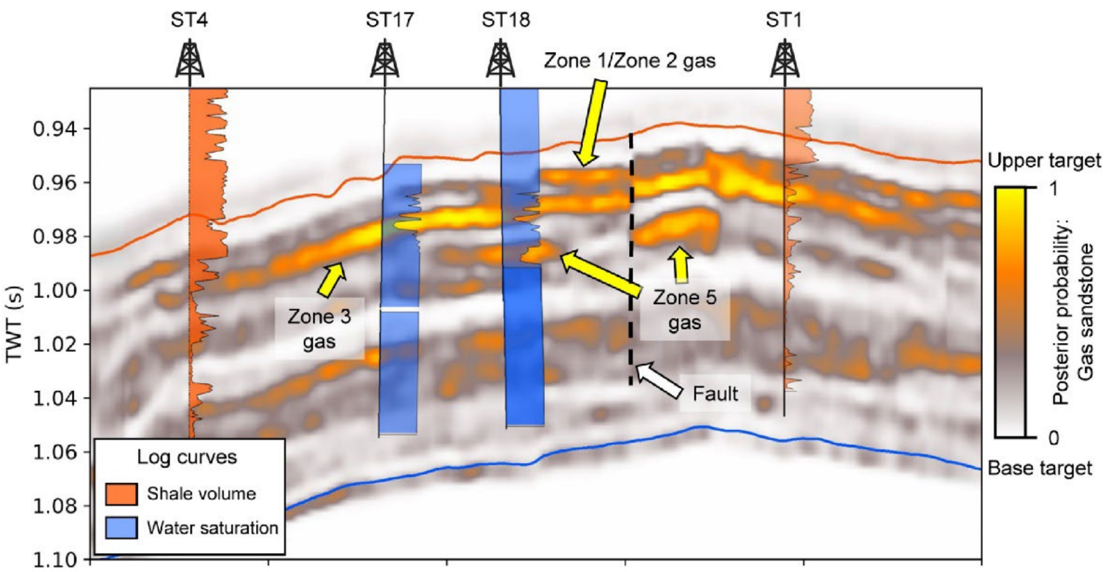

Figure 6.2.10. *Posterior probability section of gas sandstone along an arbitrary line. Water saturation and gamma ray logs from intersecting wells are plotted on top for QC.*

The main gas columns (around 70% gas saturation) in Stenlille-17 and 18 are approximately 7 and 9 m thick in zone 3, and 0 and 12 m thick in zone 5, respectively. These gas column thicknesses are in good agreement with the high-probability gas sandstone anomalies. There are also thinner gas columns in zone 1 and 2 that vary between 1-5 m in thickness at various well locations and smaller gas saturations (5–10%) that could trigger the ”fizz gas” effect for a uniform fluid mixture at the seismic scale, where it becomes difficult to seismically distinguish high and low gas saturations. However, the high-probability anomalies seem to primarily resolve the main gas accumulations, particularly within zone 3 and zone 5. The inversion also suggests some lower gas probabilities within the deeper zone 6, although not as strong as the shallower anomalies. A fault is also apparent by the abrupt time shift in the upper part of the Gassum interval, as illustrated by the black dashed line.

Figure 6.2.11 shows the posterior probability map of the gas sandstone LFC, extracted along the Upper target horizon with a +22 ms time shift applied corresponding to zone 3. A high-probability anomaly appears at the structural high and agrees well with the locations of the main injection wells into zones 1–3, namely Stenlille-2, 7, 9 and 11. On the top map, the arbitrary line in Figure 6.2.10 is illustrated by the black dashed line. On the bottom map, an additional black mask is overlaid derived from a structural dip attribute to the plane reflector, implying discontinuities, or complex reflections. The dashed white lines show some interpretations of two lineaments crossing through the gas injection area towards the top of the structure, representing faults or possibly some abrupt facies changes. The area of the high-probability anomaly corresponding to the gas injection in zone 3 is estimated to approximately 2.56 km^2.

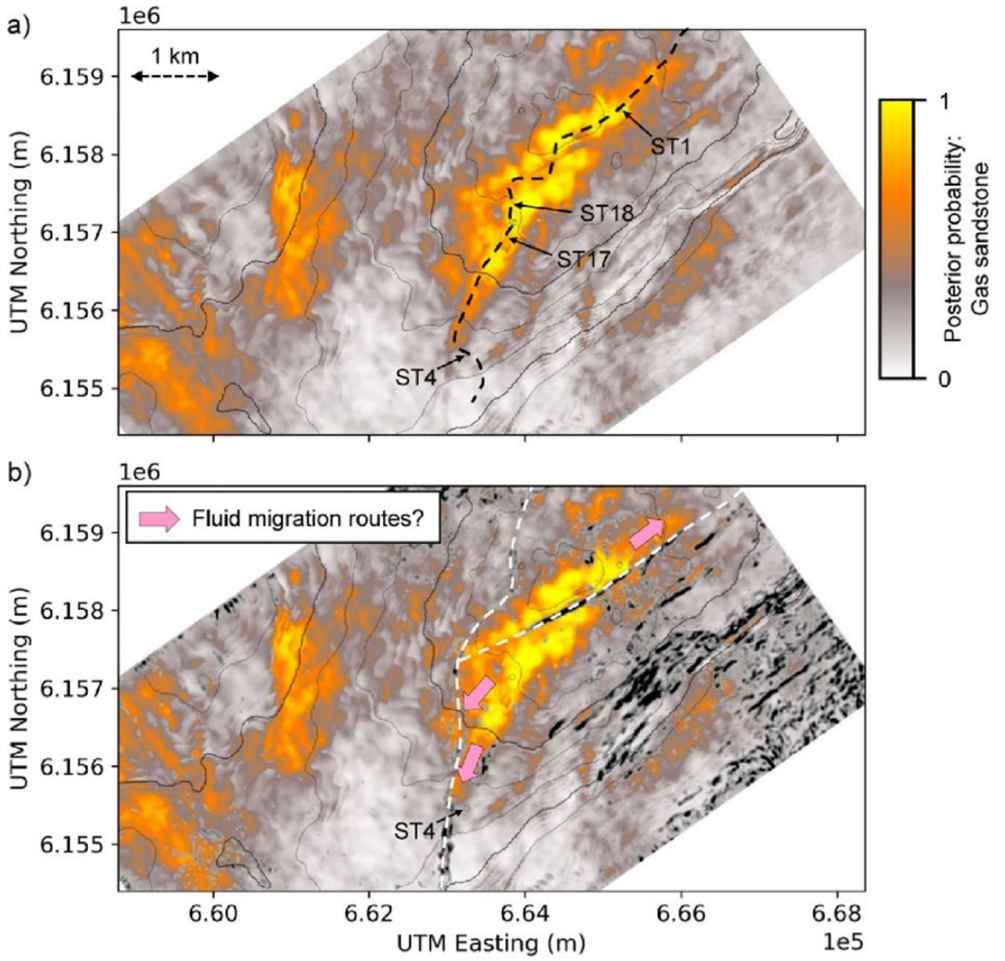

Figure 6.2.11. *Posterior probability maps of gas sandstone extracted from Upper target with +22 ms shift, corresponding to zone 3, with (a) showing the arbitrary line in Fig. 6.2.10 indicated as the black dashed line along with the intersecting wells, and (b) displaying the map corendered with a structural dip attribute seen as a black overlay mask with some interpretations shown by white dashed lines.*

Figure 6.2.12 shows the posterior probability map extracted from the Upper target horizon with a +38 ms shift corresponding to zone 5. This zone is operated as three separate compartments divided by the outlined faults as indicated in the bottom map, as the faults seem to act as fluid flow barriers. The pink arrow also points at some high-probability gas fingering which seems to follow the interpreted NW–SE fault, although the gas has not migrated as far SW towards Stenlille-4 as the gas in zone 3 in Figure 6.2.11. The area of the high-probability anomaly corresponding to the gas injection in zone 5 is estimated to approximately 1 km. Note that the gas anomaly does not conform with the top isocontour of the Upper target horizon corresponding to the reservoir apex. This is likely because the zone 5 gas injection via the anticline limbs started only two years prior to the seismic survey, and the gas plume has therefore not had sufficient time to migrate into the structural trap.

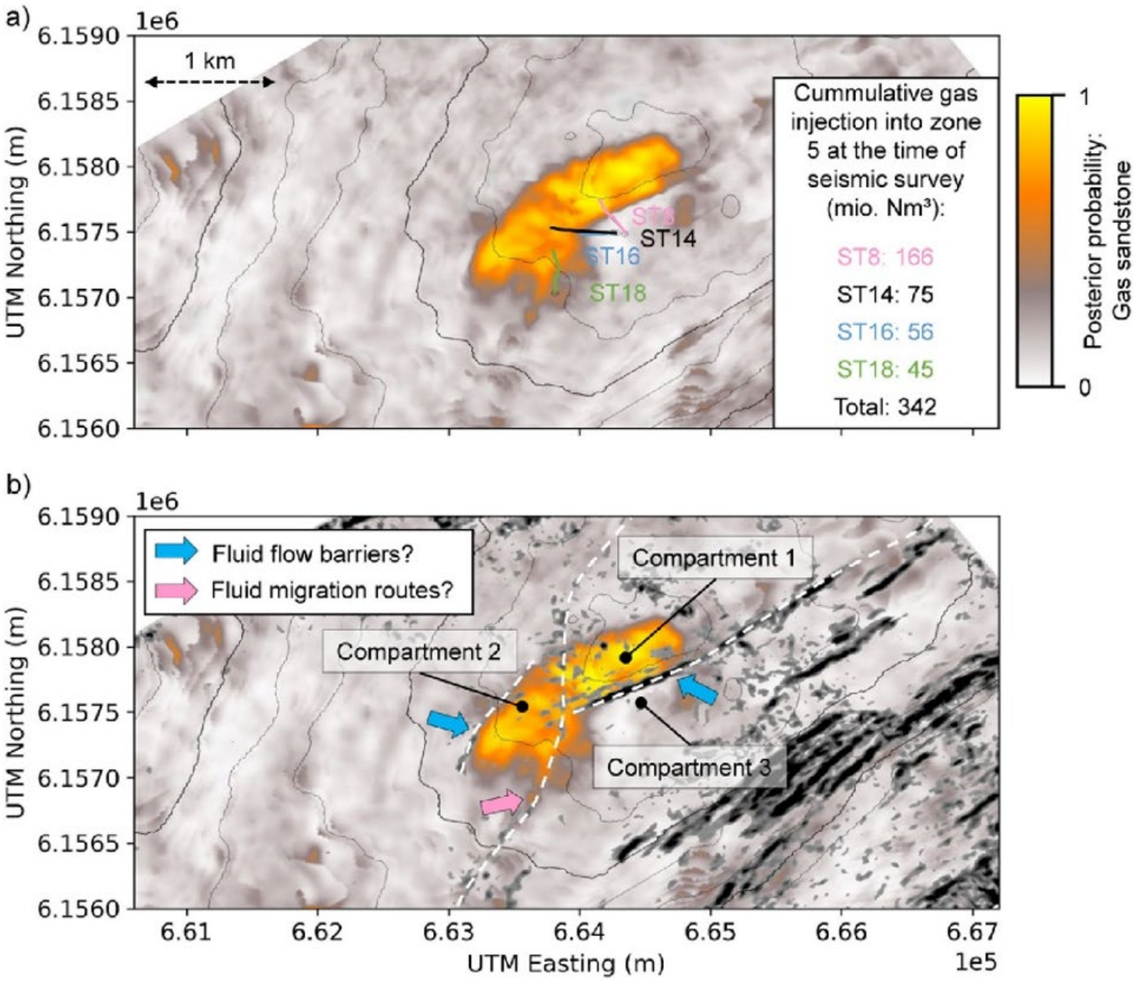

Figure 6.2.12. *Posterior probability maps of gas sandstone extracted from top of zone 5, with (a) showing the injection wells and the net gas injection volumes, and (b) displaying the map corendered with a fault attribute seen as a black overlay mask with some interpretations in white dashed lines.*

Relative impedance inversion – Delineating reservoir zonation

Besides the absolute Bayesian inversion described in the previous section, a trace integration (TI) relative inversion approach has also been tested. The TI yields a relative impedance where the aim is to shape the seismic data to look more like layers rather than interface properties, without including a prior model. This method is not meant to yield a final product in a reservoir characterization workflow based on inversion results, but it is a valuable starting point or sanity check.

The TI attribute shows a strong correlation to the Bayesian inversion and may serve as a useful volume for interpreting some of the reservoir zonation boundaries by picking and tracking along the zero-crossings. Figure 6.2.13 shows some interpretations of the various reservoir zones based on a 3D autotracker picked on the zero-crossing events in the TI volume along the arbitrary section. The horizons are in a reasonable agreement with the shale volume logs and could yield a good representation of the zonation boundaries.

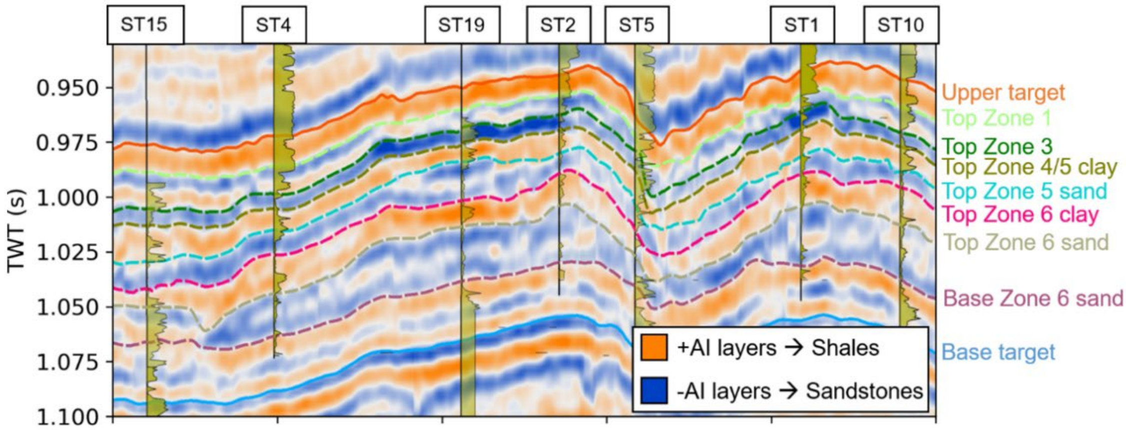

Figure 6.2.13. *Interpreting reservoir zonation based on the trace integration attribute.*

Conclusions

The following conclusions are made based on the results: (1) The rock physics and pore-fluid substitution modelling of the in situ natural gas and a modelled CO_2 fluid exhibited similar seismic responses in the Gassum Formation. This indicates that the Stenlille natural gas storage is representative for predicting the seismic response of future CO_2 storage in geological settings similar to the Gassum Formation in the Stenlille aquifer. (2) The natural gas injected into the Gassum Formation yields a low acoustic impedance contrast that separates from the other facies, allowing us to seismically resolve and distinguish the gas using a Bayesian post-stack inversion. High-probability gas sandstone anomalies were predicted and outlined within the various reservoir zones utilized for gas storage. The outlined gas distributions were consistent with well log observations and conforms with the Stenlille anticline structure in a reasonable manner. (3) A relative trace integration volume was derived that improved the resolution of thin layers, making it easier to pick and delineate the reservoir zone boundaries. In total, the quantitative interpretation results provided additional reservoir insights useful for building a robust static model for subsequent CO_2 storage de-risking, development, and management. However, the results have a significant uplift potential if modern high-quality seismic data in a pre-stack format would be available to constrain the non-uniqueness of the inverse problem and the associated uncertainties.

Tectonostratigraphic evolution at the Stenlille structure

The study is focused on the Stenlille area with a tie to the Slagelse area, which is shown in Figures 6.2.14 and 6.2.15. The key-tie composite profile in Figure 6.2.14 is chosen as it crosses the SE part of the Danish Basin towards the Ringkøbing–Fyn High and includes important deep and shallower structures. The tectonostratigraphy is constrained by seismic stratigraphic horizons correlated to key wells, where lithostratigraphy and ages are defined. The tectonostratigraphic and structural evolution of the area is summarized, based on the key profiles and well-ties, interpretation and mapping of horizons, units and faults, and horizon flattening back-stripping (Fig. 6.2.14, -15). The tectonostratigraphic and structural evolution of the area is described below mainly from sections with flattened horizons, from the Palaeozoic to the Base of the Chalk Group (Base Chalk), encompassing the main formation of the Stenlille structure. Stratigraphy below includes descriptions from the completion reports of the Slagelse-1 and Stenlille-19 wells and from GEUS.

Precambrian to Top Early Palaeozoic

The Precambrian basement (grey) and Lower Palaeozoic succession (turquoise colour) is affected by Early Palaeozoic extensional faults, which offsets the Top Basement horizon (black) and a thin uniform basal unit (below the lower green horizon) (Fig. 6.2.15a), which is onlapped by the thick upper turquoise unit, wedging out onto the two Slagelse structures. This indicates basin filling and deepening of basins connected between the Slagelse and Stenlille areas, which were partly divided by shallow structures and half-grabens (Fig. 6.2.15a). The Precambrian basement (grey) is likely crystalline as drilled south and north of the basin (Nielsen 2003, Vejbæk 1997), and is overlain by Cambrian quartzite, silt- and sandstones and Cambrian−Silurian mudstones, which are drilled in the Slagelse-1 well (Fig. 6.2.14) (Schovsbo 2011). The basins (Fig. 6.2.15a) probably subsided associated with tectonism due to the Caledonian Orogeny, with the central-north European deformation front moving towards north creating the deep foreland basin, with a thick Silurian shale succession (turquoise unit above the green horizon), drilled in the Slagelse-1 well (Schovsbo 2011).

Late Palaeozoic

Extensional faults and large wedge-shaped basins developed after deposition of the Lower Palaeozoic unit, and an unconformity (turquoise colour) with onlap above and truncation below is interpreted at the base of the Upper Palaeozoic (red) succession both in the Slagelse area and towards the Stenlille area (Fig. 6.2.14, 6.2.15b). This indicates major rifting tectonism with fault blocks, erosional truncation, and syn-rift deposition. Thick Silurian shales are separated from Zechstein by a Rotliegende succession, and thus Devonian−Carboniferous rocks are absent here at the Top Lower Palaeozoic unconformity (blue horizon: Fig. 6.2.15b). The Rotliegende Group, including syn-rift successions of sandstones, mudstones, conglomerates and reworked volcanic rocks, are known from other wells drilled into tilted hanging wall blocks (e.g., the Hans-1 well), in similar syn-rift wedges as in Fig. 6.2.14 north of the Slagelse-1 well, supporting significant Carboniferous−Early Permian regional tectonism and rifting (Vejbæk 1997, Michelsen & Nielsen 1991, Mogensen & Korstgård 2003).

The top of the Rotliegende succession is truncated by the regional Top pre-Zechstein (mid-Permian) unconformity (black horizon; Fig. 6.2.15b,c). The Top pre-Zechstein unconformity is associated with basin-wide erosional denudation and is the deepest and oldest basin-wide mappable horizon, which forms the base of the Danish Basin. It separates the pre-rift and syn-rift successions from the post-rift basin succession and formed the seafloor of the restricted shallow northern Zechstein sea where evaporites later evolved (Vejbæk 1997). Lithosphere thinning and crustal extension during Late Carboniferous–Early Permian times possibly caused the widespread Rotliegende volcanism and block faulting as described by Frederiksen et al. (2001). This was followed by lithospheric thermal contraction creating subsidence and accommodation space for Zechstein evaporites and the overlying thick Triassic successions.

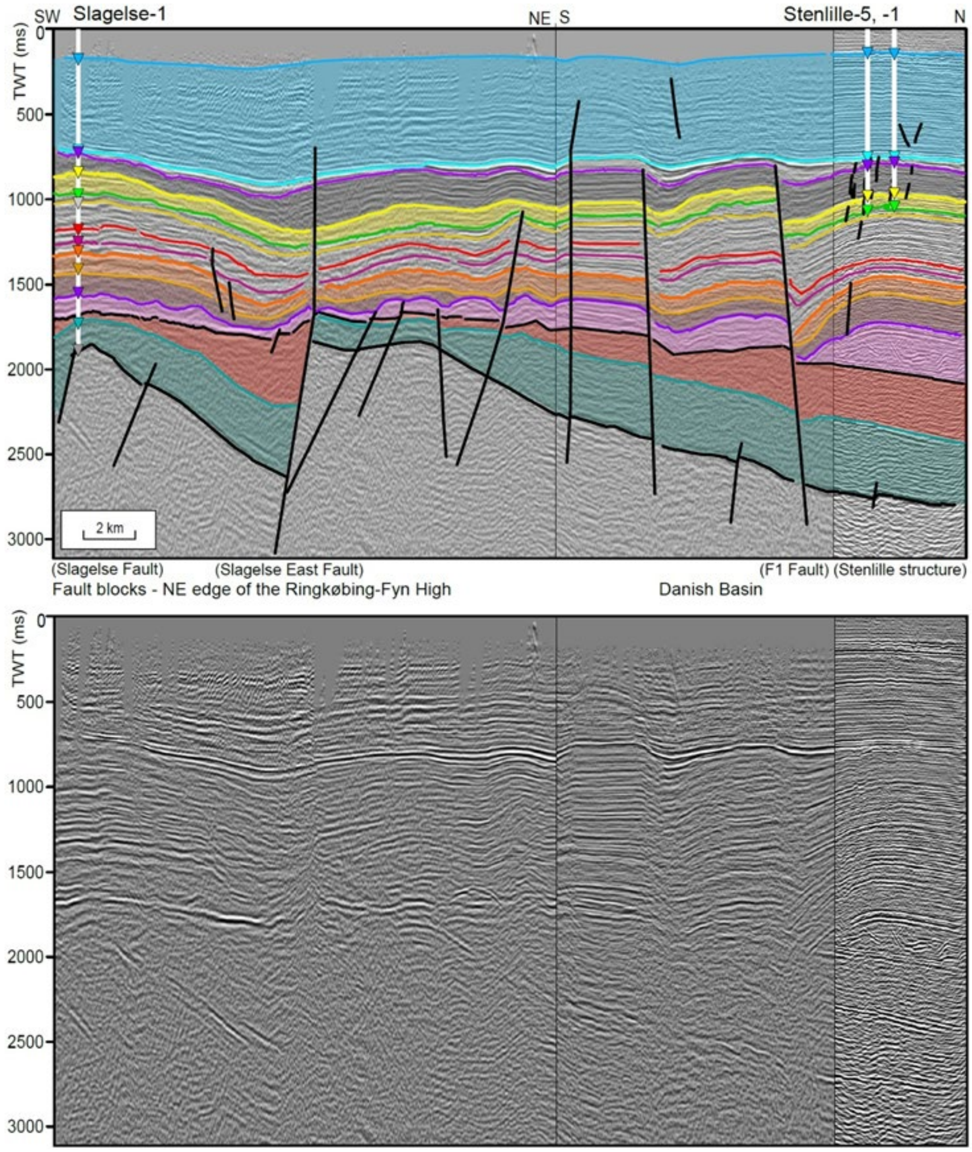

Figure 6.2.14. *Composite seismic sections in two-way time from the Slagelse-1 to the Stenlille-1,-5 wells (projected), with and without interpretation. Triangle positions mark lithostratigraphic well-ties. Major basin and structures are named. The upper blue unit indicates the Chalk Group and Danian. The Gassum (yellow unit) and Fjerritslev (dark-grey unit) Formations form the upper part of the Stenlille structure, which is formed by the deep Zechstein salt pillow (pink). Seismic sections are from SW to N: SSL72_001, SSL73_036 and DN94_D07. Fig. 6.2.15 includes the same composite profiles without the projected wells, the legend, and it also shows the location of the seismic sections. From Gregersen et al. (2022).*

The Zechstein Group (pink unit) is interpreted between the Top pre-Zechstein unconformity and the Top Zechstein (purple horizon), where the succession forms a number of minor mounds and in the Stenlille area a larger pillow (Fig. 6.2.15c-e). The unit ties into an evaporitic succession with halite, anhydrite, and dolomite in the Slagelse-1 well. The evaporites formed in an arid climate during the Late Permian time in large parts of the Danish Basin, where later mobilization led to numerous diapirs and pillows. Near the Permian−Triassic transition uplift took place which was followed by regional subsidence (Vejbæk 1997).

Triassic

The lowermost Triassic unit (brown) above the Zechstein shows variation in thickness (Fig. 6.2.15c), possibly due to incipient subsidence or secondary structures and later salt mobilization, and it thickens considerably into the Stenlille area, and this seismic stratigraphic unit is interpreted as the Lower Triassic Bunter Shale Formation by correlation to the Slagelse-1 well (Fig. 6.2.14). The unit is separated from the overlying unit (orange) by an unconformity (light orange horizon) with downlap and is fairly uniform in thickness (Fig. 6.2.15c). This unit correlates to the Bunter Sandstone Formation in both the Slagelse-1 and the Stenlille-19 wells (Fig. 6.1.1, 6.2.14). However, the completion reports show fine-grained sandstones and dominance of claystone. Further east (in Copenhagen; Fig. 3.1) sandstones of this formation are reservoir for geothermal energy (the Margretheholm wells; Fig. 3.4).

Middle−Upper Triassic units (brown with red-orange-yellow horizons) show more or less uniform thicknesses across the area, though with some local fault activity with local thickening at faults, located at flanks of the underlying Zechstein unit (Fig. 6.1.1, 6.2.15d). This may indicate reactivation of Permian faults and/or incipient salt mobilization. The Middle to Upper Triassic formations (Ørslev, Falster, Oddesund and Vinding) are mostly clay-rich formations, that occurs widespread across much of the Danish Basin (Fig. 6.1.1). Contents of dolomites, limestones, anhydrites, etc. may cause some of the intraformational strong seismic reflections, e.g., anhydrites near c. 1200 ms (Fig. 6.1.1). Middle to Upper Triassic successions thicken especially towards the Stenlille area (Fig. 6.2.15d,e). Claystones, calcareous in lower parts – more siliciclastic in upper parts, dominated the successions until the latest Triassic Rhaetian time (Slagelse-1 and Stenlille-19 completion reports).

Latest Triassic to Early Jurassic

The Gassum Formation (Rhaetian age) in the Stenlille wells can be tied to a seismic stratigraphic unit, bounded by top and base peak reflections (Fig. 5.1, 6.1.5) and with internal reflectivity, occasional mounded or with troughs interpreted as channels (Section 7.; Vosgerau et al. 2020; Smit et al. 2022). The total thickness of the formation in the Stenlille wells is approximately 140−150 meter, with the thickest and most sandstone-rich units preserved in lower part of the formation (below TS5) (Section 7.1; Vosgerau et al. 2020). The Gassum Formation can also be correlated in seismic sections from the Stenlille wells to the Slagelse-1 well, where it is 137 m thick, and the formation seems to have a more or less uniform thickness in the mapped area of the structure (Fig. 6.2.4C).

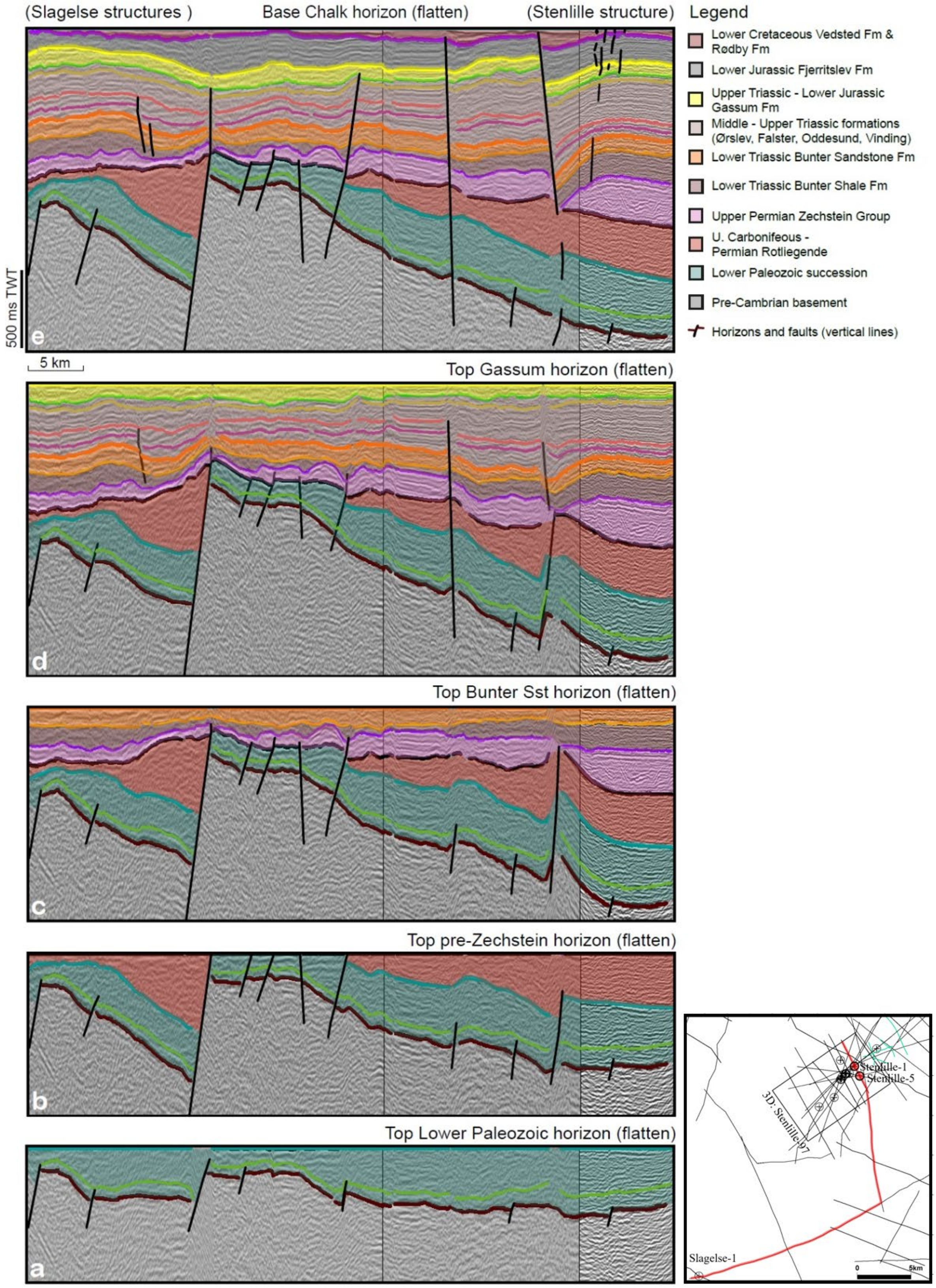

Figure 6.2.15. *Horizon flattening at key-horizons (a-e) of Fig. 6.2.14, illustrating the Palaeozoic to Cretaceous structural evolution between the Slagelse and the Stenlille structures, described in the text. See the insert map for location, and Fig. 6.2.14 for well-ties. From Gregersen et al. (2022).*

Channel positions mostly west of and partly across the present top of the Stenlille structure, lowermost in the successions, may indicate paleo-topographical highs, e.g., due to initial syn-depositional doming or sedimentary system build-up (Section 7.1; Vosgerau et al. 2020). However, the most significant doming of the structure is later at the Near Top Fjerritslev (Fig. 6.2.5, 6.2.15e). The sedimentary systems of the Gassum Formation were dominated by fluvio-deltaic, estuarine, and shoreface environments also interpreted by new detailed seismic geomorphology, core facies, and sequence stratigraphic studies of wells and 3D seismic data (Smit et al. 2022; Section 7.1). These studies also revealed sand-rich, coastal-near systems (meandering fluvial channels, point bars, and sand plates) and indications of transport directions. In addition, seismic reservoir characterization is studied in the previous section (see also Bredesen et al. 2022). The improved reservoir characterization can be used in static reservoir modelling and simulation of CO_2 injection.

Zircon provenance analysis shows that the Stenlille area received input from long distance transported sediments sourced from both the Fennoscandian Shield (Caledonian Orogen and Sveconorwegian Orogen), and from south (Variscian Orogen), and the thick mature sandstones indicate tectonism and denudation in the hinterlands as well as sufficient accommodation space at Stenlille for deposition of sand (Olivarius et al. 2022; See also Section 7.1).

The Stenlille structure has a number of faults in its top, in particular in the Gassum and through the Fjerritslev succession, and less apparently in the overlying successions (Fig. 6.2.5−6.2.8). In large parts of the structure, faults seem to displace more or less equal thicknesses, though with minor variations, of both the Gassum and Fjerritslev Formations to the Near Top Fjerritslev horizon (Fig. 6.2.4B,C; 6.2.5). This may indicate that these faults were active later than deposition of most of the Fjerritslev Fm, except for a thickening of the Fjerritslev Fm towards SE at the large F1 fault, close to the border of the mapped area (Fig. 6.2.4B).

The Stenlille F1 fault SE in the study area, south of the Stenlille structure (Fig. 6.2.14), is a large, deep normal fault, seated SE of the salt dome, which evolved from mid-Jurassic time. The F1 fault shows throws at the Top Gassum of c. 160−180 ms, with similar order of throws of deeper horizons (c. 170−200 ms) down to Top Zechstein. The Fjerritslev Formation between Top Gassum and Near Top Fjerritslev horizons thickens in the hanging wall syncline towards fault F1, indicating growth fault evolution of a primary syncline of salt doming, and the throw at the Near Top Fjerritslev is only 70−80 ms, possibly a result of erosion (Fig. 6.2.14). Apparently, it is primary the uppermost part of the Fjerritslev Formation succession (probably the F-IV member), that thickens towards the fault. The structure top is offset by faults in particular south of the Stenlille-1 well, at the southern flank of the doming structure.

Most faults in Gassum and Fjerritslev Formations in the Stenlille structure have mainly minor, normal and in some cases reverse throws, mostly less than c. 30 ms or c. 30−50 m (Fig. 6.2.5). Most faults are located along the anticlinal NE−SW trending axis of the Stenlille structure, in its top and its SE flank, and a few faults trend N-S (Fig. 6.2.5−6.2.8). The deepest-seated faults occur along the SE structure flank, and some of these sole out deep into the salt pillow (Fig. 6.1.1), indicating that they are related to the structural deformation due to the doming of the structure. The most prominent fault in the SE structure top, SE of ST-5, is the F5 fault (Fig. 6.2.5, 6.2.6). Also, the shallower Gassum−Fjerritslev faults ending at the Near Top Fjerritslev horizon are probably related to the doming of the salt pillow after late Early Jurassic time.

Faults interpreted manually, are compared to Machine Learning (ML) derived fault probability, both vertically and laterally (Fig. 6.2.5, 6.2.6; Gregersen et al. 2022, Lorentzen et al. 2022). The fault-probability shown in yellow are scaled to 80−100% probability (binary colour coded: ‘1’= 80-100% fault probability, whereas ‘0’ (no colour) < 80%) of reflection discontinuity, which represents mostly faults. The ML fault predictions are created by training a convolutional neural network model on synthetic seismic data and was subsequently applied to the Stenlille 3D dataset (Lorentzen et al. 2022). This comparison improves the understanding significantly of the fault patches and will provide more accurate and detailed fault networks. Manually interpreted faults are mainly located at clear breaks/displacements in reflections and successions, whereas the ML fault predictions are also sensitive to less visible breaks and subtle features (Fig. 6.2.5, 6.2.6). Such features may also include boundaries of channels, mounds, seismic facies change due to changed lithology, fluids, etc., but also seismic noise. The significant details of ML fault-probability traces can provide important data for evaluations of fault risks, seal-integrity, etc., not least of prospects for storage CO_2 or other resources. The manually interpreted fault polygons and the ML fault trends show consistent NE−SW fault directions both at the Top Gassum and the Near Top Fjerritslev surface maps (Fig. 6.2.6d,e). Some of the near Top Gassum faults may compart the Gassum Formation reservoir and seem to restrict predicted natural gas in some cases (See Seismic reservoir characterization section above; Bredesen et al. 2022). At the Base Chalk surface (Fig. 6.2.8e) there are less faults, but some still with NE−SW trends. This indicates relatively few clear fault connections between the Lower Cretaceous successions and the Upper Cretaceous Chalk Group. However, as breach of seals may occur at faults, such risks have to be investigated and assessed thoroughly before injecting CO_2. The long-term, safe storage of natural gas at Stenlille indicates competent sealing successions.

The Near Top Fjerritslev horizon is interpreted at a marked trough with increasing acoustic impedance, in a significant seismic stratigraphic unconformity, with onlap from overlying successions and which defines the top of the Stenlille structure (Fig. 6.1.1). The preserved uppermost Fjerritslev Fm (Toarcian age) is overlain by the Lower Cretaceous Vedsted Fm near at or slightly above this horizon (Fig. 6.1.1), and the actual boundary in the sedimentary successions is thus a major hiatus – see also discussion in Section 7.2. The erosion and hiatus may be slightly different depending on the position on the structure, and flanks of the structure would probably have less erosion and more preserved successions, possibly also including upper parts of the Fjerritslev F-IV Member. The major unconformity marks the formation of the Stenlille structure mainly due to formation of the underlying salt pillow. The unconformity may in part be equivalent to the ‘Base Middle Jurassic unconformity’ or ‘Mid-Cimmerian Unconformity’ (Nielsen 2003) associated with uplift and erosion (and a major hiatus) over structures and margins of the Danish Basin, including the Ringkøbing−Fyn High (Fig. 6.1.1).

Cretaceous

The Lower Cretaceous Vedsted and Rødby Formations are part of the seismic stratigraphic wedge, which onlapped the Near Top Fjerritslev horizon after the formation of the elevated Stenlille structural dome (Fig. 6.2.5). The dome formed primary due to salt pillow growth and probably caused erosional removal or non-deposition during Middle Jurassic to Early Cretaceous times. From the top of the Stenlille structure, near above Top Fjerritslev (at the Fjerritslev Fm/Vedsted Fm boundary), biostratigraphy shows, that the youngest Jurassic deposits are of Toarcian age and the oldest Early Cretaceous deposits are Hauterivian in age (see Section 7.2; Fig. 6.1.1). Parts of the Vedsted succession above the Near Top Fjerritslev includes prograding reflections towards SE, away from the structural crest, and minor troughs (channels or fault related) occur towards the structure (Section 7.1). The Rødby Formation is overlain by the regional Upper Cretaceous Chalk Group. In the lower to middle parts of the Chalk Group extensional faults occur (Fig. 6.2.7, 6.2.8f) as sets of small half-grabens in and below the high-reflective succession (c. 550−600 ms) trending in three directions, mostly NW−SE and WNW−ESE, and less NE−SW, due to renewed tectonism. Slight inversion may be recognized as gentle elevation over the top of the Stenlille structure (Fig. 6.2.5).

Most of the Cenozoic is missing over the Stenlille structure. Only a Paleocene succession buried shallow is described in the Final Well Report of well Stenlille-19. This succession includes the Lellinge Fm (Lellinge Grønsand of Selandian age) and the Ekofisk Fm (Danian age). The Paleocene succession is likely overlain by mostly Quaternary successions. Japsen & Bidstrup (1999) reported that c. 600 m Cenozoic successions are missing in some of the Stenlille wells.

Summary of the structural evolution

The structural reconstruction of the development of the Palaeozoic and Mesozoic to the Base Chalk facilitated by horizon flattening at several key horizons shows that the Palaeozoic structures formed during several tectonic events with the Top pre-Zechstein as a base of the present Stenlille structure. The Stenlille structure mainly evolved by the growth of a salt pillow forming the overlying structural doming anticlinal. The formation of the structure was likely initiated during deposition of the Gassum Formation. However, the structure developed more pronounced under the subsequent burial of the thicker Fjerritslev Formation. The burial probably conditioned salt migration into the domal salt-pillow, which elevated the overburden structure during the Middle Jurassic to Early Cretaceous times. Normal faults and faults with reverse and compressional indications are observed and may be caused by doming and regional compressional related tectonics. More than fifteen faults were manually interpreted and show NE−SW trends in the Gassum-Fjerritslev Formations. Machine Learning increased the understanding of the 3D fault network. Shallower faults in the lower Chalk Group show three directions: NW−SE, WNW−ESE, and NE−SW. The Near Top Fjerritslev unconformity is onlapped by the Vedsted Formation and the Rødby Formation, which is overlain by the Chalk Group, and the structure was later affected by inversion and uplift episodes.

7. Geology and parameters of the reservoirs and seals

7.1 Reservoirs – Summary of geology and parameters

The primarily reservoir for potential CO_2 storage in the Stenlille structure is the sandstone dominated Gassum Formation whereas the deeper lying sandstones of the Oddesund and Bunter Sandstone Formations form secondary reservoirs (Fig. 7.1.1). In the following description of reservoirs, emphasis is on the Gassum Formation whereas the secondary reservoirs are only described briefly. The description of the Gassum Formation below is based mainly on Vosgerau et al. (2020, in prep.) and Hovikoski & Pedersen (2020). The Gassum Formation is subdivided into 6 Reservoir Zones and internal seals by DONG (DONG 2001), which is also used in the present reservoir characterization. The Gassum Formation and the identified Reservoir Zones in the Stenlille-19 well are shown in Fig. 7.1.2 and in interpreted well logs for the Stenlille-1, -2, -5, -6, -18 wells shown in the Appendix B.

The primary reservoir: The Gassum Formation

The Gassum Formation is the best-known sandstone reservoir in the Danish onshore subsurface. It is used for geothermal energy in Thisted and Sønderborg and has also been used for seasonal storage of natural gas for more than 30 years in the Stenlille structure. The good reservoir properties of the formation have thus been proven at several places in Denmark. The formation is widespread in the Danish Basin and locally in the Danish part of the North German Basin (Fig. 7.1.3). It has a general thickness of 30–150 meters (Nielsen & Japsen 1991, Nielsen 2003). Locally it is missing due to uplift and erosion related to regional uplift in the Middle Jurassic, at the ʽBase Middle Jurassic unconformityʼ or the ʽMid-Cimmerian Unconformityʼ *sensu* Nielsen (2003), and above structures formed by vertical salt movements. The Gassum Formation is of Late Triassic–Early Jurassic age with the upper boundary showing a significant younging towards the northern, north-eastern, and eastern basin margins (Fig. 7.1.3) (Bertelsen 1978, 1980; Michelsen et al. 2003; Nielsen 2003). The upper formation boundary is thus of latest Rhaetian age in the central parts of the basin, including the area of the Stenlille structure, whereas it is of Early Sinemurian age along the basin rims (Nielsen 2003 and references therein). This diachronic development of the boundary reflects an overall backstepping of the general coastline toward the basin margins during latest Triassic – Early Jurassic time owing to an overall rise in relative sea-level, interpreted as caused by a combination of regional basin subsidence and a eustatic sea-level rise (Nielsen 2003).

In general, the Gassum Formation is dominated by fine to medium-grained, in places coarse-grained, light grey sandstones, alternating with darker colored clay- and siltstones and locally thin coal layers (Bertelsen 1978, Michelsen et al. 2003, Nielsen 2003). The sediments were deposited during repeated sea-level fluctuations in Late Triassic – Early Jurassic times when the Danish Basin was a shallow marine area. Large quantities of sand were transported into the basin by rivers which were sourced by erosion of the Fennoscandian Shield and, to a lesser degree, locally from the Ringkøbing–Fyn High in periods when this was exposed.

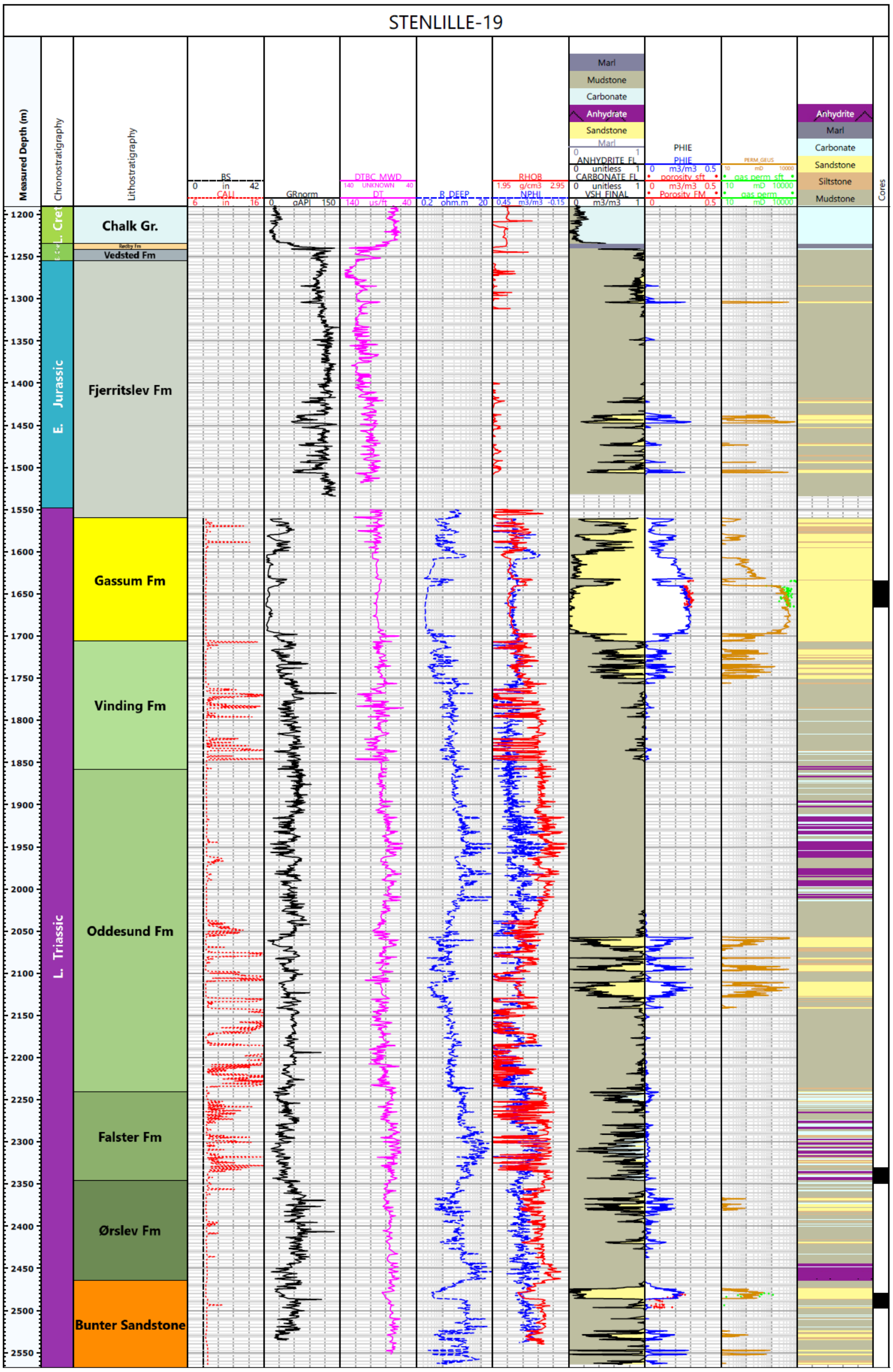

Figure 7.1.1. *Lithostratigraphic subdivision of the Stenlille-19 well with interpreted lithology and formations based on petrophysical log interpretation and information from core data, cutting samples etc. This well is the only Stenlille well that is deeper than the Vinding Formation. Sandstones of the Gassum Fm is the primary reservoir, and sandstones of the Oddesund and Bunter Sandstone Formations are potential secondary reservoirs. The Fjerritslev Fm/Vedsted Fm boundary is at 1254.5 m MD and has been moved up from 1278 m MD based on new biostratigraphy (K. Dybkjær & E. Sheldon) – see Section 7.2.*

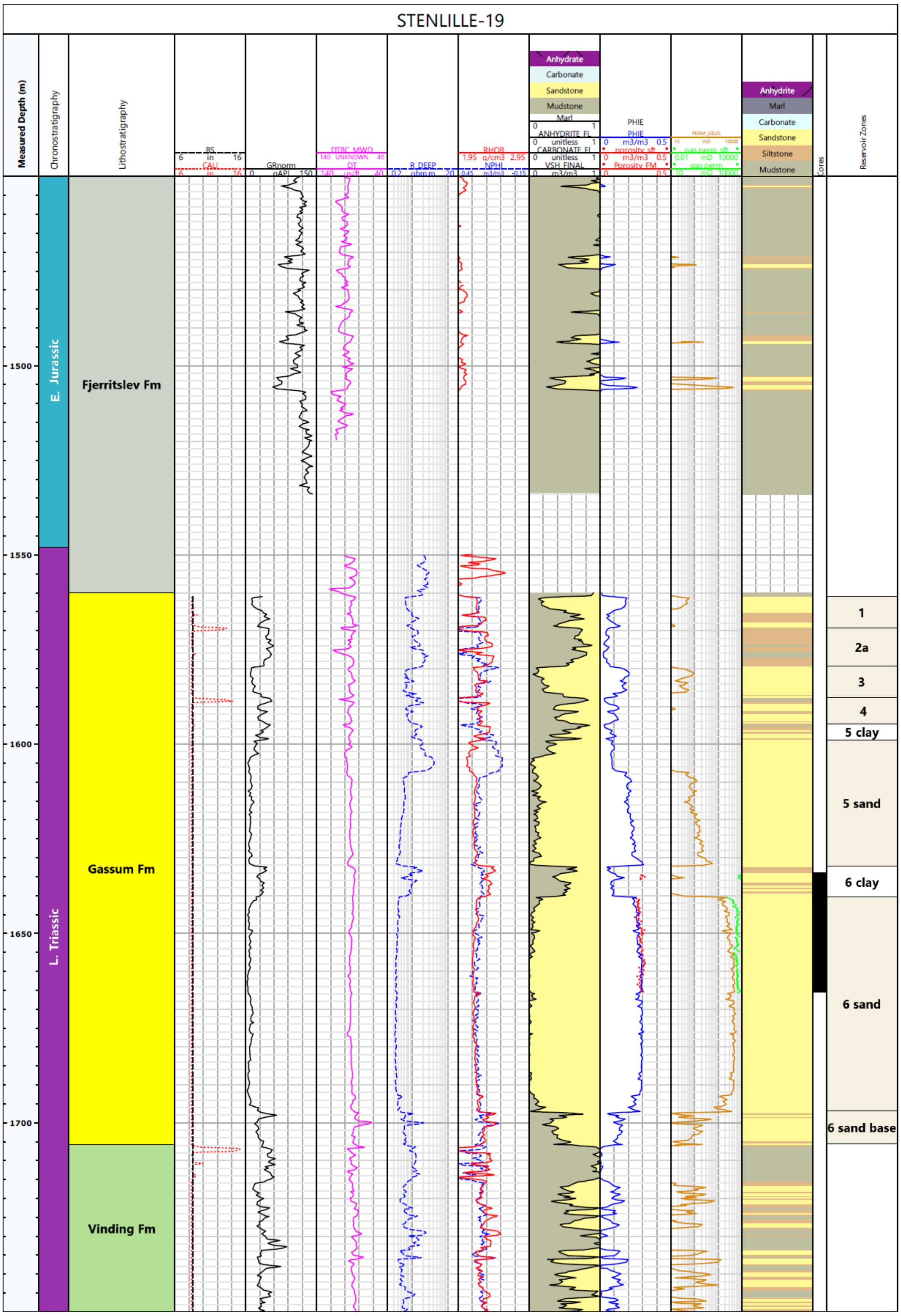

Figure 7.1.2. *The Stenlille-19 well with interpreted lithology and formations based on well-log interpretation. Zoom section of Fig. 7.1.1 to the Gassum Formation with main reservoir zones in yellow (1–6) of DONG (2001), with cored part of Zone 6 (black column). Note the good accordance between porosities derived from logs (PHIE column) and core measurements (red dots), and between permeabilities derived from logs (perm) and core measurements (green line), except in the Zone 6 clay.*

Recent provenance studies suggest that the basin was sourced also with sand from southerly Variscan source areas, perhaps transported into the basin through grabens intersecting the Ringkøbing–Fyn High.

However, a general mixed composition of zircon ages in samples from the eastern part of the basin suggests that rivers draining the Caledonian and Variscan Orogens met in the east and supplied mixed sediment towards west into the basin (Olivarius et al. 2020, 2022) (Fig. 7.1.4).

The high influxes of sediment almost balanced subsidence implying that the intracratonic basin largely remained shallow and almost flat-based, but with its deepest part located near its center (Hamberg & Nielsen 2000). Due to the flat, low-gradient basin floor and overall shallow water conditions, sediment accumulation was very sensitive to Late Triassic and Early Jurassic fluctuations in relative sea level which resulted in repeated long-distance progradation or retrogradation of the coastline. A large part of the sandstones in the formation therefore represents shoreface deposits, but significant amounts are also fluvial or estuarine in origin. This is especially the case for the lower part of the formation where pronounced high-order relative sea level falls led to the progradation of rivers into the central part of the basin and the establishment of estuaries during succeeding rise in relative sea level.

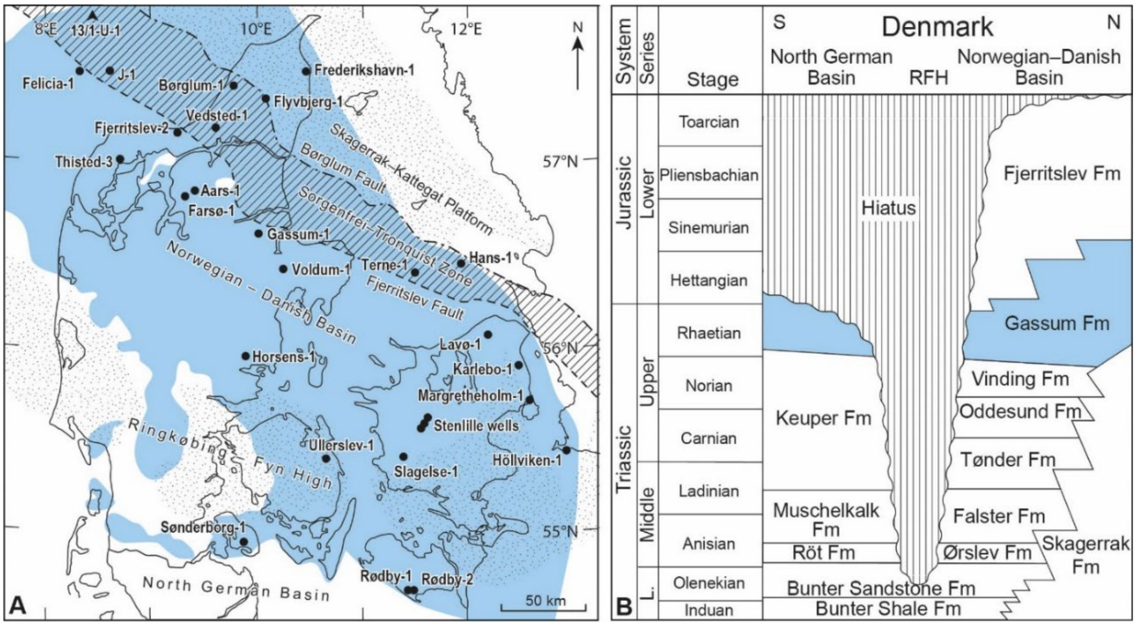

Figure 7.1.3. *A) Estimated distribution of the Gassum Formation in the Danish onshore and nearshore area shown in blue. Also shown is selected wells and main structural elements including the Norwegian–Danish Basin and the North German Basin which are separated by the Ringkøbing–Fyn High (RFH). B) Stratigraphic scheme of the Lower Triassic–Lower Jurassic succession onshore Denmark revealing among others the time-transgressive nature of the of the top of the Gassum Formation. From Olivarius et al. (2022).*

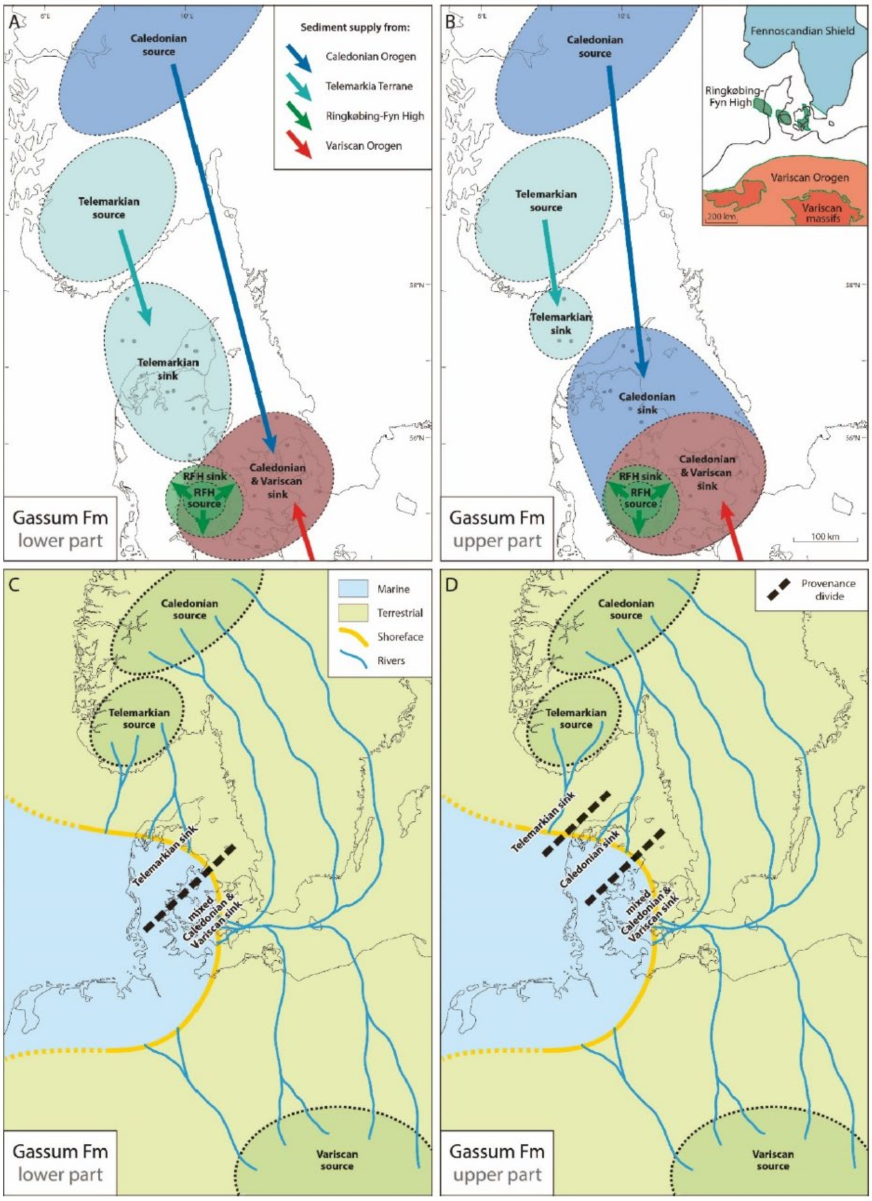

Figure 7.1.4. *Provenance of the lower (A) and upper (B) parts of the Gassum Formation showing the location of the primary source areas (Caledonian, Sveconorwegian, and Variscan) and the minimum extend of their sinks as evident from zircon U-Pb data from wells in the Danish Basin and the northern North German Basin. Sediments were locally supplied from exposed parts of the Ringkøbing–Fyn High. Tentative paleogeographic reconstructions for the lower (C) and upper (D) parts of the formation, where the primary difference is which of the Fennoscandian source areas that supplied most sediments to the basin. The maps represent snapshots since the coast-line moved back and forth due to repeated transgressions and regressions in time. From Olivarius et al. (2022).*

The Gassum Formation at Stenlille:

Depth, thickness and extent: At Stenlille, well data shows that the thickness of the Gassum Formation varies between 141 and 154 m, with a mean thickness of c. 146 m. The vertical depth to the top of the formation is slightly exceeding 1500 m at the central part of the domal structure and down to 1564 m at the flanks of the structure (Table 7.1.1). All Stenlille wells are located within the 3D seismic survey area, except ST-6 that is situated nearly 1 km NE of the north-eastern limit of the 3D survey area (Fig. 7.1.5). Seismic mapping and interpretation indicate that the Gassum Formation is present in the entire Stenlille area, with a thickness of approximately 140–160 m (Fig. 6.2.4C).

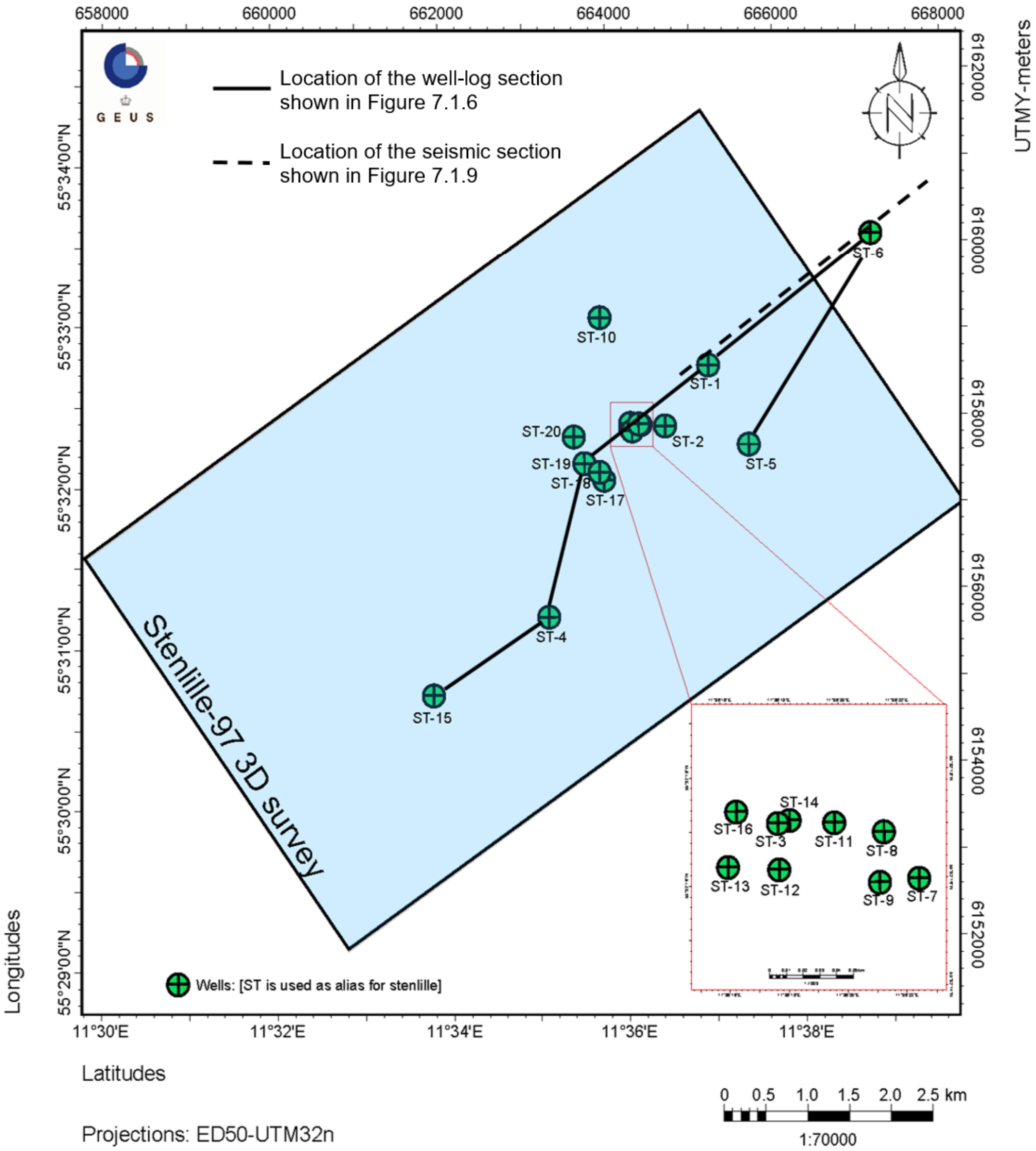

Figure 7.1.5. *Areal extent of the 3D seismic survey in Stenlille (blue rectangle) and the locations of wells of which only ST-6 to the NE is located outside the 3D survey. The marked log section (solid black line) is shown in Figure 7.1.6. Also marked, is the approximately location of a seismic section (dashed black line) shown in Figure 7.1.9.*

Table 7.1.1. *Approximately depths to the Top and Base of the Gassum Formation and its thickness in the Stenlille wells.*

Well	True Vertical Depth (meter below Kelly Bushing)		Thickness (m)
	Top Gassum Fm	Base Gassum Fm	
ST-1	1507	1650	143
ST-2	1512	1658	146
ST-3	Not penetrated		
ST-4	1514	1659	145
ST-5	1551	1692	141
ST-6	1564	1706	142
ST-7	1510	1657	147
ST-8	1505	1650	145
ST-9	1511	1653	142
ST-10	1524	1671	147
ST-11	1500	1647	147
ST-12	1503	1650	147
ST-13	1503	1650	147
ST-14	1501	1649	148
ST-15	1523	1677	154
ST-16	1503	1647	144
ST-17	1503	1649	146
ST-18	1503	1650	147
ST-19	1508	1653	145
ST-20	1505	1653	148

Subdivision: The formation is subdivided into 7 depositional sequences, SQ1–SQ7 (Fig. 7.1.6B), based on integration of sedimentological interpretations of cores and petrophysical log patterns, palynological data and interpretation of the 3D seismic survey (Stenlille-97) covering a large part of the Stenlille structure (Hovikovski et al. 2020, Lindström 2020, Vosgerau et al. 2020) (Fig. 7.1.7). The numbering of sequences and their associated surfaces follows the sequence stratigraphic nomenclature in Nielsen (2003). This was developed for the Upper Triassic–Jurassic sedimentary succession in the Danish Basin and showed that individual sequences in most cases can be correlated basin-wide from well to well.

Each sequence is based by a sequence boundary (SB) formed at the time of maximum fall in relative sea level. Lowstand systems tracts (LST) form between sequence boundaries (SB) and the first transgressive surface (TS). Transgressive systems tracts (TST) form between the TS and the maximum flooding surface (MFS). Highstand systems tracts (HST) form between the MFS and the SB of the next sequence. This simple sequence stratigraphic approach (e.g., Payton 1977) is following the divisions of Nielsen (2003). There are also other concepts (see e.g., Catuneanu 2019), but these are not discussed further here. Figure 7.1.6 shows how the depositional sequences link to depositional facies and environments.

DONG defined six reservoir zones with some internal mudstone seals in the Gassum Formation, but only the upper c. 40 m of the formation, covering Zones 1–4 and the upper part of Zone 5, is used for gas storage (Fig. 7.1.8). Overall, the lowstand systems tract (LST) and lower transgressive systems tract (TST) of the sequences consist of sandstone and correlates to DONG´s reservoir sand zones. In contrast, the remaining part of the TST of the sequences consist of mudstone and heteroliths correlating to DONG´s defined internal seals in the Gassum Formation (Fig. 7.1.8).

The seven sequences reflect an overall progradational pattern from the base of the Gassum Formation and up to SB5. SQ´s 1–3 consist mainly of shoreface deposits, whereas thick lowstand systems tracts, up to 40 m thick, of the overlying SQ´s 4 and 5 are fluvial dominated with intercalations of shoreface sandstones. The upper part of SQ5, above TS5, is 15–20 m thick in many wells, and is dominated by shoreface deposits (Fig. 7.1.6). An overall backstepping pattern is revealed by the depositional units becoming thinner and more fine-grained upwards in addition to offshore mudstone and shoreface sandstones becoming more dominant. SQ7 has a thin fluvial succession at its base in ST6 which marks the youngest event of fluvial deposition in the Stenlille area during deposition of the Gassum Formation.

High order sea-level variations formed the individual sequences and generated the complex internal reservoir architecture of the formation with lowstand intervals forming internal sandstone reservoirs and transgressive intervals of mudstone and heteroliths forming internal seals as mentioned above. Locally, these seals are truncated due to fluvial erosion related a fall in relative sea level and formation of sequence boundaries, implying that lowstand sandstones from different sequences are connected. The most intensive erosional event associated with basinward bypass of sediments relates to the formation of SB4. This sequence boundary in places led to a complete removal of the deposits of SQ3, especially in the northeastern part of the 3D survey area (Fig. 7.1.9). Many sequences are thin, which preclude that all the sequence stratigraphic surfaces identified based on the well data can be idenfied in the seismic data due to resolution. Consequently, a subdivision of sequences into systems tract is generally not posible in the seismic data. Thus, it is mainly sequence boundaries that are linked to seismic reflectors whereas transgressive surfaces and maximum flooding surfaces are more difficult to map out laterally. However, the transgressive surface TS7 corresponds approximately to the top of the Gassum Formation (Fig. 7.1.8B), which is marked by a decrease in the acoustic impedance from the Fjerritslev Fm to the Gassum Fm as a clear peak seismic reflection displayed in black or red color (Fig. 5.1, 6.1.3, 7.1.9).

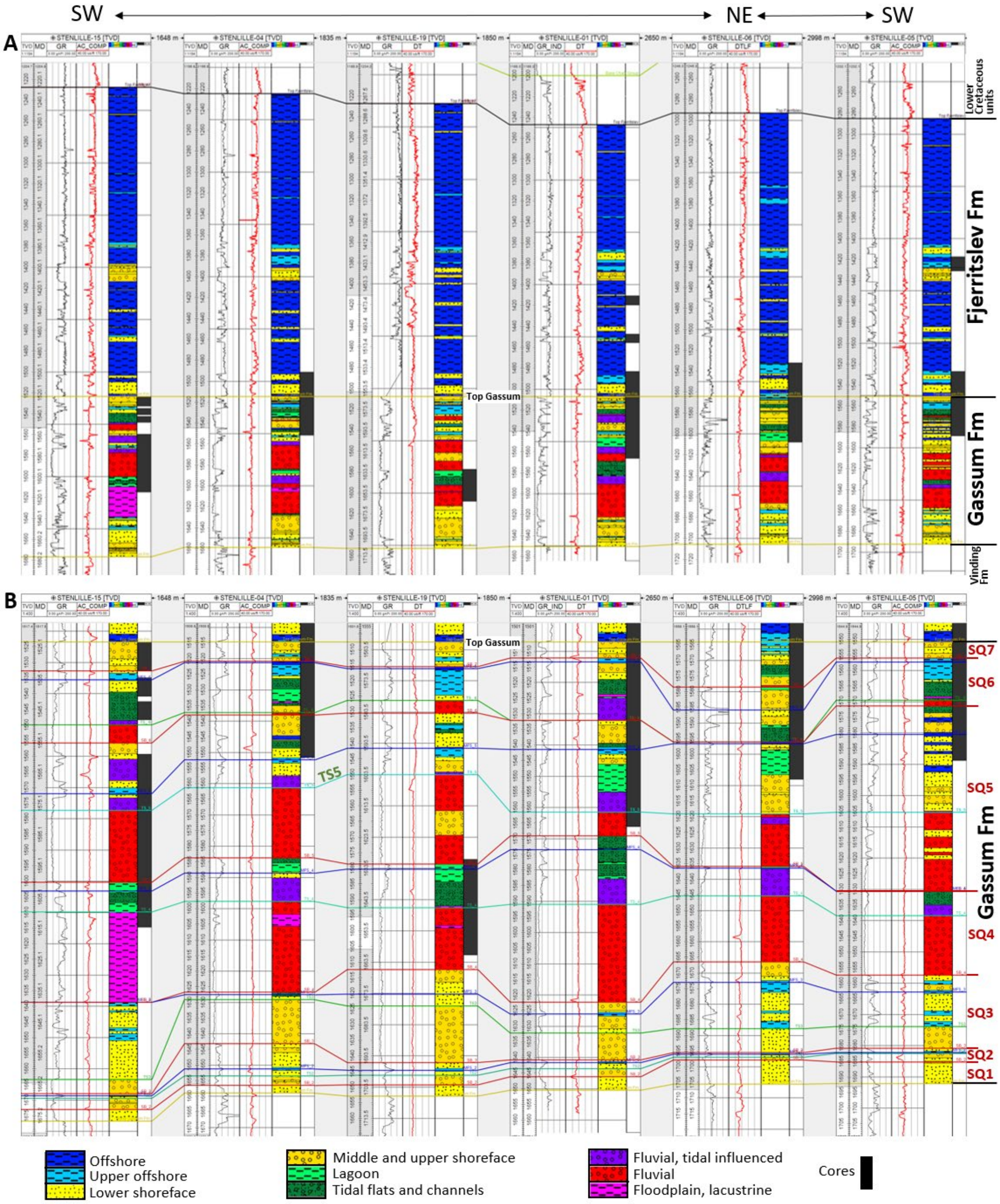

Figure 7.1.6. *A) Correlation panel of the Gassum and Fjerritslev Formations with interpreted facies associations. B) Correlation panel of the Gassum Formation showing sequence stratigraphic subdivision and interpreted facies associations. The Fjerritslev Fm/Vedsted Fm boundary is currently under revision due to new biostratigraphy (K. Dybkjær & E. Sheldon), implying a slightly shallower position than shown in the present figure (see Section 7.2). Location of log panels is shown in Figure 7.1.5. Location of log panels are shown in Figure 7.1.5.*

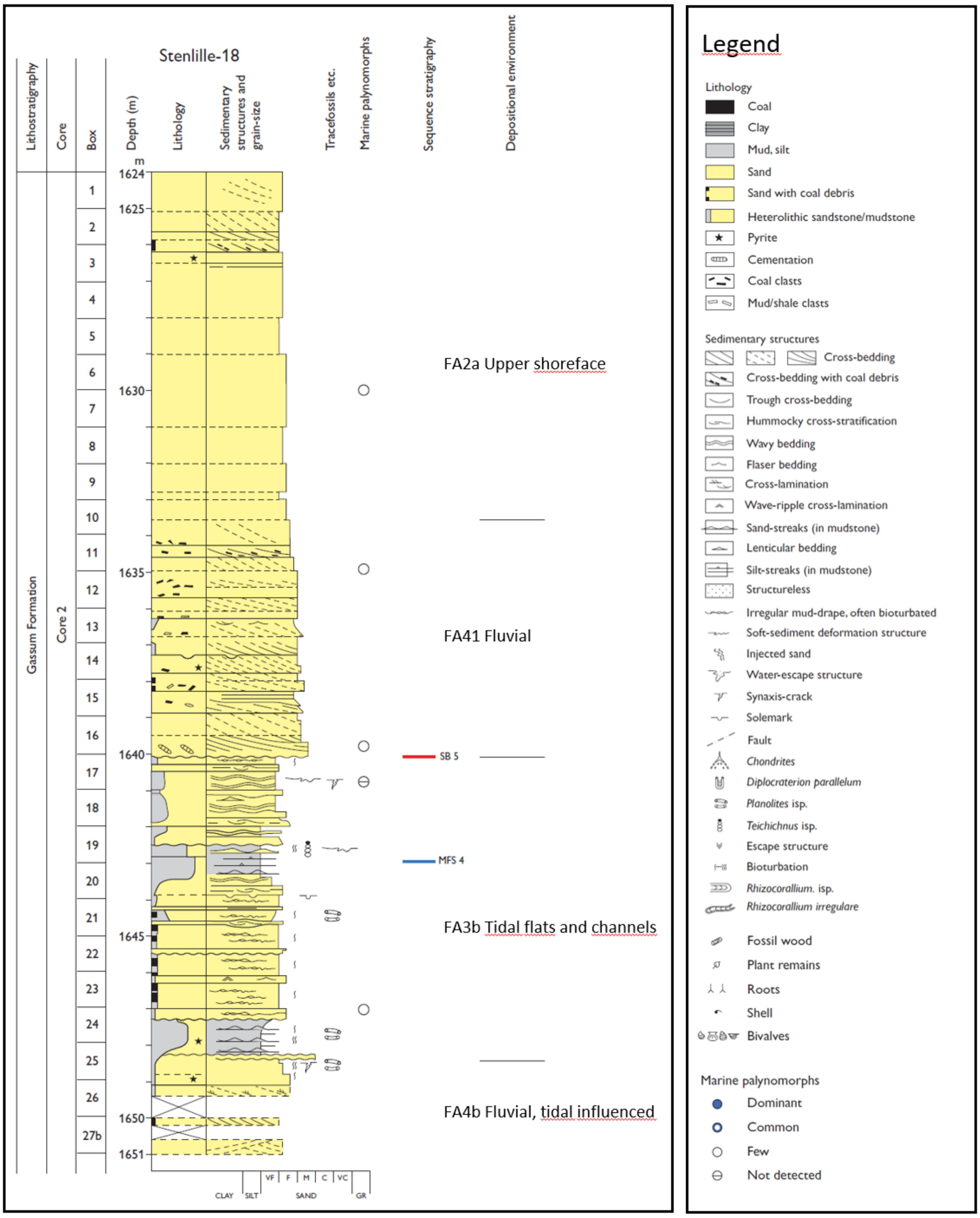

Figure 7.1.7. *An example of sedimentological description and interpretation of a core from the ST-18 well. Modified from Hovikoski & Pedersen (2020).*

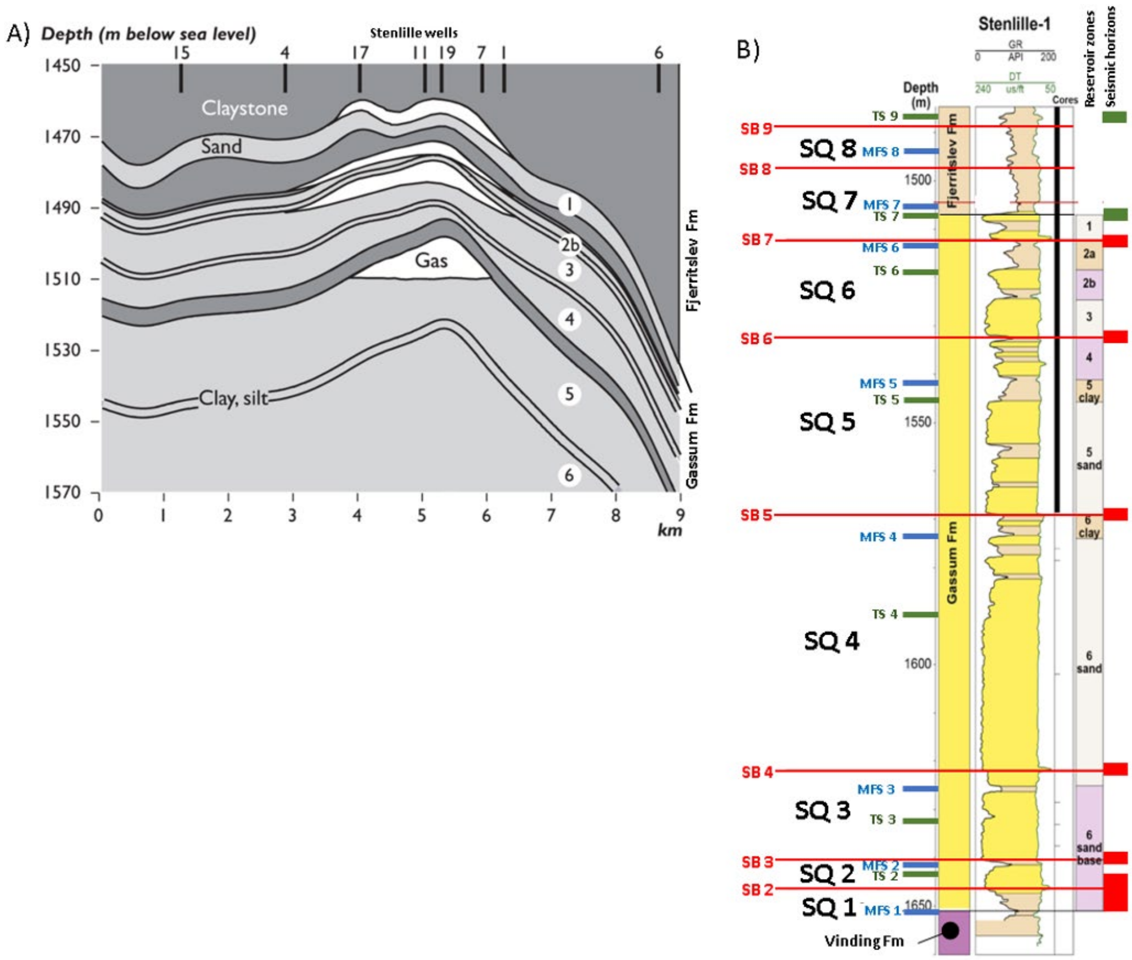

Figure 7.1.8. *A) Schematic cross-section (SW–NE) of the natural gas underground storage at Stenlille showing the various reservoir sandstone dominated zones (1–6) separated by relative thin mudstone dominated intervals (dark grey). From Laier & Øbro (2009).*

B) The Stenlille-1 well with gamma-ray log (GR) and sonic log (DT), well-tied sequence stratigraphic surfaces and sequences, reservoir zonation and to the right interpreted seismic horizons correlated to sequence stratigraphic surfaces. Yellow and brown, filling out the space between GR and DT logs, indicate intervals dominated by sandstone and mudstone, respectively. SB: sequence boundary, MFS: Maximum flooding surface, TS: Transgressive surface. The subdivision of the Gassum Formation into DONG´s reservoir zones are shown to the right (see also the well in Appendix B).

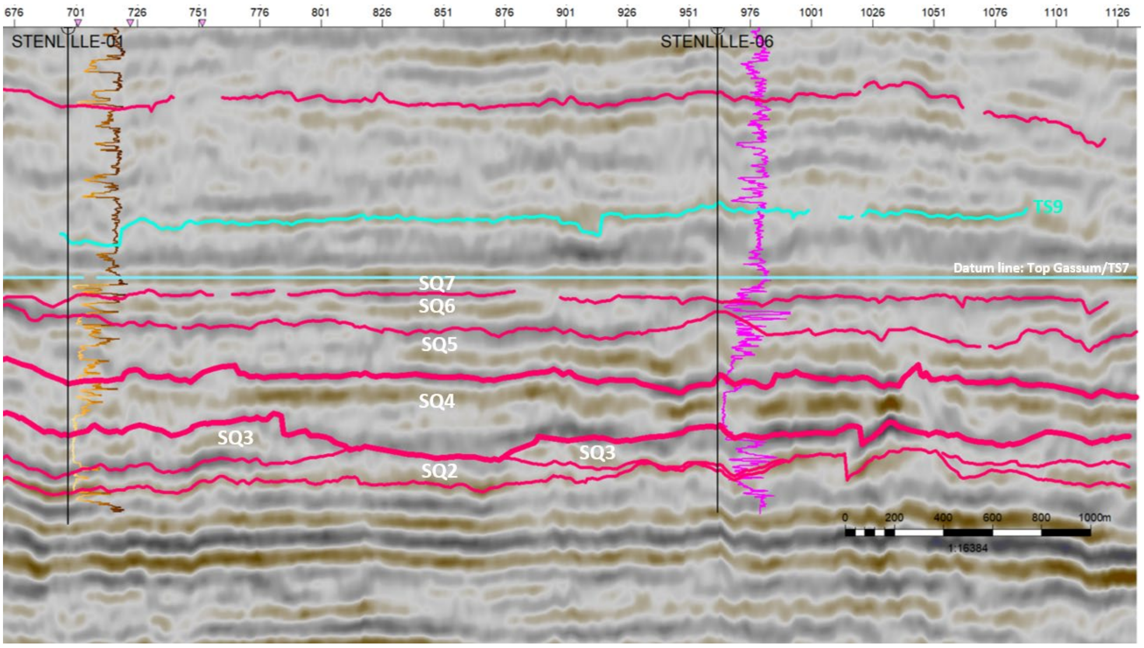

Figure 7.1.9. *SW–NE orientated 2D seismic line, DN94-D01, extending beyond the 3D survey area towards NE, and linking the ST-1 and ST-6 wells marked with their gamma-ray log motifs. The section is flattened on Top Gassum Fm (TS7) to remove later halokinetic movement and bringing seismic reflections closer to original depositional geometry. Red lines are mapped sequence boundaries of the marked sequences. Note SB4 truncating through SQ3 over a zone of c. 630 m. This incised valley is approximately up to 15 ms or c. 25–30 m deep, and thereby provides extra accommodation space available for the deposition of fluvial sand, compared to the location of the ST-1 and ST-6 wells, where the LST of SQ4 consists of fluvial sandstones in reservoir Zone 6 (Fig. 7.1.8B). Depth is in two-way travel time (milliseconds). Shown with a vertical exaggeration of 10. Location of the seismic profile is shown in Figure 7.1.5.*

Lithology, depositional environment, and provenance: The formation is interpreted to reflect a range of depositional environments including offshore, shoreface, lagoonal complex, fluvial, backshore, lakes and marsh (Fig. 7.1.6). The thickest sandstone intervals represent fluvial and shoreface LST deposits, whereas the intervening mudstone rich intervals represent offshore or lagoonal TST deposits.

Palynofacies analysis from marine facies below TS5 in general indicate marginal marine to shallow marine depositional environments, suggesting deposition in a restricted environment with limited connection to the oceans, e.g., an embayment (Lindström et al. 2020, in prep.). Palynological evidence of marginal environments is also seen in marine facies above TS5 but in general the palynofacies data indicate fully marine conditions, thus reflecting the overall backstepping of the coastline towards the basin margins and accordingly stepwise enlargement of the marine areas during the latest Rhaetian. A shallow-marine to coastal-near position in Stenlille is shown near the time (earliest Jurassic) of transgressions at or near above the Gassum Fm in Figure 3.6C.

The lowermost sequences, SQ´s 1–3, consist mainly of offshore to shoreface deposits followed by SQ´s 4 and 5 which also contain thick lowstand deposits of fluvial and subordinate shoreface sandstones (Fig. 7.1.6).

Seismic geomorphological analysis of SQ5 using mapped sequence stratigraphic horizons within the 3D seismic volume and a frequency-filtering seismic attribute show concentric shapes associated with shingled reflections and channelized incisions in 2D sections, which suggest that the fluvial sandstones were deposited in meandering river systems (Fig. 7.1.10; Smit et al. 2022).

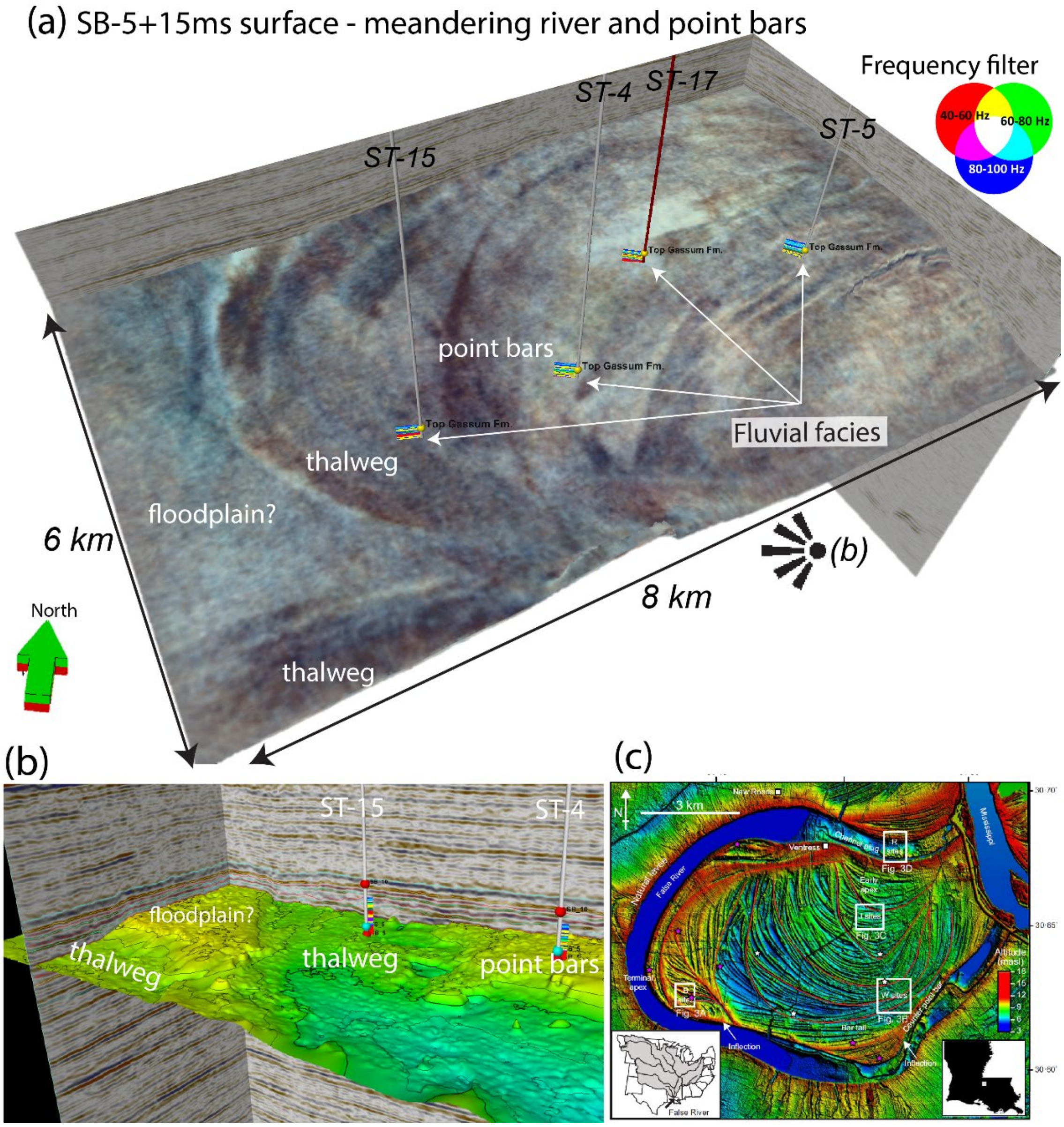

Figure 7.1.10. *A) Colour-rendering (with frequency-filtered data) of the time-shifted SB5 3D seismic horizon with 15 ms up. The concentric shapes are interpreted to reflect fluvial pointbars with the main channel (thalweg) furthest southwest. B) Time structure of mapped horizon SB5 showing the relief of the fluvial landscape. C) For comparison, an example from False River in Louisiana (USA) of similar concentric shapes representing pointbar migration formed by meandering rivers (from Clift et al. 2019).*

Incipient salt doming possibly controlled the pattern of fluvial erosion, as the 3D seismic data suggest this mainly to have occurred along the flanks of the present-day domal structure where nearly all the Stenlille wells are concentrated. Above TS5, intervals of offshore mudstone and shoreface sandstones dominate (Fig. 7.1.6), and the backstepping pattern the sequences form culminated in the overlying thick succession of offshore mudstones of the Fjerritslev Formation. Lateral variations in facies associations within the sequence systems tracts as seen for some of the sequences in Figure 7.1.6 most likely reflect lateral variability of sub-environments in a costal setting where land meets the sea and barrier islands, lagoons, estuaries and nearby rivers may alternate within short distances. Direction of depositional progradation is associated with uncertainties.

Available dip-meter measurements from ST-3, -5, -6 and -11 were evaluated and compared to cored sections, when possible, in an attempt to identify likely transport directions from sedimentary structures. Significant and reliable information on transport directions were not found, but data from ST-5 seems to suggest a general N–S coastal trend in the section represented by the lower part of core 6 changing to a WNW–ESE trend in the upper part of core 6 and to a NE–SW trend in the section represented by core 5. One fluvial cross-bed above SB 6 suggest transport toward the SSW. Data from ST-11 may suggest westward transport in the thick fluvial to fluvial-estuarine sandstone-dominated intervals.

Zircon dating from SQ´s 4 and 7 suggest that the area received sediments from southern or south-eastern source areas apart from sediments from Fennoscandia (Olivarius et al. 2020, 2022). As mentioned above, this may have occurred as a mix of fluvial systems from the north and the south that merged east of the Danish basin and transported sediment into the basin from the east and southeast in the present Baltic Sea area (Fig. 7.1.4).

Reservoir quality (porosity and permeability): The porosity variations have been determined based on interpretation of well log data that are calibrated to the core measurements, whereas the permeability estimates are based on specific porosity-permeability relationships set up for sandstone units of Gassum Formation based on the core measurements. The permeability has not been logged in any of the Stenlille wells, meaning that permeability have been evaluated from core permeability data and presumed porosity-permeability relations. Both with regards to the porosity and the permeability the core measurements correspond very well to the log derived values (Fig. 7.1.2). Thus, it is assumed that the log derived porosity and permeability also applies to the sections without cores.

When using log data, core analysis data and presumed porosity-permeability relationships, the various sandstone units and Zones can be characterized by generalized reservoir parameters, including net sand thickness, porosity, shale volume and permeability as tabulated below (Table 7.1.2). The table summarizes the results of existing well-log interpretations and current permeability assessments. The latter is outlined in detail below. The thickness of a particular zone varies across the structure and may pinch out. Similarly, the net sand thickness varies in terms of shale volume, porosity and well location. Herein 'Net sand' is defined as sandstone intervals characterized by fairly high porosities (> 10%) and low shale content (< 50%).

The porosities measured on the cores are the total porosities, i.e., including porosity within the clay minerals. The total porosity (PHIT) is also estimated from the logs; however the effective porosity is used in the characterisation of the reservoirs. The total porosities measured on the cores and the logs are in good correspondence, but when the rock includes a high volume of shale, the difference between the total porosity and the effective porosity is large. Contrary, in a clean sandstone, the total and effective porosities are similar. Looking at table 7.1.2 it is seen that in some of the reservoir zones there is a marked difference between the core porosity and the PHIE, which is caused by the clay content and in particular by the clay-bound water. This is probably also causing the high core measured values in the Zone 6 clay in ST-19 (see Fig. 7.1.2).

The conventional core analysis data point to the presence of more porosity-permeability relationships in the Gassum Formation as the depositional environment varies throughout the Late Triassic time (Fig. 7.1.11). Hence, the grain size and clay content of the Gassum Formation sandstones vary with depth and spatially. Accordingly, two distinct poro-perm models are suggested: one relation for the upper sand- and mudstone stone units (corresponding to Zones 1–5), and one relation for the lower clean sandstone unit (i.e., Zone 6). These correlations are used for estimating permeabilities in un-cored zones, meaning that the permeability assessments are derived from log data.

In particular, with respect to the Gassum Formation in the Stenlille-19 well, the average reservoir parameters as derived from the log interpretation are summarized in Table 7.1.3. The permeability range of the table is attributed to the presence of two different sandstone successions, i.e., upper sands and lower sands.

Table 7.1.2. *Generalized reservoir parameters for the Gassum Formation zones at Stenlille. The average for the reservoirs is calculated from the numbers in this table using the Zones 1, 2b, 3, 4, 5 sand, 6 sand and 6 basal unit.*

Zone (adapted from DONG)	**Net sand thick-ness** (m)	**Avg. Porosity** (%)		**Avg. Shale vol.** (%)	**Permeability** (mD)			
	Range	PHIE	Core	Vshale	Aver-age from log	max	Aver-age from core	max
1	0 – 8	21	24	25	130	956	60	568
2a	0 – 2	11	20	26	39	291	8	369
2b	0 – 8	19	23	24	134	370	84	279
3	6 – 13	25	25	13	303	879	423	6359
4	3 – 7	20	24	27	112	3438	69	382
5_clay dominated	0 – 5	13	20	32	20	104	25	442
5_sand dominated	21 - 39	25	24	12	292	697	245	549
6_clay dominated	1 – 6	17	26	32	69	1676	72	489
6_sand dominated	22 – 56	26	28	8	2999	7730	4133	9303
6_sand/clay domi-nated basal unit	7 – 34	19	N/A	17	1357	10418	N/A	N/A
Average (reser-voirs)		22	25	18	766		835	

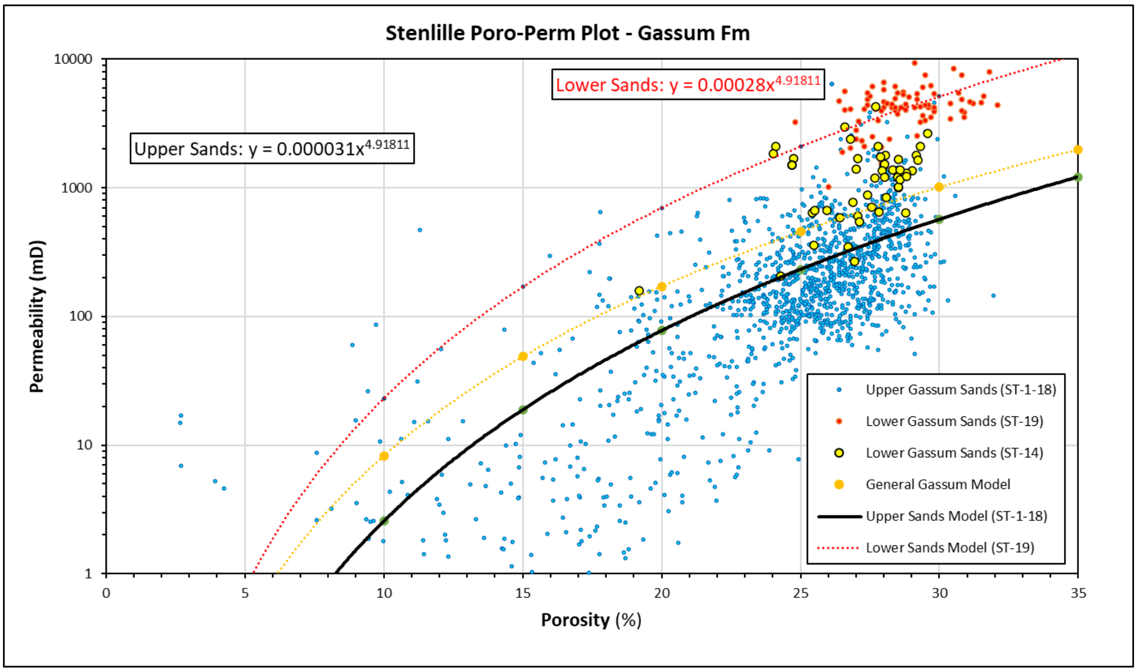

Figure 7.1.11. *Porosity-permeability relationships for the Gassum Formation sandstones. Based on conventional core analysis data from cored Stenlille wells. The black line represents the upper part of the Gassum Formation, the red line represents the lower part of the Gassum Formation. Permeability values are gas permeabilities measured in a core laboratory (GEUS, COREX etc.). The data points in orange and the orange trend line refer to the General GEUS Poro-Perm Model representing the Gassum Formation* *<u>outside</u>* *the Stenlille area (included for comparison).*

Table 7.1.3. *Generalized reservoir parameters for the Gassum Formation reservoir zones within the Stenlille-19 well.*

Well	*Zone*	Gross Sand (m)	Net Sand (m)	N/G	Avg. PHIE (%)	Avg. Core POR.	Avg. VSH (%)	Avg. PERM (mD)	Avg. Core-PERM
ST-19	*Zone 1*	8.2	4.6	0.63	15.9		26.3	32	
ST-19	*Zone 2a*	0	0.0	N/A	0		0	0	
ST-19	*Zone 2b*	N/A	N/A	N/A	N/A	N/A	N/A	N/A	N/A
ST-19	*Zone 3*	8.3	7.2	0.93	17.2		18.6	43	
ST-19	*Zone 4*	7.0	3.1	0.45	12.4		39.9	8	
ST-19	*Zone 5 clay*	4.3	0.8	0.17	11.0		33.7	4	
ST-19	*Zone 5 sand*	33.3	25.9	0.78	21.5		11.0	139	
ST-19	*Zone 6 clay*	8.2	2.0	0.25	13.1	29.9	38.8	36	
ST-19	*Zone 6 sand*	56.5	56.4	1	27.8	28.6	3.0	3732	7321
ST-19	*Zone 6 base*	8.6	6.5	0.76	14.3		35.7	247	3896

Based on these analysis the best reservoir characteristics are contained in Reservoir Zones 5 sand and 6 sand, which also are the thickest units. Zone 5 sand ranges from 21 to 39 m in thickness but also varies quite a bit in shale volume in the study area. The Reservoir Zone 5 sand has average log derived PHIE of 25%, average core porosity of 24%, average log-derived permeability of 270 mD extending up to 700 mD, and measured permeability of 250 mD with values up to 500 mD. The porosity-permeability relation in this zone may be further evaluated, as the general relation is based on all Reservoir Zones 1-5 including zones with low porosity and high clay content. It might be the case that the clean sandstones within Reservoir Zone 5 have porosity-permeability relation closer to the relation used for Reservoir Zone 6. Looking at the lowermost 25 m of Reservoir Zone 5 in the well Stenlille-19 it is estimated from the logs to be a relatively clean sandstone with average shale volume of 11% and effective porosity of 22%. Using the same porosity-permeability relation as used for Reservoir Zone 6 would take the average permeability for the Reservoir Zone 5 up to 800 mD.

The secondary reservoirs: Oddesund Fm and Bunter Sandstone Fm

The Oddesund Formation

The Oddesund Formation is largely dominated by variegated, calcareous, anhydritic claystones and siltstones and with a thick interval of evaporite beds and is interpreted as formed during prevailing brackish to hypersaline, arid conditions (Bertelsen 1980). Basically, it is thus not to be considered as a reservoir. However, locally the formation may contain intervals of sandstones as is also the case in ST-19, the only Stenlille well which penetrate the formation (Fig. 7.1.1). Input of sandstones in the otherwise fine-grained formation may have reflected increasing humidity leading to the deposition of deltaic or fluvial sand in basin marginal areas.

The sandstones are in general fine-grained, silty or slightly clayey, greenish grey or red-brown, micaceous, mainly non-calcareous and locally they contain dispersed microlignite (Bertelsen 1978). The mudstones of the lower part of the formation are interpreted to reflect deposition on flat coastal plains which were not permanently covered by water as the mudstones are predominantly reddish, common in anhydrite occurs and lack fossils (Bertelsen 1978). The sandstones from the upper part of the formation are interpreted to reflect fluvial deposition and a possible climatic change from semi-arid to more humid conditions (Bertelsen 1978).

The Oddesund Formation in the Stenlille area:

The Oddesund Formation is present in the ST-19 well in the depth interval 1858 – 2241 m MD (Fig. 7.1.1). The formation is dominated by mudstone and secondary anhydrite but also contains an interval (c. 2257–2128 m MD) of well-defined sandstone layers embedded in the mudstone (Fig. 7.1.1). The three distinct sandstone layers range in thickness from c. 2–16 m with at least the lowermost and thickest sandstone layer probably being present in the entire Stenlille structure - based on the interpretation of the available seismic data, mapped as 'Intra Oddesund sst. beds' (Fig. 6.1.1). The lithological description of the sandstones in the completion report of the ST-19 well is sparse, saying that the sandstones are very fine to fine grained, moderately sorted with subrounded grains, with calcareous cement and traces of pyrite. The color is white to light grey or olive green (DONG 2001). The thinnest sandstone is just 2 m thick and is not considered further as a reservoir for the purpose of this study.

Reservoir quality (porosity and permeability): The reservoir quality of the 3 pronounced sandstone layers in the Oddesund Formation (Fig. 7.1.1) – located in the intervals 2057–2068, 2090–2097 and 2110–2126 m MD – is not fully documented as no cores are available, meaning that sandstone permeability cannot be measured in the laboratory. However, an evaluation of the well-log data indicates fairly low shale volume and porosities up to 30%, suggesting reasonable reservoir quality. For this purpose, the porosity-permeability relation within the sand in the Oddesund Formation is expected to be similar to the Gassum Formation, and therefore a range is calculated based on the two relations outlined in Fig. 7.1.11. As the grain sizes are described as fine to very fine in the Final Well Report, the positive porosity-permeability relation shown in Fig. 7.1.11 may cause too optimistic permeability estimates. On the other hand, the volume of shale is considered lower than the average shale volume for the Reservoir Zones 1–5 (Gassum Fm) across the Stenlille area.

The average reservoir parameters as derived from the log interpretation of the ST-19 well are summarized in Table 7.1.4 including all three sandstone layers.

Table 7.1.4. *Reservoir parameters for the Oddesund Formation (Intra Oddesund sst. beds) at Stenlille based on the Stenlille-19 well (Fig. 7.1.1). Note the Gross Sand is taken from the top of the uppermost reservoir to the bottom of the lowermost reservoir, hence it is not the full thickness of the formation.*

Well	Formation	Gross Sand, m	Net Sand, m	N/G	Avg. Porosity (%)	Avg. Permeability (mD)
ST-19	Oddesund	38	28	0.74	19	135 –1222

The Bunter Sandstone Formation

The Bunter Sandstone Formation is known from deep boreholes in Denmark and Sweden and is widespread in the Danish Basin and the North German Basin. The geothermal plant at Margretheholm in Copenhagen is designed to use hot water from sandstone layers in the formation. The formation is less than 300 meters thick in the southern Danish area, and over the Ringkøbing–Fyn High the formation is either thin or absent. The high and adjacent areas were probably partially exposed in the Early Triassic (Michelsen et al. 1981). The formation consists of reddish-brown and yellow-brown, fine- to medium-grained sandstone, in addition to thick intervening intervals of siltstone and claystone. Locally, the deposits are strongly calcareous, anhydrite and micaceous. In the Danish Basin, the formation is replaced to the north by coarse-grained sandstones belonging to the Skagerrak Formation (Fig. 3.3). The Bunter Sandstone Formation was formed in the Early Triassic in a dry and hot desert climate (Fig. 3.5B). Ephemeral rivers transported sand, mainly from the Fennoscandian basement, into the central part of the Danish basin, where the sand was deposited in river channels. Vegetation was extremely sparse, and during the dry periods wind created sand dunes. Periodically eolian sand was supplied to the Danish Basin from the south (Olivarius 2015). In between the river channel and dune sand, layers of clay were deposited in lakes.

In the North German Basin, the Bunter Sandstone Formation is divided into four members, each consisting of a sandstone succession followed by a relatively thick claystone succession. Two of these members (Volpriehausen and Solling members), and partly the Defurth Member, can also be recognized in most of the deep Danish onshore wells that penetrate the Bunter Sandstone Formation (Bachmann et al. 2010, Michelsen & Clausen 2002).

The Bunter Sandstone Formation in the Stenlille area:

Only one of the Stenlille wells (ST-19) is drilled deep enough to reach the Bunter Sandstone Formation (Fig. 7.1.1). The ST-19 well penetrates the top of the formation at c. 2410 m TVD (2464 m MD). The well reveals a minimum thickness of the formation of 106 m; the base of the formation has thus not been penetrated. Seismic mapping and interpretation indicate a widespread occurrence of the formation with subtle prograding/onlapping reflections and troughs, which may indicate depositional systems with sandstones and/or local tectonics at structure flanks near ST-19 (Fig. 6.1.1). The thickness of the formation may from seismic interpretation be in the order of c. 200–250 m (Fig. 6.1.1, 7.1.1) within the 3D survey area. Michelsen & Clausen (2002) interpret the Volpriehausen, Defurth and Solling members also to be present in the ST-19 well (Fig. 7.1.12). The lithological description of the sandstones published in the ST-19 completion report says that the sandstones are fine to medium grained, well sorted with rounded grains, and with calcit cement. The colour is described as red-brown to light grey to smokey (DONG 2001).

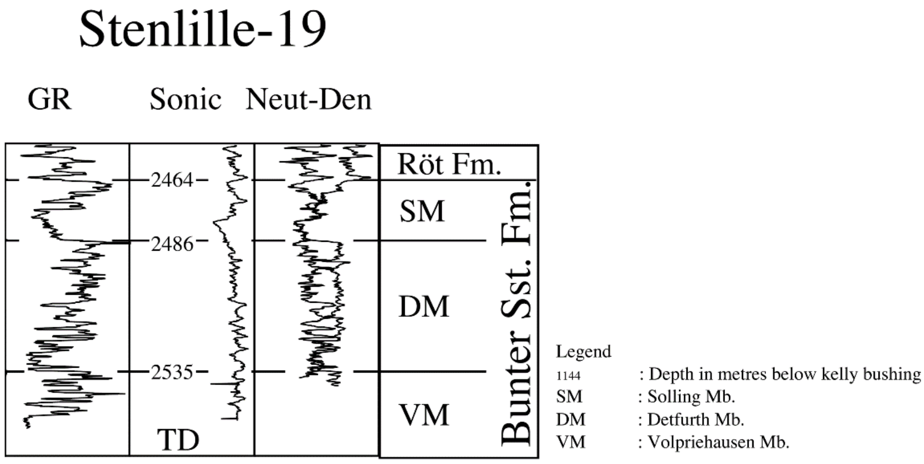

Figure 7.1.12 *Subdivision of the Bunter Sandstone Formation in the ST-19 well into the Volpriehausen, Detfurth and Solling Members. Modified from Michelsen & Clausen (2002).*

Reservoir quality (porosity and permeability): In general, the reservoir quality of the Bunter Sandstone Formation is presumed good, since the aeolian deposits that characterizes the formation have a large lateral continuity, a fairly constant thickness, and only few cementing phases that are mostly clay-free. A smaller part of the Bunter Sandstone Formation has been cored in the Stenlille-19 well (at *c.* 2500 m MD; Fig. 7.1.1) covering parts of the reservoir and the underlaying mudstone. The cored interval is approximately 20 m thick, and the conventional core analysis data are plotted in Figure 7.1.13 within the reservoir zone of the Bunter Sandstone Formation the core measured porosity ranges from 15% to 26% and corresponds well with the log derived PHIE. The core measurements of the permeability within the sandstone vary from 17 to 1132 mD.

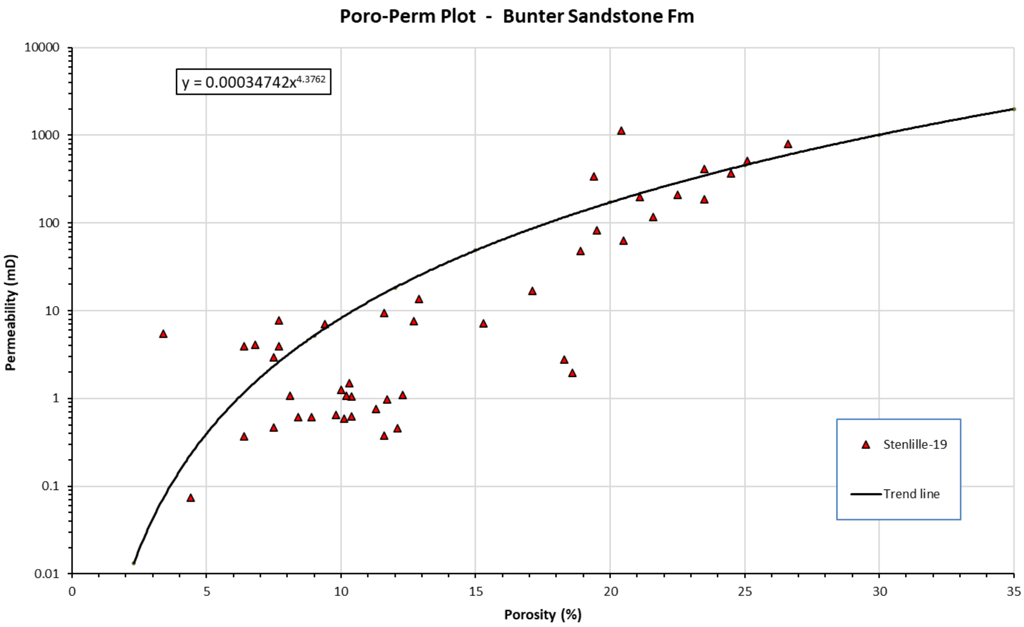

Figure 7.1.13. *Porosity-permeability relationships for the Bunter Sandstone Fm sandstones cored in the Stenlille-19 well. Based on conventional core analysis data. The black line represents the presumed trend line of the Bunter Sandstone Formation. This specific trend line is supported by core analysis data that are available from wells located outside the Stenlille area. Permeability values are gas permeabilities measured by the COREX Core Laboratory.*

With respect to the Bunter Sandstone Formation in the Stenlille-19 well, the average reservoir parameters as derived from the log interpretations and the core measurements are summarized in Table 7.1.5:

Table 7.1.5. *Generalized reservoir parameters for the Bunter Sandstone Formation at Stenlille (Stenlille-19 well). The Gross Sand is the thickness from the top to the base of the reservoir, and as there is only a single potential reservoir interval in the Bunter Sandstone Formation from ST-19 (Fig. 7.1.1), the Gross and Net sand are equal. Note that this well does not penetrate the full thickness of the Bunter Sandstone Formation.*

Well	Formation	Gross Sand (m)	Net Sand (m)	N/G	Avg. Porosity (PHIE %)	Avg. Porosity (Core %)	Avg. Perm (log, mD)	Avg. Perm (Core, mD)
ST-19	Bunter Sandstone	12	12	1	19.1	21.1	203	231

Thus a 12 m thick reservoir of fine-grained sandstone having an average effective porosity (PHIE) of 19.1% and log derived permeability of 203 compared to the measured average permeability of 231 mD, although measurements exceeding 1100 mD are seen.

7.2 Seals – Summary of geology and parameters

The primary seal of the Gassum Fm: The Fjerritslev Fm

The Lower Jurassic Fjerritslev Formation is known from more than 50 deep wells in the Danish onshore and inland water areas and the well-sections show that the present distribution is largely controlled by Middle Jurassic and younger erosional events. The lithostratigraphy and positions of the wells drilled before 1990 were compiled by Nielsen & Japsen (1991). In the Stenlille area, sandstones of the Upper Triassic Gassum Formation are used for temporal storage of natural gas with the Fjerritslev Formation constituting the seal (Fig. 2.1, 2.4, 3.1). On the storage site the Fjerritslev Formation is known from seismic data and from19 deep wells showing a thickness of c. 250–300 m (Fig. 6.2.4B; Table 7.2.1).

The Fjerritslev Formation is a succession of marine claystones and mudstones, interbedded with thin sandstone units. It is present in the Danish Basin, north of the Ringkøbing–Fyn High, and in the North German Basin south of the Ringkøbing–Fyn High, but absent on the high itself. In the central part of the Danish Basin (including the Stenlille area) the fluvial to shallow marine Gassum Formation is of Rhaetian (latest Triassic) age and is overlain by the Fjerritslev Formation of Early Jurassic age.

However, in the Sorgenfrei–Tornquist zone and on the Skagerrak–Kattegat Platform deposition of sand continued through the Hettangian and into the earliest Sinemurian and is included in the Gassum Formation (Nielsen 2003; Fig. 7.1.1). Towards the SE and E (southern Sweden and Bornholm) the Fjerritslev Formation is replaced by sandstone-dominated formations deposited in non-marine and coastal depositional environments (Gravesen et al. 1982, Surlyk et al. 1995).

At Stenlille, Middle–Upper Jurassic and lowermost Cretaceous sediments are missing, and the Fjerritslev Formation is unconformably overlain by the Lower Cretaceous Vedsted Formation (Dybkjær 1991; Fig. 3.7, 7.2.1). This is in contrast to the Sorgenfrei–Tornquist Zone where the Haldager Sand, Flyvbjerg-, and Børglum Formations were deposited in the Middle Jurassic to earliest Cretaceous (Michelsen 1989a; Michelsen et al 2003; Nielsen 2003). Palaeogeographical reconstructions suggest that the Ringkøbing–Fyn High and adjacent areas, including the Stenlille area, were characterized by deposition of terrestrial deposits or by erosion during Middle–Late Jurassic as well as in earliest Cretaceous times (Michelsen et al. 2003; Petersen et al. 2008; Fig. 3.7). The Stenlille area was also affected by growth of the Stenlille salt pillow and the regional, mid-Cimmerian tectonic phase (Gregersen et al. 2022).

On Zealand, the Fjerritslev Formation is well documented in the Stenlille area, where 19 wells penetrate the formation and thus provide data (petrophysical logs, cuttings, and cores; Section 4.4; Fig. 7.2.2). Most of the cores have been taken in the lower part of the Fjerritslev Formation and document the transition from the Gassum to the Fjerritslev Formation. In the Stenlille-1 well, the succession in core 2 has previously been referred to the Vedsted Formation (Pedersen et al. 2022), but current investigations suggest that the boundary between the Fjerritslev and Vedsted Formations may be located near the top of core 2. The Lower Cretaceous Vedsted and the Rødby Formations are overlain by the Upper Cretaceous Chalk Group, which is around 1000 m thick. The Chalk Group is overlain by 200–225 m of Cenozoic to Quaternary strata including Danian limestones, Selandian greensand and marl, and Quaternary deposits.

Age of the Fjerritslev Formation

The age of the Fjerritslev Formation is well-constrained by investigations of ammonites and bivalves (Sorgenfrei & Buch 1964), ostracods (Michelsen 1975, 1989a), and palynomorphs (Dybkjær 1988, 1991; Lindström 2015, 2017, 2019, 2020) showing that the formation covers the latest Rhaetian to the Toarcian, and possibly includes Aalenian deposits locally. In the Stenlille area the basal part of the Fjerritslev Formation is of latest Rhaetian age and the youngest part is Late Toarcian (Dybkjær 1991; Vosgerau et al. 2016; Lindström 2020).

The well-dated end-Triassic mass extinction event (ETE) is documented in cores from the lowermost part of the Fjerritslev Formation between SB-8 and TS-8 in the Stenlille wells ST-1, ST-4, ST-5, and ST-6 and provides a well-defined correlation to the Lavø-1 and Rødby-1 wells and to the latest Triassic–earliest Jurassic succession in Scania (Lindström 2012; Lindström et al. 2017; Lindström et al. in prep.). The event is represented by characteristic grey siltstones in the Stenlille wells forming a distinct marker bed that is correlated to the GSSP section at Kuhjoch in Austria, and to several successions in northern Germany (Lindström et al. 2017).

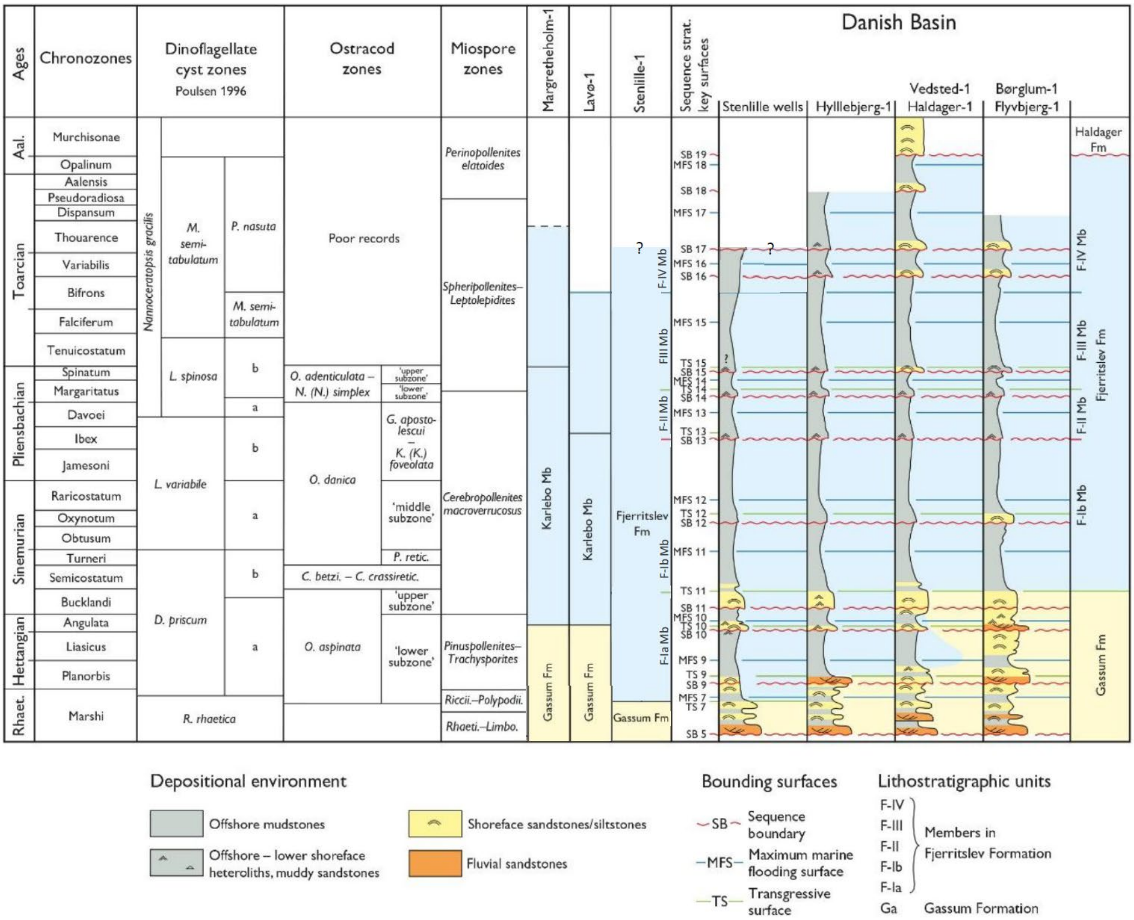

Figure 7.2.1. *Detailed litho-, bio-, and sequence stratigraphy of uppermost Upper Triassic to lowermost Middle Jurassic successions in the Danish Basin including Stenlille wells. Modified from Nielsen (2003) and Pedersen et al. (2022). A major unconformity (hiatus) separates the Lower Jurassic Fjerritslev Fm from the overlying Lower Cretaceous Vedsted Fm (Fig. 6.1.1). The precise age gab from the uppermost preserved Fjerritslev Fm to the lowermost Vedsted Fm is uncertain due to few core data and analyses. This part of the stratigraphy in Zealand is currently under revision.*

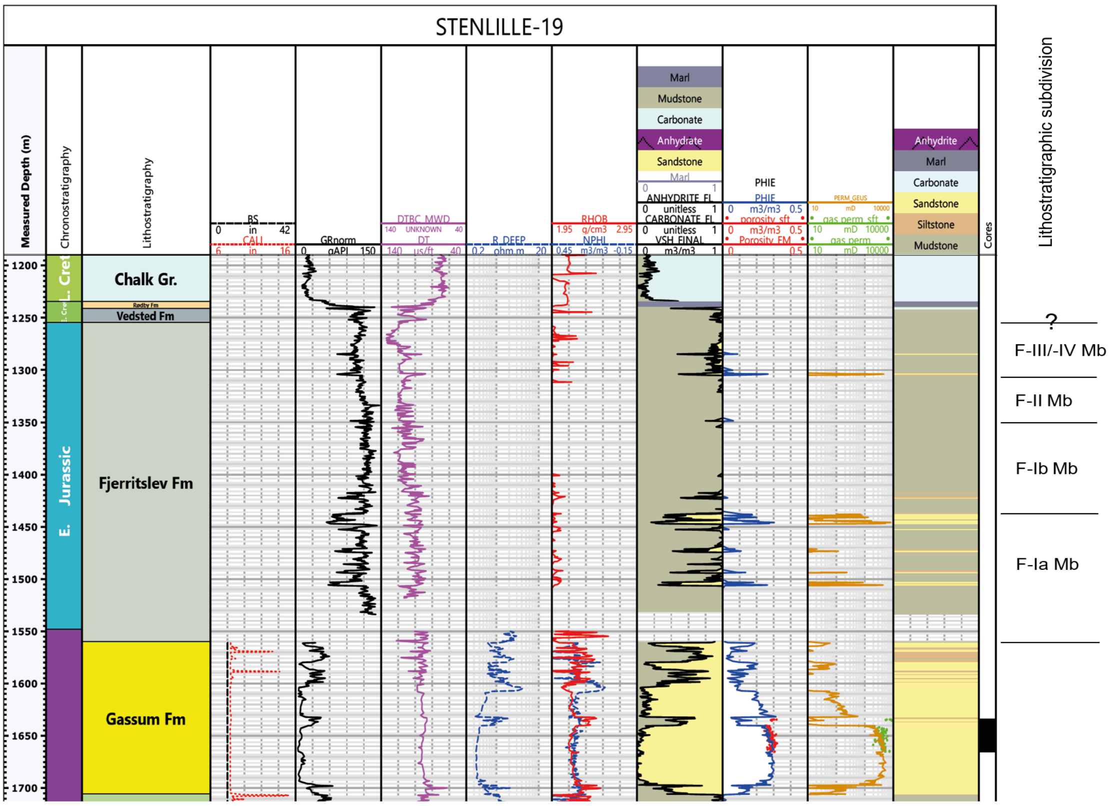

Figure 7.2.2. *Petrophysical logs from Stenlille-19 well with the primary reservoir sandstone successions of the Gassum Formation and the overlying mudstone seal successions of the Fjerritslev Formation (primary seal), followed by the Vedsted Formation to the Chalk Group (secondary seals). The Fjerritslev Formation is subdivided into members dominated by mudstones. Note that the lowermost F-Ia Member contains a number of thin sand- and siltstone layers in contrast to the other members. The uppermost two members (if both are present) are not distinguished here. The figure is a zoomed section from Fig. 7.1.1.*

Lithological subdivision

The Fjerritslev Formation was defined by Larsen (1966) and revised by Michelsen (1978, 1989a; Michelsen et al. 2003). The formation is divided into five members F-Ia, F-Ib, F-II, F-III, and F-IV using the Hyllebjerg-1 as reference section (Michelsen 1989a). A detailed correlation between wells located centrally in the Danish Basin shows that characteristic log-patterns can be traced across long distances suggesting that the formation comprises a high number of thin, but laterally continuous depositional units (Michelsen 1989b). A sequence stratigraphic division of the Gassum and Fjerritslev Formations was presented by Nielsen (2003). The base of Fjerritslev Formation is defined at TS-7 in the central part of the Danish Basin and also in the Stenlille area. The boundaries of the five members (F-Ia to F-IV) correlate to sequence stratigraphic surfaces (Table 7.2.1) (Nielsen 2003).

The log-patterns described by Michelsen (1989b) are difficult to recognize in the Stenlille wells. Here thin sandstones with large lateral continuity are present in the F-Ia Member, separated by clay- and mudstones (Fig. 7.2.3). The F-Ia Member is laterally equivalent and contemporaneous with the Lower Jurassic part of the Gassum Formation toward the basin margins. Lateral variations in thickness from wells within the Fjerritslev Formation are exemplified in Table 7.2.1, showing that the Fjerritslev Formation is c. 260–300 m thick in the Stenlille area, and slightly more range from seismic mapping (Fig. 6.2.4B). The F-Ia Member is the thickest of the members and is even thicker here than further to the northwest in the Danish Basin. In contrast, the F-Ib to F-IV Members are thin at Stenlille compared with central to northern Jutland (Table 7.2.1; Fig. 7.2.3, 7.2.4).

<table>
<tr><td colspan="2"></td><td colspan="7">Fjerritslev Formation</td><td>Age</td></tr>
<tr><td colspan="2">Location/wells</td><td colspan="2"></td><td>N. Jutland</td><td>Rø-1</td><td>ST-19</td><td>ST-2</td><td>ST-1</td><td></td></tr>
<tr><td colspan="2" rowspan="2">Depth (m) to</td><td colspan="2">Top Fjerritslev Fm</td><td>~1920</td><td>2138</td><td>1254.5</td><td>1217</td><td>1220.5</td><td>Toarcian</td></tr>
<tr><td colspan="2">Base Fjerritslev Fm</td><td>~2400</td><td>2613</td><td>1560</td><td>1511</td><td>1509</td><td>L Rhaet.–E Sinemur</td></tr>
<tr><td colspan="2"></td><td colspan="2">Thickness (m)</td><td>~500</td><td>475</td><td>305.5</td><td>294</td><td>288.5</td><td></td></tr>
<tr><td colspan="2"></td><td colspan="2">Sequence stratigraphy</td><td colspan="5">Thickness (m)</td><td>Age</td></tr>
<tr><td colspan="2"></td><td>Lower boundary</td><td>Upper boundary</td><td></td><td></td><td></td><td></td><td></td><td></td></tr>
<tr><td rowspan="5">Lithostratigraphy</td><td>F-IV Mb</td><td>SB-16 *</td><td>SB-19</td><td>30 – 50</td><td>38</td><td rowspan="2">61.5</td><td rowspan="2">61</td><td rowspan="2">63.5</td><td>Toarcian</td></tr>
<tr><td>F-III Mb</td><td>TS-14</td><td>SB-16*</td><td>150 – 200</td><td>145</td><td>Early Toarcian</td></tr>
<tr><td>F-II Mb</td><td>SB-13</td><td>TS-14</td><td>30 – 80</td><td>73</td><td>39</td><td>36</td><td>35</td><td>Pliensbachian</td></tr>
<tr><td>F-Ib Mb</td><td>TS-11</td><td>SB-13</td><td>150</td><td>141</td><td>83</td><td>84</td><td>72</td><td>Sinem.–E. Pliensb.</td></tr>
<tr><td>F-Ia Mb</td><td>TS-7 / TS-9</td><td>TS-11</td><td>75 – 80</td><td>64</td><td>122</td><td>113</td><td>118</td><td>Rhaet.–Hettangian</td></tr>
</table>

Table 7.2.1. *Thicknesses of the members of the Fjerritslev Formation in wells from Danish Basin south of the Sorgenfrei-Tornquist Zone. *: The lower boundary of the F-IV Member is positioned between MFS-15 and SB-16. The column N. Jutland shows characteristic thicknesses in Hyllebjerg-1, Kvols-1, Skive-1, and Hobro-1 wells south of the Sorgenfrei–Tornquist Zone (Michelsen 1989b). Rø-1: Rønde-1, located in the central part of the Danish Basin, between Hyllebjerg-1 and the Stenlille area further to the east. ST-1, ST-2, ST-19: Wells in the Stenlille area. Biostratigraphy in ST-1,-2,-19 from the present study (K. Dybkjær & E. Sheldon). Sequence stratigraphy after Nielsen (2003: fig. 31) and modified in this study (H. Vosgerau), also providing the calculated thicknesses.*

The F-Ia Member

In Stenlille, the F-Ia Member is bounded the sequence stratigraphic surfaces TS-7 and TS-11. The member is around 120 m thick, and the lithology and biostratigraphy in the lower part of the member is well documented in cores from several wells (Fig. 7.2.3). The member comprises a number of sedimentary facies ranging from laminated claystones to heterolithic mudstones interpreted as deposited in lower offshore to lower shoreface environments (Pedersen 1985). It differs in lithology from the overlying members by containing a number (c. 7–10) of sandstone and siltstone units, 1–20 m thick, which can be traced laterally with varying thickness (Fig. 7.2.3; Appendix B (ST-1, 2, 5, 6,18, 20). Interpretation of the well-logs show that some sandstone beds are well-sorted with high porosities and permeabilities whereas other units, with intermediate values, probably are heterolithic (Vosgerau et al. 2016). The lower part of the F-Ia Member includes a series of grey siltstone beds between SB-8 and TS-8 Lindström et al. (2015). The siltstones constitute a distinct chronostratigraphic marker bed with wave-ripple cross-lamination, water-escape structures and numerous soft-sediment deformation structures indicating deposition in a shoreface environment around fair-weather wave base. The siltstones mark a sudden shallowing compared to the black claystones below, which includes MFS-7, and to the mudstones above.

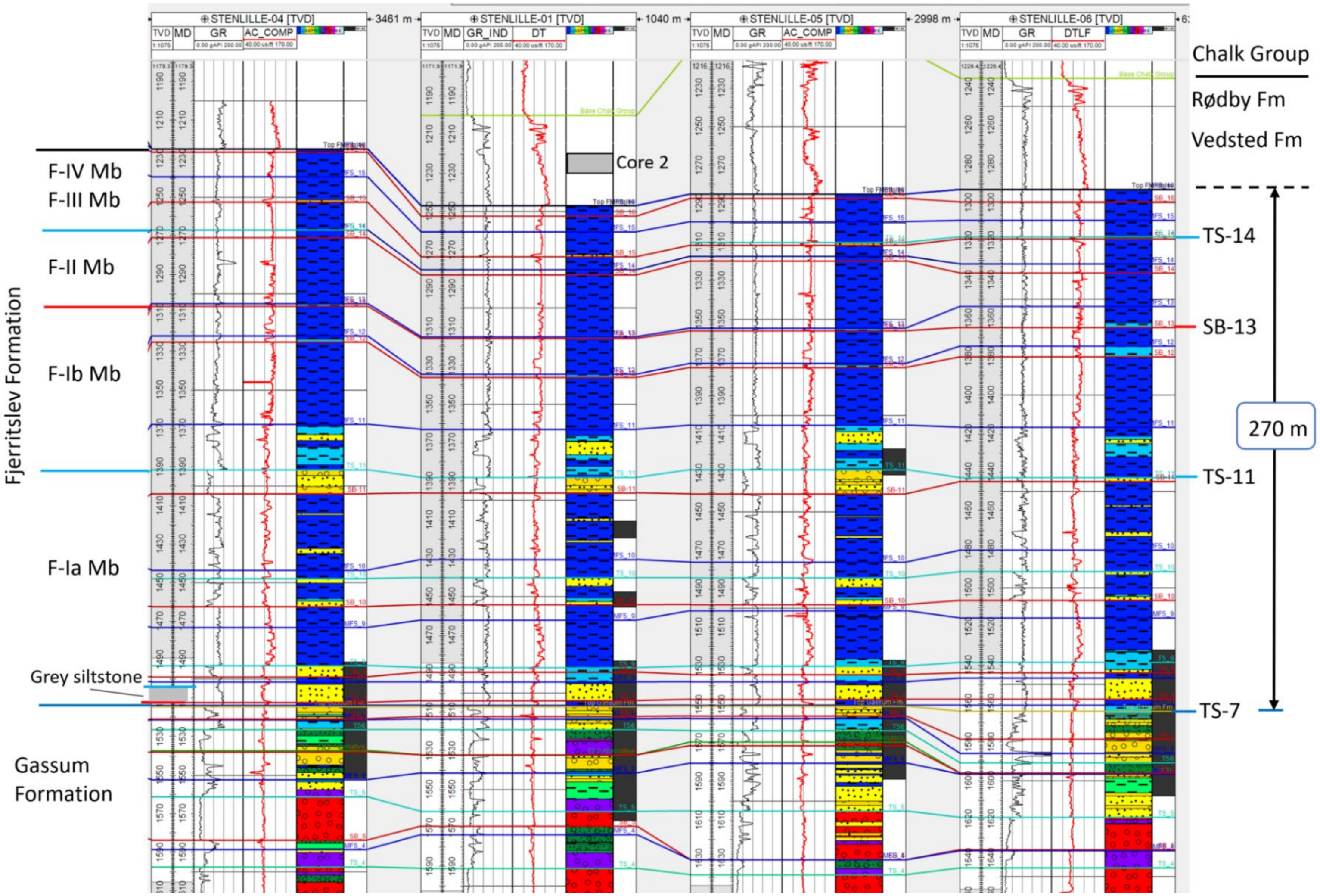

Figure 7.2.3. *Lateral changes in facies through the Fjerritslev Formation. Interpretation from petrophysical logs by H. Vosgerau. Sequence stratigraphic surfaces define the boundaries between the members in the Fjerritslev Formation. The dark blue colour represents mudstones, bluish green is siltstone and yellow is sandstones. Cored intervals are shown in black. Note that here are slight variations in the thickness of each member laterally. The Fjerritslev Fm/Vedsted Fm boundary is currently under revision due to new biostratigraphy (K. Dybkjær & E. Sheldon), implying a slightly shallower position than shown in the present figure (see Section 7.2). For location of the wells see Fig. 4.1.2.*

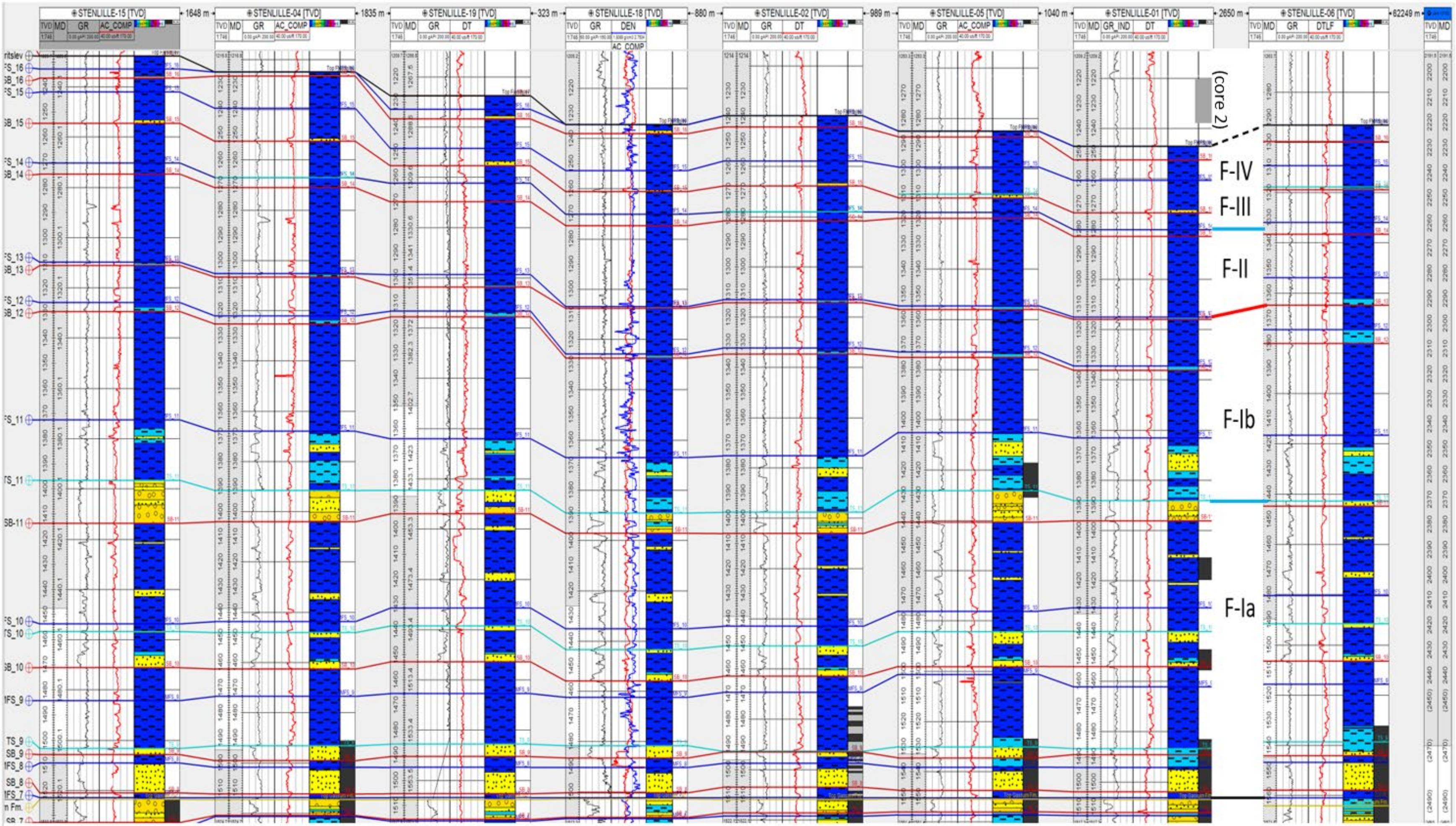

Figure 7.2.4. *Correlation of petrophysical logs and interpreted lithologies in the Fjerritslev Formation (Members F-Ia to F-IV) in wells from the Stenlille area. The logs demonstrate lateral continuity, and minor variations in lithologies and thicknesses. Lithological and sequence stratigraphic interpretation by H. Vosgerau. Cores are available mainly from the basal part of the F-Ia Member. Core 2 in Stenlille-1 is shown in grey. The top of this core is referred to the Lower Cretaceous Vedsted Fm. The Fjerritslev Fm/Vedsted Fm boundary is currently under revision due to new biostratigraphy (K. Dybkjær & E. Sheldon), implying a slightly shallower position than shown in the present figure (see Section 7.2).*

The siltstones contain the *Riccisporites-Polypodisporites* Zone, which formed during the global end-Triassic mass-extinction (ETE) that is linked to volcanic activity in the Central Atlantic Magmatic Province (CAMP), atmospheric changes, increased wildfire activity and deforestation causing increased erosion in the hinterland and larger influx of silt and sand (Fig. 7.2.5) (Petersen & Lindström 2012; Lindström et al. 2015, 2017).

The F-Ib Member

Samples from the Gassum-1 well (Fig. 3.1, eastern Jutland) show that the marine fauna of benthic bivalves perished in the lower part of the F-Ib Member probably caused by a change from normal marine to restricted (oxygen-poor) sea-floor environments (Pedersen 1986). The ostracod fauna also shows a major change in species (Michelsen 1975). The faunal changes in the F-Ib Mb are interpreted to reflect a marine transgression during the Sinemurian to Pliensbachian that also led to a lithological change in Northern Jutland where deposition of sand (Gassum Formation) was replaced by mudstones (Fjerritslev Formation; Nielsen 2003: Fig. 25, 31). The transgression is also recorded in southern Sweden and at Bornholm (Frandsen & Surlyk 2003; Donovan & Surlyk 2003). Figure 7.2.3 shows a thin sandstone unit in the basal part of the F-Ib Member interpreted as formed during the transgression. The overlying part of the F-Ib Member is lithologically uniform, characterized by fine-grained mudstones probably with a relatively high content of organic matter.

The F-II Member

In northern Jutland the F-II Member is characterized by influx of sand and silt, which resulted in deposition of heterolithic sandstones. This was not the case in the Stenlille area, where the member is fine-grained and difficult to distinguish from the F-Ib Member below and the F-III Member above. The F-II Member is bounded by SB-13 and TS-14 (Fig. 7.2.3, 7.2.4). It may be speculated, that sand, supplied from the NE, E and SE was trapped in the Øresund Basin and that the eastern part of the Danish Basin was a starved basin during deposition of the F-II Member.

The F-III and F-IV Members

The gamma-log values recorded in the Fjerritslev Formation at Stenlille show very little contrast between the F-II, F-III and F-IV members (Fig. 7.2.3). The F-III Mb is around 20 m thick, and clearly condensed in comparison with northern Jutland, where it is 150–200 m thick (Table 7.2.1). Petersen et al. (2008) examined the amount and composition of the organic matter contained in the Toarcian marine mudstones of the F-III and F-IV members in the central part of the Danish Basin. These members locally include intervals with hydrogen index (HI) values of 300–400 mg HC /g TOC (HC: hydrocarbons; TOC: total organic carbon) see also Michelsen (1989b). The high values indicate that the mudstones were deposited in deep-water with anoxic or oxygen-poor marine environments. This agrees well with the lack of benthic fauna in the F-III Member in the Gassum-1 well (Pedersen 1986). The mudstones are probably very fine-grained with a low permeability.

The F-IV Member is up to 45 m thick in the Stenlille wells (Fig. 7.2.3, 7.2.4). Palynomorphs from the F-IV Member in the Stenlille-2 well indicate that deposition of marine mudstones continued into the Toarcian (Dybkjær 1991). The thickness is comparable to that of the member in northern Jutland (Table 7.2.1), possibly because the boundary between the Fjerritslev

Formation and the overlying Haldager Sand Formation there is a major erosional unconformity (Fig. 7.2.1). The major hiatus between the Lower Jurassic Fjerritslev Formation (Toarcian F-IV Mb) and the Lower Cretaceous Vedsted Formation in Stenlille, and faulting in the Fjerritslev Fm may have been caused partly by uplift and erosion due to growth of the Stenlille salt pillow, and partly by regional uplift (Section 6.2; Gregersen et al. 2022).

Bulk mineralogy

The bulk mineralogy of the Fjerritslev Formation was examined in 12 samples from ST-5 (Mathiassen et al. 1989). The data show a positive correlation between quartz and feldspars which suggest that both of these minerals dominate the coarse silt to sand fractions. This interpretation is supported by a negative correlation between quartz (and feldspars) and clay minerals. The bulk mineralogy of mudstones from the Gassum and Fjerritslev Formations are shown in Vosgerau et al. (2016). Quartz is the dominant mineral in all samples followed by kaolinite and illite or mica. Feldspars are present in some samples. Calcite, siderite or pyrite are present in some samples, mainly in the mudstones.

Clay minerals

Mathiassen et al. (1989) also examined the clay mineral assemblage in the mudstone facies, which are characterized by clay-to fine-grained silt sized particles. Total organic carbon (TOC) and pyrite (FeS2) correlate with the clay content. The analyses of samples from the lower part of the Fjerritslev Formation in ST-5 and ST-6 show that the mudstones generally contain ≤ 60% clay minerals, quartz (≥20 %), feldspars (≤5%), pyrite (≤5%) and varying contents of calcite or siderite (Mathiassen et al. 1989). Clay mineral analyses from the Fjerritslev Formation are few, but some results were included in Vosgerau et al. (2016). They show that kaolinite is the dominant clay mineral followed by mixed-layer clays, and illite. Vermiculite is present in small amounts and smectite was not recognized. Ten samples from the Fjerritslev Formation in Kvols-1 (northern Jutland) shows little variation through the formation. All samples are dominated by kaolinite, followed by mixed-layer minerals, vermiculite and mica. A similar mineral assemblage is reported from the Lower Sinemurian section at Örby (Scania, southern Sweden). Here the clay mineralogy is characterized by kaolinite and mica throughout the section and increasing amounts of chlorite and mixed-layer minerals occur in the marine deposits (Erlström et al. 1999).

Diagenesis, burial and exhumation

Vitrinite reflectance values are a proxy for maximum temperatures during burial. Petersen et al. (2008) measured 560 vitrinite reflectance (VR) values in samples from 26 wells in the Norwegian–Danish Basin and concluded that the Fjerritslev Formation experienced a significant post Early Cretaceous uplift in most of the basin. The data closest to Stenlille area are from the Rønde-1 well and it was estimated that the Fjerritslev Formation in this well was uplifted c. 400 m. Based on study of the sonic velocities measured in Stenlille wells Japsen & Bidstrup (1999) estimated that the Fjerritslev Formation was uplifted c. 600 m during Neogene time in this area. This extra burial depth may be considered when the capacity and quality of the Fjerritslev seal is evaluated.

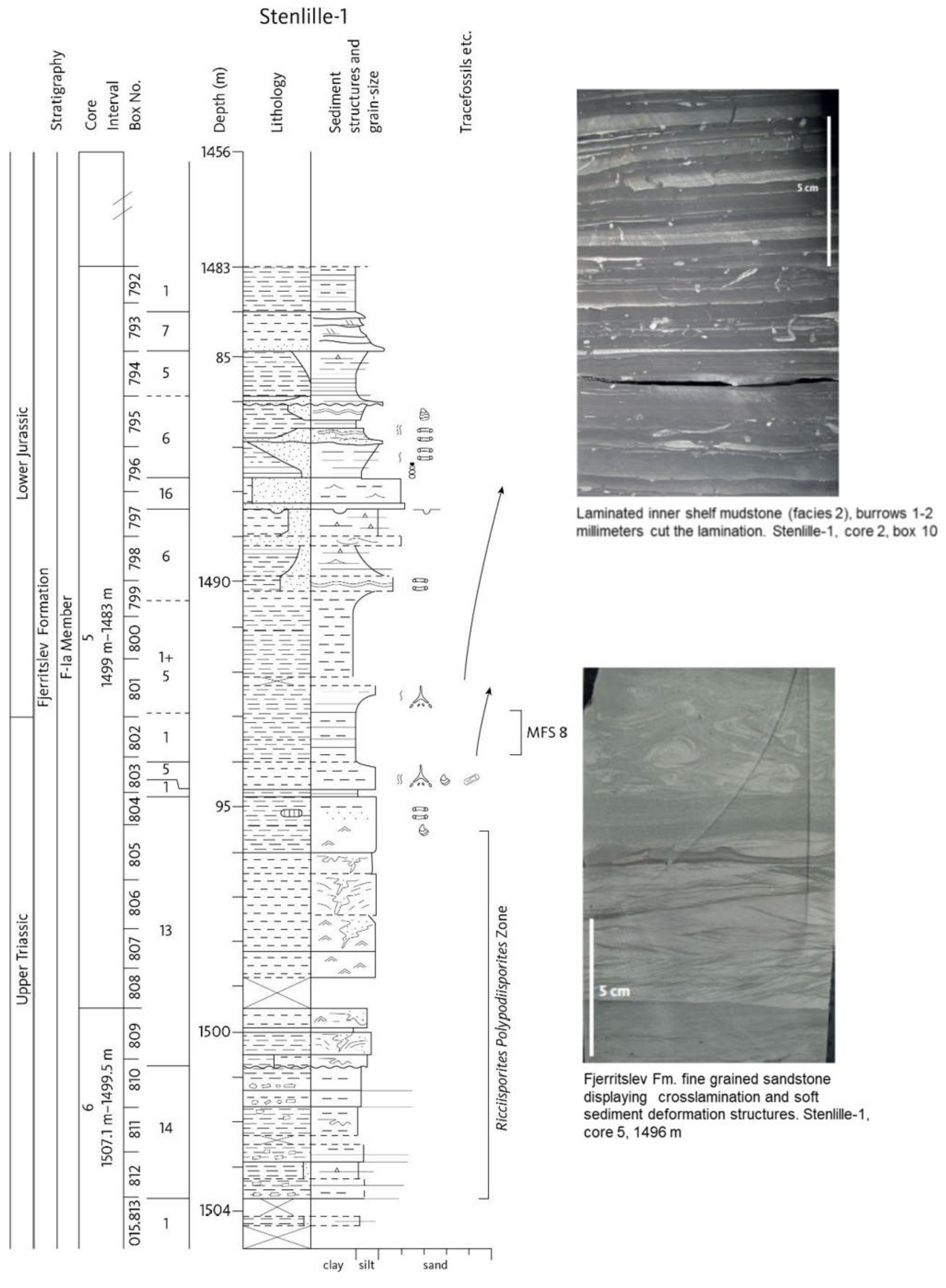

Figure 7.2.5. *Sedimentological logs of the transition from the Gassum Formation to the lowermost part of the Fjerritslev Formation (F-Ia Mb) with examples of core photos from the Stenlille-1 well. From Pedersen et al. (2022).*

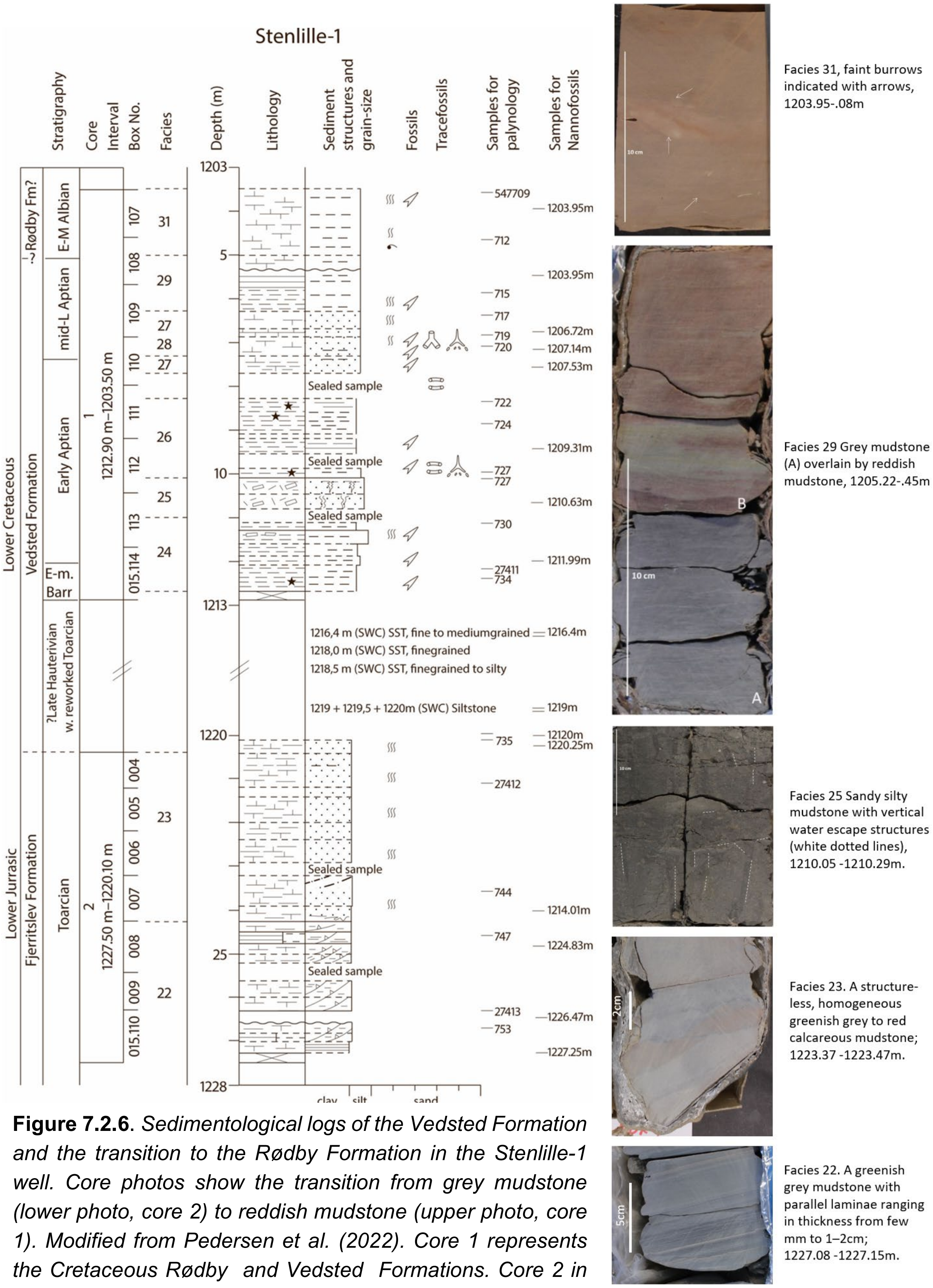

Figure 7.2.6. *Sedimentological logs of the Vedsted Formation and the transition to the Rødby Formation in the Stenlille-1 well. Core photos show the transition from grey mudstone (lower photo, core 2) to reddish mudstone (upper photo, core 1). Modified from Pedersen et al. (2022). Core 1 represents the Cretaceous Rødby and Vedsted Formations. Core 2 in Stenlille-1 (1220.1-1227.5m MD) is shown with a revised Top Fjerritslev at the dashed black line determined from new bio-stratigraphic data – See the section on the secondary seals.*

Seal capacity of the Fjerritslev Formation

The seal capacity of the Fjerritslev Formation was examined by Springer et al. (2020). They state, in their summary, that the sealing capacity of the Fjerritslev Formation has mostly been studied in the Stenlille area. Here, the seal is the >200 m thick Fjerritslev Formation (c. 240–300 m; Fig. 6.2.4B), with interbedded porous sandy-silty layers (within the F-Ia Member) that divide the seal into a lower and upper seal unit. Average porosity is 11%, and air-permeability is 160 µD. A single liquid permeability measured at in situ conditions in a massive mudstone layer from Stenlille reached a value of 3 nD, which is similar to the best petroleum caprocks known, a few other overburden measurements gave liquid permeabilities around 200 nD (Springer et al. 2020). Thus, the Fjerritslev Formation, and in particular its upper part above the F-Ia Member, is an excellent seal in the Stenlille area, where natural gas has been stored in the Gassum Formation below the seal for more than 30 years. The good quality of the seal is probably a function of mineralogic composition and the pre-Neogene maximum burial depth in combination with the great overburden thickness.

Capillary entry pressure

The critical rock property for fluid entering the seal is the capillary entry pressure of the rock. Experiences from the petroleum industry confirms that shales in general are excellent caprocks. Capillary drainage displacement experiments by Mercury injection (MICP, Mercury Injection Capillary Pressure) are a fast technique to obtain entry pressures for caprocks. The governing parameters for the capillary entry pressure are the pore-throat size distribution and the wetting properties of the rock-fluid system.

One disadvantage for using MICP to evaluate seal capacity is the fluid system used: Mercury as the displacing fluid and air vacuum as the initially saturating fluid of the rock sample. Results from the Mercury/air system must be converted into the CO_2 brine system, which depends on the ratio of the product of the contact angle and interfacial tension for the two fluid systems, which gives some uncertainties.

Using standard values for conversion of the capillary entry pressure to a brine/air system gave results in the range of 5–10 MPa (Springer et al. 2020). New MICP measurements on samples from the Fjerritslev Formation were conducted on both cores and cutting samples from the Stenlille-1 and Stenlille-2 wells. MICP measurement were also conducted on cutting samples from Stenlille-6. The new samples gave a somewhat lower range of 1–5 MPa.

The governing process for the seal capacity for CO_2 storage is the buoyancy force exerting on the caprock from the density difference between the formation water and the injected CO_2. The height of the CO_2 column in the reservoir below the caprock determines how high a pressure can be obtained (cf. Fig. 7.2.7).

Using the values from both Springer et al. (2020) and the newly obtained capillary entry data, a range of column heights can be calculated from approximate 290 m to more than 1000 meters. With the relief on the Stenlille structure measured from the top of the structure (at the Top Gassum surface) and down flank towards N or NE near the lowest contour, a relief of approximate up to c. 100–120 meters can be determined, dependent on the position on the flank and reservoir zone (See also Section 8.1; Fig. 8.1.1). If injection of CO_2 is planned to be injected from the lower part of the reservoir e.g., in order to optimize the filling of the reservoir an additional c. 30–50 meters must be added to the height, but still on the safe side up to the minimum 290 meters. Thus, it is concluded that the Fjerritslev Formation is an excellent primary seal for the Gassum Formation with good sealing capacity.

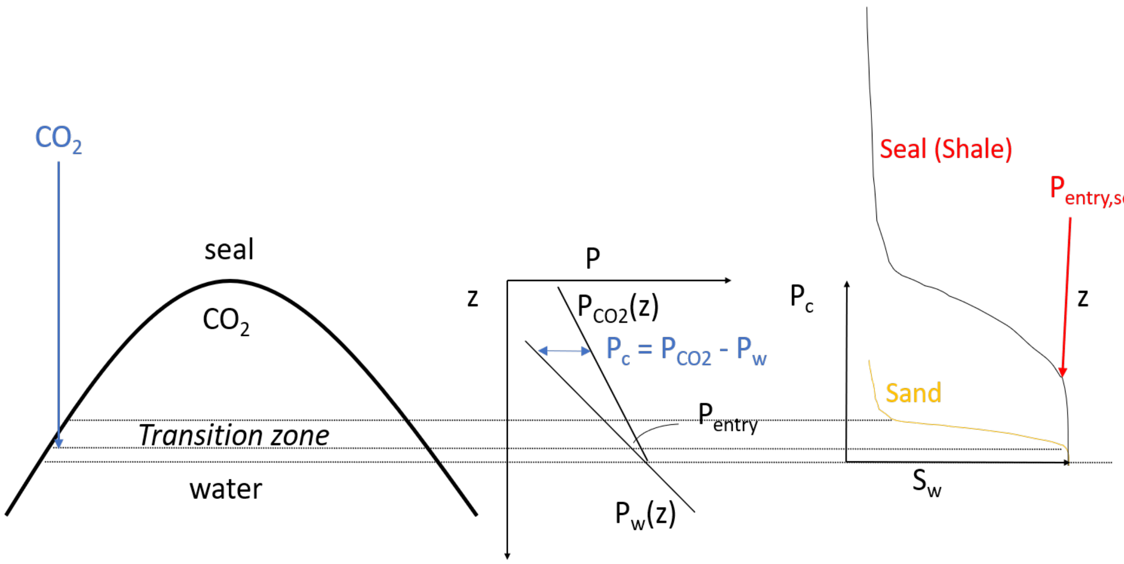

Figure 7.2.7. *Difference in the pressure gradients between the formation brine and the injected CO_2 determines the pressure or column height that the caprock can withstand ($P_{entry,seal}$). Seal and sand have substantially different capillary entry pressures.*

Secondary seals of the Gassum Fm: The Vedsted Fm, Rødby Fm and Chalk Group

The secondary seals of the Gassum Fm on the top of the Fjerritslev Fm in the Stenlille area are the Lower Cretaceous Vedsted and Rødby Formations and the lower part of the Upper Cretaceous Chalk Group (Fig. 1.4). Neither of these formations have previously been the main target for coring (Table 4.4.2). However, Stenlille-1, display one core potentially covering part of the Vedsted and Rødby Formations and Stenlille-5 has one core from the lower part of the Chalk Group. Core 2 from Stenlille-1 has previously been dated as Lower Cretaceous but new dating in this study suggests a Lower Jurassic age (Toarcian). Results from studies of Stenlille-1, and -5 will be presented here with comments on a few other Stenlille wells. The nannofossil zonation of Burnett (1998) and chronostratigraphy in Gale et al. (2020) is applied in the revised biostratigraphy of the Lower and Upper Cretaceous.

The Vedsted Fm of the Danish Basin spans the Valanginian to Albian. The lower boundary of the Vedsted Formation coincides with the transition from marine silty claystones to less silty claystones (Larsen 1966). The Rødby Formation, which overlies or in some places was deposited at the same time as the upper part of the Vedsted Fm, consists of marine red marlstones and marly chalks. Its base is suggested to be late Aptian or early Albian in age in the Danish Basin (Sorgenfrei & Buch 1964) and its upper boundary to the Late Cretaceous Chalk Group is late Albian to early Cenomanian (Lauridsen et al. 2022; Jensen et al. 1986). Mudstones and carbonate beds forming the upper part of the Vedsted Formation and the overlying Rødby Formation were deposited in a mixed siliciclastic-calcareous depositional system indicating lowstands when marly chalk and marl is dominating and highstands when pure chalk is being deposited (Ineson 1993; Ineson et al. 1997). Onset of pelagic carbonate production started in the late Early Cretaceous (late Albian) and dominated completely the depositional environment in the Danish Basin from early Cenomanian. The lower part of Upper Cretaceous is characterised by white hard chalk intercalated with marly beds.

The Lower Cretaceous Vedsted Formation varies in thickness from a maximum of 700 meters in the Fjerritslev Trough in the northern Danish Basin to around 50 meters or less in the eastern and southeastern parts of Denmark. An example of vertical variations within the Vedsted Formation exists from a new study of cores from Vinding-1 located further to the west at the southern margin of the Danish Basin (Lauridsen et al. 2022). The new biostratigraphic ages indicate presence of several hiati in the sedimentary record during Lower Cretaceous suggesting a combination of discontinuous sedimentation and several erosional events. Erosion occurred most pronounced along the basin margins. The Ringkøbing–Fyn High remained an uplifted landmass from Middle Jurassic and to Early Cretaceous time and formed the southern border of the Danish Basin (Michelsen et al. 2003). Compared to the Lower Cretaceous successions in the central part of the Danish Basin in northern Jutland, the successions in Stenlille and Vinding-1 are systematically thinner, reflecting a location with less accommodation space along the basin margin.

The Rødby Formation comprises interbedded mudstones and limestones, and a few thin sandstone beds. The upper boundary towards the Upper Cretaceous Chalk Group is supposedly transitional, and the lower part of the Upper Cretaceous section is characterised by the presence of numerous marl layers in the lower 200–300 meters.

The Vedsted Fm in Stenlille area

The Vedsted Fm in the Stenlille area has been interpreted based on petrophysical logs to measure between 11.5 to 49 m in thickness (Fig. 7.2.8). According to the completion reports the boundary between the Fjerritslev and the Vedsted Formations has supposedly been picked as a distinct log marker recognisable in all Stenlille wells. The marker has been supported by a minor change in lithology, and only one core (Stenlille-1, core 2) exists from this boundary interval to confirm this. However, it is difficult to recognize a lithological boundary in two apparently similar fine-grained sediments (Fig. 7.2.6). In some of the later completion reports (from Stenlille-8 and onwards) it is emphasized that a revision of this boundary is needed because preliminary dating in their studies have shown that a large part of the Vedsted Fm is of Early Jurassic age (e.g., Completion report 3133 p. 24). New biostratigraphic data from this present study has suggested that the boundary is at a shallower log depth confirmed by dating of Stenlille-1 and -8 and compared to published data of Stenlille-2 (Dybkjær 1991).The revised ages of Stenlille-5 suggest placing the boundary at a shallower depth. Stenlille-6 and -19 have been revised based on correlation of gamma ray log patterns from the wells and both are suggesting thinner units of Lower Cretaceous. See also the logs in Appendix B.

Material from the Lower Cretaceous part of the Stenlille cores were originally dated by Arne Buch using foraminifera and by Jens Morten Hansen using palynomorphs (Completion report_7887_Stenlille_1). However, new dating by dinoflagellates, palynomorphs and nannofossils of cores, cuttings and sidewall cores from some of the Stenlille wells (Stenlille-1, -2, -5, -8, -9 and -10) from large part of the supposedly Vedsted Fm show that the lower part of the investigated interval is apparently of Early Jurassic age (Toarcian) indicating that it belongs to the Fjerritslev Fm. Thus, further study and a revision is needed (Dybkjær, 1991 and this present study). The revised thickness is shown in Stenlille-1, -2, -5 and -8 in Fig. 7.2.8. Stenlille-9 and -10 had too few datapoint for a proper revision. Stenlille-5 is placed on the flank of the structure, and this can have created more accommodation space available for sediments compared to the wells on the top of the structure (e.g., ST-1, -2 and -8). More work is needed to evaluate the age and consequently the sequence stratigraphical frame of the remaining Stenlille cores, but the study confirms a major hiatus spanning Middle to Late Jurassic and the earliest part of Early Cretaceous (late Hauterivian) in the Stenlille area.

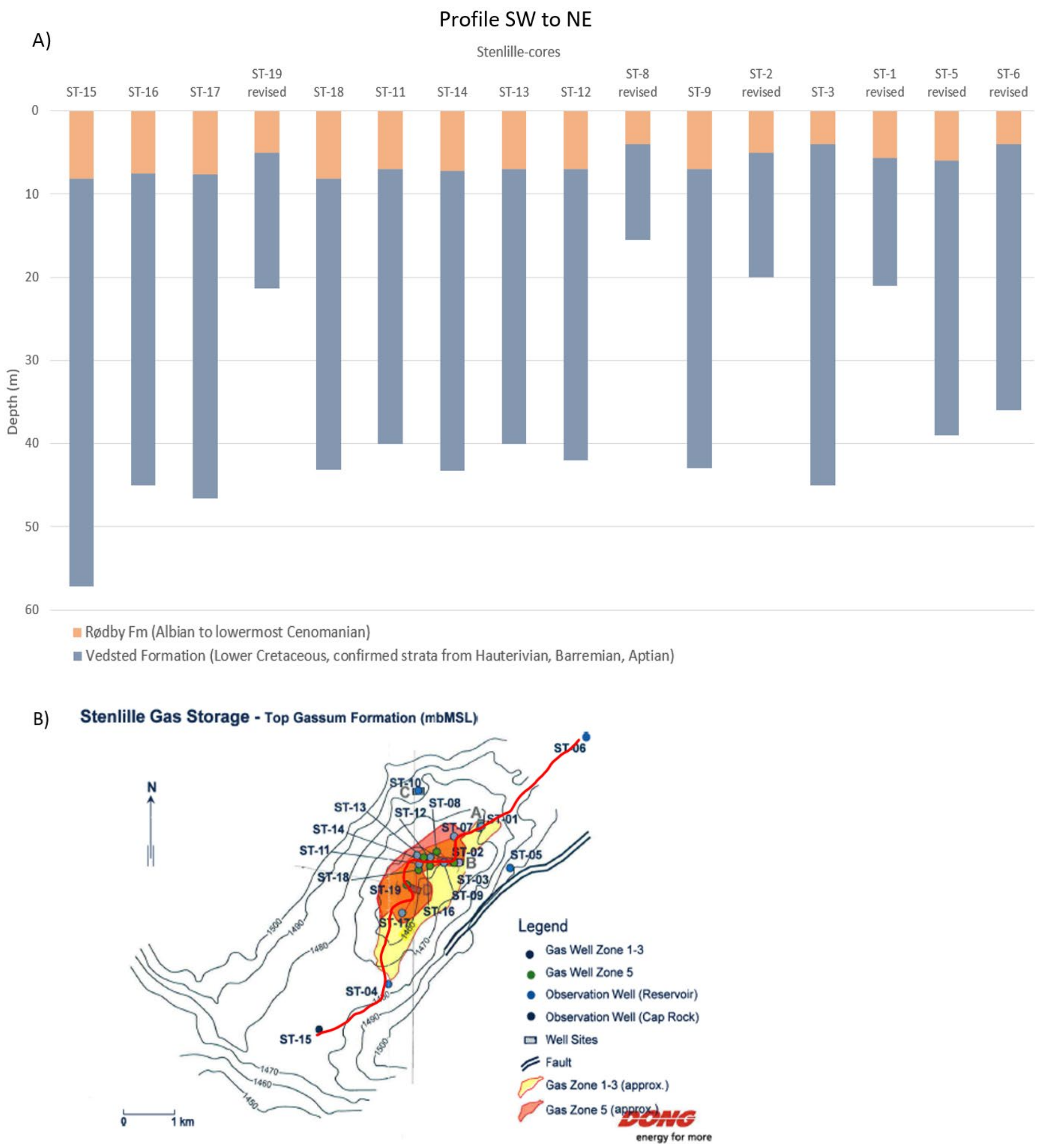

Figure 7.2.8. A) *Thickness of the Vedsted and Rødby Formations in the Stenlille area. Note that the Vedsted Fm of Stenlille-1, -5, and -8 have been revised based on biostratigraphy, and Stenlille-6 and -19 have been revised based on gamma ray log patterns. All revised wells show a significant reduction in thickness of the Vedsted Fm. The variations and implications for this difference is discussed in the text. Note that Stenlille-15 and -5 show a larger thickness due to their position on the flank of the structure.*

B) Position of the different wells in the Stenlille area and a red line showing the order as it appear on the diagram in A). Map from DONG.

Stenlille-1 with a few comments on Stenlille-5, -8, -9 and -10

The Vedsted Fm in Stenlille-1 has previously been suggested to span the interval from 1246.6 to 1205 m (41,6 m), but new data suggests that the Vedsted Fm is only half as thick in the Stenlille-1 and only confirmed in the interval from 1219.5 to 1205.2 m (15.3 m). The position of the revised boundary between the Fjerritslev and Vedsted Formations is also based on a marked decrease on the gamma ray log indicating a sequence boundary combined with new biostratigraphic data. Stenlille-1 has two cores (1 and 2) (Fig. 7.2.6). Core 2 is measuring from 1227.5 to 1220.1 m and the boundary between the Fjerritslev and Vedsted Formation is defined near the top of the core at 1220.5 m. The central part from 1220 to 1212.9 m between the two cores is not cored, but three sidewall cores have been dated. The possible boundary between the Vedsted and Rødby Formations is present in core 1. The upper part of the Rødby Fm from 1203.5 to 1200 m is not cored. No other wells from the Stenlille area have been fully cored in the Lower Cretaceous.

Core 2 representing the upper part of the Fjerritslev Fm (1227.25–1224.25 m) is a greenish grey mudstone with parallel laminae ranging in thickness from few mm to 1–2 cm (facies 22; Pedersen et al. 2022). No macrofossils are encountered, and very little organic material is preserved. Many small- scale faults are present. The dominance of mud indicate deposition mainly from suspension fall-out in a low-energy environment below fair weather wave-base. The palynomorphs suggests a shallow marine environment relatively close to the coast. The dinoflagellates and the palynomorphs indicate a possible Toarcian age, Lower Jurassic, but the presence of Lower Cretaceous dinoflagellates are also confirmed possibly related to bioturbation of the overlying Lower Cretaceous sediments.

The upper part of the core (1224.25–1220.10 m) is structureless, homogeneous greenish grey calcareous mudstone (Fig. 7.2.6; facies 23; Pedersen et al., 2022). The boundary between facies 22 and 23 is pronounced. Trace fossils are present but rare. The upper part is also representing a deposition at low energy conditions and the palynomorphs suggest that the upper part could have been deposited at a floodplain. Many of the specimens could be redeposited and the palynomorphs and dinoflagellates show a mixture of Early Jurassic and Early Cretaceous specimens with a dominance of Early Jurassic species. No nannofossils or foraminifera have been identified. The age of this part of the core has been discussed. The two facies (22 and 23) in core 2 are different from other facies so far described from the Fjerritslev Fm (G.K. Pedersen, pers. com., 2023). It is a possibility, that they represent the uppermost Lower Jurassic deposits in the Danish Basin and that they are differently developed due to the relatively shallow depositional environment close to the Ringkøbing–Fyn High. Further, the blurred biostratigraphic signal in the upper part of core 2, is possibly representing a transgressive lag with mixture of reworking caused by bioturbation and marine transgressive erosion at the base of Lower Cretaceous. The boundary between the Fjerritslev and Vedsted Formations is not reflected in a marked facies shift in the core (Fig. 7.2.6).

The central part from 1220 to 1212.9 m is not cored but cuttings and sidewall cores reveal two fine-grained sandstone to siltstone beds interbedded with a 1 m thick claystone bed. The sandstone beds are glauconitic, and the uppermost sandstone is very calcareous. The lowermost SWC at 1220 m contains no nannofossils but a rich association of Lower Jurassic palynomorphs indicating the *Spheripollenites*-*Leptolepidites* Zone of Toarcian age and a few Early Cretaceous dinoflagellates. Large pieces of coal cuticle and pieces of wood are also found indicating deposition in a floodplain environment. The Early Cretaceous species could be present due to mixing of the sediments by burrowing fauna activities. The SWC is most likely from the Fjerritslev Fm and the exact position is probably just a little bit offset in relation to the sequence boundary at 1220.5 m. SWC at 1219.0 m is containing a rather diverse Early Cretaceous palynomorph and dinoflagellate association of a possible Hauterivian age. The nannofossils are also indicating an early late Hauterivian age of BC9 to 10. Ditch cutting samples of Stenlille-5 at 1236 m is also confirming the presence of late Hauterivian zone BC9 to 10. The degree of mixing of an Early Jurassic and Early Cretaceous fossil associations is typical of a transgressive lag remaining from the Early Cretaceous transgression and following erosion and redeposition of the Lower Jurassic sediments. The boundary of the Fjerritslev and the Vedsted Formations are therefore tentatively placed at 1220.5 m based on the marked decrease at the gamma ray log indicating a possible sequence boundary. The SWC at 1216.4m is clearly of Early Cretaceous age both by the dinoflagellates and the rich association of palynomorphs. Also, the nannofossils indicate a late Hauterivian age of BC 10. The very few Early Jurassic palynomorphs are redeposited. Ditch cutting samples of Stenlille-5 confirms Hauterivian in at least 24 meters.

Core 1 is representing the upper part of the Vedsted Fm and possibly the boundary and the lower part of the Rødby Fm (Fig. 7.2.6). The lower part of core 1 (1212.90 to 1208.2m) is represented by grey silty to muddy siltstone (facies 24 and 25 of Pedersen et al., 2022) followed by grey weakly laminated mudstone (facies 26 of Pedersen et al., 2022). Facies 24 are weakly laminated to structureless with pyrite concretions whereas facies 25 display indistinct bedding and vertical water escape structures related to fluidization of the silty mudstone. Facies 26 also contains rather large pyrite concretions. Belemnites are common in most beds. The depositional environment is interpreted as distal lower shoreface to marine lower offshore and dated by foraminifera as early to mid Barremian (lower part of facies 24). SWC at 1234.5 m of Stenlille-8 is also confirming a Barremian age. Facies 24 (upper part), 25, 26 and lowermost part of facies 27 are dated by nannofossils as early Aptian, BC 20. Similar ages are confirmed in SWC of Stenlille-8 at 1228 m (upper BC18 to lowest BC21), Stenlille-9 at 1201.7 m (BC18 to BC21) and Stenlille-10 at 1216.5m (BC19 to 21). Ditch cutting samples from Stenlille-5 have confirmed Aptian ages at 1221m and 1224 m. Late Barremian is apparently missing in Stenlille-1 and other wells in the area.

The upper part of core 1 (1207.8 to 1205 m) contains, from base to top, pale olive marl (facies 27), white homogenous limestone (facies 28) and grey, yellowish, and red calcareous mudstone (facies 29 and 31) reflecting a gradual increase in carbonate content (Fig. 7.2.6). The core from 1207.14 to 1205.48 m is dated as mid to late Aptian, BC 21 to 22 by nannofossils and are facies wise like an interval in the Vinding-1 core dated also as early Aptian, BC 20 (Lauridsen et al. 2022). The boundary from the Vedsted Fm to the Rødby Fm is not well identified. The palaeoenvironment is marine and represent lower offshore to shelf deposits.

The Rødby Fm in the Stenlille area

The Rødby Fm in the Stenlille area has been interpreted based on log patterns to measure between 4 and 8.2 m in thickness (Fig. 7.2.8). The Rødby Fm is only covered partly by a core in the Stenlille-1, by sidewall cores in Stenlille-8 and by ditch cutting samples of Stenlille-5. The base of the Rødby Fm in the Danish Basin is suggested to be late Aptian to early Albian in age in the Danish Basin and ranging up into early Cenomanian.

Stenlille-1

The uppermost part (1205–1203.50 m) of core 1 is red marl cemented in some intervals and interpreted as representing the Rødby Fm (facies 31 of Pedersen et al. 2022; Fig. 7.2.6).

Few belemnites and indistinct trace fossils are found. Cuttings from the interval 1199.5 to 1203.5 m indicate reddish-brown clay- to marlstone. The red colour may be due to an increase in hematite and is interpreted as a decrease in clastic influx because of continuous transgressions and changes to more oxygen-rich conditions at the seafloor. The depositional environment is interpreted as a marine, low-energy, lower offshore environment. The boundary to Upper Cretaceous is not cored and not described in the original completion report but according to the well logs it is supposedly transitional and the lower part of the Upper Cretaceous section is characterised by many marl layers.

In Stenlille-1 and -8 the Rødby Fm has been dated by foraminifera as early to middle Albian and these ages have been confirmed by nannofossil dating in this study. In Stenlille-5 earliest Cenomanian is also present (UC1a).

The Chalk Group in Stenlille

The Chalk Group in the Stenlille areas has been divided into a "Basal Chalk" representing the oldest parts of the Chalk Group followed by a "Lower Chalk", "Campanian Chalk", "Maastrichtian Chalk" and Danian Limestone. In this report only the "Basal and Lower Chalk" will be discussed. The "Lower Chalk" consists dominantly of limestone with little chert and occasional marl horizons. Core 1 of Stenlille-5 is cored in this part of the Chalk Group (Fig. 7.2.9). The "Basal Chalk" is pink, off white, and green limestone with chert. The unit is locally hard to microcrystalline. This significant hard, lithified chalk is likely causing locally increased seismic velocities in the lowermost part of the Chalk Group towards the Base Chalk horizon (Appendix A).

***Stenlille*-5**

The boundary between Upper and Lower Cretaceous was originally planned to be the target for the cores in Stenlille-5. However, the almost 18 m long core 1 (from 1187.7 to 1169.7 m) was drilled around 25 m above the Lower/Upper Cretaceous boundary recognized in the well at 1213 m. The position of this boundary is based on petrophysical log patterns. In the original study the cores were not studied in detail and the "Basal and Lower Chalk" was not originally dated in Stenlille-5, but in this report the units have been dated by nannofossils. New data of the core of the "Lower Chalk" and ditch cutting samples of the "Basal Chalk" have been collected in Stenlille-5 and dated in this report.

The cored part of Stenlille-5 has tentatively been divided into 5 different facies based mainly on the differences in structures, carbonate, and clay content (Fig. 7.2.9). Facies 1 is a greenish marl, bioturbated with indistinct bedding and appear mainly in the lower part of the cored section. Facies 2 is lumps or lenses of chalk in a marly matrix. It is only encountered at one level. Facies 3 is white chalk with few thin mudstone laminae and stylolites. At one level slumps and intraformational clasts appear. The chalk is moderately hard to locally very hard, sub-brittle, blocky and microcrystalline.

It is the main facies. Facies 4 is green laminated marl. Facies 5 is white structureless chalk with very little marl. Few dissolution horizons with mud drapes. Facies 5 are common toward the top of the core.

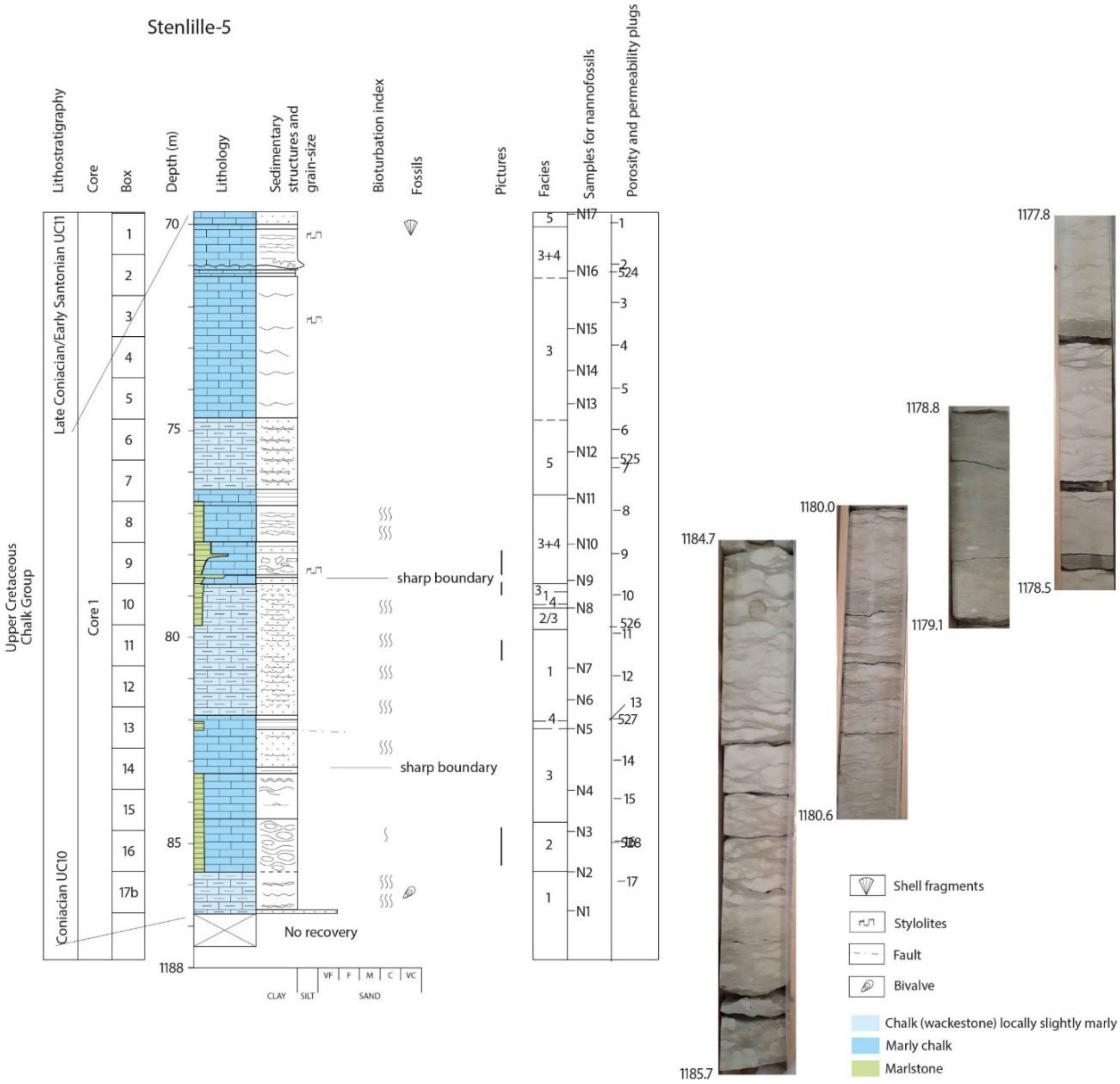

Figure 7.2.9. *Sedimentological logs of the Lower Chalk of the Chalk Group with core photos from the Stenlille-5 well. Only the lowermost and uppermost part of the core is dated. More work is needed to fully revise the core.*

In general, the chalk facies appear rich in biogenic grains and is probably reflecting a relatively shallow marine depositional environment. There is not recorded any bioturbation related to the marl beds and they are most likely very compacted. The presence of stylolites reflects chemical dissolution and is common in beds which have been buried more than 700 meters. Stenlille-5 core show many lithological similarities to the Stevns-1 core.

Two samples were taken from the Stenlille-5 core 1, for dating using nannofossil biostratigraphy. The samples were taken from the near top (1167.7m) and near base (1186.7 m) of the core (Fig. 7.2.9).

At level 1186.7 m the rich nannofossil assemblage indicates Zone UC10, middle Coniacian. At level 1169.7 m a high abundance and diversity nannofossil assemblage characterizes this sample indicating nannofossil subzone UC11c, which is the uppermost Late Coniacian to Early Santonian level. A subdivision of the core will be done soon based on collected samples from the rest of the core.

In addition, 18 ditch cutting samples were collected to identify the boundary between Lower and Upper Cretaceous and the boundary of Lower Jurassic and Lower Cretaceous. The data are listed in Figure 7.2.10. A. It is apparent from the data that Turonian is only possibly present in the Stenlille-5 with less than 15 meters. Cenomanian of the Chalk Group strata is present with no more than 22 m depending on where the boundaries are defined. The boundary between Lower and Upper Cretaceous is present within the Rødby Fm (Albian to earliest Cenomanian) and could be present from 1218 to 1212 m. The “Basal Chalk” is therefore dated as Cenomanian to possibly Turonian and measure a total of 25.3 m. The Rødby Fm is dated at Albian to lowermost Cenomanian and measures around 6 m. The Vedsted Fm is dated as Hauterivian to Aptian and measures around 33 m. The data from level 1254 to 1278 m are all possibly contaminated with material from overlying units based on the composition of species. The well is only cased in the upper and lower part of the well but in this middle part causing this probability of pollution. The data do not identify the Lower Jurassic to Lower Cretaceous boundary. If the thickness of the Rødby and Vedsted Formations of Stenlille-1 and -5 is compared. It is apparent that the thickness of the Rødby Fm is comparable, and likewise is the thickness of the Aptian and Barremian part of the Vedsted Fm, but the thickness of the Hauterivian part of the Vedsted Fm is markedly different (Fig. 7.2.10B). That can be explained with the different positions of the two wells in relation to the Stenlille structure (Fig. 6.2.5, 7.2.8B). Stenlille-1 is from the seismic interpretation (Fig. 6.2.5) positioned on the top of the structure and Stenlille-5 down at the flank. The Stenlille structure was primarily formed due growth of the underlying salt pillow (See Section 6.2) causing uplift and erosion at the top of the structure after Toarcian and probably into Early Cretaceous. During the Hauterivian the salt diapir may still have been active creating a larger accommodation space in the area around Stenlille-5 and possibly the activity also caused some redeposition of material from the upper to lower lying parts of the basin or the structure may have been pre-existing with deposition of thicker Lower Cretaceous sediments down flank. A similar pattern is identified in another well, Stenlille-6, which are also placed on the flank of the structure.

The biostratigraphic data from Stenlille-5 are very interesting and the thickness of the age units reflect the depositional environment in the Stenlille area during the Late Cretaceous. The greatest thickness of the Chalk Group is identified in the central part of the Danish Basin in the Lavø well where it measures 2000 m of which 1200 m is dated as Campanian and Maastrichtian (Stenestad 1972). In Cenomanian, the maximal thickness of chalk is 100 m, in the Turonian it is 50 m and in the Coniacian 150 m (Stenestad 1972). The Stenlille area is closer to the boundaries of the Danish Basin and the Ringkøbing–Fyn High, and the units are respectively thinner. The early part of Late Cretaceous was most likely prone to many erosional events at the rim of the Danish Basin and reflects the responses to the large regressions in late Cenomanian to early Turonian.

.

A)

Stenlille-5

Core

1169.70 m Late Coniacian

to Early Santonian (UC11c)

1186.70m Coniacian (UC10)

Ditch cuttings samples

1188 m Turonian-Cenomanian

1190 m Turonian-Cenomanian

1200 m Cenomanian

1203 m Cenomanian

1206 m Cenomanian

1209 m Cenomanian

1212 m Early Cenomanian

1215 m Earliest Cenomanian to Albian

(probably UC1a to Albian)

1218 m Earliest Cenomanian to Albian

(probably UC1a to Albian)

1221 m Aptian

1224 m Aptian

1227 m Barremian

1236 m Late Hauterivian (BC 9-10)

1245 m Late Hauterivian

1254 m ?Late Hauterivian, possibly contamination

1263 m ?Late Hauterivian, possibly contamination

1272 m Hauterivian, possibly contamination

1278 m Hauterivian, possibly contamination

B)

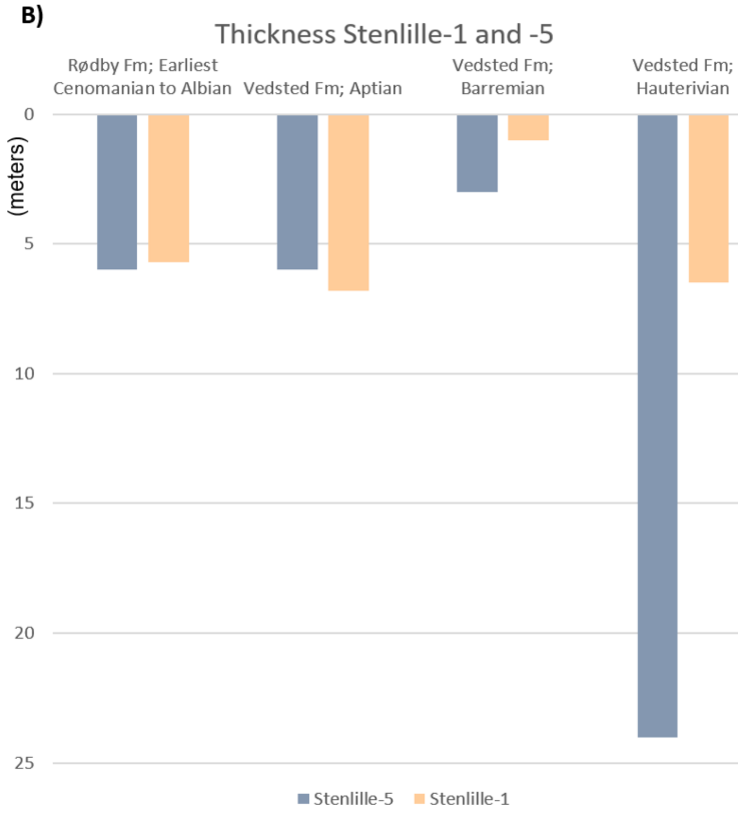

Figure 7.2.10. A) *List of nannofossil samples from Stenlille-5 both from the core 1 in Upper Cretaceous strata and from ditch cutting samples of Late and Early Cretaceous.*

B) Comparison of thickness (in meters) of Stenlille-1 and -5. Note that there is a marked difference between the wells in the Hauterivian part of the Vedsted Fm.

Porosity and permeability data of the lower part of the Chalk Group in Stenlille-5

Data from the porosity and permeability tests compiled in the mid 1980'ies are listed below (Fig. 7.2.11). The porosity and permeability data are in general very low in the chalk-rich facies 3 and 5 with an average porosity of 9.8% (facies 5) and 10.9% (facies 3) and an average permeability of 0.067 mD (facies 3) and 0.128 mD (facies 5). The clay-rich facies have an even lower porosity of 6.6% (facies 4) to 7.4% (facies 1) and permeability of 0.559mD (facies 4).

The porosity and permeability data are plotted against similar data from the Stevns-1 well (Upper Cretaceous onshore data) and offshore data from Upper Cretaceous wells. It is evident that the data from Stenlille-5 have the lowest porosity and permeability values. The relatively high porosity and permeability data from Stevns-1 (Upper Campanian to Maastrichtian) can be explained by the relatively shallow burial history (between 450 to 600 m; Nielsen et al. 2011). The offshore data from the Danish Central Graben have been more deeply buried often exceeding 3000 m, but these chalk reservoirs have preserved a relatively high porosity due to retarded compaction caused by regional overpressure of the formations (e.g., Japsen 1998). The Stenlille data is showing a normal burial compaction with no overpressure.

The non-reservoir chalk with low porosities and permeabilities of the Central Graben have been investigated to understand its capability as a pressure seal (Mallon & Swarbrick 2002, 2008). Non-reservoir chalks have permeabilities which are like siliciclastic mudstones. The studies show that both clean and argillaceous chalk diagenetic pathways result in low permeability rocks and the diversity of rock types that exhibit low permeability suggests that seals are pervasive throughout the Chalk Group. Non-reservoir chalk can therefore act as significant barriers to fluid flow and as significant pressure seals trapping high pressures beneath the Chalk Group.

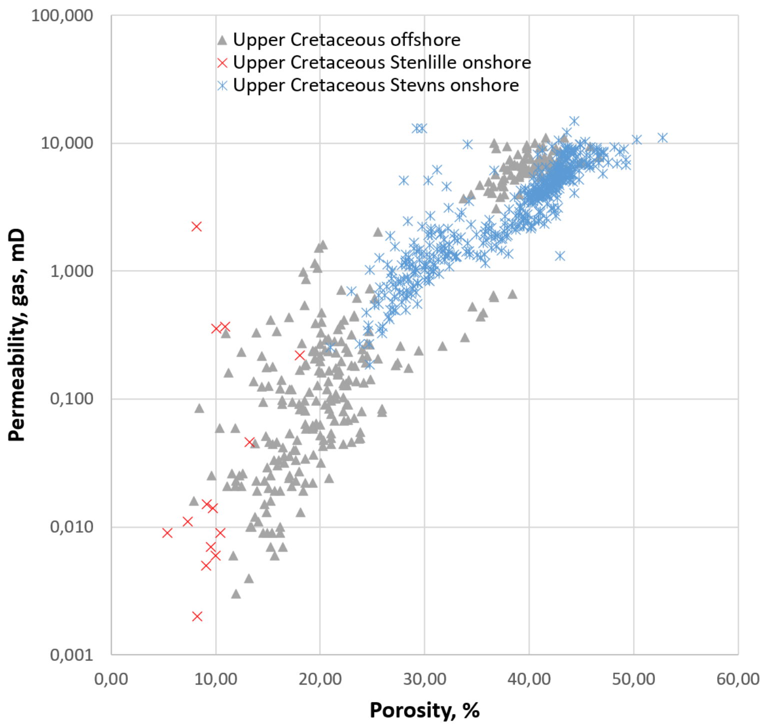

Figure 7.2.11. *Porosity and permeability plot of the Upper Cretaceous part of the Stenlille-5 core (Stenlille onshore) compared to similar data (GEUS inhouse data) from Upper Cretaceous strata from Stevns and offshore in the Danish Central Graben. The data is discussed in the text.*

Concluding remarks on the secondary seal

The porosity and permeability data from the lower part of the Chalk Group has been listed in this report. The values are generally very low and when compared with other offshore data from the Danish Basin (Stevns-1) they show an ordinary burial compaction of the Stenlille Chalk Group with no overpressure. The properties as a secondary seal have been compared with studies from the Danish Central Graben and it is most likely that the lower part of the Chalk Group will act as significant barriers to fluid flow and high pressure from the beds below.

The study has revealed new biostratigraphic data from the Lower Cretaceous Vedsted Fm, the Rødby Fm and the lower part of the Upper Cretaceous in the Stenlille area having implications on the position of the boundary between Lower Jurassic and Lower Cretaceous in all of the revised wells (Stenllle-1, -2, -5, -6, -8 and -19).

The Vedsted Fm and especially the Hauterivian part of Lower Cretaceous in the Stenlille area has in the latest part of this study showed to be thinner than expected from previous studies, and new dating of Stenlille-1, -8 and -2 has suggested a reduction in thickness of about 50%.

As mapping finished earlier, the exact well-based stratigraphic boundary between the Lower Jurassic Fjerritslev Fm and the Lower Cretaceous Vedsted Fm could not be remapped here and the previous boundary is thus tentatively named: Near Top Fjerritslev, as the Top Fjerritslev may be slightly shallower. New work is needed to exact define the new boundary with more wells, well-ties and mapping. However, the thickness from the Top Gassum to the Near Top Fjerritslev is still a good approximation to the minimum thickness of the primary seal, and as the formations here include approximately similar mudstones (Fig. 7.2.6), they both represent good seals.

Comparisons of the thickness of the Hauterivian part of the Vedsted Fm in Stenlille-1 and -5 show the salt diapir below the Stenlille structure may have been active during the Hauterivian creating a larger accommodations space in the area around Stenlille-5 or a pre-existing topography of the structure with thicker preserved deposits down the flank and onlapping the structure. Stenlille-1 was during the same period positioned near the top of the structure probably at lower water depth. The biostratigraphic data of Stenlille-1 show reworked sediments in the same time periods reflecting many erosional events.

The Vedsted Fm dated as late Hauterivian to late Aptian is in the Stenlille area is a relatively homogenous mudstone with slight variations in the content of silt and with an increase in the carbonate content in the younger parts. The formation is possibly containing several hiati during deposition due to erosional events at the position close to the basin margin.

The Rødby Formation is represented by red marl with trace fossils and belemnites. It has been dated as early to middle Albian and possibly lowermost Cenomanian in the Stenlille area.

The lower part of the Chalk Group is only partly cored in the Stenlille area. The core is located about 43 m above the Lower and Upper Cretaceous boundary. It is represented by completely bioturbated homogenous chalk interbedded with laminated and homogenous marl laminae. The cored part has been dated as middle Coniacian to possibly early Santonian. The chalk is hard to microcrystalline in some intervals.

Hiati are present between or within:

- Toarcian, Early Jurassic to Late Hauterivian, Early Cretaceous
- Late Barremian
- Late Albian
- Late Cenomanian to Turonian?

Finally, more work is needed to compare the Lower and Upper Cretaceous Stenlille data with data from other parts of the Danish Basin (e.g., Vinding-1).

8. Discussion of storage and potential risks

8.1 Volumetrics and Storage Capacity

Primary input for the estimation of potential capacity has been the seismic reinterpretation of the Gassum Fm within the current 3D-Survey (Stenlille-97) combined with extended interpretation across the newly acquired GEUS22-Stenlille 2D-survey. The detailed well analysis and a crucial element of revising the depth conversion impacts the understanding of the reservoirs and their geometry in this gentle low-relief structure (See Figure 8.1.1).

For the storage capacity estimation at Stenlille, various injection scenarios have been evaluated as the structure and reservoir units are well known and because of the added complexity of having potential competing activities within the reservoir units due to the current natural gas storage. Capacity estimation of scenarios where only the structural closure (4way closure only) is utilized has been calculated and can be compared to capacities of other structures across Denmark and as described in e.g., Hjelm et al. (2022). At Stenlille the knowledge from the natural gas storage activity allows for scenarios of sequestration in reservoirs Zones 1–4 combined and another for the Zone 5 only if these are not in communication.

As the structural closure of Stenlille currently is occupied by natural gas, capacity estimation for two additional conceptual injection scenarios have been assessed envisioning injection N–NE of the structural apex on the northern flank of the structure and these also considers injection into reservoir zones 1–4 and zone 5 only.

The scenarios are conceptually shown in map view on Figure 8.1.2 and illustrated in profile view in Figure 8.1.3. However, the injection scenarios are not envisioned to be developed simultaneously, and careful considerations have to be made regarding the current storage of natural gas and how CO_2 should evade or eventually replace the natural gas.

The 4-way top-structure storage capacities within mapped and defined closures are the primary options, whereas flank scenarios are uncertain and depend on e.g. plume flow directions and limitations, such as site-specific permeabilities, internal seals and compartmentalization. CO_2 injected downflank may to some extend be retained in parts of the flank but will most likely also migrate towards the top of the structure. Thus, the flank and 4-way top-structure scenarios may be difficult to regard separately.

The scenarios must be assessed by e.g. reservoirs simulation modelling to ensure optimal development and filling of the reservoir zones of the structure, and to ensure less uncertainty on storage capacity.

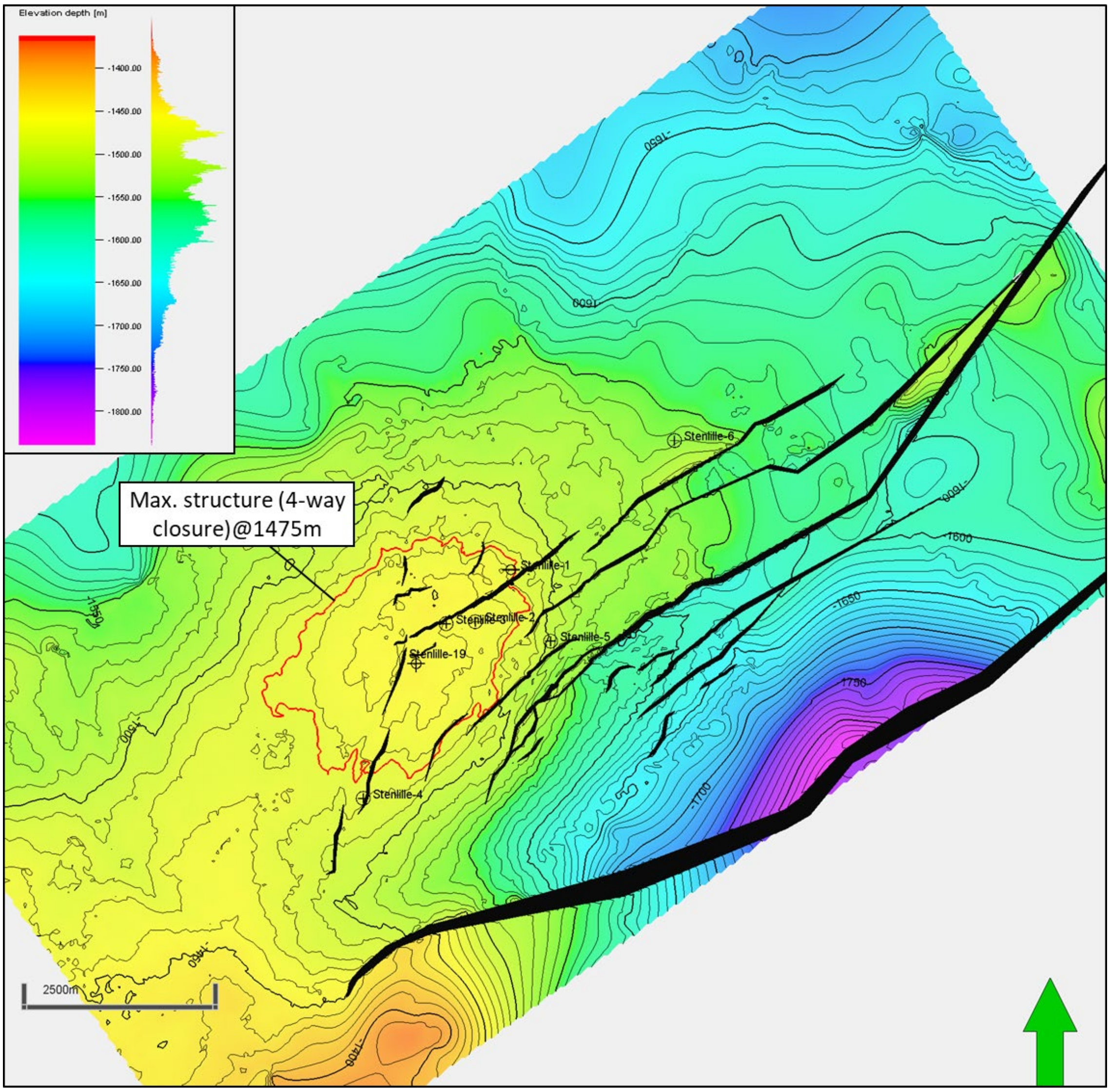

Figure 8.1.1. *The unsmoothed Top Gassum Fm depth structure map in meters (m) (generated in Petrel®, tied to wells and gridded by 50x50 meter – see Chapter 5) provides the primary input to the capacity assessment. The structure has a SW structural spill point at c. 1475 m TVDSS (deepest closing countour, marked in red). The Top Gassum map shows, that the area within the spill point is c. 5.4 km^2, and with a top point at c. 1449 m, the structure height above spill point is c. 26 m. Note that faults are mainly located towards east and mainly trends SW–NE. See also Section 6.2 for fault analyses and map location.*

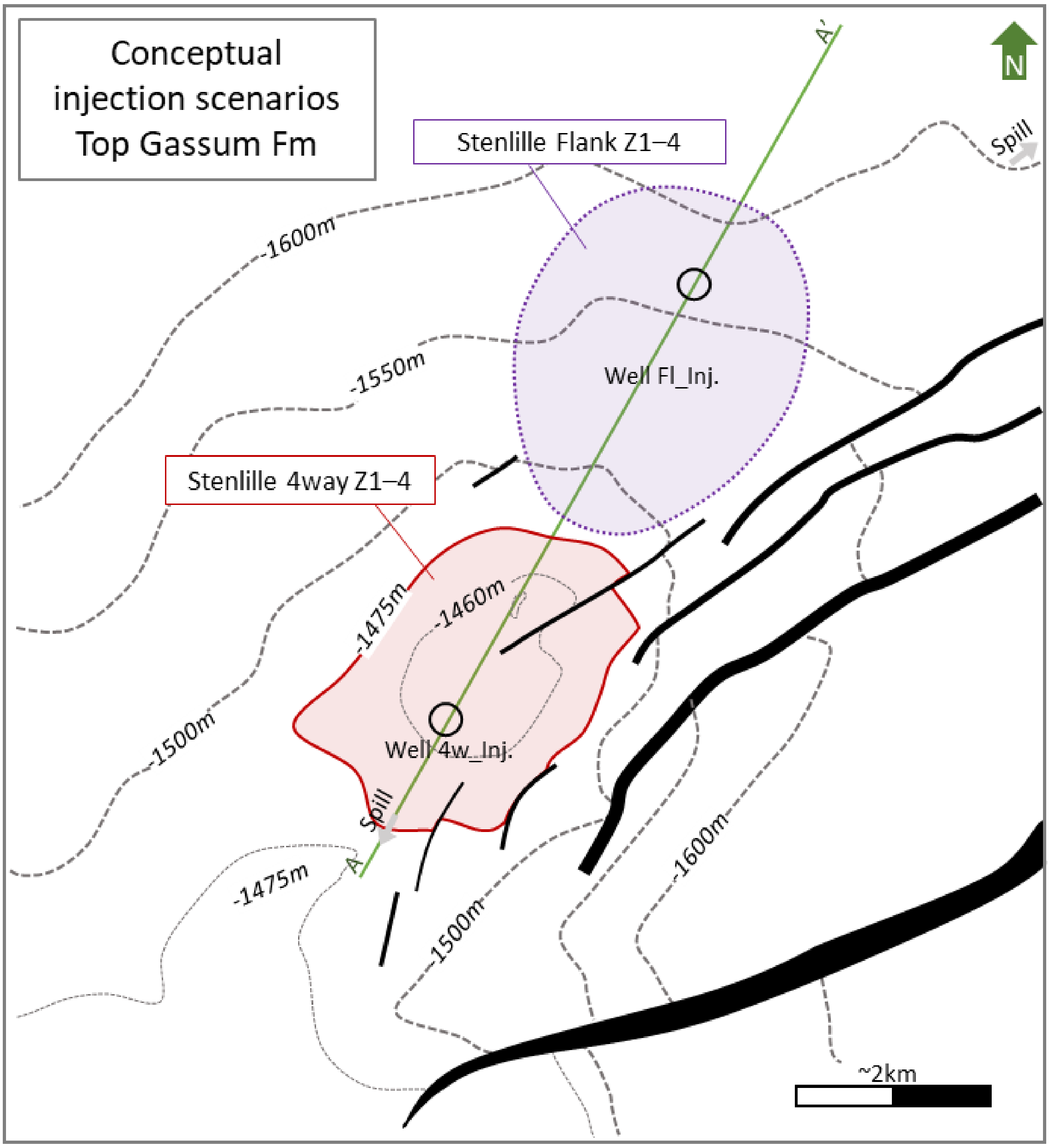

Figure 8.1.2. *Conceptual map view of two scenarios for injection in reservoir Zone 1–4. The Stenlille 4way Z1–4 assumes near crestal injection and filling of only the mapped 4way closure. This low-relief structure (26 m) does not allow for 'down-to' filling of the entire available reservoir section. Due to possible competing activity (natural gas storage) in the reservoir an additional scenario has conceptually been build. This scenario involves injection on the northern flank away from potential faults and away from an assumed NE spill point. The Stenlille Flank Z1–4 injection scenario assumes almost radial initial growth of the CO_2 plume and later density driven migration toward the structural apex leaving an oval shaped plume years after end of injection. Similar scenarios are made for reservoir Zone 5. A conceptual profile (A–A') across the setting is shown in Figure 8.1.3. The shape and size of injection scenarios is purely conceptual. Actual subsurface condition such as the detail natures of the Gassum Fm geometry, compartmentalization, porosity, pressures, number of injections points, CO_2 density and injection rates, -quantity and -duration etc. will affect the actual extent of the CO_2 plume.*

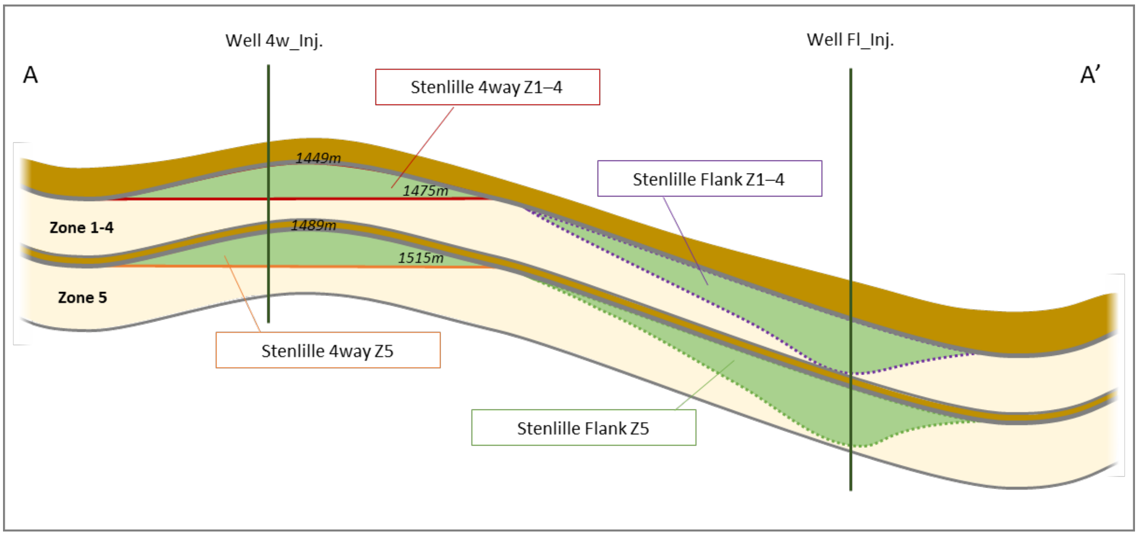

Figure 8.1.3. *Conceptual profile across the Stenlille structure illustrating the configuration of the four scenarios of which storage capacity has been estimated. Two scenarios are calculated for the potential within the 4way structural closures for the reservoir Zone 1–4 and for Zone 5. Two additional Flank scenarios for the reservoir units where estimated assuming an inverted asymmetrical cone geometry of the CO_2 plume from radial injection flow from well and late density driven migration towards the structural apex. This geometry reflects results observed from reservoir modelling of similar settings (Internal GEUS work).*

Volumetric input parameters

Gross Rock Volume (GRV)

The GRV of the structure reservoir units have been calculated using the Area and Thickness vs. Depth methodology described by e.g., James et al. (2013). Area vs. Depth tables have been extracted from the mapped and depth converted top reservoir surfaces and reservoir gross thicknesses were estimated from petrophysical work on the local wells. A most likely volume-scenario was establish based on model values derived directly from the mapping and petrophysical analysis. In order to include the uncertainty on the GRV across the Stenlille structure, a minimum and a maximum scenario were also calculated. As shown in Figure 8.1.4, three scenarios were set up for the areal extent to address the uncertainty in interpretations, mapping and depth conversion and scenarios were incorporating for the gross thickness uncertainty across the entire structure.

GRV from area and thickness vs depth calculations were constructed for the four scenarios defined by min., mode and max. as exemplified in Figure 8.1.5. It is assumed that the GRV distribution follows a Pert distribution defined by the min., mode and max. values. The Pert distribution is believed to give suitable representation for naturally occurring events following the subjective endpoint input estimates (Clark 1962). For the Gassum Fms reservoir units the assumption input for the GRV and the GRV scenarios are given in Table 8.1.1.

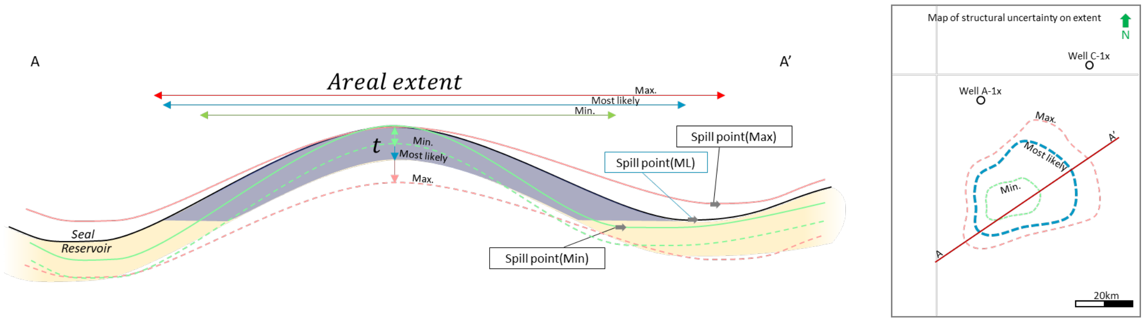

Figure 8.1.4. *Conceptual profile (A–A') across a potential structure. The uncertainty in mapping the structure gives hypothetically min. and max. scenarios that might look very different from the most likely mapped scenario. Variance in area extent and in gross thickness (t) assumptions will affect the gross rock volume of the structure, but the GRV uncertainty can be estimated and utilized in the capacity estimation.*

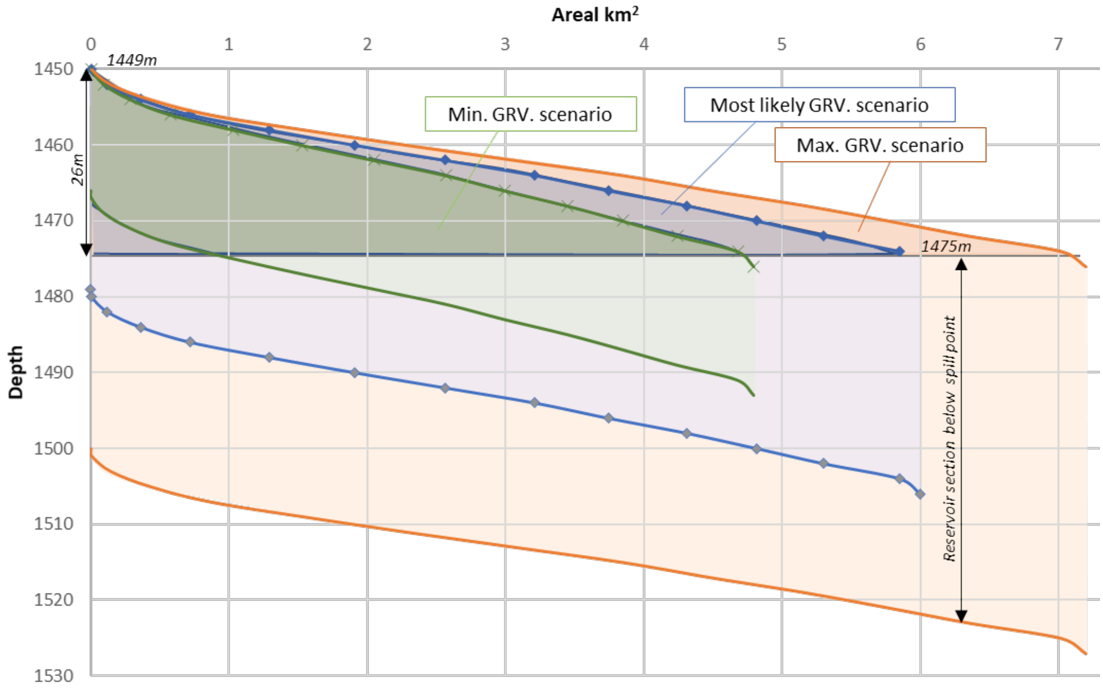

Figure 8.1.5. *Area and Thickness vs. Depth plots for min., max., and most likely GRV scenarios in the Stenlille 4way Z1–4 capacity estimation. The end-members of the GRV uncertainty range comes from variance in area and thickness. The low relief on the Stenlille structure shows that the 4-way closure only holds a minor part of the full reservoir potential within the structure. The max./min. GRV ratio is below 2 in this example which reflect that the controlling factor on GRV for the Stenlille 4-way closure is the low relief above the spill point (1475m), which only allows small upside capacity for this structural confined reservoir.*

Gross Rock Volume Assumptions												
Unit	Apex [m.TVDSS]	Reach* [m.TVDSS]	Spill point [m.TVDSS]	Area [km²]			Thickness [Gross. m]			GRV [1e⁶m³]		
				Min.	Mode	Max.	Min.	Mode	Max.	Min.	Mode	Max.
Stenlille 4way Z1–4	1449	1449	**1475**	4.34	**5.42**	6.50	20	**30**	40	53.9	**68.5**	82.2
Stenlille 4way Z5	1489	1489	**1515**	4.34	**5.42**	6.50	25	**33.3**	45	48.6	**60.7**	72.8
Stenlille Flank Z1–4	*1449*	*1480*	***1610***	*4.70*	***6.70***	*8.70*	*20*	***30***	*50*	*93.2*	***199.6***	*431.6*
Stenlille Flank Z5	*1489*	*1525*	***1650***	*4.70*	***6.70***	*8.70*	*20*	***33.3***	*55*	*93.2*	***221.6***	*472*

Table 8.1.1. *Gross Rock Volume assumption input and resultant GRVs for the suggested volume scenarios. *Reach; indicate the depth that a plume is allowed to reach, in this context 5 meters from the potential max extent of the current allotted natural gas storage. Flank scenarios (grey) are more uncertain and included as examples of other possible storage options.*

Net to Gross ratio

The N/G-ratios estimated from the petrophysical analysis of the Stenlille wells in Section 7.1 are adapted to average N/G-values across the entire structural Gross Rock Volume. Some variance from wells are expected due to lateral variation. To reflect this uncertainty, a distribution for the average N/G was subjectively constructed honouring well data and a Pert uncertainty function has been applied across the range.

Porosity

The porosity (ϕ) average was estimated from petrophysical analysis of the available Stenlille wells as described in Section 7.1. The well-derived estimate is considered as a reasonable average porosity across the entire structure (approx. set as Mode value). Some variance is expected as lateral and depth variations might occur. To reflect this, an average porosity distribution has been constructed defining the min. and max. of the distribution around +/- 20% (minor variation may occur). A Pert distribution has been applied for this element.

CO_2 density

The average in-situ density of CO_2 was estimated using the 'Calculation of thermodynamic state variables of carbon dioxide' web-tool essentially based on Span & Wagner (1996) (see also e.g., http://www.peacesoftware.de/einigewerte/co2_e.html). An average reservoir pressure was calculated on the assumption that the reservoir is under hydrostatic pressure and a single pressure point midway between apex and max spill point was selected representing the entire reservoir pressure average. Temperature for this midway point was calculated assuming an average annual surface temperature of 8°C and a geothermal gradient of 30,6°C/km (Fuchs et al. 2020). The geothermal gradient may be associated with some uncertainty as it slightly higher than regional trend (27°C/km). Assumptions and calculated densities for the individual reservoir units are tabulated in Table 8.1.2. For a quick estimation of the uncertainty on CO_2 density, various P-T scenarios were tested and in general terms a -3% (min.) and +5% (max.) variation from the calculated mode was applied for building a distribution (Pert). All calculations showed that CO_2 would be in supercritical state and as a general rule of thumb CO_2 will be at supercritical state below 800 meters depth.

Table 8.1.2. *CO_2 fluid parameter assumption and estimated values.*

Scenario	Apex depth (TVDSS. m)	Spill point depth (TVDSS. m)	Structural relief (m)	Mid reservoir depth (m)	Pressure (HydroS.)(MPa)	Mid Res. Temp. (C)	CO2 density (Kg / m3)
Stenlille 4way Z1–4	1449	1475	26	1466	14.34	54,0	619.9
Stenlille 4way Z5	1489	1515	26	1506	14.73	55.2	632.9
Stenlille Flank Z1–4	*1480*	*1620*	*140*	*1545*	*15.21*	*56.7*	*640.1*
Stenlille Flank Z5	*1520*	*1660*	*140*	*1585*	*15.60*	*57.9*	*637.5*

Storage efficiency

Storage efficiency is heavily influenced by local subsurface confinement, reservoir performance, compartmentalisation etc. (geological factors) on one hand, and injection design and operation (financial controlled factors) on the other (Wang et al. 2013). A sufficient analogue storage efficiency database is not available to this study and accurate storage efficiency factor-ranges lacks at this early stage of maturation. This emphasises the need for further investigations of subsurface and development scenarios to better understand the potential storage efficiency ranges. In this evaluation, a range from 10% to 50% with a mode of 40% is used as a possible range, although we emphasise the need for further work on this. A Pert distribution for this element has also been applied. In Tables 8.1.3 through 8.1.6, input parameter distributions are listed (all selected to follow Pert distributions defined by min., max. and mode). An example of parameter distribution shapes is displayed in Figure 8.1.6.

Input summary

Table 8.1.3. *Input parameters for the Stenlille 4way Z1–4 scenario.*

Parameter	Assumption		
	Min	Mode	Max
GRV ($10^6 m^3$)	53.89	68.51	82.2
Net/Gross	0.6	0.67	0.8
Porosity	0.2	0.23	0.27
Storage eff.	0.1	0.4	0.5
In situ CO_2 density (kg/m^3)	601	620	650

Table 8.1.4. *Input parameters for the Stenlille 4way Z5 scenario.*

Parameter	Assumption		
	Min	Mode	Max
GRV ($10^6 m^3$)	48.56	60.7	72.84
Net/Gross	0.65	0.78	0.9
Porosity	0.21	0.25	0.28
Storage eff.	0.1	0.4	0.5
In situ CO_2 density (kg/m^3)	614	633	665

Table 8.1.5. *Input parameters for the Stenlille Flank Z1–4 scenario.*

Parameter	Assumption		
	Min	Mode	Max
GRV ($10^6 m^3$)	93.2	199.6	431.6
Net/Gross	0.6	0.67	0.85
Porosity	0.2	0.23	0.28
Storage eff.	0.1	0.3	0.35
In situ CO_2 density (kg/m^3)	621	640	672

Table 8.1.6. *Input parameters for the Stenlille Flank Z5 scenario.*

Parameter	Assumption		
	Min	Mode	Max
GRV ($10^6 m^3$)	93.2	221.6	472
Net/Gross	0.64	0.8	0.9
Porosity	0.2	0.24	0.28
Storage eff.	0.1	0.3	0.35
In situ CO_2 density (kg/m^3)	618	638	669

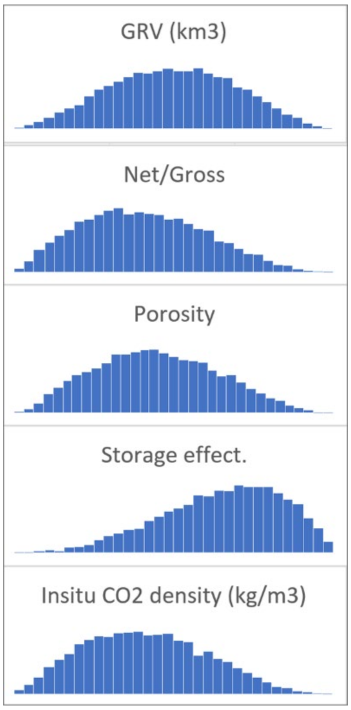

Figure 8.1.6. *Example of the distribution shapes (Pert dist.) for the input paremeters (*Table 8.1.4*).*

8.2 Storage capacity Results

The modelled capacities were made on the assumption that the current subsurface storage at Stenlille also works as storage site for CO_2. It is assumed that the known efficient reservoir-seal pairs from the Stenlille crest also is capable of retaining CO_2 in the reservoirs on flanks of the structure, although this needs to be tested by further geological investigation. In Table 8.2.1 through 8.2.5 the results of the Monte Carlo simulations are tabulated below, indicating both the available pore volume within the defined scenario, the effective volume accessible for CO_2 storage (applying the Storage Efficiency factor to pore volume) and the mass of CO_2 in mega-tons (MT) that can be stored. The tables present the 90%, 50% and 10% percentiles (P10, P50 and P10) corresponding to the probability to exceed the given capacity/volume value. Mean values of the resultant outcome distribution are also tabulated and is considered the "best" single value representation for the entire distribution. A mean storage capacity of 2.4 MT CO_2 is calculated for the Stenlille 4way Z1–4 scenario and 2.7 MT CO_2 for the underlying Stenlille 4way Z5 scenario reflects that only limited capacity is structurally confined and governed by the low relief structural setting. The two Flank injection scenarios show 6.2 and 8.0 MT CO_2 for the Z1–4 and Z5 units, respectively indicating a larger potential if the entire reservoir section can be utilised for injection. Uncertainties for the modelled capacities for the Stenlille 4way scenarios are fairly limited due to the high level of data from both wells and the available 3D seismic data (Figure 8.2.1). The largest storage capacity uncertainty is linked with the uncertainty in reservoir gross rock volume estimation and storage efficiency, as illustrated in Figure 8.1.2. and Figure 8.2.2. In comparison, CO_2 density at reservoir conditions is of minor concern. For the capacity estimation the of the Flank scenarios of the uncertainty range increases as data and the knowledge here on the flank decreases.

Table 8.2.1. *Stenlille 4way Z1–4 storage capacity potential.*

Results	P90	P50	P10	Mean
Buoyant trapping pore volume (Km^3)	0.009	0.011	0.012	**0.011**
Buoyant eff. storage volume (Km^3)	0.003	0.004	0.005	**0.004**
Buoyant storage capacity (MT CO_2)	1.7	2.5	3.2	**2.4**

Table 8.2.2. *Stenlille 4way Z5 storage capacity potential.*

Results	P90	P50	P10	Mean
Buoyant trapping pore volume (Km^3)	0.010	0.012	0.013	**0.012**
Buoyant eff. storage volume (Km^3)	0.003	0.004	0.006	**0.004**
Buoyant storage capacity (MT CO_2)	1.9	2.7	3.5	**2.7**

Table 8.2.3. *Stenlille Flank Z1–4 storage capacity potential.*

Results	P90	P50	P10	Mean
Buoyant trapping pore volume (Km^3)	0.022	0.035	0.050	**0.036**
Buoyant eff. storage volume (Km^3)	0.006	0.009	0.014	**0.010**
Buoyant storage capacity (MT CO_2)	3.7	6.0	9.2	**6.2**

Table 8.2.4. *Stenlille Flank Z5 storage capacity potential.*

Results	P90	P50	P10	Mean
Buoyant trapping pore volume (Km^3)	0.028	0.045	0.065	**0.046**
Buoyant eff. storage volume (Km^3)	0.007	0.012	0.019	**0.013**
Buoyant storage capacity (MT CO_2)	4.7	7.7	11.8	**8.0**

Table 8.2.5. *Overview of the capacity for the four selected injection scenarios. Summation should not be done as these are very different development scenarios.*

Scenario	Storage capacity (MT CO2)			
	P90	P50	P10	Mean
Stenlille 4way Z1–4	1.7	2.5	3.2	**2.4**
Stenlille 4way Z5	1.9	2.7	3.5	**2.7**
Stenlille Flank Z1–4	3.7	6.0	9.2	**6.2**
Stenlille Flank Z5	4.7	7.7	11.8	**8.0**

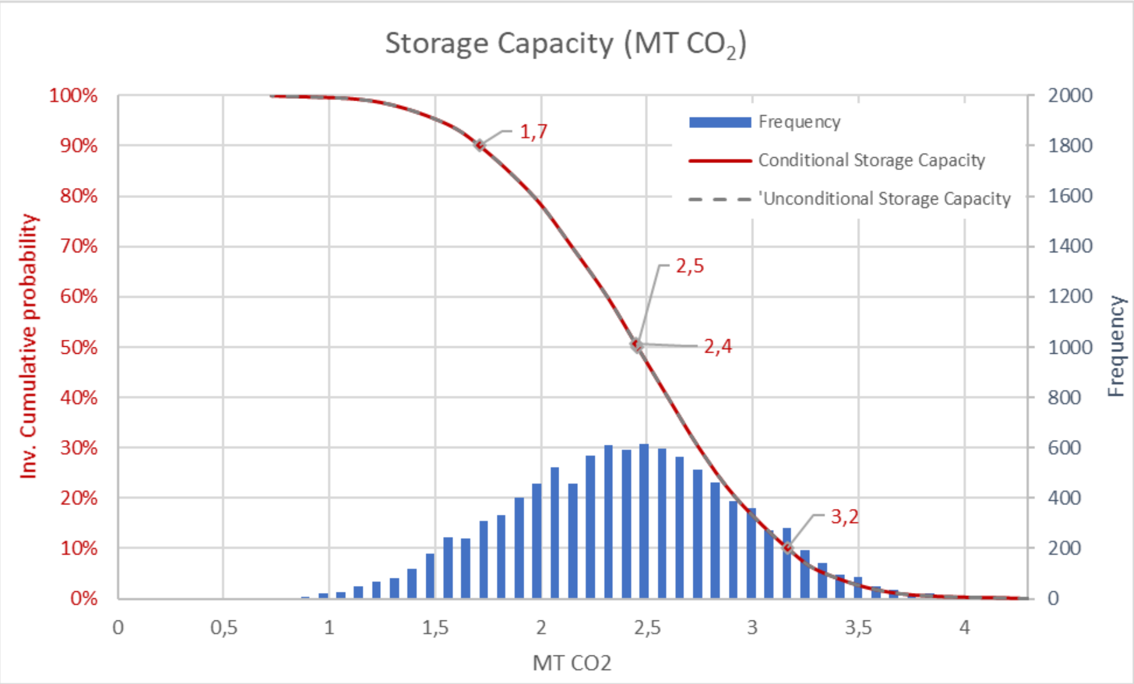

Figure 8.2.1. *Modelled statistical distribution of the Stenlille 4way Z1–4 storage capacity potential that illustrates the inverse cumulative probability function for CO_2 capacity and distribution frequency. The distribution shows that some uncertainty still resides within a well-known structure.*

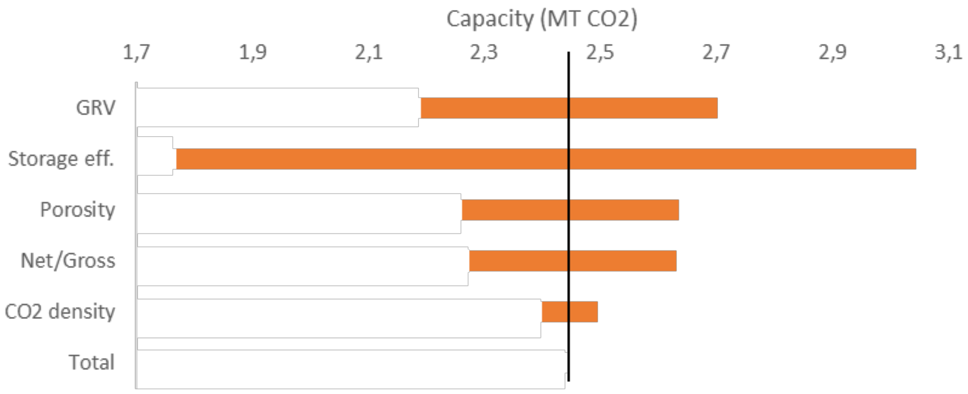

Figure 8.2.2. *Sensitivity (Tornado) plot of how the various input parameters affect the total storage capacity estimate mean (2.45 MT CO_2) of the Stenlille 4way Z1–4 unit. The horizontal bars for each parameter indicate change in storage capacity given that only that parameter is changed leaving all other constant (end levels being P90 and P10, respectively, in the parameter input range).*

Concluding Capacity Comments

It is not envisioned that all scenarios could be developed simultaneous, and the conceptual flank scenarios could be considered as indication of one well injection scenario with a hypothetical plume extent and therefore summation of the four scenarios may not be meaningful. However, two combined scenarios may be possible depending on the actual subsurface conditions and modelling.

The 4-way top-structure storage capacities within mapped and defined closures are the primary options, whereas flank scenarios are uncertain and depend on e.g. plume flow directions and limitations, such as site-specific permeabilities, internal seals and compartmentalisations. CO_2 injected downflank may to some extend be retained in parts of the flank but will most likely also migrate towards the top of the structure. Thus, the flank and 4-way top-structure scenarios may be difficult to regard separately.

Earlier regional screening has suggested that the potential on the Stenlille was in the order of c. 62 MT CO_2 (Larsen et al. 2003). However, the present study finds that the areal extent of the structure is smaller than indicated by the regional maps, and that the structural relief is a limiting factor on the capacity, and unfortunately also very sensitive to depth conversion. Therefore, the full Gassum thickness (130 m) may not be utilized for structural confined storage as previously assumed. A possible mean storage capacity estimate for a Gassum Fm development on Stenlille, may be in the order of c. 6–10 MT CO_2. The 4-way top-structure capacities are primary, probably with some additional retainment capacity in the flank of more uncertain volumes, and thus a wide capacity range is given. However, the capacity and possible scenario combinations must be investigated further by e.g., reservoirs simulation modelling to ensure optimal development and filling of the reservoir zones of the structure, and to ensure less uncertainty.

Additional storage capacity may be available in the Stenlille structure, such as in reservoir Zone 6 of the Gassum Formation, and also deeper within the Oddesund and Bunter Sandstone Formations. However, potential reservoir sandstones in the two deepest formations are only known from the Stenlille-19 well, and this study has not evaluated the potential extend of these deeper reservoir sandstones and the associated storage capacity upside.

8.3 Potential risks

The present report provides an updated geological mapping describing reservoir-seal couples, the extent, thickness, closure, reservoir quality and volume of the primary reservoir formation, as well as larger faults, but does not comprise a dedicated study of risks or risk assessment of the structure for potential storage of CO_2. Thus, the report provides a geological characterization and maturation of these identified elements and points out geological related potential risk issues, that are recommended to be included for further evaluation and maturation, e.g., in risk assessment studies. Risks treated here are primary geological parameters incompletely understood, that may negatively affect the CO_2 storage potential. Not all risks can be identified at this early stage, while other risks identified at this stage will be mitigated by collection of new geophysical and geological data and further investigations, which together can shed new light on the critical parameters and risks. The few risks described below are not considered a full list, but rather emphasizes important points that needs further attention in future studies and data collections.

Faulting of the Gassum-Fjerritslev Fm reservoir-seal pair is considered the primary risk at the current level of understanding. Despite very thickly developed seals, the faults through the Fjerritslev Fm seal and some of them up to shallower successions introduce a potential risk of vertical leakage from storage in the Gassum Formation that needs to be addressed when maturing the structure further. Faulting of the reservoirs is known to be associated with reservoir compartmentalization in at least three large compartment areas divided by faults in the Stenlille structure, where natural gas is stored. The main compartments are divided by SSW–NNE fault trend (mainly the F13 and F14 faults) in the southern part of the structure and by a SW–NE fault trend (mainly the F11 fault) along the more central part of the structure near its apex (Fig. 6.2.6). The mapped faults are typically located from less than hundred meter to a few kilometres apart, and the short distance may reduce reservoir communication and storage efficiency, and thus lower the storage efficiency in these parts and increase the number of injection wells required to fill the structure. The mapped faults are most dense in the SE flank of the structure with mainly SW–NE trending complex faults, mostly up to near top of Fjerritslev Fm, and may in some cases connect further up into the Chalk Group, where faults of other directions are also detected. Thus, should it later be decided, CO_2 injection and the potential migration pathway should be safely away from these faults, and not on the eastern to southern flank of the structure. Also, the saddle-point and lowest closure at the Top Gassum (Fig. 6.2.3C, 8.1.1) in the southern part of the structure (near the ST-4 well) and at the north-eastern saddle-point and deepest closure of the structure, have some uncertainty, and storage near these areas is therefore recommended to be avoid based on the current data and interpretations.

The long-term monitoring and analyses of groundwater over the Stenlille structure has only detected one escape of gas, related to a technical problem in the ST-14 well during injection in 1995, and was not a leakage of the stored natural gas from the Gassum Formation reservoir through the natural seal barriers (Laier 2012; Dahl-Jensen et al. 2021). The monitoring thus indicates that the seal capacity for natural gas has been effective for decades. Denmark is a low risk area for earthquakes though small earthquakes do occur (Fig. 8.2.1). Earthquake hazard for Denmark can be found in Voss al. (2015), where also lists of felt and damaging earthquakes can be found. In Figure 8.2.2 all known earthquakes on Zealand are shown. The largest is ML 4.0 (ML is the local magnitude or the local Richterscale) in 1930 ESE of Stevns (Lehmann 1931). Also, the smaller, but widely felt, earthquake in 2001 close to

Holbæk is described (Larsen et al. 2008). Most earthquakes within Zealand are registered in the western part of Isefjord and the southern end of Roskilde fjord (Fig. 8.2.1). The depths of the earthquakes are very uncertain, but they are located within Earth's crust. A monitoring study was carried out around Gas Storage Denmark (GSD) gas storage facility close to Stenlille (Fig. 8.2.2). Six seismic stations were in operation for almost three years, and no local events were detected. The detection limit within the storage area was calculated to be at least ML 0.0 (Dahl-Jensen et al. 2021).

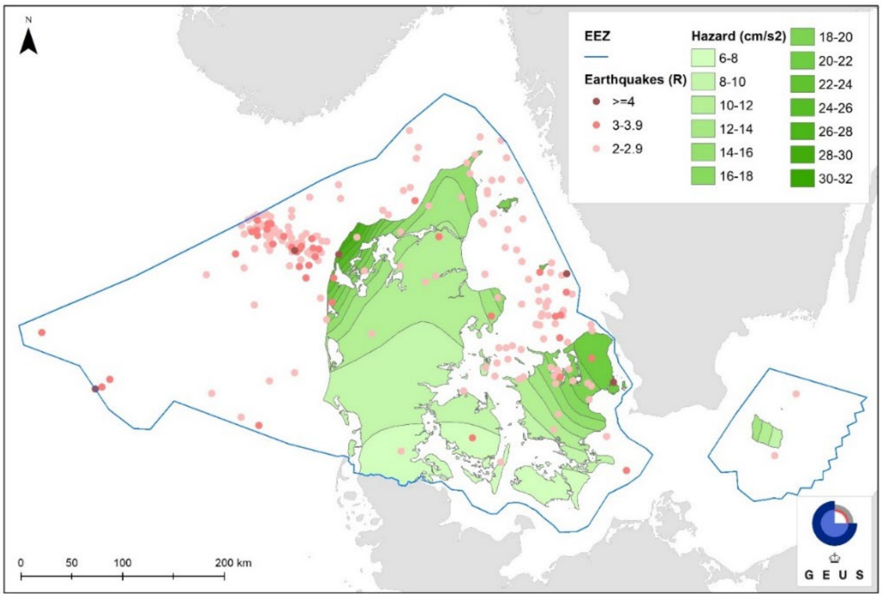

Figure 8.2.1. *The coloured contours are redrawn onshore from Voss et al. (2015) and show the estimated hazards given by the peak ground accelerations [cm/s2] for a return period of 475 years. This corresponds to a 90% non-exceedance probability in 50 years. Given values are only valid onshore Denmark. The contours are based on a validated catalogue of earthquakes over Magnitude 3 from 1960 to 2013. As the attenuation of earthquakes (ground motion prediction) has not been determined specifically for Denmark, the global reference model by Spudich et al. (1997) that describes attenuation from normal faults in hard-rock conditions was used.*

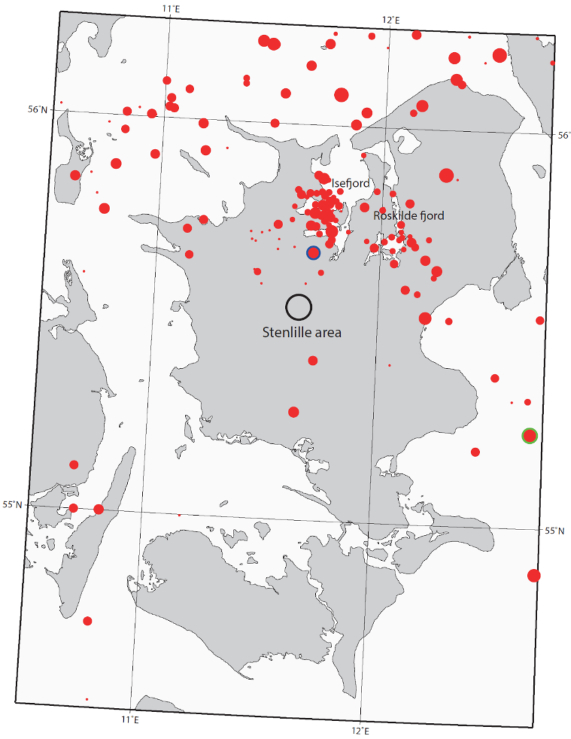

Figure 8.2.2. *All known earthquakes until the end of 2022, located since 1930 within 54.5–56.25N/10.5–12.75E. The magnitude (shown by the size of the red dots) varies from ML 4.0 and down. All known and assumed explosions have been removed, but some may remain, mainly offshore. 1930 Øresund ML 4.9 earthquake: green circle boundary; 2001 Holbæk ML 2.8 earthquake: blue circle boundary. The approximate position of the Stenlille area investigated in this report is marked with a black circle.*

9. Conclusions

This study showed, that the Stenlille structure forms a well-defined structural anticlinal dome, cored by a salt pillow of Zechstein salt overlain by thick Triassic−Lower Jurassic, and younger successions. The structure includes three reservoir−seal couples (shallow to deep), the Gassum Fm−Fjerritslev Fm (primary couple), and the deeper Intra Oddesund sandstone beds−mudstones (Oddesund Fm) and the Bunter Sandstone Fm−Ørslev Fm, all three forming structural closures. This report has focus on the primary reservoir-seal couple.

The structure is covered by the most comprehensive database onshore Denmark with 20 wells, a 3D seismic survey, and 2D seismic lines. Five new lines were acquired in February 2022, to increase coverage of the NE structure flank, outside the 3D data. However, new 3D seismic data is recommended outside or overlapping the present 3D seismic area, and in particular where injection wells may be planned and up-flank. This study is focused on the primary reservoir sandstones of the Gassum Formation of Rhaetian age overlain by the Fjerritslev Formation primary seal successions of latest Rhaetian to Early Jurassic ages. The formations are known from nearly all 20 Stenlille wells.

The Gassum Formation is c. 140−160 m thick and is lateral continuous based on the Stenlille wells and the seismic mapping. The two lowermost and thickest reservoir zones (5 and 6) have the best reservoir properties, with up to c. 25 % and c. 27 % porosity in average, respectively, and a permeability up to c. 300 mD and 4000 mD in average, respectively. The uppermost reservoir sand zones (1, 2b, 3 and 4) have good, but slightly more moderate reservoir properties with a summarized average of c. 23 % porosity and an average permeability up to c. 170 mD. Although reservoir Zone 3 is relatively thin compared to Zones 5 and 6, it has specific reservoir properties comparable to the lowermost zones, with average porosities of 25% and permeability of 350 mD. The Net to Gross ratio of the Gassum Fm sandstone in e.g., the ST-19 well is for these six zones in average c. 0.76 in total, and c. 0.67 for Zones 1–4 sand (0.93 for Zone 3), 0.78 for Zone 5, and 1 for Zone 6 sand. The reservoir zones 1–3 and 5 is currently utilized for storage of natural gas.

Seal successions are described for the three reservoirs. The Gassum Fm is overlain by the c. 240−300 m thick, lateral continuous claystone and mudstone-dominated Fjerritslev Fm, the main part of which is considered an excellent main seal for storage in the Gassum Fm. The lower formation part contains some thin silt and sandstone layers, if some CO_2 should escape the underlying reservoirs. The Lower Cretaceous Vedsted Fm to Rødby Fm succession, that onlap and overlie the Fjerritslev Fm is considered a secondary seal, which is covered by the km-thick Chalk Group and younger successions. This seal succession is proven effective by more than 30 years of safe storage of natural gas used for consumers.

Faults are located and described from 2D and 3D seismic data with focus on the Gassum Fm and Fjerritslev Fm. The mapping and machine learning work in this study showed that faults in the Triassic–Jurassic successions mainly are trending SW–NE, with less in more northern directions and have rather moderate throws. Towards east and south faults become denser and they appear to increase in length, both vertically and laterally, and also throws of successions seem to increase moderately. The primary geological risks for efficient CO_2 storage as identified at this stage is considered the presence of faults offsetting both reservoirs and overlying seals. Faults can affect compartmentalization (known from the Stenlille natural gas production in the Gassum Fm) and a mechanical weakening of the seal, which is recommended to be mitigated by further data acquisition and analyses in order to mature the Stenlille structure for CO_2 storage.

The calculations in this study show a limited storage capacity of the Gassum Formation. The storage capacity of the Gassum Formation is estimated for four out of several possible scenarios, here including the 4way closure and a conceptual Flank scenario for reservoir Zone 1–4 and Zone 5, respectively. The mean storage capacities of CO_2 in the Gassum Formation of the Stenlille structure are estimated respectively for each of the scenarios and are within the 4way closure: 2.4 MT CO_2 of Zone 1–4 and 2.7 MT CO_2 of Zone 5. The possible Flank scenarios may be in the order of 6.2 MT CO_2 of Zone 1–4 and 8.0 MT CO_2 of Zone 5. As the scenarios are different, the values may not be summarized. However, possibly two of the scenarios may be combined. Possible mean storage capacity estimates for the Gassum Formation in the Stenlille structure, may be in the order of c. 6–10 MT CO_2. However, the capacity and possible scenario combinations must be investigated further by more site-specific assessments and reservoirs simulation modelling. There may also be potential for CO_2 storage in the lower reservoir sandstones of the Gassum Formation (Zone 6), and deeper in sandstones of the Oddesund and Bunter Sandstone Formations, but their storage capacities have not been investigated here. Sandstone-dominated units in the Oddesund Formation and Bunter Sandstone Formations are only documented in one well (ST-19) and variations of thicknesses and reservoir properties are expected across the structure. See Chapters 5, 7 and 8 for more details on the reservoirs.

10. Recommendations for further work

New 2D seismic data has been acquired in the north-eastern part of the Stenlille structure and has improved the database with five seismic sections. The new data together with the existing data provided a comprehensive database for the present updated mapping and analyses of the size, spill-point, volume, details of reservoir- and seal successions, and faults of the Stenlille structure, for this initial maturation. However, it is recommended, that a further maturation of the structure should include new seismic acquisition and a risk assessment with seal integrity study, including leakage risk at faults and wells.

New 3D seismic acquisition over the potential injection- and storage areas is recommended, for more detailed interpretation prior to CO_2 injection. Acquisition of 3D seismic data over the northern and north-eastern part of the Stenlille structure can add important new data towards mitigating the fault related risks and develop scenarios for well design. It can also provide data for improved modelling of CO_2 migration. Later, repeated 3D surveys in same area can also contribute to monitor the extent of the CO_2 migration, together with other monitoring (e.g., via wells, seismometers, sampling, satellite, etc.). Such data will also enable a more precise definition of trap closures and reservoir outline, which again will feed into a refined storage volume calculation.

The modelled storage capacity is associated with variability-ranges and uncertainty, which e.g., are dependent on volume and closure definition. The structure is small on the Top Gassum mapped surface with a low relief from the deepest closure (spill-point) to the top structure, and its geometry is sensitive to mapping and depth conversion constraints. Thus, it is recommended to still improve the database (incl. new 2D and 3D seismic data), mapping and time-to-depth models. A further key element for the quantification of the storage potential of the structure is the understanding of the storage efficiency. The storage efficiency factor is mostly dependent on reservoir performance and thus potential heterogeneity, permeability, and compartmentalization, but also by economic aspects such as well density, well layout and injection design. Better understanding of the reservoir and simulation of reservoir flow could constrain storage efficiency better and thus narrow the estimated final capacity range.

In this study faults have been identified and described, mainly in the primary reservoir and seal. The study showed that the west to north-western part of the structure seems less affected by faults in the Gassum and Fjerritslev Formations compared to the more central to south-eastern parts. Thus, any possible CO_2 injection in the Gassum Fm should be away from the faults and not in the south-eastern to southern part of the structure. An area close to the saddle-point at the Top Gassum level in the southern part of the structure (near the ST-4 well) and NE part should also be avoided. Besides the potential storage of CO_2 within closure and flank as considered here, potential effects from injection and storage on reservoir and seal at the specific site(s) should also be considered, including mineral solubility, mineral trapping, pressure and stress effects, risks, existing wells etc.

It is also recommended to revise the Danish Triassic to Cretaceous lithostratigraphy, biostratigraphy and sequence stratigraphy, in the eastern part of the Norwegian−Danish Basin, with reference to discussions in this report, and also in relation to the North German Basin and Swedish formations.

New necessary data acquisition and sampling, analyses and evaluations should be carried out for further maturation, including risk analyses, to cover geological and other technical uncertainties and risks.

References

Anthonsen, K.L., Aagaard, P., Bergmo, P.E.S., Gislason, S.R., Lothe, A.E., Mortensen, G.M. and Snæbjörnsdóttir, S.Ó. 2014. Characterisation and selection of the most prospective CO2 storage sites in the Nordic region. Energy Procedia 63, 4884–4896. https://doi.org/10.1016/j.egypro.2014.11.519

Bachmann, G.H., Geluk, M.C., Warrington, G., Becker-Roman, A., Beutler, G., Hagdorn, H., Hounslow, M.W., Nitsch, E., Röhling, H.-G., Simon, T. and Szulc, A. 2010. Triassic. In: Doornenbal, J.C. & Stevenson, A.G. (eds): Petroleum Geological Atlas of the Southern Permian Basin Area. EAGE Publications b.v. (Houten), 149–173.

Bertelsen, F. 1978. The Upper Triassic – Lower Jurassic Vinding and Gassum Formations of the Norwegian–Danish Basin. Danmarks Geologiske Undersøgelse Serie B, Nr. 3, 26 pp. https://geusjournals.org/index.php/serieb/issue/view/927

Bertelsen, F. 1980. Lithostratigraphy and depositional history of the Danish Triassic. Geological Survey of Denmark. Series B, No. 4, 59 pp. https://geusjournals.org/index.php/serieb/issue/view/928

Boldreel, L.O., Andersen, M.S., Vosgerau, H., Mathiesen, A., Kamla, E. and Nielsen, L.H. *in review*. Late Palaeozoic-Cenozoic evolution of the onshore Danish area based on seismic reflection and well data. GEUS Bulletin.

Bredesen, K. 2020. Capture, Storage and Use of CO_2 (CCUS): Quantitative seismic interpretation (rock physics models, seismic inversion, AVO and attribute analysis) (Part of work package 5 in the CCUS project). Danmarks og Grønlands Geologiske Undersøgelse Rapport 2020/52, 9 pp. https://doi.org/10.22008/gpub/34549

Bredesen, K. 2022. Assessing rock physics and seismic characteristics of the Gassum Formation in the Stenlille aquifer gas storage – A reservoir analog for the Havnsø CO_2 storage prospect, Denmark. International Journal of Greenhouse Gas Control, 114, 103583. https://doi.org/10.1016/j.ijggc.2022.103583

Bredesen, K., Lorentzen, M., Smit, F.W.H. and Gregersen, U. 2022. Quantitative seismic interpretation of the Gassum Formation at the Stenlille aquifer gas storage. GHGT-16 Conference Proceedings (2022); SSRN Electronic Journal, November, 2022, 12 pp. https://doi.org/10.2139/ssrn.4276697

Burnett, J.A. 1998. Upper Cretaceous. In: Bown, P.R. (ed.): Calcareous Nannofossil Biostratigraphy. British Micropalaeontological Society Series. Chapman & Hall/Kluwer Academic, 132–199.

Catuneanu, O. 2019. Model-independent sequence stratigraphy. Earth-Science Reviews 188, 312–388.

CGG, 1998. Final report of seismic data processing. Survey: STENLILLE-97 3D survey. October, 1997-May, 1998. Conpagnie Générale de Géophysique for Dansk Naturgas A/S (DONG). France, May 1998.

Chadwick, R.A., Zweigel, P., Gregersen, U., Kirby, G.A., Holloway, S. and Johannesen, P.N. 2004. Geological reservoir characterization of a CO2 storage site: The Utsira Sand, Sleipner, northern North Sea. Energy, 29 (9−10), 2004. p. 1371–1381. https://doi.org/10.1016/j.energy.2004.03.071

Clark, C.E. 1962. The PERT model for the distribution of an activity Time. Operations Research 10, 405–406. https://doi.org/10.1287/opre.10.3.405

Clift, P.D., Olson, E.D., Lechnowskyj, A., Moran, M.G., Barbato, A. and Lorenzo, J.M. 2019. Grain-size variability within a mega-scale point-bar system, False River, Louisiana. Sedimentology 66, 2, 408–434. https://doi.org/10.1111/sed.12528

Dahl-Jensen, T., Jakobsen, R., Bundgaard Bech, T., Møller Nielsen, C., Nyrop Albers, C., Voss, P.H. and Larsen, T.B. 2021. Monitoring for seismological and geochemical groundwater effects of high-volume pumping of natural gas at the Stenlille underground gas storage facility, Denmark. GEUS Bulletin 47, 8pp. https://doi.org/10.34194/geusb.v47.5552

Danish Ministry of Climate, Energy and Utilities, Denmark's Integrated National Energy and Climate Plan under the Regulation of the European Parliament and of the Council on the Governance of the Energy Union and Climate Action, 2019.

Datalog Technology 2000. Stenlille-19. End of well report.

DGU 1981. Stenlille-1. Geological well completion report.

DONG 2001. ST-19 (Stenlille-19). Final well report. H. Schokker, Copenhagen, 14-02-2001.

Donovan, D.T. & Surlyk, F. 2003. Lower Jurassic (Pliensbachian) ammonites from Bornholm, Baltic Sea, Denmark. Geological Survey of Denmark and Greenland Bulletin 1, 555–583.

Dybkjær, K. 1988. Palynological zonation and stratigraphy of the Jurassic section in the Gassum No. 1-borehole, Denmark. Geological Survey of Denmark Ser. A, No. 21, 73 pp.

Dybkjær, K. 1991. Palynological zonation and palynofacies investigation of the Fjerritslev Formation (Lower Jurassic - basal Middle Jurassic) in the Danish Subbasin. Danmarks Geologiske Undersøgelse Serie A, no. 30, 150 p. https://doi.org/10.34194/seriea.v30.7050

Erlström, M., Sivhed, U. and Surlyk, F. 1999. A backstepping, fluviatile-paralic-marine succession, Sinemurian, Lower Jurassic, Skåne, southern Sweden. Bulletin of the Geological Society of Denmark 46, 1–12.

Frandsen, N. & Surlyk, F. 2003. An offshore transgressive–regressive mudstone-dominated succession from the Sinemurian of Skåne, Sweden. Geological Survey of Denmark and Greenland Bulletin 1, 543–554.

Frederiksen, S., Nielsen, S.B. and Balling, N. 2001. A numerical dynamic model for the Norwegian−Danish Basin. Tectonophysics, 343, 165−183. https://doi.org/10.1016/S0040-1951(01)00223-2.

Frykman, P. 2020. Capture, Storage and Use of CO2 (CCUS). 3D static reservoir model of the Havnsø structure (Part of Work package 6 in the CCUS project). Danmarks og Grønlands Geologiske Undersøgelse Rapport 2020/44, 29 pp. https://doi.org/10.22008/gpub/34541

Fuchs, S., Balling, N. and Mathiesen, A. 2020. Deep basin temperature and heat-flow field in Denmark – New insights from borehole analysis and 3D geothermal modelling. Geothermics, 83. DOI: http://doi.org/10.1016/j.geothermics.2019.101722

Gale, A.S., Mutterlose, J. and Batenburg, S. 2000. The Cretaceous Period. In: Gradstein, F.M.,Ogg, J.G., & Ogg, G.M. (eds): Geological Time Scale 2020. 1023-1086. Amsterdam: Elsevier B.V. https://doi.org/10.1016/B978-0-12-824360-2.00027-9

Gravesen, P., Rolle, F. and Surlyk, F. 1982. LIthostratigraphy and sedimentary evolution of the Triassic, Jurassic and Lower Cretaceous of Bornholm, Denmark. Danmarks Geologiske Undersøgelse Serie B. No. 7, 51 pp.

Gregersen, U., Vosgerau, H., Laghari, S., Bredesen, K., Rasmussen, R. and Mathiesen, A. 2020. Capture, Storage and Use of CO_2 (CCUS): Seismic interpretation of existing 2D and 3D seismic data around the Havnsø structure (Part of work package 5 in the CCUS project). Danmarks og Grønlands Geologiske Undersøgelse Rapport 2020/33; GEUS. 60 pp. https://doi.org/10.22008/gpub/34530

Gregersen, U., Smit, F.W.H., Lorentzen, M., Vosgerau, H., Bredesen, K., Hjelm, L., Mathiesen, A. and Laghari, S. 2022. Tectonostratigraphy and Structural Evolution of the Stenlille Structure in Zealand, Denmark – a Site for Natural Gas and CO2 Storage. GHGT-16 Conference Proceedings (2022); SSRN Electronic Journal Nov. 2022 & Geophysics eJournal 4 (85) Dec. 2022, 12 pp. SSRN: http://dx.doi.org/10.2139/ssrn.4275875

Hamberg, L. & Nielsen, L.H. 2000. Shingled, sharp-based shoreface sandstones: depositional response to stepwise forced regression in a shallow basin, Upper Triassic Gassum Formation, Denmark. In: Hunt, D. and Gawthorpe, R.L. (eds): Sedimentary Responses to Forced Regressions. Geological Society, London, Special Publications, 172, 69–89. https://doi.org/10.1144/GSL.SP.2000.172.01.04

Hjelm L., Anthonsen K.L., Dideriksen K., Nielsen C.M., Nielsen L.H. and Mathiesen A. 2022. Capture, Storage and Use of CO2 (CCUS). Evaluation of the CO2 storage potential in Denmark. Vol.1: Report & Vol 2: Appendix A and B [Published as 2 separate volumes both with Series number 2020/46]. Danmarks og Grønlands Geologiske Undersøgelse Rapport 2020/46; GEUS. 141 pp. https://doi.org/10.22008/gpub/34543

Holmslykke, H.D., Olivarius, M., Kjøller, C. and Didriksen, K. 2020. Capture, Storage and Use of CO_2 (CCUS): Reservoir characterisation and hydrogeochemical reactions between CO_2 and reservoir rock (Part of work package 5 in the CCUS project). Danmarks og Grønlands Geologiske Undersøgelse Rapport 2020/29, 63 pp. https://doi.org/10.22008/gpub/34526

Hovikoski, J. & Pedersen, G.K. 2020. Capture, Storage and Use of CO_2 (CCUS): Sedimentological description of Gassum and Fjerritslev Formations from cores in the Stenlille area, with interpretations of depositional environments (Part of Work package 6 in the CCUS project). Danmarks og Grønlands Geologiske Undersøgelse Rapport 2020/42, 60 pp. https://doi.org/10.22008/gpub/34539

Ineson, J.R. 1993. The Lower Cretaceous chalk play in the Danish Central Trough. Geological Society, London, Petroleum Geology Conference series, 4, 175–183.

Ineson, J.R., Jutson, D.J. and Schiøler, P. 1997. Mid-Cretaceous sequence stratigraphy in the Danish Central Trough. Danmarks og Grønlands Geologiske Undersøgelser Rapport 1997/109, 60 pp.

IPCC (Intergovernmental Panel on Climate Change) 2022. Climate Change 2022: Mitigation of Climate Change. Working Group III contribution to the Sixth Assessment Report of the Intergovernmental Panel on Climate Change. UN, New York. 2913 pp.

Jakobsen, R. 2020. Capture, Storage and Use of CO2 (CCUS): CO2 leakage and effects of aquatic systems – monitoring and remediation (Part of Work package 7 in the CCUS project). Danmarks og Grønlands Geologiske Undersøgelse Rapport 2020/39, 28 pp. https://doi.org/10.22008/gpub/34536.

James, B., Grundy, A.T. and Sykes, M.A. 2013. The Depth-Area-Thickness (DAT) Method for Calculating Gross Rock Volume: A Better Way to Model Hydrocarbon Contact

Uncertainty, AAPG International Conference & Exhibition. AAPG Search and Discovery Article #90166©2013, Cartagena, Colombia, 8-11 September.

Japsen, P. 1998. Regional velocity–depth anomalies, North Sea chalk: a record of overpressure and Neogene uplift and erosion. AAPG Bull., 82, 2031–2074.

Japsen, P. & Bidstrup, T. 1999. Quantification of late Cenozoic erosion in Denmark based on sonic data and basin modelling. Bulletin of the Geological Society of Denmark, 46, 79–99. https://doi.org/10.37570/bgsd-1999-46-08

Japsen, P., Green, P.F., Nielsen, L.H., Rasmussen, E.S. and Bidstrup, T. 2007. Mesozoic–Cenozoic exhumation events in the eastern North Sea Basin: a multi-disciplinary approach based on palaeothermal, palaeoburial, stratigraphic and seismic data. Basin Research 19, 451–490.

Jensen, T.F, Holm, L., Frandsen, N. and Michelsen, O. 1986 Jurassic-Lower Cretaceous Lithostratigraphic Nomenclature for the Danish Central Trough. Danmarks Geologiske Undersøgelse Serie A 12, 65 pp. https://doi.org/10.34194/seriea.v12.7031

Keiding, M. 2021. Capture, Storage and Use of CO2 (CCUS). Geophysical Methods to monitor injection and storage of CO2 (Part of Work package 7 in the CCUS project). Danmarks og Grønlands Geologiske Undersøgelse Rapport 2020/40. GEUS. https://doi.org/10.22008/gpub/34537

Kristensen, L. 2020. Capture, Storage and Use of CO2 (CCUS). Reservoir data – Stenlille area (Part of Work package 6 in the CCUS project). Danmarks og Grønlands Geologiske Undersøgelse Rapport 2020/28, 55 pp. https://doi.org/10.22008/gpub/34525

Laier, T. 2012. Results of monitoring groundwater above the natural gas underground storage at Stenlille, Denmark. GEUS Bulletin 26, 45–48. https://doi.org/10.34194/geusb.v26.4748

Laier, T. & Øbro, H. 2009. Environmental and safety monitoring of the natural gas underground storage at Stenlille, Denmark. Geological Society, London, Special Publications, 313, 81–92. https://doi.org/10.1144/SP313.6

Larsen, G. 1966: Rhaetic–Jurassic– Lower Cretaceous sediments un the Danish Embayment (A heavy-mineral study). Geological Survey of Denmark, II Series, No. 91, 127 p. plus plates. https://doi.org/10.34194/raekke2.v91.6882

Larsen, M., Bidstrup, T., Dalhoff F. 2003. Mapping of deep saline aquifers in Denmark with potential for future CO2 storage. Geological Survey of Denmark and Greenland, Rapport 2003/39, 83 pp.

Larsen, T. B., Gregersen, S., Voss, P. H., Bidstrup, T. and Orozova-Bekkevold, V. 2008. The earthquake that shook central Sjælland, Denmark, November 6, 2001. Bulletin of the Geological Society of Denmark, 56. 1–11.

Larsen, T.B., Voss, P.H. and Dahl-Jensen, T. 2020. Capture, Storage and Use of CO_2 (CCUS): Seismology in relation to safe storage of CO2 (Part of Work package 7 in the CCUS project). Danmarks og Grønlands Geologiske Undersøgelse Rapport 2020/41, 29 pp. https://doi.org/10.22008/gpub/34538

Lauridsen, B.W., Lode, S., Sheldon, E., Frykman, P., Anderskouv, K and Ineson, J. 2022. Lower Cretaceous (Hauterivian–Aptian) pelagic carbonates in the Danish Basin: new data from the Vinding-1 well, central Jylland, Danmark. Bulletin of the Geological Society of Denmark, 71, 7–29. https://doi.org/10.37570/bgsd-2022-71-02

Lehmann, I. 1931. Jordskælvet den 1. November 1930. Naturens Verden 15, 219–235.

Lindström, S. 2016. Palynofloral patterns of terrestrial ecosystem change during the end-Triassic event – a review. Geological Magazine 153, Special issue 02, 223–251.

Lindström, S. 2020. Capture, Storage and Use of CO_2 (CCUS): Palynology of the Gassum and lowermost Fjerritslev formations in the Stenlille area: biostratigraphic and palaeoenvironmental implications (Part of work package 5 in the CCUS project). Danmarks og Grønlands Geologiske Undersøgelse Rapport 2020/36, 35 pp. https://doi.org/10.22008/gpub/34533

Lindström, S. & Erlström, M. 2011. The Jurassic–Cretaceous transition of the Fårarp-1 core, southern Sweden: Sedimentological and phytological indications of climate change. Palaeogeography, Palaeoclimatology, Palaeoecology 308, 445–475.

Lindström, S., van de Schootbrugge, B., Dybkjær, K., Pedersen, G.K., Fiebig, J., Nielsen, L.H., Richoz, S. 2012. No causal link between terrestrial ecoystem change and methane release during the end-Triassic mass extinction. Geology 40, 531–534. DOI: 10.1130/G32928.1 WOSUID: WOS:000304515000013

Lindström, S., Pedersen, G.K., van de Schootbrugge, B, Hansen, K.H., Kuhlmann, N., Thein, J.T., Johansson, L., Petersen, H.I., Alwmark, C., Dybkjær, K., Weibel, R., Erlström, M., Nielsen, L.H. Oschmann, W. and Tegner, C. 2015. Intense and widespread seismicity during the end-Triassic mass extinction due to emplacement of a large igneous province. Geology 43, 387–390. (publ. online 2015.03.19). DOI: 10.1130/G36444.1 WOSUID: WOS:000357619400025

Lindström, S., van de Schootbrugge, B., Hansen, K.H., Pedersen, G.K., Alsen, P., Thibault, N., Dybkjær, K., Bjerrum, C.J. and Nielsen, L.H. 2017. A new correlation of Triassic–Jurassic boundary successions in NW Europe, Nevada and Peru, and the Central Atlantic Magmatic Province: A time-line for the end-Triassic mass extinction. Palaeogeography, Palaeoclimatology, Palaeoecology 478, 80–102. [Available online 21 December 2016]. DOI: 10.1016/j.palaeo.2016.12.025 WOSUID: WOS:000402355900006

Lindström, S., Sanei, H., van der Schootbrugge, B., Pedersen, G.K., Lesher, C.E., Tegner, C., Heunisch, C., Dybkjær, K., and Outridge, P.M. 2019. Volcanic mercury and mutagenesis in land plants during the end-Triassic mass extinction. Science Advances 5, 13 p. (eaaw4018 23 October 2019). DOI: 10.1126/sciadv.aaw4018

Lindström, S., Sanei, H., van der Schootbrugge, B., Pedersen, G.K., Lesher, C.E., Tegner, C., Heunisch, C., Dybkjær, K., and Outridge, P.M. 2019. Volcanic mercury and mutagenesis in land plants during the end-Triassic mass extinction. Science Advances 5, 13 p. (eaaw4018 23 October 2019). DOI: 10.1126/sciadv.aaw4018

Lindström, S., Callegaro, S., Davies, J., Tegner, C., van de Schootbrugge, B., Pedersen, G.K., Youbi, N., Sanei, H. and Marzoli, A. 2021. Tracing volcanic emissions from the Central Atlantic Magmatic Province in the sedimentary record. Earth-Science Reviews 212 (2021, 27 pages). Manuscript for special issue in Earth-Science Review. Available online 20.11.2020.

Lindström, S. et al. *in prep*. Palynostratigraphy and sedimentology of the Triassic–Jurassic boundary succession at Stenlille (Danish Basin, Denmark).

Lorentzen, M., Bredesen, K., Gregersen, U., Smit, F.W.H. and Laghari, S. 2022. Fault Mapping of the Gassum Formation Reservoir and the Fjerritslev Formation Caprock Interval at the Stenlille Gas Storage Site Using a Pre-Trained Convolutional Neural Network. GHGT-

16 Conference Proceedings (2022); Geophysics eJournal, 4(86), December, 2022, 12 pp. SSRN: http://dx.doi.org/10.2139/ssrn.4277405

Mallon, A.J. & Swarbrick, R.E. 2002. A compaction trend for non-reservoir North Sea Chalk, Marine and Petroleum Geology, 19, 10, 527–539.

Mallon, A.J. & Swarbrick, R.E. 2008. Diagenetic characteristics of low permeability, non-reservoir chalk from the Central North Sea, Marine and Petroleum Geology, 25, 10, 1097–1108. https://doi.org/10.1016/j.marpetgeo.2007.12.001

Malehmir, A. & Papadopoulou, M. 2022. Innovative land seismic data acquisition for geological CO_2 storage in Stenlille, Denmark. Final Acquisition and Processing Report of the GEUS2022-STENLILLE survey. Uppsala University, July 2022, 42 pp. (*Available via* the Geological Survey of Denmark and Greenland, Copenhagen: www.geus.dk).

Mathiassen, D.R., Kristensen, L., Japsen, P., Rasmussen, E.S. and Michelsen, O. 1989. Evaluering af Gassum og Fjerritslev Formationerne på Stenlille strukturen. Bidrag til vurdering af gaslager. Danmarks Geologiske Undersøgelse, fortrolig rapport nr. 3, 1989.

Mathiesen, A., Dam, G., Fyhn, M.B.W., Kristensen, L., Mørk, F., Petersen, H.I. and Schovsbo, N.H. 2022. Foreløbig evaluering af CO_2 lagringspotentiale af de saline akviferer i Nordsøen. Grønlands Geologiske Undersøgelse Rapport 2022/15, 151 pp. + App.

Mathiesen, A., Kristensen, L., Nielsen, C.M., Weibel, R., Hjuler, M.L., Røgen, B., Mahler, A. and Nielsen, L.H. 2013. Assessment of sedimentary geothermal aquifer parameters in Denmark with focus on transmissivity. European Geothermal Congress 2013, Pisa, 3–7 June 2013.

Michelsen, O. 1975. Lower Jurassic biostratigraphy and ostracods of the Danish Embayment. Danmarks Geologiske Undersøgelse II. Række 104, 1-287. https://doi.org/10.34194/raekke2.v104.6895.

Michelsen, O. 1976. Preliminary report on the Jurassic lithostratigraphic nomenclature in the Danish North Sea area. Danmarks Geologiske Undersøgelse, Årbog 1975, 105–116.

Michelsen, O. 1978. Stratigraphy and distribution of Jurassic deposits of the Norwegian–Danish Basin. Danmarks Geologiske Undersøgelse Serie B, Nr. 2, 28 pp. https://doi.org/10.34194/serieb.v2.7057

Michelsen, O. 1989a. Revision of the Jurassic lithostratigraphy of the Danish Subbasin. Danmarks Geologiske Undersøgelse, Serie A, Nr. 24, 23 pp.

Michelsen, O. 1989b. Log-sequence analysis and environmental aspects of the Lower Jurassic Fjerritslev Formation in the Danish Subbasin. Danmarks Geologiske Undersøgelse, Serie A, Nr. 25, 23 pp.

Michelsen, O. & Bertelsen, F. 1979. Geotermiske reservoirformationer i den danske lagserie. Danmarks Geologiske Undersøgelse, Årbog 1978, 151–164.

Michelsen, O. & Clausen, O.R. 2002. Detailed stratigraphic subdivision and regional correlation of the southern Danish Triassic succession. Marine and Petroleum Geology, 19, 563–587. https://doi.org/10.1016/S0264-8172(02)00028-4

Michelsen O. & Nielsen, L.H. 1991. Well records on the Phanerozoic stratigraphy in the Fennoscandian Border Zone, Denmark: Hans-1, Sæby-1, and Terne-1 wells. Geological Survey of Denmark – DGU Serie A, 29. 38 pp. https://doi.org/10.34194/seriea.v29.7049

Michelsen, O. & Nielsen, L.H., 1993: Structural development of the Fennoscandian Border Zone, offshore Denmark. Marine and Petroleum Geology Vol 10, 124–134.

Michelsen, O., Nielsen, L.H., Johannessen, P.N., Andsbjerg, J. and Surlyk, F. 2003. Jurassic lithostratigraphy and stratigraphic development onshore and offshore Denmark. In: Ineson, J.R. and Surlyk, F. (eds): The Jurassic of Denmark and Greenland. Geological Survey of Denmark and Greenland Bulletin 1, p. 145–216. https://doi.org/10.34194/geusb.v1.4651

Michelsen, O., Saxov, S. Leth, J.A., Andersen, C., Balling, N., Breiner, N., Holm, L., Jensen, K., Kristensen, J.I., Laier, T., Nygaard, E., Olsen, J.C., Poulsen, K.D., Priisholm, S., Raade, T.B., Sørensen, T.R. & Würtz, J. 1981. Kortlægning af potentielle geotermiske reservoirer I Danmark. Danmarks Geologiske Undersøgelse Serie B, Nr. 5, 96 pp.

Mogensen, T.E. & Korstgård, J.A. 2003. Triassic and Jurassic transtension along part of the Sorgenfrei-Tornquist Zone in the Danish Kattegat. GEUS Bulletin, 1. p. 437–458. https://doi.org/10.34194/geusb.v1.4680

Nielsen, L.H. 2003. Late Triassic – Jurassic development of the Danish Basin and the Fennoscandian Border Zone, southern Scandinavia. In: Ineson, J.R. and Surlyk, F. (eds): The Jurassic of Denmark and Greenland. Geological Survey of Denmark and Greenland Bulletin 1, p. 459–526. https://doi.org/10.34194/geusb.v1.4681

Nielsen, L.H. & Japsen, P. 1991. Deep wells in Denmark 1935-1990. Lithostratigraphic subdivision. Danmarks Geologiske Undersøgelse, DGU Serie A, No. 31, 177 pp.

Nielsen, L., Boldreel, L.O., Hansen, T.M, Lykke-Andersen, H., Stemmerik, L., Surlyk, F. and Thybo, H. 2011. Integrated seismic analysis of the Chalk Group in eastern Denmark – Implications for estimates of maximum palaeo-burial in southwest Scandinavia. Tectonophysics, 511, 14-26. doi:10.1016/j.tecto.2011.08.010

Nielsen, L.H., Larsen, F. and Frandsen, N. 1989. Upper Triassic–Lower Jurassic tidal deposits of the Gassum Formation on Sjælland, Denmark. Geological Survey of Denmark. DGU Series A, No. 23, 1–30. https://doi.org/10.34194/seriea.v23.7043

Nielsen, L.H., Petersen, H.I., Dybkjær, K. and Surlyk, F. 2010. Lake-mire deposition, earthquakes and wildfires along a basin margin fault; Rønne Graben, Middle Jurassic, Denmark. Palaeogeography, Palaeoclimatology, Palaeoecology 292, 103–26.

Olivarius, M., Heredia, B.D., Malkki, S.N., Thomsen, T.B. and Vosgerau, H. 2020. Capture, Storage and Use of CO2 (CCUS): Provenance of the of Gassum Formation: Implications for reservoir distribution and mineralogy (Part of Work package 6 in the CCUS project). Danmarks og Grønlands Geologiske Undersøgelse Rapport 2020/38, 35 pp. https://doi.org/10.22008/gpub/34535

Olivarius, M., Vosgerau, H., Nielsen, L.H., Weibel, R., Malkki, S.N., Heredia, B.D. and Thomsen, T.B. 2022. Maturity Matters in Provenance Analysis: Mineralogical Differences Explained by Sediment Transport from Fennoscandian and Variscian Sources. Geosciences 2022, 12(8), 308. 24 pp. https://doi.org/10.3390/geosciences12080308

Olivarius, M., Weibel, R., Hjuler, M. L., Kristensen, L., Mathiesen, A., Nielsen, L. H., & Kjøller, C. (2015). Diagenetic effects on porosity–permeability relationships in red beds of the Lower Triassic Bunter Sandstone Formation in the North German Basin. Sedimentary Geology, 321, 139-153.

Papadopoulou, M., Malehmir, A., Zappalá, S., Gregersen, U., Nielsen, L. and Hjelm, L. 2022. Innovative land seismic data acquisitions for CO2 and energy storage applications. EAGE – Near Surface Geoscience ’22 conference, Belgrade, Serbia. Extended abstract. Vol. 2022, p. 1–5. https://doi.org/10.3997/2214-4609.202220098

Payton, C.E. 1977. Seismic Stratigraphy – applications to hydrocarbon exploration. The American Association of Petroleum Geologists – AAPG Memoir 26, Tulsa, Oklahoma, USA. 516 pp.

Pedersen, G.K. 1985. Thin, fine-grained storm layers in a shelf sequence: an example from the Lower Jurassic in the Stenlille 1 Well, Denmark. Journal of the Geological Society of London 142, 357–374. DOI: 10.1144/gsjgs.142.2.0357 WOSUID: WOS:A1985AFN5800010

Pedersen, G.K. 1986. Changes in the bivalve assemblage of an early Jurassic mudstone sequence (the Fjerritslev Formation in the Gassum 1 Well, Denmark). Palaeogeography, Palaeoclimatology, Palaeoecology 53, 139–168. DOI: 10.1016/0031-0182(86)90042-8 WOSUID: WOS: A1986A988800002

Pedersen, G.K., Lauridsen, B.W., Sheldon, E. and Midtgaard, H.H., 2022. Studies of geological properties and conditions for deep disposal of radioactive waste, Denmark. Phase 1, report no. 4. Jurassic and Lower Cretaceous claystone distribution, sedimentology, and properties. Danmarks og Grønlands Geologiske Undersøgelse Rapport 2021/55; GEUS. 105 pp and appendices. https://doi.org/10.22008/gpub/34615

Petersen, H. I., Nielsen, L. H., Bojesen-Koefoed, J. A., Mathiesen, A., Kristensen, L. and Dalhoff, F. 2008. Evaluation of the quality, thermal maturity and distribution of potential source rocks in the Danish part of the Norwegian–Danish Basin. Geological Survey of Denmark and Greenland Bulletin, 16, 66 pp. https://doi.org/10.34194/geusb.v16.4989

Petersen, H.I. & Lindström, S. 2012. Synchronous wildfire activity and mire deforestation at the Triassic–Jurassic boundary. PLoS ONE 7(10): e47236. Doi:10.1371/journal.pone0047236

Rasmussen, E.S. & Nielsen, A.T. 2020. Danmarks Geologi – En kort introduktion. Junior Geologerne. https://junior-geologerne.dk/wp-content/uploads/2020/06/Junior-Geologerne_Danmarks_geologi.pdf

Schovsbo N.H. 2011. The Lower Palaeozoic sequence in the Slagelse-1 well. Stratigraphical, lithological and geochemical evaluation. Danmarks og Grønlands Geologiske Undersøgelse Rapport 2011/84; GEUS. 49 pp. https://doi.org/10.22008/gpub/28811.

Smit, F.W.H., Gregersen, U., Lorentzen, M., Bredesen, K., Pedersen, G.K., Hovikoski, J. and Vosgerau, H. 2022. Seismic Geomorphology of the Upper Triassic – Lower Jurassic Gassum Formation – Improved Reservoir Characterization in the Stenlille (Denmark) CCS Demonstration Site. GHGT-16 Conference Proceedings (2022); Geophysics eJournal, 4 (83), December 2022, 11 pp. SSRN: https://papers.ssrn.com/abstract=4277360

Sorgenfrei, T. & Buch, A. 1964. Deep Tests in Denmark 1935–1959. Danmarks Geologiske Undersøgelse, Række III, Nr. 36, 146 p. https://doi.org/10.34194/raekke3.v36.6941

Span, R. & Wagner, W. 1996. A new equation of state for carbon dioxide covering the fluid region from the triple-point temperature to 1100K at pressures up to 800 MPa, J. Phys. Chem. Ref. Data, 25, 1509–1596.

Springer, N., Didriksen, K., Holmslykke, H.D., Kjøller, C., Olivarius, M. and Schovsbo, N. 2020. Capture, Storage and Use of CO2 (CCUS): Seal capacity and geochemical modelling (Part of work package 5 in the CCUS project). Danmarks og Grønlands Geologiske Undersøgelse Rapport 2020/30; GEUS. 42 pp. https://doi.org/10.22008/gpub/34527

Springer, N., Lotentzen, H., Fries, K. and Lindgreen, H. 2010. Caprock seal capacity evaluation of the Fjerritslev and Børglum Formations. Contribution to the EFP-project AQUA-DK. Danmarks og Grønlands Geologiske Undersøgelse Rapport nr. 112.

Spudich, P., Fletcher, J., Hellweg, M., Boatwright, J., Sullivan, C., Joyner, W., Hanks, T., Boore, D.M., McGarr, A. and Baker, L. 1997. SEA96—A new predictive relation for earthquake ground motions in extensional tectonic regimes. Seismological Research Letters 68(1), 190–198.

Stenestad, E., 1972. Træk af det danske bassins udvikling i Øvre Kridt. Dansk Geologisk Forening Aarsskrift, 1971, 63–69.

Surlyk, F. Arndorff, L., Hamann, N.E., Hamberg, L., Johannessen, P.N., Koppelhus, E.B., Nielsen, L.H., Noe-Nygaard, N., Pedersen, G.K. and Petersen, H.I. 1995. High-resolution sequence stratigraphy of the Hettangian–Sinemurian paralic succession, Bornholm, Denmark. Sedimentology 42, 323–354. DOI: 10.1111/j.1365-3091.1995.tb02105.x WOSUID: WOS:A1995QR46100007

THOR, 1997. 3D Stenlille-97 Final acquisition report. THOR Geophysikalische Prospektion GmbH seismic acquisition report for DONG A/S. Germany, December 1997.

Vejbæk O.V. 1997. Dybe strukturer i danske sedimentære bassiner. Geologisk Tidsskrift 1997/4; p. 1–31. https://2dgf.dk/xpdf/gt1997-4-1-31.pdf.

Vejbæk, O.V. & Britze, P. 1994. Geological map of Denmark 1:750.000. Top pre-Zechstein. Danmarks Geologiske Undersøgelse Map series, 45, 9 pp.

Vosgerau, H., Gregersen, U., Hjuler, M.L., Holmslykke, H.D., Kristensen, L., Lindström, S., Mathiesen, A., Nielsen, C.M., Olivarius, M., Pedersen, G.K. and Nielsen, L.H. 2016. Reservoir prognosis of the Gassum Formation and the Karlebo Member within two areas of interest in northern Copenhagen. The EUDP project "Geothermal pilot well, phase 1b". GEUS Rapport 2016/56. 138 pp + app 1–5. https://doi.org/10.22008/gpub/32477

Vosgerau, H., Gregersen, U. and Laghari, S. 2020. Capture, Storage and Use of CO2 (CCUS): Seismic interpretation of existing 3D seismic data around the Stenlille structure within the framework of sequence stratigraphy and with focus on the Gassum Formation (Part of Work package 6 in the CCUS project). Danmarks og Grønlands Geologiske Undersøgelse Rapport 2020/34; GEUS. 53 pp. https://doi.org/10.22008/gpub/34531

Vosgerau et al. in prep. The reservoir architecture of the Upper Triassic–Lower Jurassic Gassum Formation at two potential CO2 storage sites, the Stenlille and Havnsø structures, Denmark.

Voss, P., Dahl-Jensen, T. and Larsen, T. B. 2015. Earthquake Hazard in Denmark. Geological Survey of Denmark and Greenland report 2015/24, 53 pp.

Wang, Y., Zhangb, K. and Wua, N. 2013. Numerical Investigation of the Storage Efficiency Factor for CO2 Geological Sequestration in Saline Formations, Energy Procedia, Volume 37, 5267-5274.

Appendix A – Depth conversion (see Chapter 5)

APPENDIX A – Depth conversion (Chapter 5)

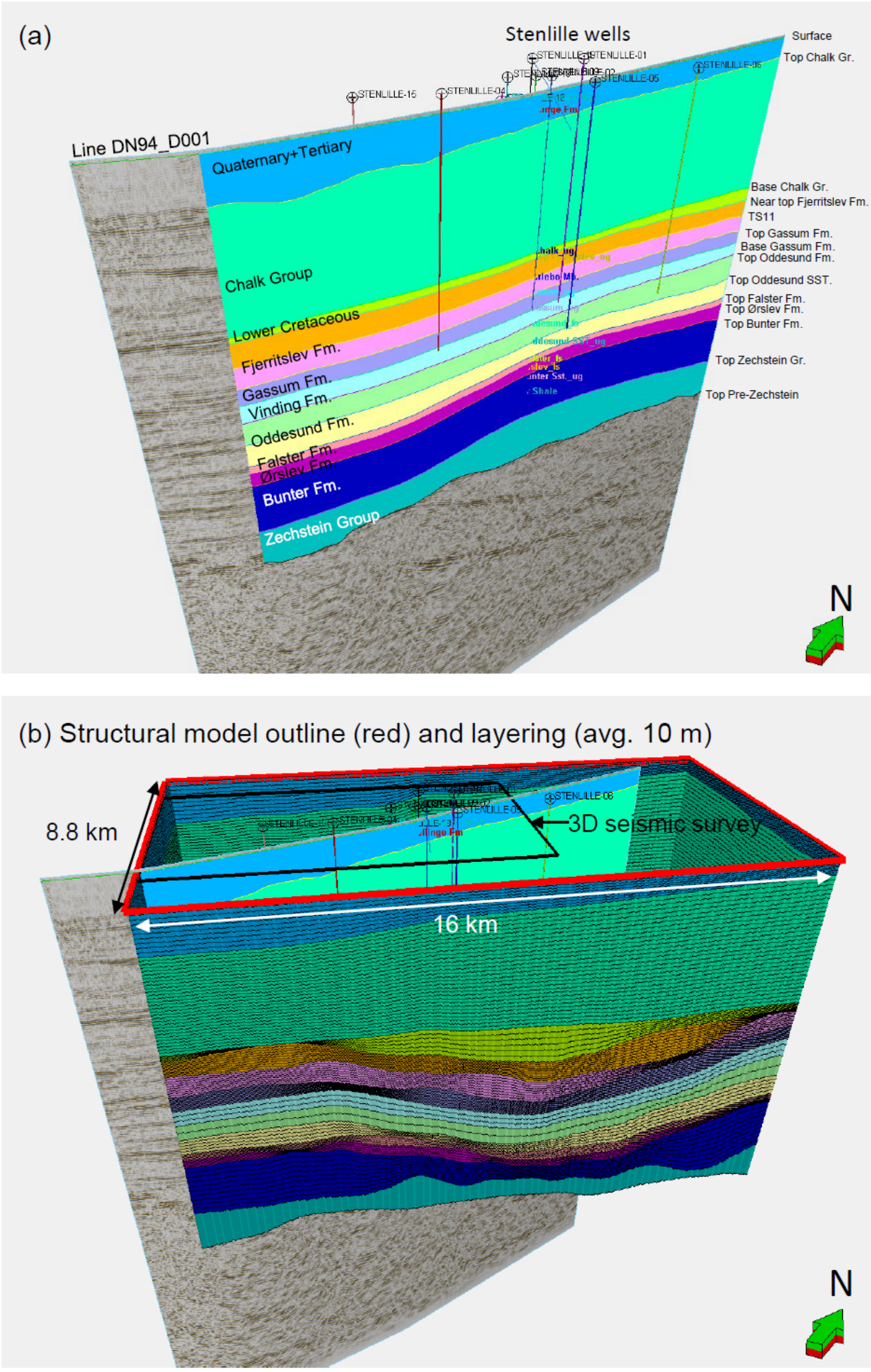

A-1 (a) Mapped seismic horizons from 3D seismic survey and 2D datasets, and zonation used in the velocity model. (b) Outline of the structural model (red line, 8.8x16 km) and 3D seismic survey (black), showing a significant extension of the velocity model beyond the 3D seismic survey. Layering per zone is based on an average thickness of 10 m per layer.

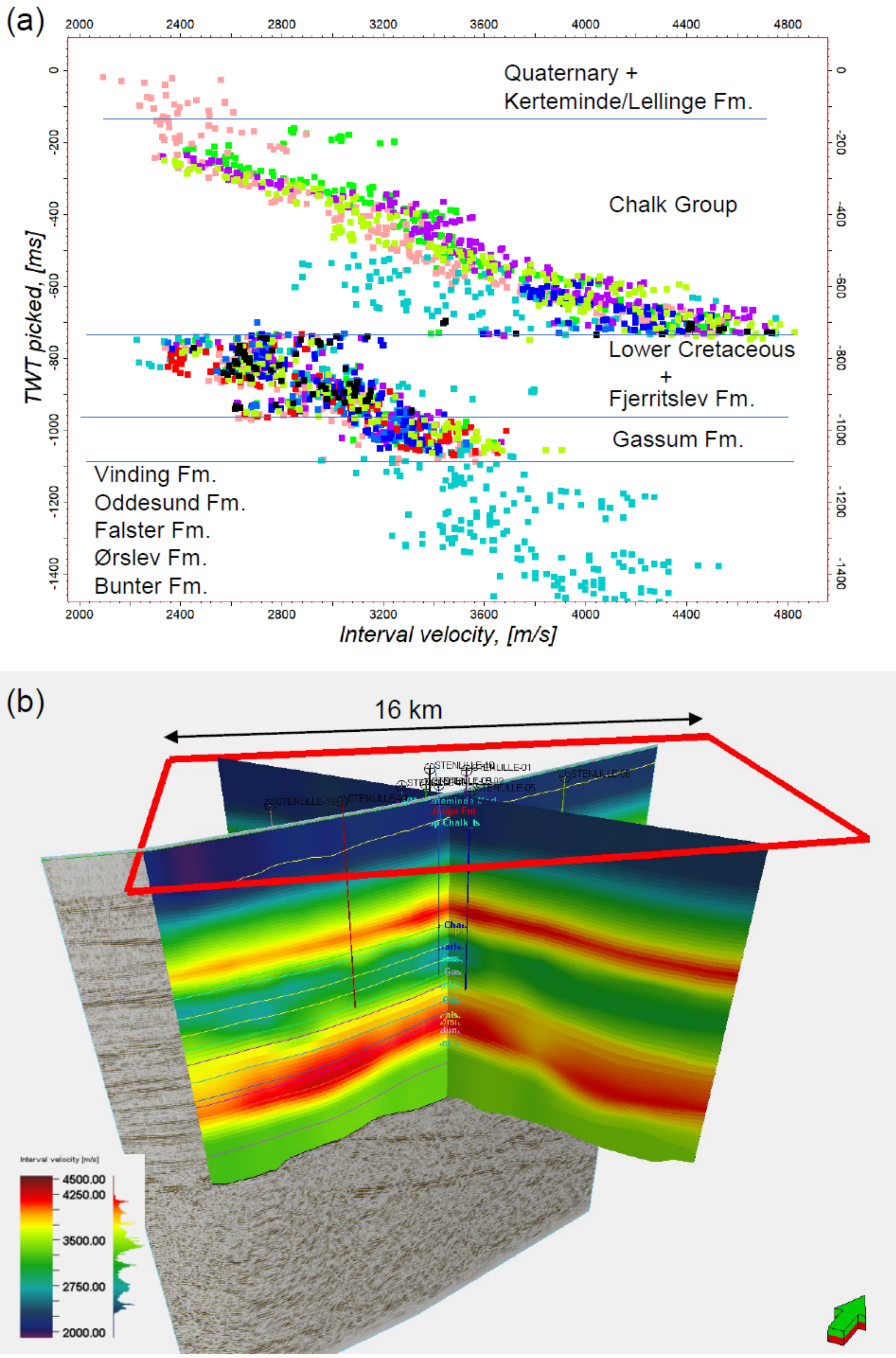

A-2 Velocity data as input to the velocity model. (a) Cross plot of interval velocity (x-axis) and Two-Way-Time (y-axis), derived from Time-Depth-Relationships (TDRs) in nine wells (ST-1/2/4/5/6/9/10/15/19) that were tied to seismic data. Colours reflect the different wells. Note variable data density, especially pre-Chalk Group, and post Gassum Fm. (b) Extrapolated seismic migration velocity data (from 3D seismic survey) using the structural grid and full-tension option. These data are used as 3D trends in the kriging procedure. Note the high velocities (red) e.g. in the lower Chalk Group.

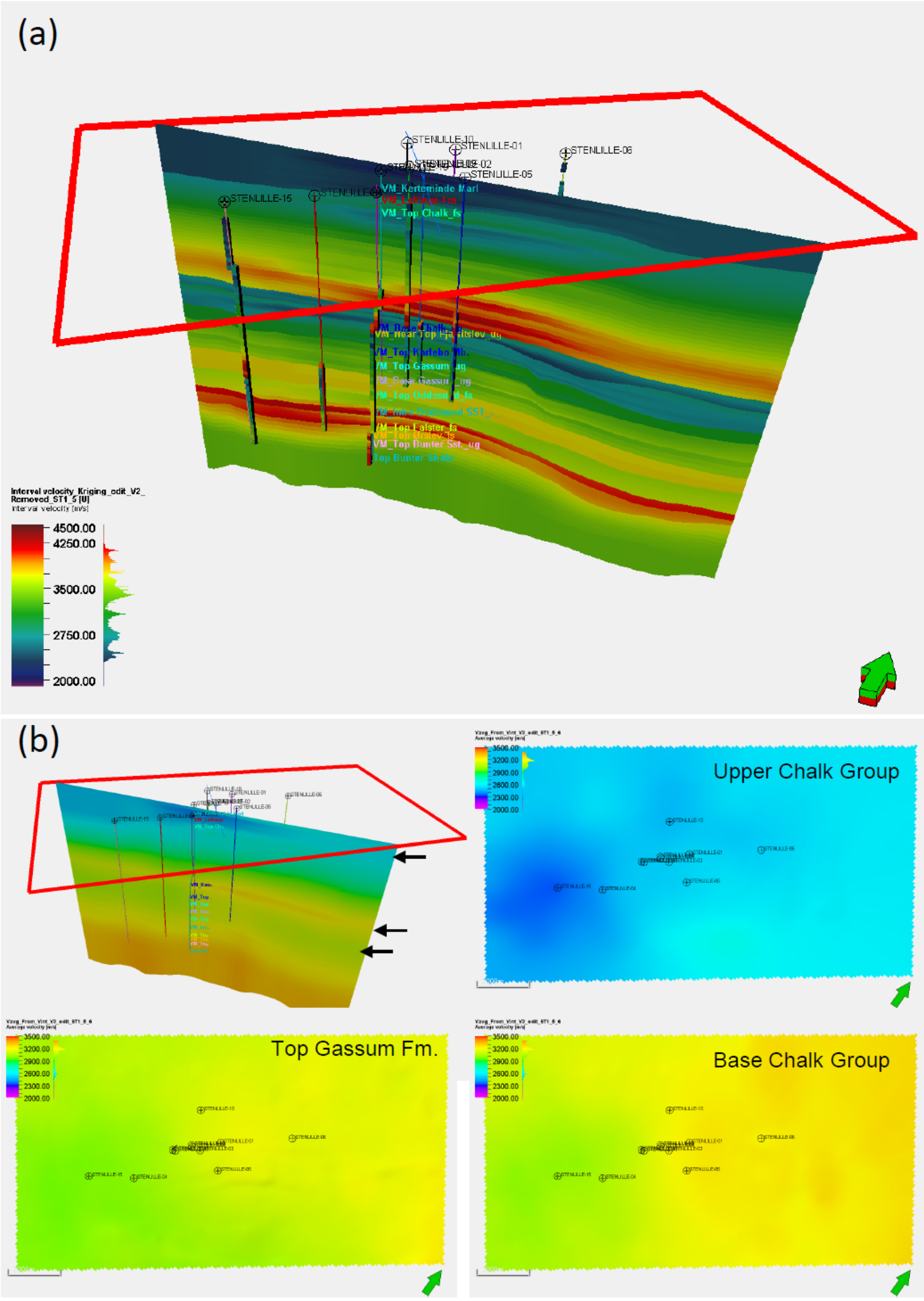

A-3 (a) Final 3D grid with interval velocities. A kriging method was used to extrapolate interval velocities from the TDRs in nine wells, considering lateral and vertical changes observed from data analysis (obtaining minor/major axis of the variograms per zone), and using the extrapolated 3D seismic migration velocities as a trend. (b) A Petrel workflow was used to convert the interval velocity grid to average velocity grid, and stratigraphic horizons extracted from the average velocity grid are shown for three horizons. Note the lower velocity (green/blue) in the ST-15 area (left) due to incisions into the Chalk Group, making this higher velocity unit thinner here, and affected the depth conversion (e.g. reduced the time mapped closure-size).

APPENDIX A – Depth conversion (Chapter 5)

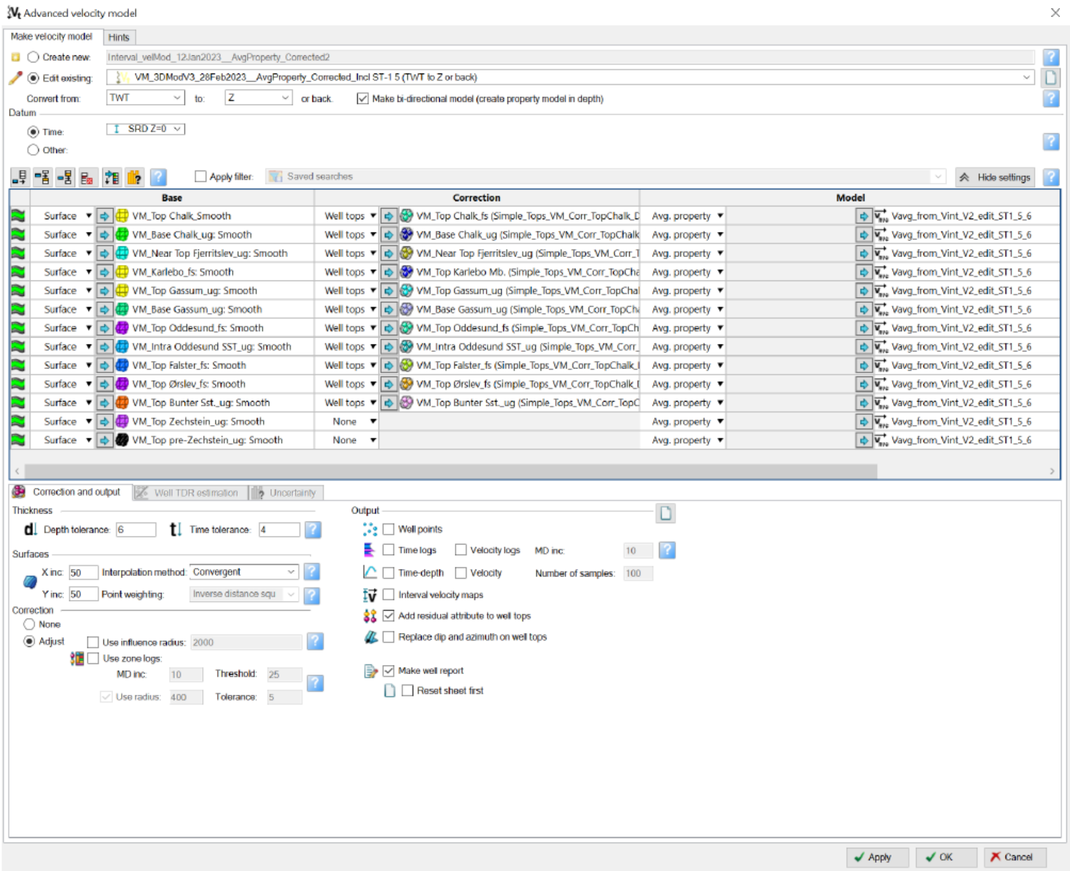

A-4 Advanced velocity model building interface in Petrel showing TWT surfaces (tied to TWT marker depths in wells prior to this step), depth well markers (meters), and velocity function using the average velocity 3D grid seen in figure A-4b. A correction to the velocity field is applied by minimizing the difference between depth in meters of 3D horizon and well marker.

Appendix B – Stenlille well-log interpretation (ST-1,2,5,6,18)

APPENDIX B - Stenlille well-log interpretation

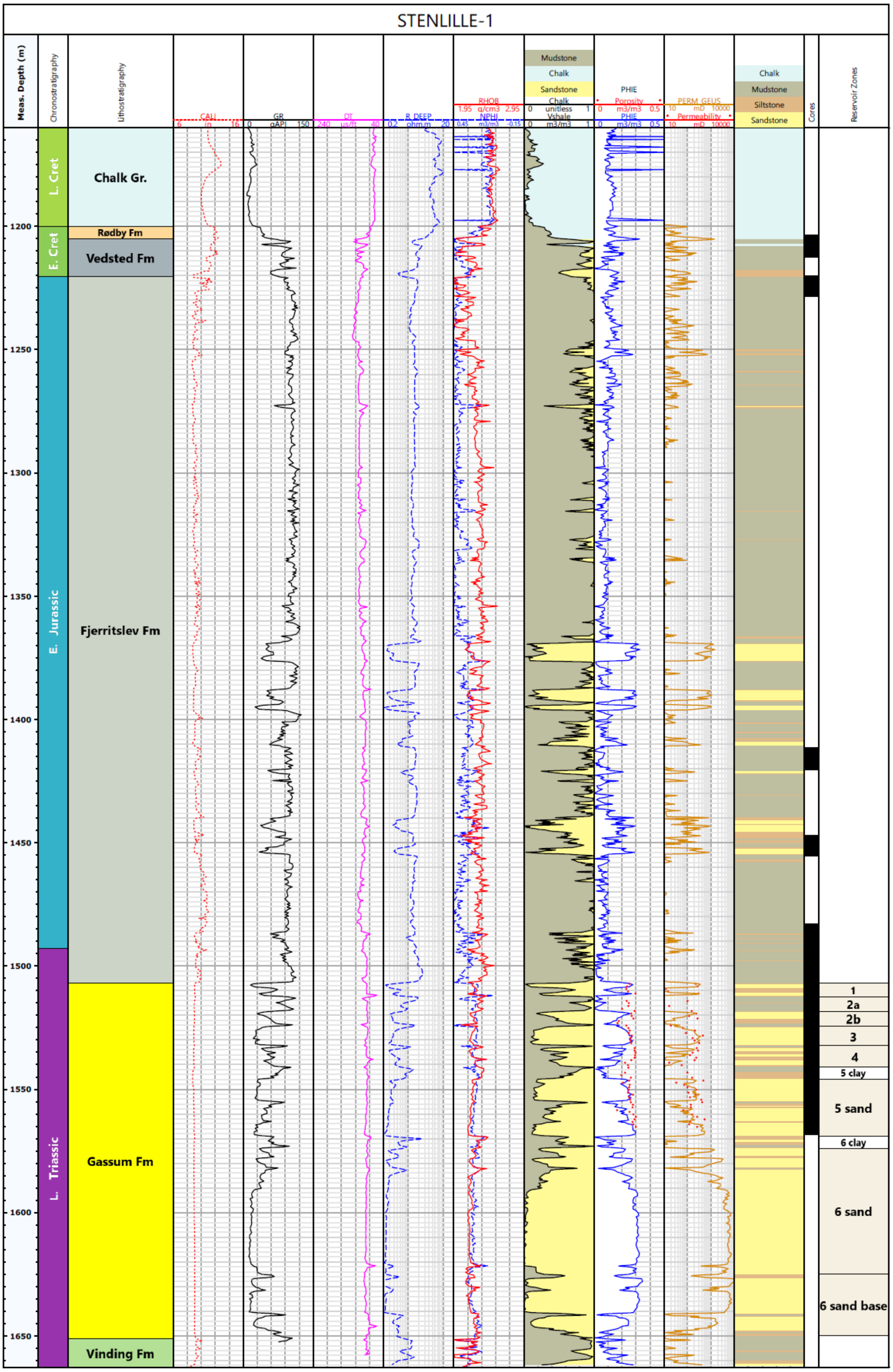

GEUS Rapport 2022/26

APPENDIX B - Stenlille well-log interpretation

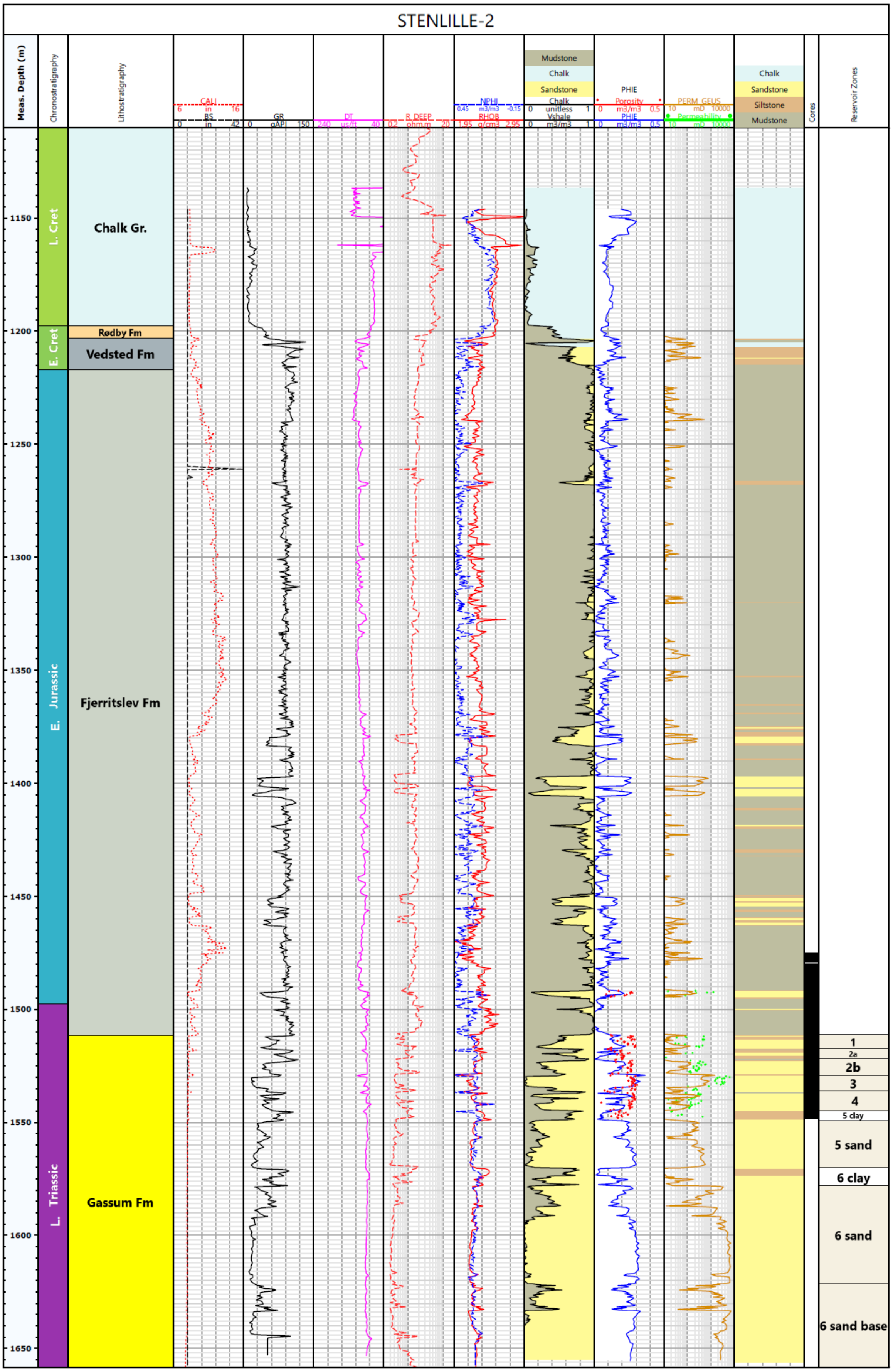

GEUS Rapport 2022/26

APPENDIX B - Stenlille well-log interpretation

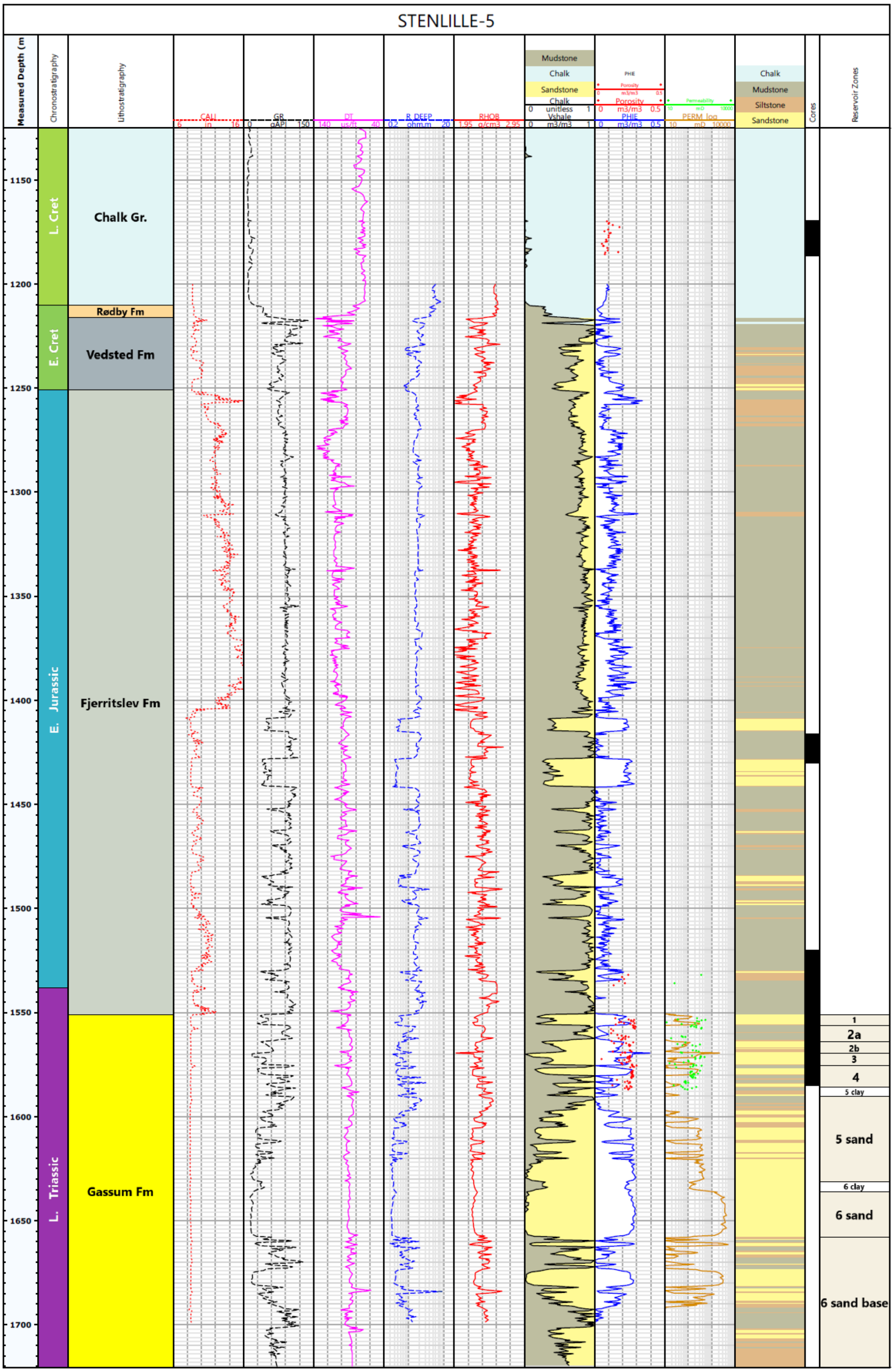

GEUS Rapport 2022/26

APPENDIX B - Stenlille well-log interpretation

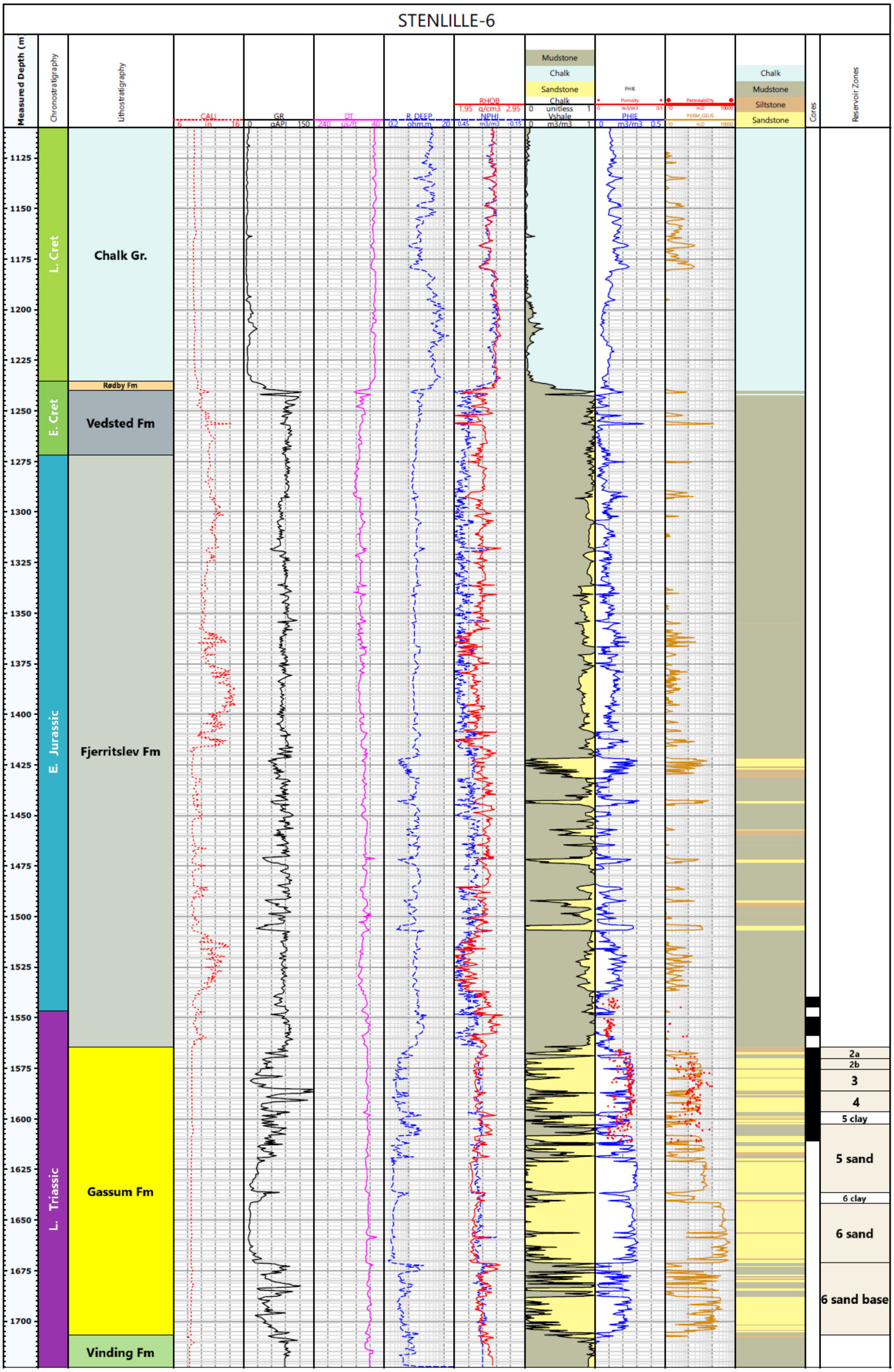

GEUS Rapport 2022/26

APPENDIX B - Stenlille well-log interpretation

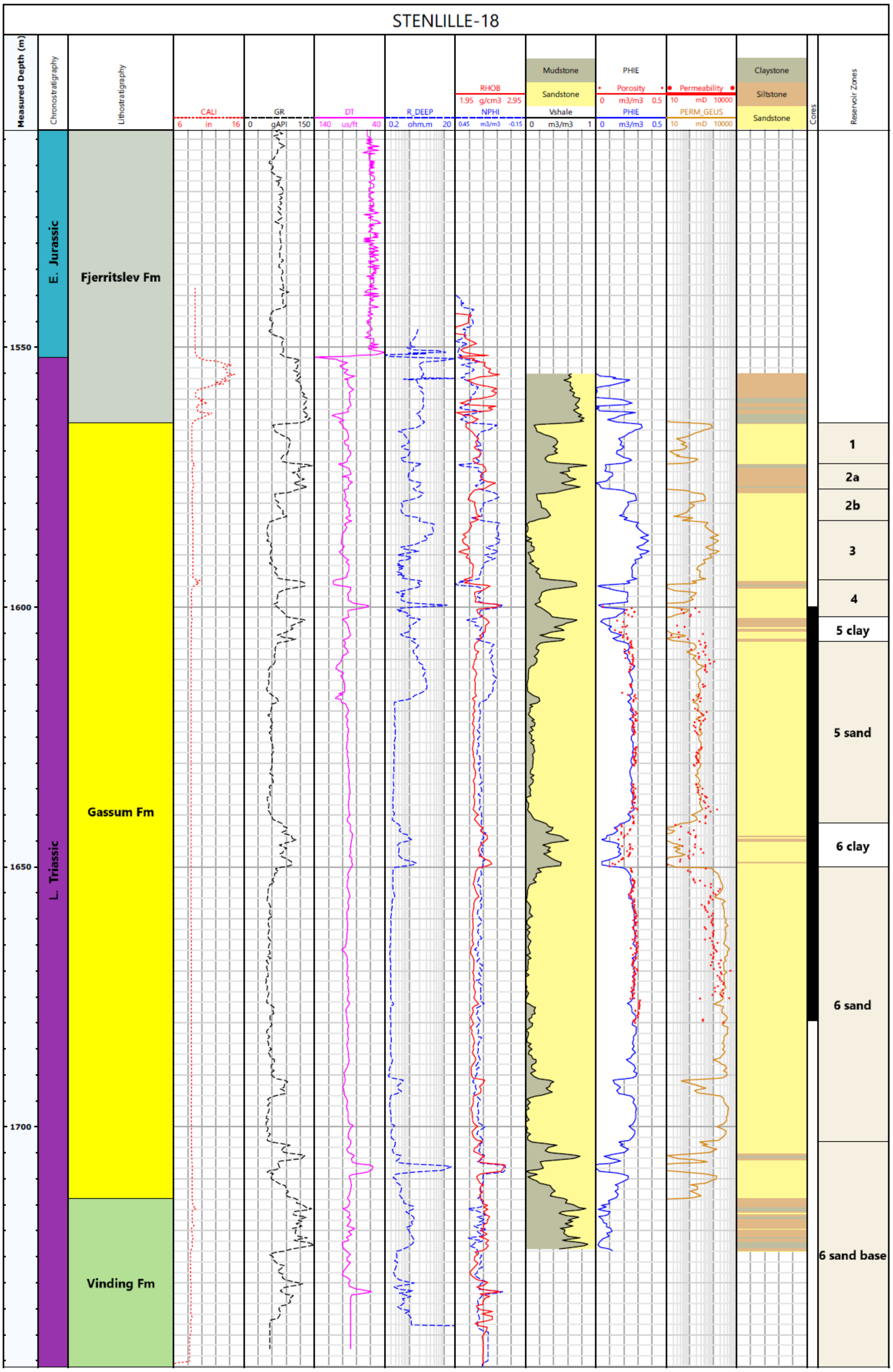

GEUS Rapport 2022/26

Danish Ministry of Climate, Energy and Utilities

Geological survey of
Denmark and Greenland (GEUS)

Øster Voldgade 10
DK-1350 Copenhagen K
Denmark

GEUS is a research and advisory institution in the Danish Ministry of Climate, Energy and Utilities

Erratum:

New 2D seismic data (GEUS2022-HAVNSOE survey) was acquired in the autumn 2022 with processing and reprocessing finalized in the autumn 2023, after the conclusion of this report: Danmarks og Grønlands Geologiske Undersøgelse Rapport 2022/26. A scope of the new seismic survey was to provide new improved data for mapping and facilitating correlation of the dense database at the Stenlille structure to the Havnsø structure to the west.

The regional correlation of the new seismic 2D data from the Stenlille-19 well (in the 3D survey area) and to the sea level at the west coast of Zealand has indicated, that the 3D seismic data cube (Stenlille-97) is located approx. 40 ms too shallow to fit the mean sea level of the marine data.